UNITED STATES AIR FORCE

SUMMER RESEARCH PROGRAM -- 1997

SUMMER FACULTY RESEARCH PROGRAM FINAL REPORTS

VOLUME 2B

ARMSTRONG LABORATORY

RESEARCH & DEVELOPMENT LABORATORIES

5800 Uplander Way

Culver City, CA 90230-6608

Program Director, RDL
Gary Moore

Program Manager, AFOSR
Major Linda Steel-Goodwin

Program Manager, RDL
Scott Licoscos

Program Administrator, RDL
Johnetta Thompson

Program Administrator, RDL
Rebecca Kelly-Clemmons

Submitted to:

AIR FORCE OFFICE OF SCIENTIFIC RESEARCH

Bolling Air Force Base

Washington, D.C.

December 1997

20010319 064

AQM01-06-1196

REPORT DOCUMENTATION PAGE

AFRL-SR-BL-TR-00-

0752

Public reporting burden for this collection of information is estimated to average 1 hour per response, including the time for reviewing instructio ... ng and reviewing the collection of information. Send comments regarding this burden estimate or any other aspect of this collection of information, includi ... for Information Operations and Reports, 1215 Jefferson Davis Highway, Suite 1204, Arlington, VA 22202-4302, and to the Office of Management and Budge

1. AGENCY USE ONLY *(Leave blank)*

2. REPORT DATE
December, 1997

3. R

4. TITLE AND SUBTITLE
1997 Summer Research Program (SRP), Summer Faculty Research Program (SFRP), Final Reports, Volume 2B, Armstrong Laboratory

5. FUNDING NUMBERS
F49620-93-C-0063

6. AUTHOR(S)
Gary Moore

7. PERFORMING ORGANIZATION NAME(S) AND ADDRESS(ES)
Research & Development Laboratories (RDL)
5800 Uplander Way
Culver City, CA 90230-6608

8. PERFORMING ORGANIZATION REPORT NUMBER

9. SPONSORING/MONITORING AGENCY NAME(S) AND ADDRESS(ES)
Air Force Office of Scientific Research (AFOSR)
801 N. Randolph St.
Arlington, VA 22203-1977

10. SPONSORING/MONITORING AGENCY REPORT NUMBER

11. SUPPLEMENTARY NOTES

12a. DISTRIBUTION AVAILABILITY STATEMENT
Approved for Public Release

12b. DISTRIBUTION CODE

13. ABSTRACT *(Maximum 200 words)*

The United States Air Force Summer Research Program (USAF-SRP) is designed to introduce university, college, and technical institute faculty members, graduate students, and high school students to Air Force research. This is accomplished by the faculty members (Summer Faculty Research Program, (SFRP)), graduate students (Graduate Student Research Program (GSRP)), and high school students (High School Apprenticeship Program (HSAP)) being selected on a nationally advertised competitive basis during the summer intersession period to perform research at Air Force Research Laboratory (AFRL) Technical Directorates, Air Force Air Logistics Centers (ALC), and other AF Laboratories. This volume consists of a program overview, program management statistics, and the final technical reports from the SFRP participants at the Armstrong Laboratory.

14. SUBJECT TERMS
Air Force Research, Air Force, Engineering, Laboratories, Reports, Summer, Universities, Faculty, Graduate Student, High School Student

15. NUMBER OF PAGES

16. PRICE CODE

17. SECURITY CLASSIFICATION OF REPORT	18. SECURITY CLASSIFICATION OF THIS PAGE	19. SECURITY CLASSIFICATION OF ABSTRACT	20. LIMITATION OF ABSTRACT
Unclassified	Unclassified	Unclassified	UL

Standard Form 298 (Rev. 2-89) (EG)
Prescribed by ANSI Std. 239.18
Designed using Perform Pro, WHS/DIOR, Oct 94

GENERAL INSTRUCTIONS FOR COMPLETING SF 298

The Report Documentation Page (RDP) is used in announcing and cataloging reports. It is important that this information be consistent with the rest of the report, particularly the cover and title page. Instructions for filling in each block of the form follow. It is important to ***stay within the lines*** to meet ***optical scanning requirements.***

Block 1. Agency Use Only *(Leave blank).*

Block 2. Report Date. Full publication date including day, month, and year, if available
(e.g. 1 Jan 88). Must cite at least the year.

Block 3. Type of Report and Dates Covered. State whether report is interim, final, etc. If applicable, enter inclusive report dates (e.g. 10 Jun 87 - 30 Jun 88).

Block 4. Title and Subtitle. A title is taken from the part of the report that provides the most meaningful and complete information. When a report is prepared in more than one volume, repeat the primary title, add volume number, and include subtitle for the specific volume. On classified documents enter the title classification in parentheses.

Block 5. Funding Numbers. To include contract and grant numbers; may include program element number(s), project number(s), task number(s), and work unit number(s). Use the following labels:

C - Contract	**PR** - Project
G - Grant	**TA** - Task
PE - Program Element	**WU** - Work Unit Accession No.

Block 6. Author(s). Name(s) of person(s) responsible for writing the report, performing the research, or credited with the content of the report. If editor or compiler, this should follow the name(s).

Block 7. Performing Organization Name(s) and Address(es). Self-explanatory.

Block 8. Performing Organization Report Number. Enter the unique alphanumeric report number(s) assigned by the organization performing the report.

Block 9. Sponsoring/Monitoring Agency Name(s) and Address(es). Self-explanatory.

Block 10. Sponsoring/Monitoring Agency Report Number. *(If known)*

Block 11. Supplementary Notes. Enter information not included elsewhere such as: Prepared in cooperation with....; Trans. of....; To be published in.... When a report is revised, include a statement whether the new report supersedes or supplements the older report.

Block 12a. Distribution/Availability Statement. Denotes public availability or limitations. Cite any availability to the public. Enter additional limitations or special markings in all capitals (e.g. NOFORN, REL, ITAR).

DOD - See DoDD 5230.24, "Distribution Statements on Technical Documents."
DOE - See authorities.
NASA - See Handbook NHB 2200.2.
NTIS - Leave blank.

Block 12b. Distribution Code.

DOD - Leave blank.
DOE - Enter DOE distribution categories from the Standard Distribution for Unclassified Scientific and Technical Reports.
Leave blank.
NASA - Leave blank.
NTIS -

Block 13. Abstract. Include a brief *(Maximum 200 words)* factual summary of the most significant information contained in the report.

Block 14. Subject Terms. Keywords or phrases identifying major subjects in the report.

Block 15. Number of Pages. Enter the total number of pages.

Block 16. Price Code. Enter appropriate price code *(NTIS only).*

Blocks 17. - 19. Security Classifications. Self- explanatory. Enter U.S. Security Classification in accordance with U.S. Security Regulations (i.e., UNCLASSIFIED). If form contains classified information, stamp classification on the top and bottom of the page.

Block 20. Limitation of Abstract. This block must be completed to assign a limitation to the abstract. Enter either UL (unlimited) or SAR (same as report). An entry in this block is necessary if the abstract is to be limited. If blank, the abstract is assumed to be unlimited.

SFRP FINAL REPORT TABLE OF CONTENTS i-xviii

APPENDICIES:

PREFACE

Reports in this volume are numbered consecutively beginning with number 1. Each report is paginated with the report number followed by consecutive page numbers, e.g., 1-1, 1-2, 1-3; 2-1, 2-2, 2-3.

Due to its length, Volume 2 is bound in two parts, 2A and 2B. Volume 2A contains #1-20. Volume 2B contains reports #21-36. The Table of Contents for Volume 2 is included in both parts.

This document is one of a set of 16 volumes describing the 1997 AFOSR Summer Research Program. The following volumes comprise the set:

VOLUME	TITLE
1	Program Management Report
	Summer Faculty Research Program (SFRP) Reports
2A & 2B	Armstrong Laboratory
3A & 3B	Phillips Laboratory
4A & 4B	Rome Laboratory
5A, 5B & 5C	Wright Laboratory
6	Arnold Engineering Development Center, U.S. Air Force Academy, Air Logistic Centers, and Wilford Hall Medical Center
	Graduate Student Research Program (GSRP) Reports
7	Armstrong Laboratory
8	Phillips Laboratory
9	Rome Laboratory
10A & 10B	Wright Laboratory
11	Arnold Engineering Development Center, U.S. Air Force Academy, Air Logistic Centers, and Wilford Hall Medical Center
	High School Apprenticeship Program (HSAP) Reports
12A & 12B	Armstrong Laboratory
13	Phillips Laboratory
14	Rome Laboratory
15A&15B	Wright Laboratory
16	Arnold Engineering Development Center

SRP Final Report Table of Contents

SRP Final Report Table of Contents

SRP Final Report Table of Contents

SRP Final Report Table of Contents

SRP Final Report Table of Contents

SRP Final Report Table of Contents

SRP Final Report Table of Contents

SRP Final Report Table of Contents

SRP Final Report Table of Contents

SRP Final Report Table of Contents

SRP Final Report Table of Contents

SRP Final Report Table of Contents

SRP Final Report Table of Contents

SRP Final Report Table of Contents

SRP Final Report Table of Contents

SRP Final Report Table of Contents

SRP Final Report Table of Contents

SRP Final Report Table of Contents

1. INTRODUCTION

The Summer Research Program (SRP), sponsored by the Air Force Office of Scientific Research (AFOSR), offers paid opportunities for university faculty, graduate students, and high school students to conduct research in U.S. Air Force research laboratories nationwide during the summer.

Introduced by AFOSR in 1978, this innovative program is based on the concept of teaming academic researchers with Air Force scientists in the same disciplines using laboratory facilities and equipment not often available at associates' institutions.

The Summer Faculty Research Program (SFRP) is open annually to approximately 150 faculty members with at least two years of teaching and/or research experience in accredited U.S. colleges, universities, or technical institutions. SFRP associates must be either U.S. citizens or permanent residents.

The Graduate Student Research Program (GSRP) is open annually to approximately 100 graduate students holding a bachelor's or a master's degree; GSRP associates must be U.S. citizens enrolled full time at an accredited institution.

The High School Apprentice Program (HSAP) annually selects about 125 high school students located within a twenty mile commuting distance of participating Air Force laboratories.

AFOSR also offers its research associates an opportunity, under the Summer Research Extension Program (SREP), to continue their AFOSR-sponsored research at their home institutions through the award of research grants. In 1994 the maximum amount of each grant was increased from $20,000 to $25,000, and the number of AFOSR-sponsored grants decreased from 75 to 60. A separate annual report is compiled on the SREP.

The numbers of projected summer research participants in each of the three categories and SREP "grants" are usually increased through direct sponsorship by participating laboratories.

AFOSR's SRP has well served its objectives of building critical links between Air Force research laboratories and the academic community, opening avenues of communications and forging new research relationships between Air Force and academic technical experts in areas of national interest, and strengthening the nation's efforts to sustain careers in science and engineering. The success of the SRP can be gauged from its growth from inception (see Table 1) and from the favorable responses the 1997 participants expressed in end-of-tour SRP evaluations (Appendix B).

AFOSR contracts for administration of the SRP by civilian contractors. The contract was first awarded to Research & Development Laboratories (RDL) in September 1990. After completion of the

1990 contract, RDL (in 1993) won the recompetition for the basic year and four 1-year options.

2. PARTICIPATION IN THE SUMMER RESEARCH PROGRAM

The SRP began with faculty associates in 1979; graduate students were added in 1982 and high school students in 1986. The following table shows the number of associates in the program each year.

YEAR	SRP Participation, by Year			TOTAL
	SFRP	GSRP	HSAP	
1979	70			70
1980	87			87
1981	87			87
1982	91	17		108
1983	101	53		154
1984	152	84		236
1985	154	92		246
1986	158	100	42	300
1987	159	101	73	333
1988	153	107	101	361
1989	168	102	103	373
1990	165	121	132	418
1991	170	142	132	444
1992	185	121	159	464
1993	187	117	136	440
1994	192	117	133	442
1995	190	115	137	442
1996	188	109	138	435
1997	148	98	140	427

Beginning in 1993, due to budget cuts, some of the laboratories weren't able to afford to fund as many associates as in previous years. Since then, the number of funded positions has remained fairly constant at a slightly lower level.

3. RECRUITING AND SELECTION

The SRP is conducted on a nationally advertised and competitive-selection basis. The advertising for faculty and graduate students consisted primarily of the mailing of 8,000 52-page SRP brochures to chairpersons of departments relevant to AFOSR research and to administrators of grants in accredited universities, colleges, and technical institutions. Historically Black Colleges and Universities (HBCUs) and Minority Institutions (MIs) were included. Brochures also went to all participating USAF laboratories, the previous year's participants, and numerous individual requesters (over 1000 annually).

RDL placed advertisements in the following publications: *Black Issues in Higher Education, Winds of Change,* and *IEEE Spectrum.* Because no participants list either *Physics Today* or *Chemical & Engineering News* as being their source of learning about the program for the past several years, advertisements in these magazines were dropped, and the funds were used to cover increases in brochure printing costs.

High school applicants can participate only in laboratories located no more than 20 miles from their residence. Tailored brochures on the HSAP were sent to the head counselors of 180 high schools in the vicinity of participating laboratories, with instructions for publicizing the program in their schools. High school students selected to serve at Wright Laboratory's Armament Directorate (Eglin Air Force Base, Florida) serve eleven weeks as opposed to the eight weeks normally worked by high school students at all other participating laboratories.

Each SFRP or GSRP applicant is given a first, second, and third choice of laboratory. High school students who have more than one laboratory or directorate near their homes are also given first, second, and third choices.

Laboratories make their selections and prioritize their nominees. AFOSR then determines the number to be funded at each laboratory and approves laboratories' selections.

Subsequently, laboratories use their own funds to sponsor additional candidates. Some selectees do not accept the appointment, so alternate candidates are chosen. This multi-step selection procedure results in some candidates being notified of their acceptance after scheduled deadlines. The total applicants and participants for 1997 are shown in this table.

1997 Applicants and Participants			
PARTICIPANT CATEGORY	TOTAL APPLICANTS	SELECTEES	DECLINING SELECTEES
SFRP	490	188	32
(HBCU/MI)	(0)	(0)	(0)
GSRP	202	98	9
(HBCU/MI)	(0)	(0)	(0)
HSAP	433	140	14
TOTAL	1125	426	55

4. SITE VISITS

During June and July of 1997, representatives of both AFOSR/NI and RDL visited each participating laboratory to provide briefings, answer questions, and resolve problems for both laboratory personnel and participants. The objective was to ensure that the SRP would be as constructive as possible for all participants. Both SRP participants and RDL representatives found these visits beneficial. At many of the laboratories, this was the only opportunity for all participants to meet at one time to share their experiences and exchange ideas.

5. HISTORICALLY BLACK COLLEGES AND UNIVERSITIES AND MINORITY INSTITUTIONS (HBCU/MIs)

Before 1993, an RDL program representative visited from seven to ten different HBCU/MIs annually to promote interest in the SRP among the faculty and graduate students. These efforts were marginally effective, yielding a doubling of HBCI/MI applicants. In an effort to achieve AFOSR's goal of 10% of all applicants and selectees being HBCU/MI qualified, the RDL team decided to try other avenues of approach to increase the number of qualified applicants. Through the combined efforts of the AFOSR Program Office at Bolling AFB and RDL, two very active minority groups were found, HACU (Hispanic American Colleges and Universities) and AISES (American Indian Science and Engineering Society). RDL is in communication with representatives of each of these organizations on a monthly basis to keep up with the their activities and special events. Both organizations have widely-distributed magazines/quarterlies in which RDL placed ads.

Since 1994 the number of both SFRP and GSRP HBCU/MI applicants and participants has increased ten-fold, from about two dozen SFRP applicants and a half dozen selectees to over 100 applicants and two dozen selectees, and a half-dozen GSRP applicants and two or three selectees to 18 applicants and 7 or 8 selectees. Since 1993, the SFRP had a two-fold applicant increase and a two-fold selectee increase. Since 1993, the GSRP had a three-fold applicant increase and a three to four-fold increase in selectees.

In addition to RDL's special recruiting efforts, AFOSR attempts each year to obtain additional funding or use leftover funding from cancellations the past year to fund HBCU/MI associates. This year, 5 HBCU/MI SFRPs declined after they were selected (and there was no one qualified to replace them with). The following table records HBCU/MI participation in this program.

SRP HBCU/MI Participation, By Year				
YEAR	**SFRP**		**GSRP**	
	Applicants	**Participants**	**Applicants**	**Participants**
1985	76	23	15	11
1986	70	18	20	10
1987	82	32	32	10
1988	53	17	23	14
1989	39	15	13	4
1990	43	14	17	3
1991	42	13	8	5
1992	70	13	9	5
1993	60	13	6	2
1994	90	16	11	6
1995	90	21	20	8
1996	119	27	18	7

6. SRP FUNDING SOURCES

Funding sources for the 1997 SRP were the AFOSR-provided slots for the basic contract and laboratory funds. Funding sources by category for the 1997 SRP selected participants are shown here.

1997 SRP FUNDING CATEGORY	SFRP	GSRP	HSAP
AFOSR Basic Allocation Funds	141	89	123
USAF Laboratory Funds	48	9	17
HBCU/MI By AFOSR (Using Procured Addn'l Funds)	0	0	N/A
TOTAL	9	98	140

SFRP - 188 were selected, but thirty two canceled too late to be replaced.
GSRP - 98 were selected, but nine canceled too late to be replaced.
HSAP - 140 were selected, but fourteen canceled too late to be replaced.

7. COMPENSATION FOR PARTICIPANTS

Compensation for SRP participants, per five-day work week, is shown in this table.

1997 SRP Associate Compensation

PARTICIPANT CATEGORY	1991	1992	1993	1994	1995	1996	1997
Faculty Members	$690	$718	$740	$740	$740	$770	$770
Graduate Student (Master's Degree)	$425	$442	$455	$455	$455	$470	$470
Graduate Student (Bachelor's Degree)	$365	$380	$391	$391	$391	$400	$400
High School Student (First Year)	$200	$200	$200	$200	$200	$200	$200
High School Student (Subsequent Years)	$240	$240	$240	$240	$240	$240	$240

The program also offered associates whose homes were more than 50 miles from the laboratory an expense allowance (seven days per week) of $50/day for faculty and $40/day for graduate students. Transportation to the laboratory at the beginning of their tour and back to their home destinations at the end was also reimbursed for these participants. Of the combined SFRP and GSRP associates, 65 % (194 out of 286) claimed travel reimbursements at an average round-trip cost of $776.

Faculty members were encouraged to visit their laboratories before their summer tour began. All costs of these orientation visits were reimbursed. Forty-three percent (85 out of 188) of faculty associates took orientation trips at an average cost of $388. By contrast, in 1993, 58 % of SFRP associates took

orientation visits at an average cost of $685; that was the highest percentage of associates opting to take an orientation trip since RDL has administered the SRP, and the highest average cost of an orientation trip. These 1993 numbers are included to show the fluctuation which can occur in these numbers for planning purposes.

Program participants submitted biweekly vouchers countersigned by their laboratory research focal point, and RDL issued paychecks so as to arrive in associates' hands two weeks later.

This is the second year of using direct deposit for the SFRP and GSRP associates. The process went much more smoothly with respect to obtaining required information from the associates, only 7% of the associates' information needed clarification in order for direct deposit to properly function as opposed to 10% from last year. The remaining associates received their stipend and expense payments via checks sent in the US mail.

HSAP program participants were considered actual RDL employees, and their respective state and federal income tax and Social Security were withheld from their paychecks. By the nature of their independent research, SFRP and GSRP program participants were considered to be consultants or independent contractors. As such, SFRP and GSRP associates were responsible for their own income taxes, Social Security, and insurance.

8. CONTENTS OF THE 1997 REPORT

The complete set of reports for the 1997 SRP includes this program management report (Volume 1) augmented by fifteen volumes of final research reports by the 1997 associates, as indicated below:

1997 SRP Final Report Volume Assignments

LABORATORY	SFRP	GSRP	HSAP
Armstrong	2	7	12
Phillips	3	8	13
Rome	4	9	14
Wright	5A, 5B	10	15
AEDC, ALCs, WHMC	6	11	16

APPENDIX A -- PROGRAM STATISTICAL SUMMARY

A. Colleges/Universities Represented

Selected SFRP associates represented 169 different colleges, universities, and institutions, GSRP associates represented 95 different colleges, universities, and institutions.

B. States Represented

SFRP -Applicants came from 47 states plus Washington D.C. Selectees represent 44 states.

GSRP - Applicants came from 44 states. Selectees represent 32 states.

HSAP - Applicants came from thirteen states. Selectees represent nine states.

Total Number of Participants	
SFRP	189
GSRP	97
HSAP	140
TOTAL	426

Degrees Represented			
	SFRP	GSRP	TOTAL
Doctoral	184	0	184
Master's	2	41	43
Bachelor's	0	56	56
TOTAL	186	97	298

SFRP Academic Titles	
Assistant Professor	64
Associate Professor	70
Professor	40
Instructor	0
Chairman	1
Visiting Professor	1
Visiting Assoc. Prof.	1
Research Associate	9
TOTAL	186

Source of Learning About the SRP

Category	Applicants	Selectees
Applied/participated in prior years	28%	34%
Colleague familiar with SRP	19%	16%
Brochure mailed to institution	23%	17%
Contact with Air Force laboratory	17%	23%
IEEE Spectrum	2%	1%
BIIHE	1%	1%
Other source	10%	8%
TOTAL	100%	100%

APPENDIX B -- SRP EVALUATION RESPONSES

1. OVERVIEW

Evaluations were completed and returned to RDL by four groups at the completion of the SRP. The number of respondents in each group is shown below.

Table B-1. Total SRP Evaluations Received

Evaluation Group	Responses
SFRP & GSRPs	275
HSAPs	113
USAF Laboratory Focal Points	84
USAF Laboratory HSAP Mentors	6

All groups indicate unanimous enthusiasm for the SRP experience.

The summarized recommendations for program improvement from both associates and laboratory personnel are listed below:

A. Better preparation on the labs' part prior to associates' arrival (i.e., office space, computer assets, clearly defined scope of work).

B. Faculty Associates suggest higher stipends for SFRP associates.

C. Both HSAP Air Force laboratory mentors and associates would like the summer tour extended from the current 8 weeks to either 10 or 11 weeks; the groups state it takes 4-6 weeks just to get high school students up-to-speed on what's going on at laboratory. (Note: this same argument was used to raise the faculty and graduate student participation time a few years ago.)

2. 1997 USAF LABORATORY FOCAL POINT (LFP) EVALUATION RESPONSES

The summarized results listed below are from the 84 LFP evaluations received.

1. LFP evaluations received and associate preferences:

Table B-2. Air Force LFP Evaluation Responses (By Type)

		How Many Associates Would You Prefer To Get ?								(% Response)			
		SFRP				GSRP (w/Univ Professor)				GSRP (w/o Univ Professor)			
Lab	Evals Recv'd	0	1	2	3+	0	1	2	3+	0	1	2	3+
AEDC	0	-	-	-	-	-	-	-	-	-	-	-	-
WHMC	0	-	-	-	-	-	-	-	-	-	-	-	-
AL	7	28	28	28	14	54	14	28	0	86	0	14	0
USAFA	1	0	100	0	0	100	0	0	0	0	100	0	0
PL	25	40	40	16	4	88	12	0	0	84	12	4	0
RL	5	60	40	0	0	80	10	0	0	100	0	0	0
WL	46	30	43	20	6	78	17	4	0	93	4	2	0
Total	84	32%	50%	13%	5%	80%	11%	6%	0%	73%	23%	4%	0%

LFP Evaluation Summary. The summarized responses, by laboratory, are listed on the following page. LFPs were asked to rate the following questions on a scale from 1 (below average) to 5 (above average).

2. LFPs involved in SRP associate application evaluation process:
   a. Time available for evaluation of applications:
   b. Adequacy of applications for selection process:
3. Value of orientation trips:
4. Length of research tour:
5. a. Benefits of associate's work to laboratory:
   b. Benefits of associate's work to Air Force:
6. a. Enhancement of research qualifications for LFP and staff:
   b. Enhancement of research qualifications for SFRP associate:
   c. Enhancement of research qualifications for GSRP associate:
7. a. Enhancement of knowledge for LFP and staff:
   b. Enhancement of knowledge for SFRP associate:
   c. Enhancement of knowledge for GSRP associate:
8. Value of Air Force and university links:
9. Potential for future collaboration:
10. a. Your working relationship with SFRP:
    b. Your working relationship with GSRP:
11. Expenditure of your time worthwhile:

(Continued on next page)

12. Quality of program literature for associate:
13. a. Quality of RDL's communications with you:
    b. Quality of RDL's communications with associates:
14. Overall assessment of SRP:

Table B-3. Laboratory Focal Point Reponses to above questions

	AEDC	*AL*	*USAFA*	*PL*	*RL*	*WHMC*	*WL*
# Evals Recv'd	0	7	1	14	5	0	46
Question #							
2	-	86 %	0 %	88 %	80 %	-	85 %
2a	-	4.3	n/a	3.8	4.0	-	3.6
2b	-	4.0	n/a	3.9	4.5	-	4.1
3	-	4.5	n/a	4.3	4.3	-	3.7
4	-	4.1	4.0	4.1	4.2	-	3.9
5a	-	4.3	5.0	4.3	4.6	-	4.4
5b	-	4.5	n/a	4.2	4.6	-	4.3
6a	-	4.5	5.0	4.0	4.4	-	4.3
6b	-	4.3	n/a	4.1	5.0	-	4.4
6c	-	3.7	5.0	3.5	5.0	-	4.3
7a	-	4.7	5.0	4.0	4.4	-	4.3
7b	-	4.3	n/a	4.2	5.0	-	4.4
7c	-	4.0	5.0	3.9	5.0	-	4.3
8	-	4.6	4.0	4.5	4.6	-	4.3
9	-	4.9	5.0	4.4	4.8	-	4.2
10a	-	5.0	n/a	4.6	4.6	-	4.6
10b	-	4.7	5.0	3.9	5.0	-	4.4
11	-	4.6	5.0	4.4	4.8	-	4.4
12	-	4.0	4.0	4.0	4.2	-	3.8
13a	-	3.2	4.0	3.5	3.8	-	3.4
13b	-	3.4	4.0	3.6	4.5	-	3.6
14	-	4.4	5.0	4.4	4.8	-	4.4

3. 1997 SFRP & GSRP EVALUATION RESPONSES

The summarized results listed below are from the 257 SFRP/GSRP evaluations received.

Associates were asked to rate the following questions on a scale from 1 (below average) to 5 (above average) - by Air Force base results and over-all results of the 1997 evaluations are listed after the questions.

1. The match between the laboratories research and your field:
2. Your working relationship with your LFP:
3. Enhancement of your academic qualifications:
4. Enhancement of your research qualifications:
5. Lab readiness for you: LFP, task, plan:
6. Lab readiness for you: equipment, supplies, facilities:
7. Lab resources:
8. Lab research and administrative support:
9. Adequacy of brochure and associate handbook:
10. RDL communications with you:
11. Overall payment procedures:
12. Overall assessment of the SRP:
13. a. Would you apply again?
    b. Will you continue this or related research?
14. Was length of your tour satisfactory?
15. Percentage of associates who experienced difficulties in finding housing:
16. Where did you stay during your SRP tour?
    a. At Home:
    b. With Friend:
    c. On Local Economy:
    d. Base Quarters:
17. Value of orientation visit:
    a. Essential:
    b. Convenient:
    c. Not Worth Cost:
    d. Not Used:

SFRP and GSRP associate's responses are listed in tabular format on the following page.

Table B-4. 1997 SFRP & GSRP Associate Responses to SRP Evaluation

	Arnold	Brooks	Edwards	Eglin	Griffis	Hanscom	Kelly	Kirtland	Lackland	Robins	Tyndall	WPAFB	average
# res	6	48	6	14	31	19	3	32	1	2	10	85	257
1	4.8	4.4	4.6	4.7	4.4	4.9	4.6	4.6	5.0	5.0	4.0	4.7	4.6
2	5.0	4.6	4.1	4.9	4.7	4.7	5.0	4.7	5.0	5.0	4.6	4.8	4.7
3	4.5	4.4	4.0	4.6	4.3	4.2	4.3	4.4	5.0	5.0	4.5	4.3	4.4
4	4.3	4.5	3.8	4.6	4.4	4.4	4.3	4.6	5.0	4.0	4.4	4.5	4.5
5	4.5	4.3	3.3	4.8	4.4	4.5	4.3	4.2	5.0	5.0	3.9	4.4	4.4
6	4.3	4.3	3.7	4.7	4.4	4.5	4.0	3.8	5.0	5.0	3.8	4.2	4.2
7	4.5	4.4	4.2	4.8	4.5	4.3	4.3	4.1	5.0	5.0	4.3	4.3	4.4
8	4.5	4.6	3.0	4.9	4.4	4.3	4.3	4.5	5.0	5.0	4.7	4.5	4.5
9	4.7	4.5	4.7	4.5	4.3	4.5	4.7	4.3	5.0	5.0	4.1	4.5	4.5
10	4.2	4.4	4.7	4.4	4.1	4.1	4.0	4.2	5.0	4.5	3.6	4.4	4.3
11	3.8	4.1	4.5	4.0	3.9	4.1	4.0	4.0	3.0	4.0	3.7	4.0	4.0
12	5.7	4.7	4.3	4.9	4.5	4.9	4.7	4.6	5.0	4.5	4.6	4.5	4.6
Numbers below are percentages													
13a	83	90	83	93	87	75	100	81	100	100	100	86	87
13b	100	89	83	100	94	98	100	94	100	100	100	94	93
14	83	96	100	90	87	80	100	92	100	100	70	84	88
15	17	6	0	33	20	76	33	25	0	100	20	8	39
16a	-	26	17	9	38	23	33	4	-	-	-	30	
16b	100	33	-	40	-	8	-	-	-	-	36	2	
16c	-	41	83	40	62	69	67	96	100	100	64	68	
16d	-	-	-	-	-	-	-	-	-	-	-	0	
17a	-	33	100	17	50	14	67	39	-	50	40	31	35
17b	-	21	-	17	10	14	-	24	-	50	20	16	16
17c	-	-	-	-	10	7	-	-	-	-	-	2	3
17d	100	46	-	66	30	69	33	37	100	-	40	51	46

4. 1997 USAF LABORATORY HSAP MENTOR EVALUATION RESPONSES

Not enough evaluations received (5 total) from Mentors to do useful summary.

5. 1997 HSAP EVALUATION RESPONSES

The summarized results listed below are from the 113 HSAP evaluations received.

HSAP apprentices were asked to rate the following questions on a scale from
1 (below average) to 5 (above average)

1. Your influence on selection of topic/type of work.
2. Working relationship with mentor, other lab scientists.
3. Enhancement of your academic qualifications.
4. Technically challenging work.
5. Lab readiness for you: mentor, task, work plan, equipment.
6. Influence on your career.
7. Increased interest in math/science.
8. Lab research & administrative support.
9. Adequacy of RDL's Apprentice Handbook and administrative materials.
10. Responsiveness of RDL communications.
11. Overall payment procedures.
12. Overall assessment of SRP value to you.
13. Would you apply again next year? Yes (92 %)
14. Will you pursue future studies related to this research? Yes (68 %)
15. Was Tour length satisfactory? Yes (82 %)

	Arnold	Brooks	Edwards	Eglin	Griffiss	Hanscom	Kirtland	Tyndall	WPAFB	Totals
# resp	5	19	7	15	13	2	7	5	40	113
1	2.8	3.3	3.4	3.5	3.4	4.0	3.2	3.6	3.6	3.4
2	4.4	4.6	4.5	4.8	4.6	4.0	4.4	4.0	4.6	4.6
3	4.0	4.2	4.1	4.3	4.5	5.0	4.3	4.6	4.4	4.4
4	3.6	3.9	4.0	4.5	4.2	5.0	4.6	3.8	4.3	4.2
5	4.4	4.1	3.7	4.5	4.1	3.0	3.9	3.6	3.9	4.0
6	3.2	3.6	3.6	4.1	3.8	5.0	3.3	3.8	3.6	3.7
7	2.8	4.1	4.0	3.9	3.9	5.0	3.6	4.0	4.0	3.9
8	3.8	4.1	4.0	4.3	4.0	4.0	4.3	3.8	4.3	4.2
9	4.4	3.6	4.1	4.1	3.5	4.0	3.9	4.0	3.7	3.8
10	4.0	3.8	4.1	3.7	4.1	4.0	3.9	2.4	3.8	3.8
11	4.2	4.2	3.7	3.9	3.8	3.0	3.7	2.6	3.7	3.8
12	4.0	4.5	4.9	4.6	4.6	5.0	4.6	4.2	4.3	4.5
Numbers below are percentages										
13	60%	95%	100%	100%	85%	100%	100%	100%	90%	92%
14	20%	80%	71%	80%	54%	100%	71%	80%	65%	68%
15	100%	70%	71%	100%	100%	50%	86%	60%	80%	82%

MEDIATING EFFECT OF ONSET RATE ON THE RELATIONSHIP BETWEEN +Gz AND LBNP TOLERANCE

David A. Ludwig, Ph.D.
Associate Professor
Department of Mathematical Sciences

University of North Carolina, Greensboro
1000 Spring Garden Street
Greensboro, NC 27412-5001

Final Report for:
Summer Faculty Research Program
Armstrong Laboratory

Sponsored by:
Air Force Office of Scientific Research
Bolling Air Force Base, DC

and

Armstrong Laboratory

August 1997

MEDIATING EFFECT OF ONSET RATE ON THE RELATIONSHIP BETWEEN +Gz AND LBNP TOLERANCE

David A. Ludwig, Ph.D.
Associate Professor
Department of Mathematical Sciences
University of North Carolina, Greensboro

ABSTRACT

Research attempting to establish a relationship between human response to lower body negative pressure (LBNP) and +Gz acceleration has in general, disregarded the moderating effects of negative pressure and +Gz onset rates. Seventeen males (24-34 years) were tested in a seated LBNP chamber and received three pressure onset schedules of 0.067, 0.33, and 2.0 mmHg/s. Relaxed acceleration tolerance was assessed on a 6.1 m centrifuge using three gradual onset rates of 0.2, 0.05, and 0.01 +Gz/s. LBNP and +Gz tolerances were subjected to principle components (factor) analysis to investigate the underlying correlation structure. The factor model suggested a two dimensional solution consisting of an acceleration factor and an orthostatic factor. The general pattern of the factor loadings indicates the relationship between tolerances of the two forms of orthostatic stress (acceleration and LBNP) is a function of how fast each stress is delivered. The correlation between LBNP tolerance and acceleration tolerance increases as LBNP onset is increased, or +Gz onset is decreased. Although both LBNP and +Gz exposure can lead to eventual loss of consciousness, syncopal events associated with intolerance to either stress are a function of somewhat different cardiovascular mechanisms. There are however, specific situations where LBNP may constitute a viable substitute for +Gz.

MEDIATING EFFECT OF ONSET RATE ON THE RELATIONSHIP BETWEEN +Gz AND LBNP TOLERANCE

David A. Ludwig, Ph.D.

INTRODUCTION

Redistribution of blood from head-to-toe is a principal mechanism underlying loss of consciousness in pilots during sustained radial acceleration (+Gz) (2,3). Laboratory investigations designed to identify +Gz tolerant pilots (10), enhance +Gz tolerance through training (4), and develop +Gz countermeasures (7) have been conducted using human-rated centrifuges. However, the use of a centrifuge can prove costly in regard to required facilities and personnel. As a result, lower body negative pressure (LBNP) has been considered as a potential low-cost surrogate for +Gz since it can induce similar tachycardia, hypotension, and eventual loss of consciousness.

Based on the premise that LBNP and +Gz produce similar physiological changes, investigators have hypothesized that LBNP can be used to predict, enhance, or maintain an individual's tolerance to high levels of +Gz stress. This idea was supported by Lategola and Trent (8) who indicated that, :

> "The cost of purchasing and operating a human centrifuge is substantial. Lower body negative pressure is considered an acceptable experimental substitute for the +Gz stress of the centrifuge. This inexpensive device should provide access to seated +Gz studies by any investigator who cannot afford the cost of acquiring or operating a human centrifuge."

Despite this claim, their report did not provide any data to support this conclusion. Similarly, Verghese and Prasad (15) state, "The LBNP chamber is easy to fabricate and can be used to assess the tolerance of subjects likely to be subjected to high levels of +Gz stress." Again, no

data were available to support this opinion. Nevertheless, the idea that lower body decompression could serve as a substitute for +Gz has prompted some to speculate on experimental protocols that relate LBNP findings to high +Gz environments. Vettes et al. (16) stated, " Aeronautical medicine can also benefit from the lower body negative pressure test not only as a clinical orthostatic test but especially as a means of investigating cardiovascular adaptation capacity to the positive longitudinal accelerations known as +Gz".

The potential for using LBNP as a surrogate for centrifugation requires consideration and evaluation of several measurement aspects that can influence the appropriateness of cardiovascular comparisons between LBNP and +Gz. In contrast to a pilot's upright, seated posture, LBNP is traditionally performed in the supine position (17). This postural difference influences initial fluid distribution, especially in the baseline condition (12). In addition, progressive stepped LBNP profiles are uniquely different from the continuous elevation of +Gz stress experienced by centrifuge subjects or pilots. Finally, redistribution of fluid is distinctly different between the two stresses (13). Reduced ambient pressure below the iliac crests of the pelvis, induced by LBNP, isolates sequestration of blood to the lower abdominal region and legs, while +Gz physically pushes blood across a hydrostatic column from the head toward the feet in all organs of the body. With characteristics unique to LBNP and +Gz, it is clear that the potential to substitute +Gz acceleration with LBNP, in research or pilot training, will require the development of LBNP equipment and protocols that will more closely simulate the onset of loss of consciousness induced by +Gz.

The purpose of this study was to investigate the hypotheses that +Gz tolerance can be predicted by LBNP tolerance. To accomplish this objective, an experiment was designed to examine the correlation structure of LBNP and +Gz tolerance as a function of +Gz and LBNP onset rates.

METHODS AND MATERIALS

Subjects. Prior to testing and subject recruitment, the study protocol was reviewed and approved by the Advisory Committee on Human Experimentation at the Armstrong Laboratory, Brooks AFB. Seventeen, nonsmoking, normotensive men (volunteers), with a mean (SD) age of 24 (3) yr, mean height of 176 (6) cm, and mean weight of 79.1 (9.6) kg, gave written consent to participate in this study in accordance with AFR-169-3. Participation was contingent on a positive medical screening that constituted a detailed medical history and physical examination. All subjects were qualified centrifuge riders who were familiar with a variety of centrifuge protocols. Subjects were asked to abstain from consumption of caffeine containing beverages, alcohol, or strenuous exercise for at least 14 hours prior to testing.

Centrifuge protocol. Centrifuge testing was conducted on the 6.1 m radius centrifuge at Brooks AFB, San Antonio, TX. Subjects rode in an upright seat (13° seat-back angle) without G-suit and were instructed to remain as relaxed as possible. Electromyography (EMG) of the quadriceps and gastrocnemius muscles provided a method to monitor muscle tension and remind the subjects to remain relaxed. A standard three lead electrocardiogram (ECG) was used to monitor heart rate.

Subjects rode the centrifuge until they experienced approximately 100% peripheral or 50% central visual field lose. Although subjects terminated each run based upon a subjective evaluation of their visual field loss, an objective record was obtained by way of a subject-controlled high resolution visual field tracker (Figure 1, Panel A). This device consisted of a curvilinear array of 120 white lights located at 1° increments around a 76 cm radius. While fixing sight on a central red light, subjects "balanced" the white light on the periphery of their visual field by triggering a micro-switch on the gondola joystick. The position of the white lights was continuously recorded on a chart recorder, and following each run, was used to verify a

subjective endpoint. A more complete description of this tracking light bar is given by Gillingham and McNaughton (5). Subjects could stop the centrifuge at any time by releasing their grip on a touch-sensitive, hand-held microswitch (i.e. electronic brake activator).

G tolerance was evaluated at onset rates of 0.2 (fast), 0.05 (medium), and 0.01 (slow) +Gz/s. During a centrifuge session, each subject was tested at each onset rate. A 15-min. rest interval was used between onset rates within a centrifuge testing session. A small pilot study indicated this rest period was sufficient for the heart rate to return to baseline levels. Between tests, subjects remained seated in the centrifuge gondola and were permitted to drink water ad libitum. To decrease measurement error, and subsequently increase the reliability of the subjects +Gz tolerance at each onset rate, each subject returned for centrifuge testing on three separate days (9). A minimum of one day and a maximum of seven days were used between centrifuge testing sessions. The nine tests per subject were systematically randomized in a three-by-three Latin square (three onsets by three days) to counterbalance, within each subject, the order of onset administration. The three +Gz tolerance values at each onset were averaged and used in the statistical analysis.

Seated LBNP protocol. A seated LBNP chamber was used to test the tolerance of subjects to lower body decompression (Figure 1, Panel B). The chamber was designed so that body position was the same as that for centrifuge testing. Seatback angle was kept at 13° and legs were positioned and supported in the same manner as during centrifuge testing. To ensure subjects remained relaxed, EMG was used to monitor tension in the quadriceps and the gastrocnemius. Heart rate was monitored with a standard three-lead ECG.

It was determined from a small pilot study, that visual field loss experienced during LBNP differed from that during centrifugation. Rather than reporting a general narrowing of the visual field, subjects reported a "generalized clouding" (i.e., bleaching). For this reason, the visual

light bar was not used during LBNP testing. Subjects terminated the LBNP test when they began to experience an overall deterioration of vision which was usually accompanied by a feeling of imminent syncope. Subjects could stop the depressurization to the chamber at any time by releasing their grip on a touch-sensitive, hand-held microswitch.

Each subject was given an orientation exposure to the LBNP chamber several days prior to the beginning of testing. Subjects were tested at three pressure onset rates of -2.0 (fast), -0.3 (medium), and -0.067 (slow) mmHg/s. The testing schedule was the same as used for determining +Gz tolerance. During three separate LBNP testing sessions, each subject was tested at each pressure onset (i.e., three determinations per onset). Testing of subjects was systematically randomized in a three-by-three Latin Square (three onsets by three days) to counterbalance, within each subject, the order of pressure onset administration. This provided three determinations of LBNP tolerance per subject per pressure onset. LBNP tolerance (mm/Hg) was averaged over the three determinations and used in the statistical analysis.

Statistical analysis. The 17 subjects by six measures of tolerance (three +Gz and three LBNP) data matrix was subjected to principle component factor analysis followed by an oblique rotation (promax) of the initially extracted factors. The number of component factors was determined by the solution producing a simple structure of factor loadings with the minimum number of factors needed to account for a majority of the variance in the six tolerance measures.

With this statistical procedure, we attempted to account for total covariation among variables in fewer dimensions (factors) than defined by each of the individual measures (6 measures of tolerance). Factors emerge by forming linear combinations of the original measures in such a way as to account for as much variation in the original measures as possible. The form of each linear combination depends on the intercorrelation structure of the

original measures while the number of linear combinations depends on the underlying dimensionality. If the component variables are redundant, the intercorrelation structure can be described in fewer dimensions than that defined by the original number of measurements (i.e., six). Factor analysis attempts to define and describe this redundancy. The end result is a factor table which reflects the correlation (loading) of each of the original variables with the linear combinations. High loadings indicate that a particular variable has high representation within that linear combination. A factor is defined by the collection of variables having high loadings on that factor (i.e., a collection of redundant variables). The final factor solution describes the underlying intercorrelation pattern in the original measures. A more detailed conceptual and mathematical explanation of this technique is given by Kleinbaum and Kupper (6).

RESULTS

Evaluation of the eigenvalues from the unrotated principle components, percent of explained variance, communalities, and rotated factor loadings indicated a two factor solution was the most parsimonious statistical model. The two factor solution explained 79.5% of the total variance in the original six variables. After oblique rotation, 58% of the explained variance was accounted for by the first factor and 42% by the second factor. The inter-factor correlation was small (.15), suggesting the constructs underlying the two factors are relatively independent. All of the final communality estimates were greater than .80 except for the fast onset LBNP (.51). This indicates the variance associated with the fast onset LBNP protocol was somewhat unique and not completely accounted for within the final factor solution.

Table 1 presents the rotated factor loadings, post-rotation eigenvalues, communalities, and percent of explained variance for the two-factor solution. All of the +Gz protocols (fast, medium, and slow) had high loadings on the first factor (>.80). The fast onset LBNP protocol

had a moderate loading (.68) on the first factor, while the loadings associated with the slow and medium onset LBNP protocols were low (<.16). The slow and medium onset LBNP protocols had high loadings on the second factor (>.90). The remainder of the loadings on the second factor were low (<.15), except for a marginal loading associated with the slow onset +Gz (.33). Thus, the first factor suggests an underlying +Gz component (+Gz Factor), while the second factor suggests an underlying LBNP component (LBNP Factor).

Although the LBNP loadings on the +Gz factor are small, they increase in a linear fashion as the LBNP onset increases. This trend also occurs for the +Gz loadings on the LBNP factor. As +Gz onset rate slows, the +Gz loadings increase on the LBNP factor. The overall factor solution indicates the two tolerances have very distinct features, while the loading pattern also suggests some "common ground" between LBNP and +Gz tolerance. The factor loadings tend to converge to a common factor when +Gz onset rate and/or the LBNP onset rate are changed. When the LBNP onset rate is increased, LBNP tolerance correlates more highly with +Gz tolerance. Similarly, when +Gz onset is slowed, +Gz tolerance correlates more highly with LBNP tolerance. The fast +Gz loading on the LBNP factor and the slow LBNP loading on the +Gz factor are both negative. This suggests a divergence both between the slow LBNP protocol and +Gz tolerance, and the fast +Gz protocol and LBNP tolerance.

Zero order correlations and descriptive statistics for the +Gz and LBNP tolerances are presented in Table 2. The table is arranged to reflect the general pattern of relationships uncovered by the factor analysis. The residual correlation matrix based on the two factor solution is presented in Table 3. These data reflect how accurately the two factor solution can reproduce the original six factor correlation matrix. Larger residual values indicate relationships not compatible with the two factor solution. All of the residual values greater than .10 were associated with fast onset LBNP tolerance. The diagonal elements of the residual correlation matrix are uniqueness values. These values represent how much of the variance for a

particular variable is unique to that variable and not accounted for in the factor solution. Uniqueness values are inversely related to the communalities presented in Table 1. Fast onset LBNP tolerances had the largest uniqueness value (.49). The pattern of residual values and the uniqueness values suggest overlap of LBNP tolerance with +Gz tolerance when the LBNP onset is increased.

DISCUSSION

Is tolerance to progressive LBNP and +Gz the same thing? The results of the current investigation suggest that although LBNP and +Gz tolerance are separate, unique attributes, together they define the underlying latent component of tolerance to progressive orthostatic challenge. Just like the latent construct of general intelligence is composed of verbal and quantitative skills, LBNP and +Gz tolerance are underlying dimensions of tolerance to general orthostatic stress. Perhaps a more interesting question is, "Does changing the protocol for determining LBNP and +Gz tolerance change the composite definition of tolerance to general orthostatic stress?" In other words, "Is the determination of LBNP and +Gz tolerance method dependent?" These results suggest that this is, in fact, the case. Different protocols produce different relationships between LBNP and +Gz tolerance.

There is no doubt progressive LBNP and +Gz are two very different stresses. Positive Gz creates an active "pushing" force from head-to-toe, while LBNP creates a more passive "holding" or blood redistribution restricting force applied to the legs and lower torso. No matter what onset schedule is used, the two stresses are fundamentally different. Yet, there is surely both unique and common physiology attempting to counteract the effect of both types of stresses. The results of the current investigation suggest that when the passive nature of progressive LBNP is made to "look" more active by increasing the onset rate, and +Gz is made to look more passive by slowing the onset rate, the physiological mechanisms involved in

counteracting these stresses tends to involve more common systems. The unique physiology associated with each stress is still present, but there tends to be more "physiological overlap" when LBNP onset is increased and +Gz onset is decreased.

The results also suggest that the fastest LBNP onset rate may not have been fast enough. Although fast LBNP tolerance tended to correlate with +Gz tolerances, the factor loadings and residual matrix indicated there was a moderate amount of unique variance associated with the fast LBNP onset. During early testing of the LBNP chamber, we experimented with faster LBNP onsets, including a very rapid lower body decompression protocol (0 to -200 mmHg in 5.5 s). Although this protocol was discontinued due to concerns for the welfare and safety of the subjects, it is interesting to note that experienced centrifuge riders remarked how similar it felt to rapid onset centrifuge testing. Furthermore, subjects tested using this rapid decompression protocol experienced petechiae on the legs. Despite the very fast decompression, subjects tolerated the -200 mmHg high pressure plateau for as long as 20 s before experiencing presyncopal symptoms. This is in contrast to near instantaneous greyout during rapid onset +Gz. Also, as previously mentioned (see LBNP methods), presyncopal visual symptoms tended to be different across the two stresses. The time course of presyncopal events during exposure to LBNP and +Gz suggests very different orthostatic challenges.

Can LBNP be used as a substitute for radial acceleration? There are both unique and common physiological systems associated with LBNP and +Gz stress (14). While the physiological effects of slow onset (<.02 G/s) low level (<.3Gz) centrifugation may be adequately simulated with seated LBNP protocols (11), LBNP simulation of rapid onset +Gz does not seem appropriate or practical. Even when LBNP is used to simulating slow onset, low level centrifugation, there is no hydrostatic gradient against arterial pressure between the trunk and head. How LBNP is applied also needs to be considered. The current findings suggest

traditional slow onset pressure protocols do not stimulate physiological systems common to both LBNP and +Gz. LBNP and +Gz tolerances do not correlate unless lower body decompression is delivered at a relatively fast rate. Therefore, LBNP should be considered an incomplete substitute for +Gz.

There may be some situations in which LBNP might be used as a model for centrifugation. For example, Baldin et al. (1) used LBNP to examine cerebral artery blood flow following presyncopal LBNP. The hemodynamics associated with post decompression might be similar to those associated with post, unprotected, centrifugation (I.e., afterload physiology). It would therefore seem reasonable that the time course of cerebral blood flow after LBNP would be similar to that observed after centrifugation.

The decompression speed needed to accurately simulate the physiological effects of high +Gz (i.e., operational levels) or estimate individual +Gz tolerance, seems to be beyond sensible safety guidelines. However, LBNP might be used in conjunction with flight simulation (i.e. flying and tracking tasks) to provide a more realistic flight simulator experience (i.e., feel) Integrating LBNP into a flight simulator would require pilots to attenuate to the problem of G induced loss of consciousness (GLOC) while continuing to track targets and fly the simulator. Although LBNP simulated G stress would not be as high as that experienced in the more advanced fighters, it would provide an important stimulus currently ignored during cognitive flight simulation. Since task management is perhaps the most important aspect of flying today's high performance aircraft, it is important that flight simulation provide as many tasks as possible that pilots will be required to manage during actual flight.

REFERENCES

1. Balldin UI, Krock LP, Hopper NL, Squires WG. Cerebral artery blood flow velocity changes following rapid release of lower body negative pressure. Aviat. Space Environ. Med. 1996; 67:19-22.

2. Burton RR, Leverett SD, Jr, Michaelson ED. Man at high sustained +Gz acceleration: a review. Aerospace Med. 1974; 45:115-36.

3. Burton RR, Whinnery JE. Operational G-induced loss of consciousness: something old something new. Aviat. Space Environ. Med. 1985; 56:812-7.

4. Gillingham KK, Fosdick JP. High-G training for fighter aircrew. Aviat. Space Environ. Med. 1988; 59:12-9.

5. Gillingham KK, McNaughton GB. Visual field contraction during G stress at 13° 45° and 65° seatback angles. Aviat. Space Environ. Med. 1977; 48:91-6.

6. Kleinbaum DG, Kupper LL. Applied regression analysis and other multivariable methods. Boston: Duxbury, 1978; 376-405.

7. Krutz RW, Burton RR. The effect of uniform body pressurization on +Gz tolerance and protection. In: Preprints of the 1974 Annual Scientific Meeting. Alexandria, VA: Aerospace Med. Assoc. 62-4, 1974.

8. Lategola MT, Trent CC. Lower body negative pressure box for +Gz simulation in the upright seated position. Aviat. Space Environ. Med. 1979, 50:1182-4.

9. Ludwig DA, Krock LP. Errors in measurement of +Gz acceleration tolerance. Aviat. Space Environ. Med. 1991; 62:261-5.

10. Parkhurst MJ, Leverett SD, Shubrooks SJ. Human tolerance to high sustained +Gz acceleration. Aerospace Med. 1972; 43:708-12.

11. Polese A, Sandler H, Montgomery LD. Hemodynamic responses to seated and supine lower body negative pressure: comparison with +Gz acceleration. Aviat. Space Environ. Med. 1992; 63:467-75.

12. Rowell LB. Human cardiovascular control. New York: Oxford University Press, 1993; 137-53.

13. Self DA, White CD, Shaffstall RM, et al. Differences between syncope resulting from rapid onset acceleration and orthostatic stress. Aviat. Space Environ. Med. 1996; 67:547-54.

14. Suvorov PM, Voloshin VG, D'yachenko LN, Krivets VF. Investigation of hemodynamics with exposure to decompression and acceleration. Kosmicheskaya Biolgiya i Meditsina. 1972; 6(3):59-64.

15. Verghese CA, Prasad, ASK. Lower body negative pressure system for simulation of +Gz-induced physiological strain. Aviat. Space Environ. Med. 1993, 64:165-9.

16. Vettes B, Vieillefond H. Value of the lower body negative pressure test in aerospace medicine. Neuilly-sur-Seine, France: NATO Advisory Group for Aerospace Research and Development, 1983; AGARDograph No. 277E:189-92.

17. Wolthuis RA, Bergman SA, Nicogossian AE. Physiological effects of locally applied reduced pressure in man. Physiol. Rev. 1974; 54:566-95.

TABLE 1

ROTATED FACTOR SOLUTION (PROMAX) FOR
+Gz AND LBNP PROTOCOLS

	FACTOR		
Variable	I	II	Communality
Gz (Fast)	**.87**	-.35	.81
Gz (Med.)	**.94**	.01	.90
Gz (Slow)	**.80**	.33	.86
LBNP (Fast)	**.68**	.11	.51
LBNP (Med.)	.16	**.92**	.93
LBNP (Slow)	-.13	**.95**	.90
Eigenvalue	2.78	1.99	
% Variance	46.33	33.17	
Cum. % Var.	46.33	79.50	

Note: Factor loadings are adjusted for the inter-correlation of the factors (.15). Only unique variance explained by each factor is reflected in the loadings.

TABLE 2

CORRELATION MATRIX OF +Gz (g) AND LBNP (mmHg) TOLERANCES

	Gz (Fast)	Gz (Med.)	Gz (Slow)	LBNP (Fast)	LBNP (Med.)	LBNP (Slow)
Gz (Fast)	1.0	.77	.54	.40	-.05	-.23
Gz (Med.)		1.0	.86	.54	.25	.07
Gz (Slow)			1.0	.52	.53	.32
LBNP (Fast)				1.0	.37	.00
LBNP (Med.)					1.0	.83
LBNP(Slow)						1.0
MEAN (n=17)	5.0	4.6	4.1	233.5	113.2	66.1
S.D.	1.0	0.7	0.6	27.4	17.8	13.6

TABLE 3

RESIDUAL CORRELATION MATRIX OF +Gz (g) AND LBNP (mmHg) TOLERANCES

	Gz (Fast)	Gz (Med.)	Gz (Slow)	LBNP (Fast)	LBNP (Med.)	LBNP (Slow)
Gz (Fast)	.19	-.02	-.06	**-.15**	.02	.09
Gz (Med.)		.09	.03	**-.14**	-.05	.04
Gz (Slow)			.14	**-.13**	-.04	-.02
LBNP (Fast)				.49	.05	**-.12**
LBNP (Med.)					.07	-.05
LBNP(Slow)						.09

Note: Diagonal elements are uniqueness values.

FIGURE 1

A

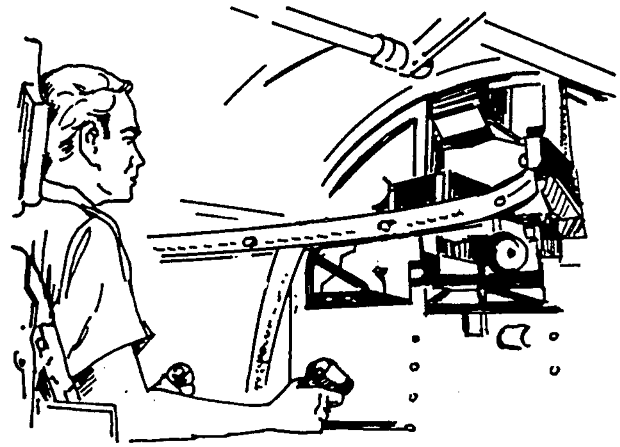

B

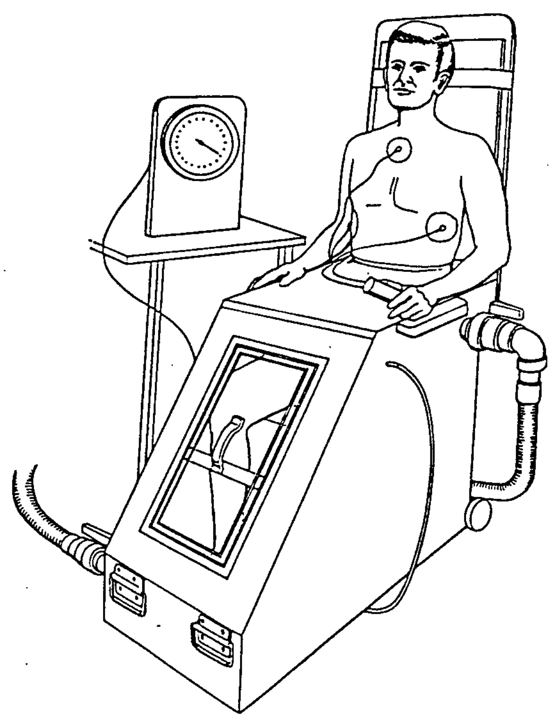

THE EFFECTS OF TASK STRUCTURE ON COGNITIVE ORGANIZING PRINCIPLES IMPLICATIONS FOR COMPLEX DISPLAY DESIGN PRACTICES

Robert P. Mahan
Associate Professor
Department of Psychology

The University of Georgia
Athens, Georgia 30602

Final Report for:
Summer Research Program
Armstrong Laboratory

Sponsored by:
Air Force Office of Scientific Research
Bolling Air Force Base, Washington, DC

And

Armstrong Laboratory

September 1997

THE EFFECTS OF TASK STRUCTURE ON COGNITIVE ORGANIZING PRINCIPLES: IMPLICATIONS FOR COMPLEX DISPLAY DESIGN PRACTICES

Robert P. Mahan
Associate Professor

Philip Dunwoody
Department of Psychology
University of Georgia

Abstract

The exponential growth of automated systems is generating demands for sophisticated display design protocols. In general, cognitive engineering practices provide display design solutions that enhance the operator's ability to manage and control complex systems. However, they often do so without adequate modeling of the cognitive system requirements for this process. In effect, while the task and display properties are well defined, the cognitive system of the user remains covert and hidden from the modeling process. This report illustrates that different cognitive organizing principles are induced by different task representations. Further, performance is dependent on the congruent mapping between task, display, and cognitive organizing principle of the operator. By externalizing the organizational principle used by an operator in a given task context, in theory one can develop representations and displays that are congruent with task and cognitive system.

THE EFFECTS OF TASK STRUCTURE ON COGNITIVE ORGANIZING PRINCIPLES: IMPLICATIONS FOR COMPLEX DISPLAY DESIGN PRACTICES

Robert P. Mahan and Philip Dunwoody

Introduction

The prospect of operators needing to manage greater amounts of data and information in real-time technology-based systems is continuing to drive innovative research and development strategies for creating efficient information representation protocols. However, while there is valuable work being conducted in developing theoretical frameworks for rationally guiding the design of decision support systems aimed at information rich work environments, current design strategies tend to remain haphazard and largely technology driven in nature. Innovation in sensor technology and advances in computer graphics are providing new ways to capture and represent heretofore unmeasured and unseen system data. The emergence of powerful and relatively inexpensive realtime processing capabilities (e.g., desktop SGI) is making it particularly important to understand the cognitive dynamics associated with technology based systems. For example, graphical information displays are now commonly used to encode multidimensional data structures by exploiting various perceptual organizing principles such as color, size, visual angle, depth, orientation and others (see Wickens and Carswell, 1995 for review). Future efforts will most certainly have operators working within reality systems using 3-D perspective, information flow fields and other perceptual-based features (Schiflett, 1997).

Yet, despite advances in system technology, it remains relatively unclear how features of complex systems influence the properties of the cognitive system in the user. For example, much of the display engineering research has focused on specific details of the task-display properties. These details have been well defined and rendered explicit in numerous display engineering efforts. Wickens and Andre (1990) present a compelling framework for engineering design based on a proximity compatibility relationship where spatial properties of the task are mapped to an interface in an effort to activate particular perceptual mechanisms in the operator. In the use of object-like configural displays, performance has been viewed as a category matching process where operators identify values in system parameters that are compared with learned system category states, or

internal model defining category membership (see Wickens, 1995; Coury et al, 1989; Bennett and Flach, 1992).

However, the properties of the internal mental models that are central features to the representation compatibility arguments have tended to remain relatively covert and hidden from the modeling process. The internalized state of the cognitive system and the fact that it is not expressed in a manner that explicates its properties limits engineering solutions because operational outcomes are a joint product of the task-display-cognitive system, where it only the task-display system that is fully understood. In effect, we still know little about the information organization principles and their relationship to information representation protocols beyond the consensus that display representations should match in some way the mental models of the users.

In an effort to generate a theoretical framework that helps externalize the cognitive system of a decision maker and thereby explicate hidden details of the task-cognition system boundary, Hammond (1980, 1990; Hammond et al, 1987) focused on the nature of information organizing principles activated by the properties of the task. The cognitive continuum theory (CCT) specifically predicts properties of the mental model of the users when engaged specific task domains. The adaptable theory asserts that task properties induce particular information organizing principles in operators that range between analytical noncompensatory models to intuitive compensatory models. A fundamental substantive contribution made by the cognitive continuum theory lies in the notion that cognitive efficiency, and thus performance, is in part, a function of the **congruence** between the properties of the task and the cognitive organizing principles employed by the decision maker . The theory essentially describes a system of two continuua- one associated with the task, and the other associated with the cognitive disposition of the individual. Oversimplifying the theory (see Hammond, 1981; Hammond et al., 1987), the assertion is that various properties of the task "**induce** " a particular mode of cognition lying somewhere between the analytical and intuitive poles on the cognitive continuum. For example, a simple, highly structured deterministic task (e.g., simple mental arithmetic) is likely to induce a mode of cognition (i.e., organizing principle) at the analytical end of the continuum. Here, the psychological/behavioral consequences of such an organizing principle is that a very proceduralized set of operations are executed, at a somewhat methodical pace with a relatively high degree of accuracy, where the subject is highly aware of the organizing principle. In contrast, a

complex, ill-structured and ambiguous task is likely to induce a mode of cognition in the person that is closer to the intuitive end of the continuum. The intuitive cognitive mode would tend to be associated with a holistic organizing principle, executed quickly and with lower overall accuracy when compared to some normative standard, and where the subject would manifest less awareness of the actual organizing principle being used in performance. In effect, the closer the congruence between the properties of the task and the model of the cognitive system given the structure of the task, the more efficient cognition is likely to be. Thus, for example, an individual utilizing analytical skills to solve a very complex ill-defined problem (and vice versa) will likely display incongruence between the organizing principle that is analytic in this case, and the properties of the task, which call for a very different organizing principle that is intuitive in nature. This incongruence will ultimately lead to inefficient cognition.

The congruence construct has emerged out of the correspondence metatheoretical orientation of Popper's three world view (1963, 1972), and has been viewed as important for successful performance by a number of researchers. For example, Hockey, (1983) refers to the matching of cognitive resources with resource demands of the task in his variable activation state theory on stress. Wickens and Andre (1990) argue the construct of proximity compatibility as the relational match between the spatial properties of the task and those of representations and displays. Tversky and Kahneman (1983) describe conditions that induce particular cognitive activities in their tests of the conjunction rule. Simon (1978, 1990) discusses how the concept of rationality must be modified in order to include intuitive elements that are compatible with an uncertain world. In these and other cases, the premise, either implicitly or explicitly stated, is that cognition must match particular features of the task.

The present study examined the congruence concept using a threat identification task where task complexity and representational format were manipulated. The hypotheses tested were guided by the nature of task induced cognitive properties defined within the framework of the cognitive continuum theory congruence principle (see table 1). In general it was hypothesized that a low complexity task structure would be best served by a numeric representational format because this task/format combination would induce a congruent analytically-based organizing principle. The simplicity of the task, its limited dimensional nature, and its objective indexing of system

parameters (i.e., numerically represented) would facilitate a computational (analytical) response to task characteristics (see Hammond, 1980, 1987). Analytical cognition is demarcated by a variety of unique properties such as, sequential cue use, slow information processing, low confidence in outcomes and high confidence in process, few but large errors, high consistency, and task specific organizing principle to name a few.

In contrast, a complex task structure would favor an iconic graphic format, which would induce an intuitive-based organizing principle geared to information complexity. Here, complexity, both in number of dimensions as well as their intercorrelated statistical nature is viewed as resource intensive characteristic that has been shown an important catalyst in the induction of intuitive organizing principles (Hammond, et al., 1987; Hammond, 1990, 1996). Intuitive cognition is highlighted by a rapid form of information processing, simultaneous cue usage, high confidence in outcomes and low confidence in process, normal error distribution, inconsistent cue usage, perceptual based cue evaluation as well as others.

Method

Participants

Participants were thirty undergraduate psychology students selected from the University of Georgia Research Participant Pool or which 40 percent were female. The mean age of the participants was 23.5, SD = 2.5 ranging from 20 to 26. Participants were provided course credit for complete participation in the study. Monetary incentives were also provided to the participants with the top three performers in the study receiving $50.00, $30.00, and $20.00 for 1st, 2nd, and 3rd, respectively.

Task Overview

Research participants worked on a threat identification simulation that was adapted from the Team Interactive Decision Exercise for Teams Incorporating Distributed Expertise (TIDE2) (see Hollenbeck et al, 1995) and modified to allow numeric and iconic protocols necessary for study, as well a provide a specific single user interface.

The software was programed to simulate a threat identification exercise where participants were presented with a number of attribute values on an object and asked to render a judgment on the status of the object based on the integration of the attribute information. Participants were taught how to weigh and integrate the attribute information in producing judgments of object state

(discussed below).

The simulation is configurable and can be programed to represent a number of task domains. However, in this study the simulation was programed to represent a naval command threat assessment scenario similar to the TIDE^2 task used by Hollenbeck et al (1995). The participants were assigned the role of a aircraft carrier commander whose goal was to protect the ship from hostile airborne enemy by patrolling the airspace surrounding the carrier. In this role, the commander had access to a variety to tactical assets that provided him/her with information concerning objects appearing in the airspace. The task was to evaluate the information on a object on the basis of attributed values such as, air speed, size, direction, angle and render a judgment as to the appropriate response to make toward that object. Judgments were rendered on a 7-point scale that varied in the intensity of the military response directed toward the object from <u>ignore</u> (the most benign response) to <u>defend</u> (destroy the target). Intermediate values of intensity or aggressiveness were also available, and included (2) review, (3) monitor, (4) warn, (5) ready, and (6) lock-on (see Hollenbeck et al, 1995 for review).

<u>Participant Instruction</u>. Participants were instructed on how to perform the task. First, the participants were given a very detailed verbal description of the threat assessment exercise they would be performing during the experiment. They were informed that the task was a simulation of a military command and control judgment task in which their responsibility was to patrol the air space around a carrier. Participants were instructed to rate how threatening the approaching aircraft was on a scale from one to seven based on the information provided. Each attribute was described in detail by the experimenter. For example, in the numeric display condition participants were informed that aircraft speed was represented in mph and that 100-300mph was a slow speed, 301-550mph was average speed, and 551-800mph was a fast speed. In the iconic display condition, participants were informed that aircraft speed was represented by an arrow projecting from the aircraft. A short arrow length indicated the aircraft was moving at a slow speed (100-300mph), a medium arrow length indicated the aircraft was moving at an average speed (301-550mph), and a long arrow length indicated the aircraft was moving at a fast speed (551-800mph). All attributes were described in this manner and participants were given a list of the attributes and their description that they could refer to throughout the task. After the attributes were described participants were given a description of the possible judgment values and an explanation of the

feedback screen. At this point participants were informed that because this was a performance oriented study, monetary awards would be given for the top three performers. Participants were encouraged to ask questions throughout this period. After questions were answered the task was started and participants were asked to confirm that they understood the presentation of all attributes, their judgment options, and the feedback screen. This confirmation was given by participants within the first eight trials and no further questions were permitted.

Research Design. Two levels of analysis were performed on the data in test of the congruence principle. The first was an ideographic evaluation that examined each participant's judgment protocol for reliability, as well as its fit within the hypothetical framework advanced in the study. The ideographic evaluation is part and parcel of the adaptive perspective used here where (1) judgment behavior is viewed as being mediated by a unique correspondence between the judge and the ecology in which he/she is embedded, and (2) as a result of this unique and personal correspondence, an evaluation of the reliability of the judges relationship within this ecology is tantamount to a test of the adaptive character of this relationship (see Hammond, McClelland, and Mumpower, 1980 for review).

The second level of analysis was nomothetic in nature where a 2 X3X 2 mixed analysis of variance design was used to evaluate the within factors experience and representational format manipulation which were crossed with the between factor task complexity manipulation.

Independent Variables. Three independent variables: Experience, Display, and Task Complexity were used. Experience was a three level within factors variable that provided the study with three epochs of judgments to examine. Similarly, two levels of the within subject factor representational format (Display) were used (n = 30). The first level presented the object attribute information to the participants in a numeric tabular form. Figure # shows an example of the numeric display. The information on target objects was present simultaneously on the screen in both display conditions. The second display format presented the information to the participants in a iconic graphic manner where object attribute information sources were configured as separate graphical icons, with the exception of the altitude indicator which remained numeric in nature.

Subjects were randomly assigned to each of two levels of the between subjects factor task complexity (n=15). Complexity was defined as the amount of information necessary to make judgments of target threat. In the low complexity condition participants were taught to use a

decision rule that contained <u>six</u> attribute information values of which only <u>four</u> were known to the participants. In order to simulate components of a probabilistic decision task, two attributes were not visible to the participants. The invisible attributes created a barrier to perfect learning as well as perfect performance since the outcome information from each judgment was based on the entire criterion model (i.e., six information sources). The high complexity condition required participants to weigh and integrate nine information sources of which only seven were visible.

<u>Low Complexity Criterion</u>

$$\underline{\mathbf{Y}_{\mathbf{low}}} = (.201)X1 + (.177)X2 + (.265)X3 + (.303)X4 + \underbrace{\mathbf{(.181)X5 + (.308)X6}}_{\text{Mystery Values}} \quad (1.0)$$

<u>High Complexity Criterion</u>

$$\underline{\mathbf{Y}_{\mathbf{high}}} = (.210)X1 + (.042)X2 + (.256)X3 + (-.027)X4 + \underbrace{\mathbf{(.191)X5 + (.398)X6}}_{\text{Mystery Values}} + (.124)X7 + (.411)X8 + (.110)X9 \quad (2.0)$$

Threat attribute values were defined as follows: X1 = speed, X2 = size, X3 = Direction, X4 = Range, X5 = Radar Type, X6 = Altitude, X7 = IFF, X8 = Corridor Status, X9 = Angle of Target Vector.

<u>Performance Measures</u>. A lens model analysis of judgment task performance was conducted. The lens model can be mathematically characterized by defining the relationship among the components of the model and judgment task performance. Tucker (1964) described it as follows:

$$r_a = GR_sR_e + C[(1 - R_s^2)(1 - R_e^2)]^{.5} \quad (3.0)$$

The correlational performance an individual achieves (i.e., achievement index) r_a, is a function of four distinct components: the linear multiple correlation between the cue values and the criterion, R_e, (environmental predictability), which indexes the uppermost predictability of the judgment task; the linear multiple correlation between the cue values and an individual's judgments of the criterion, R_s, (consistency index), which represents the ability of the subjects to control the execution of their knowledge regarding the judgment task; the extent to which the linear model of the individual judge correlates with the linear model of the criterion, G, (matching index), which measures overall task knowledge; and the extent to which the nonlinear residual variance in the model of the individual correlates with the nonlinear residual variance in the model of the criterion, designated C. Nonlinear or configural variance was negligible in this study, so the C index was not included in the analysis.

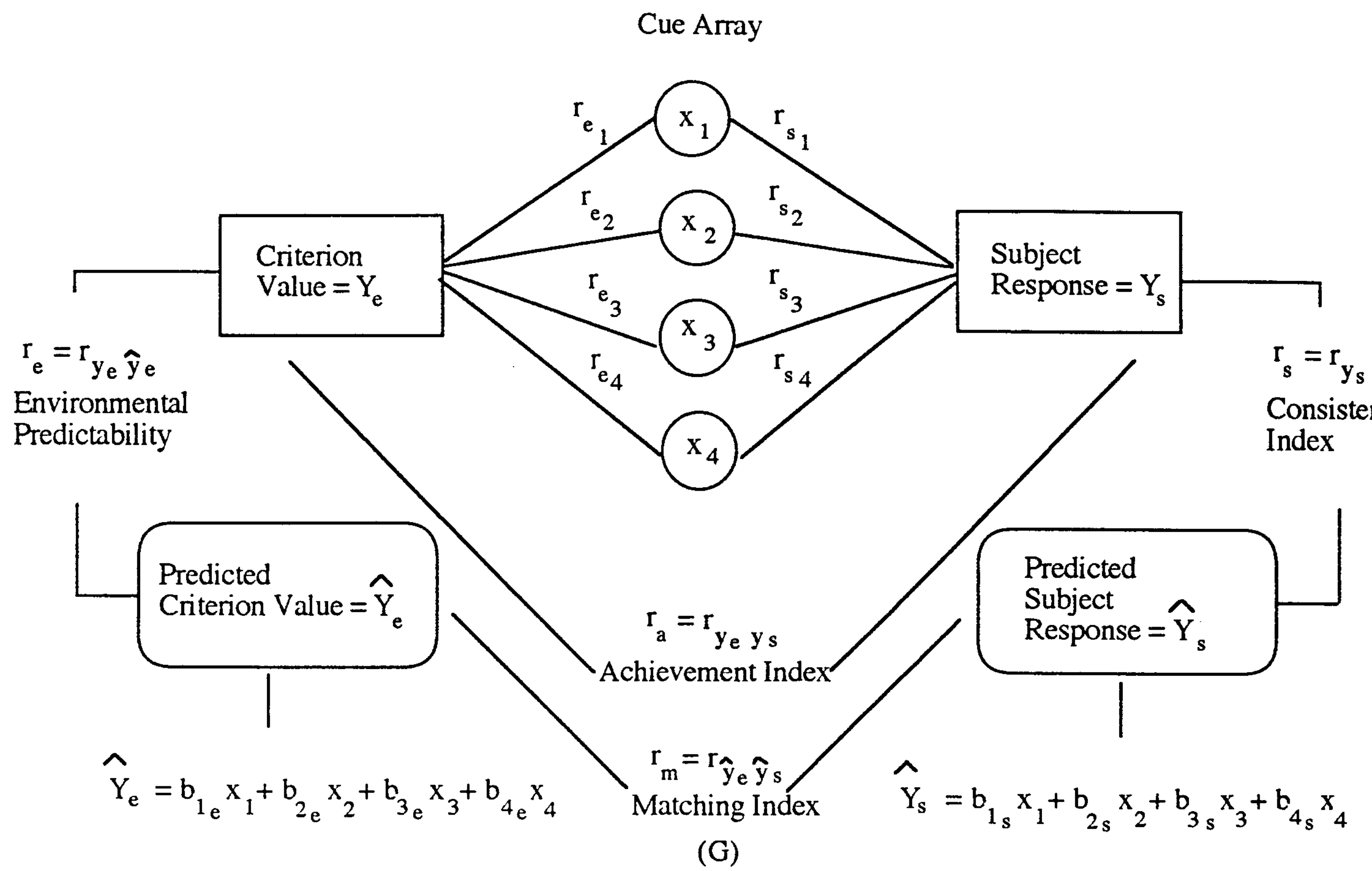

Figure 2. Formal Model of Expert Judge and Environment Interaction (From Mahan, 1992a).

Achievement (r_a) provided an index of over-all judgment accuracy. In addition, several measures that identified the mode of cognition were used. Kurtosis in the Mean Difference scores between judgment of threat identification and criterion values was used as a method to quantify error distributions for participants. A measure of implicitness toward the policy used to weight and integrate target attribute values was also computed. Here, the measure was conceived as the absolute difference between participants' subjective relative weights of attribute information and that of the least square solution of their respective policies converted to relative weights. The subjective relative eights were defined at the conclusion of the experiment where participants were asked to distribute 100 points over the attribute set in a manner that reflected the diagnostic value of each attribute in participants' judgments (Cook and Stewart, 1975). The relative weight transformation applied to the least squares policy solution was generated in a manner that allowed direct comparisons between subjective relative weights and the least squares Beta weights in the policies for each participant. The relative weighting procedure used here is a common method employed to circumvent many of the problems associated with the use of standardized regression coefficients to reflect cue importance (Anderson, 1974; Cooksey, 1996). The Beta weights in each participant's policy is divided by the Sum of the policy Beta weights to generate a set of relative weights. Implicitness then is defined as the absolute difference between the least squares policy and subjective estimates. The assertion taken was the greater the difference, the more implicit the policy.

$$rw_{\beta i} = \frac{|\beta i|}{\sum_{i=1}^{k} |\beta i|} \tag{4.0}$$

Finally, a confidence assessment was solicited from the subjects that quantified the level of belief that their subjective weights did indeed correspond to the least squares regression of judgments on target attribute arrays, or the way in which they were in reality using the information. This measure provided some insight on the knowledge over the method used to weigh the attribute information in judgments of target threat.

Procedure. Once participants were taught to perform the simulation, the study commenced. The participants performed 99 trials in each of two display formats. The formats were counterbalanced across the 30 participants. Fifteen of the participants performed the Low complexity task while fifteen performed the High complexity task. Once subjects had performed the simulation, they were debriefed. The debriefing included measuring subjective relative weights, as well as confidence rating on the subjective weights.

Results

Ideographic Descriptive Assessment

Participants were first evaluated on a case by case basis in order to determine the correspondence between outcomes and hypotheses of performance at the level of the individual. This approach is consistent with Brunswikian efforts to verify the stability (reliability) of individual indices of performance prior to nomothetic evaluations (see Hammond, et al, 1980; Cooksey, 1996).

Table 1 displays the descriptive results of the interactions between format and complexity manipulations. The focus within this table is the proportion of subjects that fall consistent with the hypotheses concerning congruence between task and display format. Five of the six outcome cells were identified as representing support for the congruence principle. The hypothesis that the numeric format should be associated with higher levels of achievement, consistency, and matching under low complexity conditions appeared supported for consistency with strong support given for matching outcomes. However, the achievement results failed to produce the correct directional outcome. Similarly, the hypothesis that the visual format would be superior at supporting higher levels of performance under the high complexity condition appeared supportive with positive outcomes for all three performance indices.

Table 1. Proportion of Participants Meeting Hypothetical Predictions for Congruence.

	LOW COMPLEXITY	**HIGH COMPLEXITY**
	Numeric > Visual	Numeric < Visual
Achievement (r_a)	*2/13*	**13/17**
		Numeric > Visual
Consistency (R_s)	**8/13**	**10/17**
		Numeric < Visual
Matching (G)	**12/13**	**11/17**

Nomothetic Evaluations

Factorial 2 X 2 mixed univariate ANOVA was used to evaluate average performance indices as

well as indices of cognitive mode. A univariate approach was taken in order to maximize the clarity with which the manipulations could be understood on the conceptually independent lens model indices. Table 2 displays the results of the factorial evaluation for the lens model performance indices which include power estimation values.

Table 2. Mixed Task X (Format X Subjects) Anova Table on Averaged Fisher Z Transformed Lens Model Performance Indices

Performance Index	SS	DF	MS	F	Sig	Power
Achievement (r_a)						
Within + Residual	3.67	28	.13			
Task	.19	1	.19	1.43	.242	.209
Within + Residual	1.58	28	.06			
Format	.4	1	.4	7.02	.013**	.723
Task X Format	.09	1	.09	1.67	.207	.238
Consistency (R_s)						
Within + Residual	1.57	28	.06			
Task	.03	1	.03	< 1	.49	.113
Within + Residual	.96	28	.03			
Format	.01	1	.01	< 1	.608	.057
Task X Format	.01	1	.01	< 1	.554	.066
Matching (G)						
Within + Residual	5.17	28	.18			
Task	1.5	1	1.5	8.12	.008***	.784
Within + Residual	2.52	28	.09			
Format	.65	1	.65	7.28	.012**	.738
Task X Format	1.35	1	1.35	15.03	.001***	.962

The factorial results of the Lens Model analysis demonstrated that the primary effects found in the study were associated with the achievement (ra) and matching (G) indices. Consistency (Rs) values did not produce statistically significant outcomes. Matching (G) appeared the most robust outcome with statistically significant outcomes associated with main and interaction effects. Finally, power estimates revealed that the significant outcomes were associated with adequate power values of .7 and above while the nonsignificant effects were associated with much lower power values.

Mode of Cognition

The mode of cognitive activity which in this study was used to provide evidence for a particular cognitive system state was evaluated using the same mixed factorial design that was used for the

performance indices. Table 3 displays the results of the factorial analysis.

Table 3. Mixed Task X (Format X Subjects) Anova Table on Cognitive Mode Values

Cognitive Mode Index	SS	DF	MS	F	Sig	Power
Kurtosis of Error						
Within + Residual	11.69	27	.43			
Task	.06	1	.06	< 1	.716	.055
Within + Residual	12.36	27	.46			
Format	4.4	1	4.4	9.62	.004***	.847
Task X Format	1.13	1	1.13	2.46	1.28	.328
Implicitness						
Within + Residual	.77	26	.03			
Task	.83	1	.83	27.87	.000***	.999
Within + Residual	.27	26	.01			
Format	.1	1	.1	9.26	.005***	.832
Task X Format	.02	1	.02	2.07	.162	.283
Confidence						
Within + Residual	49.64	26	1.91			
Task	.12	1	.12	< 1	.804	.049
Within + Residual	23.08	26	.89			
Format	1.75	1	1.75	1.97	.172	.272
Task X Format	.68	1	.68	< 1	.389	.160

The results of the Mode analysis shows that both Kurtosis and implicitness values demonstrated statistically significant outcomes, while the confidence values failed to achieve significant outcomes. In addition, the power values appear to indicate that significant outcomes were again associated with adequate power values, while the nonsignificant outcomes were limited to, in some cases, extremely small values.

Discussion

The accurate assessment by human operators in the state of complex multidimensional systems has been directly linked to the manner in which the information about the systems is packaged and represented (Carswell and Wickens, 1987; Woods, Wise, and Hanes, 1981; Casey, 1986; Wickens and Carswell, 1995). Iconic and object oriented graphic displays appear to be a especially useful in tasks requiring information integration, particularly when the indicators of a

system are intercorrelated (Goldsmith and Schvanevedlt, 1981; Bennet and Flach, 1992; Wickens and Carswell, 1995). In contrast to correlated system dimension, systems that can be decomposed into orthogonal information dimension are thought to be better served by representations that maintain the uniqueness of the information sources through separable data displays (Goldsmith and Schvanevedlt, 1981; Coury, Boulette, and Smith, 1989; Wickens, 1986).

The aim of testing the cognitive continuum congruence construct emerges from the observation that despite advances in engineering and applied cognitive science solutions to difficult human computer interaction problems, the cognitive system of the operator often remains covert and hidden from the modeling process. This study demonstrates, in part, that (1) the idea for congruence between cognitive organizing principles and representation formats has potential in defining many of the heretofore unmeasured details of the task-cognition interaction, and (2) the congruence principle, through lens model functionalism, provides a possible means to explicate and externalize important features of cognitive system of a user.

In the present study the tasks used were differentiated by both the number of parameters and the number of significant intercorrelations among cues. The results provide some solid support for the congruence principle hypothesized to account for the effects of task and format configurations on the state of the cognitive system. The low complexity (simple) task appeared best served by a numeric display format which induced a congruent analytically anchored organizing principle in the operators. In contrast, a complex task appeared best served by an iconic display that induced a congruent organizing principle that tended to be more intuitively anchored in nature. The support generated in favor of the congruence principle is particularly interesting considering the effects have most likely been underestimated due to the constraints on methodological power.

The CCT postulates that an analytical mode of information processing is typically induced by a number of task properties including the number of cues, and the presence of the intercorrelations among cues. The low complexity criterion rule in equation 1.0 shows that decision makers were shown only four cues. Cues five and six were hidden from participants and thus called mystery cues. The mystery cues provided an element of uncertainty to the task by concealing a source of variation from participants that outcome feedback was not able to reveal. The uncertainty

component was viewed as important feature in representing an operational threat assessment task where some information is likely to be absence and not available to the operators. Thus, participants could only generate perfect augments of threat by chance alone. However, since the task required parsing only four cues and since the four cues had very low intercorrelations, an organizing principle that favored analytical decomposition of cue information by the participants would be induced by the task (Hammond, 1996).

While, the achievement (ra) values were not supported by the hypothesis that the numeric display would be superior to iconic with only 2 of 13 participants generating higher ra values under numeric condition, both consistency and matching indices did point in the hypothesized direction. The interpretation given for the achievement values, which is a measure of overall performance, suggests that the iconic display of information best supported overall performance on the low complexity task.

In contrast, consistency (Rs), which is a measure of the control each decision maker exerted over the execution of his/her decision knowledge, was highest for the majority of participants with 8 of 13 generating the largest index values using the numeric display (Table 2). The interpretation here is that the numeric display helped provide a means to consistently integrate the cue information over judgments of the threat criterion. The implication of analytical decomposition of information is that a specific rule (i.e., organizing principle) can be more easily applied to the data by the subjects in an explicit manner. Further, since the rule tends to be explicit, in part, because one is able to decompose the problem into orthogonal components, the rule is more easily applied the same way judgment after judgment (see Cooksey, 1996; Hammond, 1996; Mahan, 1994; Simon, 1983). Thus, the reliability of the decision maker's execution of judgment policy information remains high.

Similarly, the matching index values were highest for the 12 of 13 participants using the numeric display under low complexity conditions. The matching index is considered a knowledge index in the sense that in order for this index to be high, a decision maker must maintain the diagnostic rank order value of the cues that is in the model of the criterion. Thus, if a decision maker maintains this monotonic rank ordering during decision activities, he/she will generate high matching values, which is what was found for the numeric display of information. The interpretation given this finding is that the numeric display assisted participants in parsing the

decision problem into four relatively orthogonal pieces that helped participants explicitly understand through feedback the weights that should be applied to each cue value.

The iconic display in the low complexity case is less effective at supporting the decision makers ability to parse individual information components because of the fact the cue values are encoded as a perceptual feature of an object (see Wickens and Carswell, 1995 for review). Thus, the iconic display did not allow for mode of cognition that reflected the analytical decomposition of cue information.

In contrast to the low complexity task outcomes, the high complexity task presented the decision makers with a greater number of information cues that were moderately intercorrelated. Equation 2.0 shows that decision makers were exposed to a nine cue criterion rule which included a single inverted cue (negative b weight), and with the same mystery cues that were present in the low complexity criterion. Thus, the decision makers saw seven cues in the high complexity condition.

The iconic display presented cues as objects where cue values were encoded as perceptual features such as veridical size of aircraft, the perceptual distance between an aircraft and the aircraft carrier, the size of air corridor, and others. Here, the decision makers were required to perceptually measure the cue values which assisted in inducing an intuitive response to the decision problem which matched the task complexity features. Table 2 shows that the majority (13 or 17) of decision makers generated the highest achievement values using the iconic display. Thus, overall performance was best in the high complexity- iconic display combination condition for most participants.

It was also expected that the numeric display would indeed generate the highest consistency values (Rs). Here the numeric display presents decision makers with an artificially decomposed decision problem. That is, the decision problem appears as an analytic problem where an explicit analytic organizing principle can be reliably executed across judgments. However, in this case, an analytic strategy does not account for task properties such as intercorrelated cues, thus the organizing principle is incorrect. This is shown in the lower overall achievement values associated with the numeric display. While the judgments of threat are executed more reliability (consistently) with the numeric display, they are consistently <u>wrong</u>.

<u>Nomothetic Evaluations</u>

The factorial outcomes mirrored, in part, the ideographic descriptive evaluations above. A limiting constraint on the factorial analyses was the low statistical power particularly associated with interaction effects, which were integral to testing task-display hypotheses concerning cognitive state.

Average achievement on the threat identification simulation was superior for the iconic display regardless of the complexity of the task, and thus did not support the congruence principle. However, a likely reason for the failure of the congruence principle to account for achievement is the fact that the two tasks were probably not all that different. That is, while the tasks were configured to represent positions relatively close to the poles of the task continuum, in reality it is likely they were both located midway on the continuum.

The implication is that both tasks tended to induce quasi-rational processing because both tasks were located at a midpoint on the task continuum. Since both tasks required decision makers to effectively deal with uncertainty and cue intercorrelations, the icon display was superior. The absence of differences in average consistency index values, and the fact that they remained high across formats testifies to the fact that analytical elements in the organizing principles in both tasks were present. Here, one predicts that an analytical organizing principle will tend to be executed consistently because of the explicit nature of the rule being applied to the information. The fact that both task-display configurations represented the information cues as separate and distinct components of the decision problem may have led to the decision problem being partially organized as an analytical rule.

The judgment matching index has been viewed as reflecting the subject's understanding of the properties underlying accurate task performance (Hammond & Summer, 1972; Hammond et al., 1977; Hammond, McClelland & Mumpower, 1980; Brehmer & Joyce, 1988). The matching index measures the extent to which subjects can distinguish among the cues on the basis of their diagnostic value in predicting the criterion variable. The significant interaction between task and display (Table 3, Figure 4) showed that the numeric display appeared to best match the low complexity task while the iconic display best matched the high complexity task. Here, it was evident that task understanding was a function of the congruence between task, display, and information organizing principle.

The factorial results of the implicitness (self awareness) measure mirrored the performance profile

for task knowledge (Matching), and helped validate the organizing principle used by decision makers. Figure 5 shows that the level of implicitness was dependent on the task-display condition combination where the complex task generated the highest values when iconically represented and the low complexity task the smallest value when numerically displayed. These results suggest that during conditions where the depth properties of the task were complex and the surface properties were iconically displayed, the organizing principle became more implicit and less subject to conscious awareness by decision makers. In contrast, when the depth character of the task was simple (low complexity) and the surface character was defined by a numeric display, low implicitness scores were recorded. Thus, the organizing principle used under the low complexity-numeric display condition combination tended to be explicit, and consistent with a formulaic analytical response by decision makers to the threat identification task.

The error distribution found in the study, in part, supported the predictions made by the congruence principle. CCT asserts that the the application of a explicit analytical logic-based, highly retraceable organizing principle produces consistent decision behavior. Thus, identical information sources produce identical decisions and decision behavior. Hammond (1996, 1986) notes that this type of coherence-based decision behavior has a propensity for small error. That is, on average, people are able to execute the analytical formula precisely over and over (but see Klinemunz, 1985). However, when there is a error (a mistake in a parameter within the formula) a very large error results. Thus, when executing analytical organizing principles the prediction for a leptokurtic error distribution results.

In contrast to the behavior manifest from an analytical organizing principle, an intuitive principle tends to be more dynamic in nature. That is, the absence of a formula to use on the information means that the implicitly organized rule will undergo changes from decision to decision, which reflects the absence in control over the organizing principle (low consistency). However, this behavior will be manifest as oscillations around some central decision response. That is, the slight changes in the principle from decision to decision will create small deviations around a mean decision point. This produces a platokurtic error distribution that tends to be very peaked with small tails unlike the analytical counterpart (flat with large tails).

Summary

In many display engineering research efforts the cognitive system of the decision makers remains a mystery and covert in nature. Thus, establishing theoretical frameworks that postulate performance constructs based on matching, compatibility, and or congruence between task and display systems are difficult to achieve. Explicating and measuring properties of the cognitive system in the user will assist with theoretical efforts designed to improves and support performance in complex systems. Understanding how particular properties of the cognitive system are changed in response to changes in the depth and surface features of a task should provide information on more efficient system design techniques.

The present study in part validates the congruence principle elaborated in the CCT that the cognitive system must be congruent with the task and display systems being used. While, the study suffered from limited statistical power, the results nevertheless suggest that the congruence principle may be useful in producing coherent display design principles, and thus should undergo continued research.

REFERENCES

Anderson, N. H. (1974). Information integration theory: A brief survey. In D. Krantz, R. C. Atkinson, R. D. Luce, & P. Suppes (Eds.), Contemporary developments in mathematical psychology, (Vol. 2, pp. 237-305). San Francisco: W. H. Freeman.

Bennet, B. B., & Flach, J. M. (1992). Graphical displays: Implications for divided attention, focused attention, and problem solving. *Human Factors, 34*(5), 513-533.

Brehmer, B., & Joyce, C. R. B. (1988). Human judgment: the SJT view. Amsterdam; Oxford: North Holland.

Carswell, C. M., & Wickens, C. D. (1987). Information integration and the object display: An integration of task demands and display superiority. *Ergonomics, 30,* 511-527.

Casey, E. J., & Wickens, C. D. (1986). Visual display representation of multidimensional systems (Tech Report CPL-86-2/MDA903-83-K-0255): University of Illinois Cognitive Psychology Lab.

Cook, R. L., & Stewart, T. R. (1975). A comparison of seven methods for obtaining subjective descriptions of judgmental policy. *Organizational Behavior and Human Performance, 13,* 31-45.

Cooksey, R. W. (1996). Judgment analysis: Theory, methods, and applications. San Diego, CA: Academic Press.

PRELIMINARY REPORT ON THE EFFECTS OF VARIETIES OF FEEDBACK TRAINING ON SINGLE TARGET TIME-TO-CONTACT JUDGMENTS

Philip H. Marshall

Professor

Department of Psychology

Texas Tech University

Lubbock, TX 79409

Final Report for:

Summer Faculty Research Program

Armstrong Laboratory

Sponsored by:

Air Force Office of Scientific Research

Bolling Air Force Base, DC

and

Armstrong Laboratory

August 1997

PRELIMINARY REPORT ON THE EFFECTS OF VARIETIES OF FEEDBACK TRAINING ON SINGLE TARGET TIME-TO-CONTACT JUDGMENTS

Philip H. Marshall
Professor
Department of Psychology
Texas Tech University

Abstract

This preliminary study examined the effectiveness of various forms of information feedback training on single target time-to-contact judgments. Following a baseline testing condition, 80 participants were divided into four groups for additional trials that included one of four feedback conditions: no feedback, verbal only, visual only, or both verbal and visual. After filler task activities involving verbal and mathematics skills, a retest was conducted with non-feedback trials. The results indicated that informative feedback conditions resulted in improved performance compared to the no feedback condition, and that, in general, moderate performance gains persisted until retest. It is suggested that there be further research in the development and evaluation of more effective training methods for time-to-contact and related dynamic vision and timing skills in a context that allows for repeated training and assessment trials.

PRELIMINARY REPORT ON THE EFFECTS OF VARIETIES OF FEEDBACK TRAINING ON SINGLE TARGET TIME-TO-CONTACT JUDGMENT

Philip H. Marshall

Introduction

For some time there has been a research interest in the ability of human observers to make time-to-contact (TTC) judgments. In one version of this task, an observer watches a target traveling horizontally (at constant velocity) along a path for several seconds before that target disappears. The object is to predict (usually by pressing a button) when the target would reach a predetermined end point or finish line. Researchers have suggested this ability to be solely a function of information from the optic array (Lee, 1976; Tresilian, 1991), while others have suggested the involvement of various cognitive processes and mechanism such as memory, imagery, and internal clocks (see Tresilian, 1995). There has also been limited research on the effects of non-target stimuli on performance during the TTC task (Marshall & Dunlap, 1996), with the result that TTC performance, while remaining noticeably less than ideal, is not affected adversely by a variety of non-target characteristics such as their number, direction and speed of movement. There also is some evidence for beneficial strategic cognitive processing occurring during TTC tasks (Marshall & Dunlap, 1996; Fischer, Hickey, Pellegrino, & Law, 1994).

One of the most problematical results from the TTC literature is the inefficiency with which participants perform this task. Performance is often characterized by increasing underestimation of TTC (responding earlier than the target would have made contact) as actual TTC increases, and by increased variability at longer actual TTCs (Schiff & Detwiler, 1979; Caird & Hancock, 1991). Considering an operational time interval of from 0- up to 10-sec, a common phenomenon is the increasing underestimation of TTC as actual TTC increases. Hypothetical data shown in Figure 1 are typical of the usual result. An actual TTC of 8-sec can be underestimated by as much as 2-sec (or 25%), a considerable amount of time given the extremely fast closure speeds found in many of the situations where TTC performance accuracy is essential, and where an error could be very costly. Given this poor performance, the immediate objectives of the present research were to determine if TTC performance could be improved with practice, to determine if some conditions of

practice would be more beneficial, and to determine the short-term retention characteristics of such training. If training does improve performance, the long-term objective of this research is to develop a training program for sustained improvement of TTC accuracy.

Within the context of a relative prediction motion task, Fischer, Hickey, Pelligrino and Law (1994) have shown that for certain conditions practice with a variety of types of feedback can improve performance on a relative arrival time task where subjects have to predict which of two targets will arrive first at a target. Further, the effects of practice with feedback were found to be stable, lasting for at least one day. Their results, however, suggest that conscious strategies, and the conditions under which they prove successful, override or mitigate the effectiveness of feedback and improvement on this task. That is, in their study feedback improved performance only when there were no other ways (i.e., "heuristic strategies") for subjects to predict arrival time.

Marshall and Dunlap (1996) have argued that the more complex the TTC task (i.e., anything more than a single target moving in the display) the more likely that any one of a number of cognitive strategies can be used by the subject who approaches the task as a problem to be solved. The Fischer et al. (1994) study involved a relatively complex TTC task, and showed that conscious heuristic strategies can in fact play an important role in the presumed efficacy of practice. Therefore, in the present research a simpler TTC task was used to provide a replication of Fischer et al. (1994) in a situation less likely to foster the development of such strategies, and hence more likely to provide direct access to fundamental TTC capabilities.

Methodology

Design. The design of this study followed the sequence of baseline, practice, interpolated filler activity, and finally, retest. All participants performed in a baseline phase during which their base TTC performance efficiency could be determined. This was followed by one of four types of interpolated feedback practice conditions: no feedback, just visual, just verbal, and both visual and verbal. Changes in performance during these periods were determined by dividing each segment into three blocks of trials. Finally, after some time had passed doing irrelevant interpolated activity, participants performed a retest on the original baseline task with no feedback. The following questions were considered: What are the effects (e.g., improvement) of different forms of response

feedback on TTC performance within the feedback practice session? Do these effects persist over a reasonable length of time?

Participants. The participants in this study were 80, male, Air Force basic military recruits. All participants were right handed, and had normal or corrected to normal vision.

Materials and equipment: The participants viewed a series of visual presentations on a computer monitor (15 inch), and made TTC decisions by depressing a key on a computer mouse. What might have been seen on a typical trial is presented in the top panel of Figure 2. Upon an initiation of a trial, a triangular target, initially resting against a vertical line, moved for 2-sec. from left to right at a constant velocity, and then disappeared. The participant pressed the mouse button when the target, now invisible but presumably continuing to travel, reached the finish line, the right hand vertical line. All trials had the same appearance, and the same positioning of the finish line, but the starting location, the remaining travel time (TTC), and the velocities varied. There were ten different TTCs, the travel duration remaining after the target disappeared, and they were 2-, 3-, 4.5-, 6-, 7.5-, and 9-sec. There were 15 different lengths of paths, each with a different velocity, for each of the six TTC durations (see Table 1).

During the practice (second) portion of the study, and depending on to which condition a participant had been assigned, a different message appeared on screen after the participant responded. The bottom panel of Figure 2 shows the possibilities for the three types of feedback screens: just the written message, just the visual target marker display, or both of these two. In the no feedback condition the screen informed the participant to "wait." Before this second phase the participants in the positive feedback conditions were informed to use the feedback to help them improve their performance, while the participants in the no feedback condition were simply told that there would be a brief pause to help them get ready for the next trial.

Procedure. On each of the two days of data collection participants were randomly assigned to a feedback condition upon arrival at the laboratory which contained 40 computer test stations for their use. The assignment of participants to conditions resulted in somewhat unequal numbers, with 20 participants in the no,and both verbal and visual feedback conditions, 22 in the verbal only, and 18 in the visual only feedback conditions. After viewing brief instructions that described the task, and after performing several task familiarization trials, the baseline task began. The

sequence of baseline trials was randomly determined for each participant, with the restriction that within each 30 trials there were five trials for each of the six TTC values. Therefore, the distribution of overall travel lengths (and associated velocities) varied for each participant. Trials within the baseline condition proceeded with minimal time between trials. A trial was concluded immediately upon the pressing of the mouse button, whereupon the scene for the next trial appeared without delay. Upon the presentation of the scene for the next trial the participant pressed the spacebar to initiate that trial (i.e., the target started to move). Finally, there was a one-minute rest break following trials 30 and 60.

The training sessions followed immediately after the baseline trials. Table 2 gives the instructions the participants received. In the no feedback condition, to compensate for the time that the feedback groups were allowed to see and understand their feedback, after the participant pressed the mouse button on each trial there was a pause of 3-sec. before the scene for the next trial appeared on the screen.

In the verbal only condition after the participant pressed the button on each trial there was a statement centered above the display appeared for 3-sec. stating, for example, *Too early (or too late) 1.15 sec.*. See Figure 2 for a sample. Also, in this condition, and in the verbal and visual feedback conditions, a button press within +/- 5 pixels of the finish line resulted in the verbal display saying "*On time!!*" Although this was a sort of verbal feedback for all participants, it did not indicate amount of error. Since the role of feedback is to change or improve performance, this message was not considered to be informative about how the participant might improve performance on the next trial.

In the visual only condition after the participant pressed the button on each trial a target shape appeared for 3-sec. at the location where the press had occurred relative to the actual TTC (see Figure 2).

In the condition wherein both verbal and visual feedback occurred after the participant pressed the button on each trial, both the written message and the target marker display were presented for 4-sec. (see Figure 2)

There were 90, newly randomized feedback/training trials divided into three blocks according to the same randomization requirements and scene specifications used during the

baseline condition.

Following the training session there was a break of approximately 47-min. from this task while the subjects performed on an unrelated test battery consisting of verbal and mathematical abilities tests. The average time spent performing these filler tasks was about 47-min. After performing this battery of filler tasks there was a retest which consisted of a replication of the baseline conditions, presented with a new random order of the 90 trials.

Results

There were three basic questions posed concerning this research. Was the performance of the participants in each of the four feedback groups relatively equivalent during baseline performance, as one would expect from the randomized assignment to those subsequently experienced conditions? Was there a difference in the immediate effectiveness of the four feedback conditions? Was there any positive lasting effect of any of the feedback conditions?

An analysis of variance was conducted to answer these questions, and the data entered for each participant per condition were the mean TTC judgments collapsed over the five trials for each TTC in each of the three blocks of each testing segment (baseline, training, retest). One would expect that the four groups would have similar performance during the baseline segment, that the effectiveness of the feedback conditions during training might show some immediate differences, and that there might be lingering effects due to training at retesting.

An initial analysis of variance showed that the four feedback groups did not differ during the baseline segments ($p > .13$). To examine the effects of feedback training, the major analysis of variance had the four feedback conditions as a between-subjects variable, and segments (baseline, training, retest), blocks, and TTC as within-subjects variables. There were significant main effects for segments and TTC ($p < .0001$), and for the interaction of those two factors with training condition, F (30, 760)=2.55, $p < .001$. The data from that interaction are shown in Figure 3 which also shows the ideal performance level that could have been achieved. It can be seen that TTC performance for all feedback conditions, except that involving no feedback, improved during the training phase, but that performance deteriorated during the retest phase.

A follow up analysis of variance on performance during just the training phase yielded a

significant effect for the interaction between feedback conditions and TTC, $\underline{F}$ (15, 380)=6.58, $\underline{p}$ < .0001. That effect is shown in Figure 4, and it can be seen that all three informative feedback conditions yielded comparable levels of improved performance during training, and all were more effective than the no feedback condition. The no feedback condition does, however, evidence some improvement during the training segment, at least for intermediate durations of TTC. A possible explanation for that is some form of "Hawthorne" effect since in order to explain the 3-sec. delay between trials participants in the no feedback group were told that the pause might help them get ready ("prep") for the next trial. One might speculate that this instruction was sufficiently motivational to raise performance levels over the just completed 90 trials of baseline

Conclusions

In general, the results of Fischer et al. (1994) were replicated and extended to the single target case. The varieties of informative feedback that were used can improve performance on a TTC task, and no form of that feedback was particularly superior to any other. The gains approached, but did not reach, ideal performance, and one may wonder if there are other training conditions that could improve performance beyond the observed levels. Also, the gains in performance observed during the limited training session diminished by retesting. It is possible that the combined effects of the durations of baseline (about 20-min.), training (about 20-min.), and filler activities (about 47-min.) fatigued the participants to the point of lowering motivational and performance levels, so it is unclear from this study just to what extent and for how long the benefits of practice can be sustained. The participants were not able to rest or to be excused from the experimental session for any prolonged period of time, nor was it possible to recall the participants at a later date for a follow up evaluation. Nonetheless, the results are promising. Further research needs to be conducted to establish the optimum training conditions for TTC skills. It is important that such research be conducted in a situation that allows for extensive training beyond the limited number of trials possible in the experimental context of this study so that there can be a determination of just how much improvement is possible. It is also crucial that future research be conducted in a context that allows for repeated assessment of the permanence of any improvements. It would also be desirable to assess the robustness of any transfer of improved

TTC skills to novel task situations under a variety of conditions that may include the presence of stressors. Further, TTC abilities may be related to several other fundamental cognitive processes involved in dynamic visual processing and timing performance. This study offers the promise that those skills also may be conducive to training protocols. Conceivably, one could develop a training battery that encompassed a number of these skills, and that could be used from time to time to maintain these abilities at high levels.

References

Caird, J.K., & Hancock, P.A. (1994). The perception of arrival time for different oncoming vehicles at an intersection. Ecological Psychology, 6, 83-109.

Fischer, S.C., Hickey, D.T., Pellegrino, J.W., & Law, D.J (1994). Strategic processing in dynamic spatial reasoning tasks. Learning and Individual Differences, 6, 65-105.

Lee, D.N. (1976). A theory of visual control of braking based on information about time-to-collision. Perception, 5, 437-459.

Marshall, P.H., & Dunlap, R.D., (1996, unpublished report). Time-to-contact judgments in the presence of static and dynamic objects: A preliminary report. Armstrong Laboratory, Brooks Air Force Base, San Antonio, TX, August.

Schiff, W. & Detwiler, M.L. (1979). Information used in judging impending collision. Perception, 8, 647-656.

Tresilian, J.R. (1991). Empirical and theoretical issues in the perception of time to contact. Journal of Experimental Psychology: Human Perception and Performance, 17, 865-876.

Tresilian, J.R. (1995). Perceptual and cognitive processes in time-to-contact estimation. Analysis of prediction motion and relative judgment tasks. Perception and Psychophysics, 57, 231-245.

Acknowledgements

I would like to thank Dr. William Tirre of Armstrong Laboratory, Brooks Air Force Base, San Antonio, Texas for encouraging and facilitating all aspects of this project, and Ms. Karen Raouf whose programming expertise was essential for the efficient and speedy implementation of this study. Comments may be sent by email to *p.h.marshall@ttu.edu.*

Table 1

The Target Velocities (pixels/sec) for Fifteen Lengths (distances traveled) at Each TTC

Total Distance Traveled (pixels)	TTC (sec.) 2.0	3.0	4.5	6	7.5	9.0
257	64.25	51.4	39.54	32.13	27.05	23.36
270	67.50	54.00	41.54	33.75	28.42	24.55
283	70.75	56.60	43.54	35.38	29.79	25.73
296	74.00	59.20	45.54	37.00	31.16	26.91
309	77.25	61.80	47.54	38.63	32.53	28.09
322	80.50	64.40	49.54	40.25	33.89	29.27
335	83.75	67.00	51.54	41.88	35.26	30.45
348	87.00	69.60	53.54	43.50	36.63	31.64
361	90.25	72.20	55.54	45.13	38.00	32.82
374	93.50	74.80	57.54	46.75	39.37	34.00
387	96.75	77.40	59.54	48.38	40.74	35.18
400	100.00	80.00	61.54	50.00	42.11	36.36
413	103.25	82.60	63.54	68.83	43.47	37.54
426	106.5	8520	65.54	53.25	44.84	38.73
439	109.75	87.80	67.54	54.88	46.21	39.91

Table 2

Instructions Given at the Beginning of the Feedback Training Segment for Each Condition

All groups received:

"This task will be the same as the one you just took."

Then, depending on condition, participants saw:

None	The difference is that you will have a prep time before each trial that may help to improve your accuracy.
Verbal	The difference is that you will be told how close to the line you were. Use this information to improve your accuracy.
Visual	The difference is that you will be shown how close to the line you were. Use this information to improve your accuracy.
Verbal and Visual	The difference is that you will be told and shown how close to the line you were. Use this information to improve your accuracy.

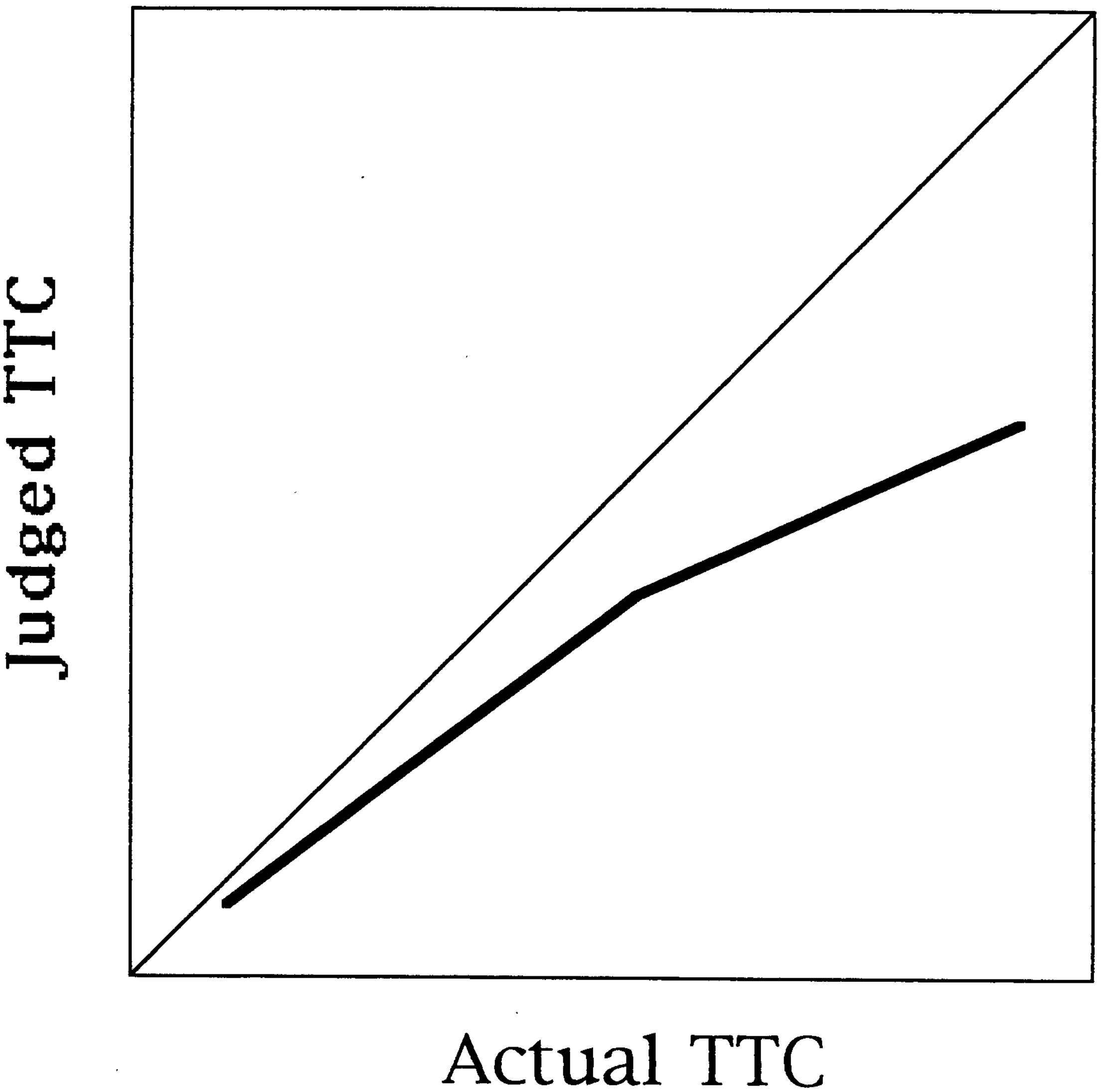

Figure 1. Typically, performance falls off of the diagonal, indicating increasingly less accurate TTC judgments for longer actual TTCs.

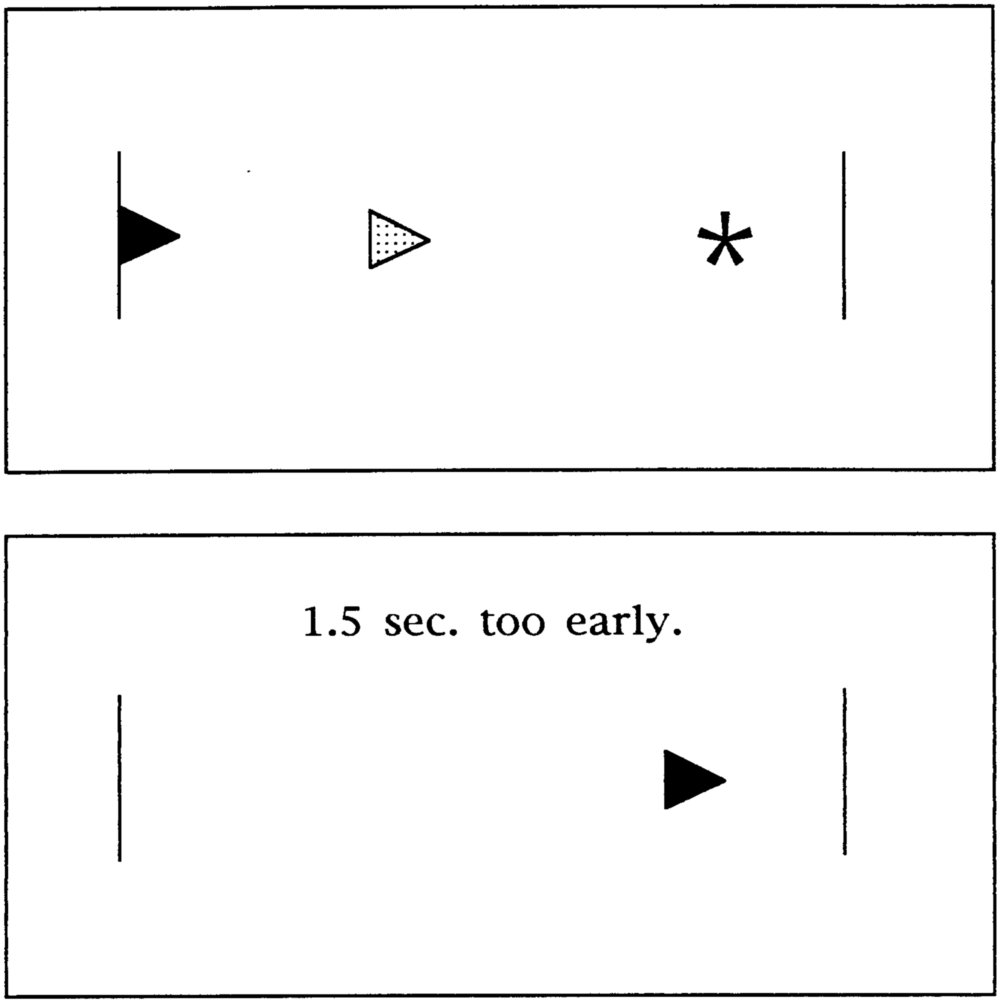

Figure 2. The top panel depicts the sequence of events on any given trial. The target starts to move, disappears, then the participant responds.

The bottom panel depicts both verbal and visual feedback for that trial. The leading point of the target marker indicates the button press. Other conditions of feedback varied accordingly: none, just the verbal message, or just the visual response marker.

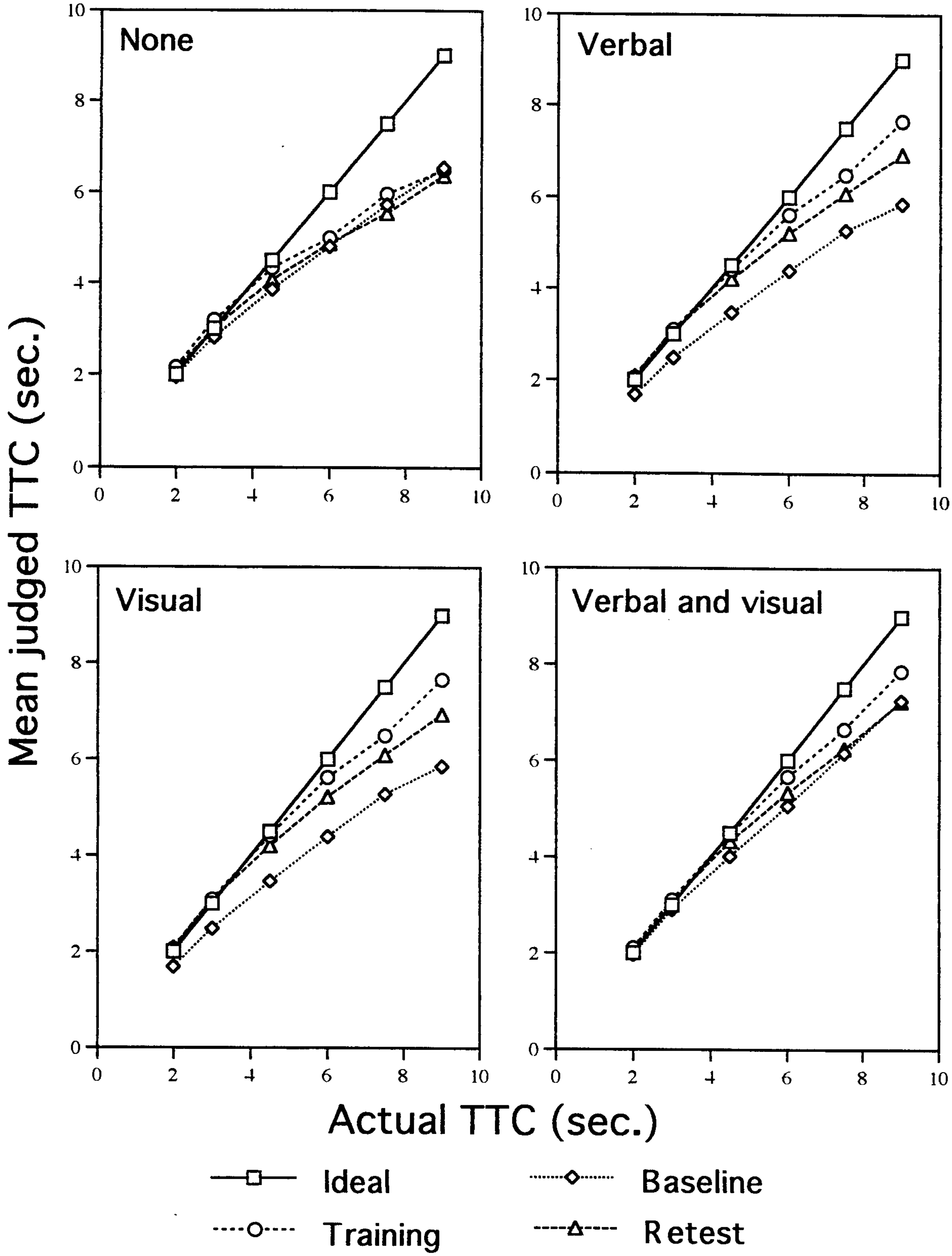

Figure 3. TTC performance for each training condition during baseline, training and retest.

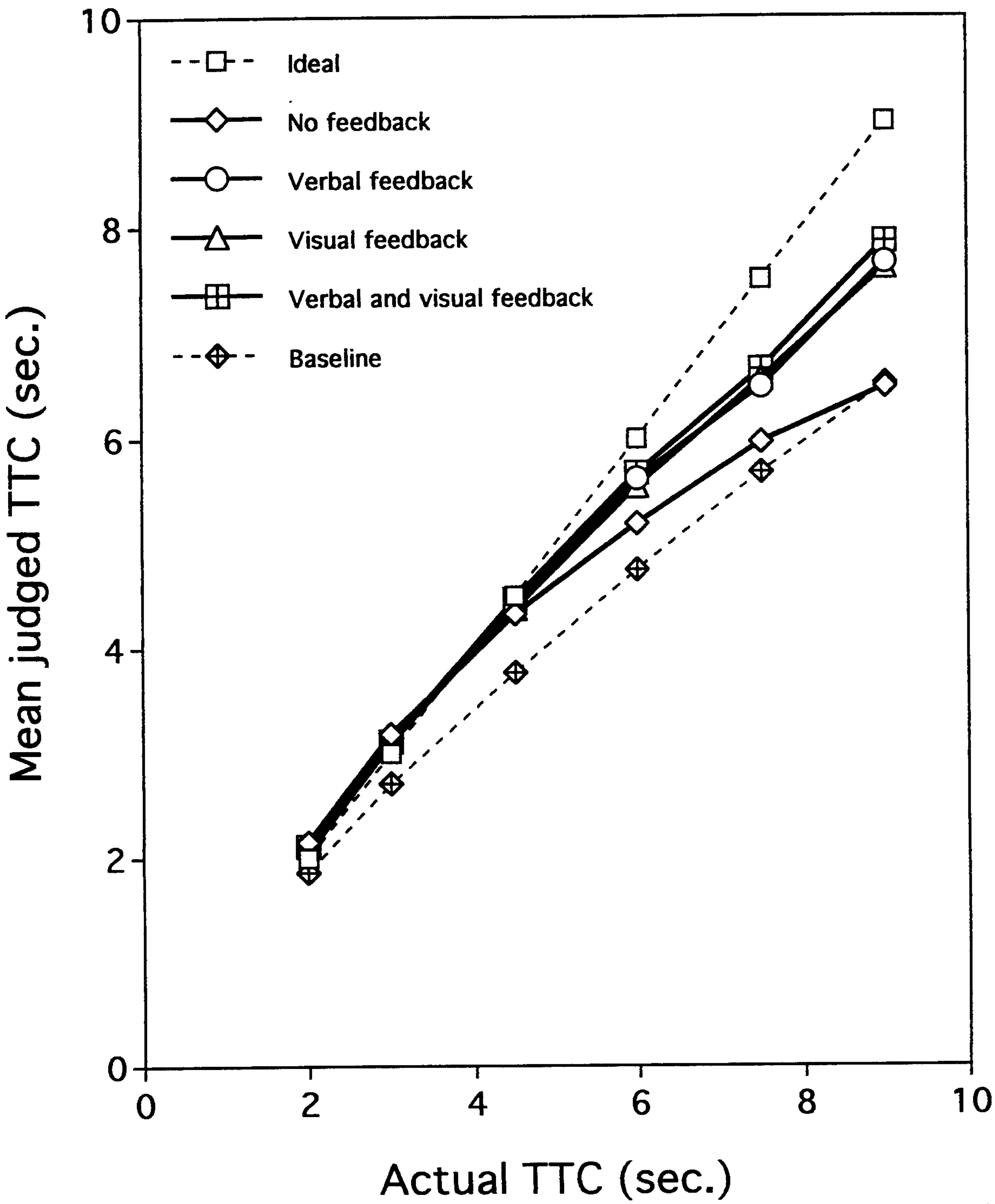

Figure 4. Mean judged TTC during training as a function of feedback condition. Also shown are mean performance during baseline and ideal performance.

Bruce Mutter's report was not available at the time of publication.

THE DETECTION OF COLOR BREAKUP IN FIELD SEQUENTIAL COLOR DISPLAYS

Allen L. Nagy
Professor
Psychology Department

Wright State University
Psychology Department
Fawcett Hall
Dayton, OH 45435

Final Report for:
Summer Faculty Research Program
Armstrong Laboratory

Sponsored by:
Air Force Office of Scientific Research
Bolling Air Force Base, DC

and

Armstrong Laboratory

August, 1997

THE DETECTION OF COLOR BREAKUP IN FIELD SEQUENTIAL COLOR DISPLAYS

Allen L. Nagy
Professor
Psychology Department
Wright State University

Abstract

Field-sequential color displays are of interest because of the need for small, high resolution color displays. Under many conditions, these displays suffer from the drawback that color breakup is perceived when the eyes are moved, a stimulus on the display is moved, or the display moves. Experiments were performed to determine thresholds for color breakup as a function of observer adaptation level, stimulus contrast, and the retinal velocity of the stimulus. The data were used to develop a model based on the spatial and temporal properties of the color coding mechanisms in the human visual system. The purpose was to develop a model that could be used to predict the detectability of color breakup in sequential color displays under a wide variety of viewing conditions.

THE DETECTION OF COLOR BREAKUP IN FIELD SEQUENTIAL COLOR DISPLAYS

Allen L. Nagy

INTRODUCTION

Helmet mounted displays (HMD) require high spatial resolution in order to convey an adequate amount of information. Recent advances in display technology have resulted in the development of small, full color, high resolution liquid crystal displays (LCD). Typically, such a display uses three chromatic filters which filter the emitted light. The three filters are typically chosen to maximize the color gamut of the display. Because of the qualities mentioned above, such a display is an ideal candidate for HMDs: small, light weight, and full color. Unfortunately, because a head-mounted display is usually viewed under high magnification, the spatial resolution is still not as high as desired in such displays.

Resolution is limited because of the very nature of a conventional color display. A conventional color display is composed of individual pixels, each of which contains three spatially separated components that are typically red, green, or blue. Because the visual system integrates information over space, the individual components in each pixel are not visible when the display is viewed from a sufficient distance and the appearance of each pixel is determined by the sum of the components. A whole gamut of colors can be produced in each pixel by varying the relative intensities of the three components in each pixel. Therefore, in a conventional three primary color display, a third of the total number of pixel components convey the red information, a third the green information, and another third the blue information. To match the resolution of a black and white display of comparable size, three times as many pixel components are necessary for a three primary color display.

One possible solution to this limitation in spatial resolution is to present the chromatic information in a temporal format rather than a spatial format. Instead of presenting the chromatic information spatially as in conventional displays, the three primarily color components can be presented rapidly in time within each pixel. If the sequence of presentation is performed at a rate fast enough, the visual system is unable to resolve the individual fields and temporally integrates the three fields. Presenting the primaries temporally offers a substantial gain in spatial resolution since all the pixel components available in the display can be used at any one time. In other words, a sequential color display offers a gain of a factor of three in spatial resolution compared to a conventional display.

Because it takes three sequential fields (one red, one green and one blue) to display the equivalent of one conventional frame, the field rate of sequential color display systems that have been designed typically has been three

times that of conventional systems. The higher field rate requirement demands that not only one field be presented every 1/180th of a sec (for a 180 Hz system) but also that the rise and decay of the liquid crystal or phosphor be fast enough to allow for such field rate. Even if these demands are met by a liquid crystal or phosphor, other problems, more perceptual than technological, remain. For example, moving objects presented sequentially tend to "breakup". Perceptually, a sequentially presented moving object appears with distinctive colored stripes on both its leading and trailing edges. This breakup is often referred to as the "color breakup" artifact. Another artifact, which is also visible in a conventional monochrome display system and is often called "object breakup", is a luminance breakup which often appears as luminance flicker. Typically, as the speed of the moving object in a sequential color display is increased, object breakup appears first. If the speed of the object is increased further, the color breakup artifact becomes visible. If the speed of the object is increased even more, the leading and tailing chromatic edges on the moving stimulus become larger and more visible. Viewers generally report that the color breakup is more distracting and annoying than the object breakup. The visibility of color breakup artifacts have limited the use and development of sequential color displays.

The color breakup artifact can be understood in terms of the image produced by a display presented temporally on the retina. Assuming a stationary eye, a moving object in a sequential color display may result in red, green and blue images that do not overlap on the retina. For example, suppose a vertical bar moving in a left-to-right direction is presented in a sequential color display. Because the primary colors are presented sequentially in time and because the bar is moving, the red, green and blue fields will be presented to different areas of the retina and the bar may resemble a red, green, and blue grating with a spatial frequency dependent on the velocity of the bar and the field rate. The spatial frequency of the grating can be described by:

$$\text{cycles/deg} = F/3V \tag{1}$$

where F is the field rate of the display, and V is the velocity of the moving bar expressed in angular velocity. Equation 1 provides a description of the spatial pattern produced on the retina which is useful in determining whether color breakup will be visible.

In previous work Arend, Lubin, Gille, and Larimer (1994) used the Sarong Vision Model to predict color breakup in visual displays. The model was based on the spatial and temporal properties of the achromatic or luminance coding mechanism in the human visual system, but did not include properties of the chromatic mechanisms. Arend et al proposed that color breakup would be seen whenever the achromatic mechanism could detect breakup of an object in a display. It is well known that the spatial and temporal properties of the chromatic

mechanisms differ markedly from those of the achromatic mechanism. With regard to spatial patterns the chromatic mechanisms cannot detect patterns with spatial frequencies greater than approximately 11 cycles per degree (Mullen, 1985) while the luminance coding mechanism may detect patterns with spatial frequencies as high as 60 cycles per degree. For temporal patterns the chromatic mechanisms cannot detect temporal frequencies above approximately 18 Hz. (Boynton, 1992) while the achromatic mechanisms may detect temporal frequencies up to 60 Hz. Thus it might be expected that chromatic breakup would not be visible under all conditions in which the achromatic mechanism might detect breakup. The purpose of this project was to obtain data on the detection of color breakup in a sequential color display that might be related to the spatial and temporal properties of the human color coding mechanisms in order to develop a model that might be used to predict the detection of color breakup under a wide variety of viewing conditions. Thresholds for perceiving color breakup in a thin vertical bar moving across the display field were measured under a wide variety of viewing conditions including different adaptation levels, different contrast levels, and different stimulus velocities. In order to compare the results with previous work on the spatial temporal properties of the color coding mechanisms, the stimuli were specified in terms of cone contrast signals (Stromeyer et al, 1983) generated within each of the two color-opponent mechanisms known to code color in the retina and optic nerve (Boynton, 1992). Measures of the field rates at the threshold for color breakup were converted into spatial frequencies of the pattern generated on the retina so that the results might be compared to Mullen's data (1985) on the contrast sensitivity function for chromatic spatial patterns. Mullen's experiments suggest that the artifactual chromatic patterns generated by a moving stimulus in a sequential color display should not be detectable if those patterns consist of spatial frequencies higher than approximately 11 cycles per degree. The results obtained were used to test this hypothesis over a wide variety of viewing conditions.

METHODS

Six observers participated in the experiment. Their ages ranged from 28 to 50 years. All observers had normal near and far Snellen acuity. Observers were also screened for normal color vision using the Ishihara pseudoisochromatic plates and Farnsworth F2 tritan plate illuminated by a Macbeth Easel lamp. Five of the 6 observers already had participated in a similar study involving the same apparatus and were therefore highly practiced and familiar with the task. The sixth observer was familiar with psychophysical procedures, such as the one used in this study, and completed a training period in order to be able to provide consistent and stable thresholds.

The experiment was done on a computer controlled Maxwellian viewing system illustrated schematically in Figure 1.

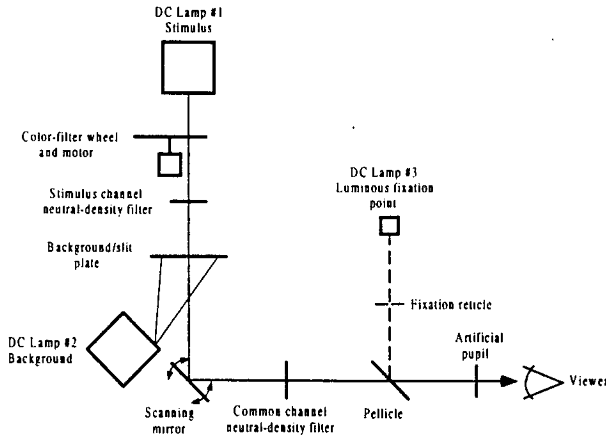

Figure 1. Simplified illustration of the FSC apparatus.

The color field sequential presentation was generated by placing a color wheel in the path of the stimulus channel. Field rates were under the observer's control. The stimulus channel was subsequently directed through a thin vertical slit drilled into a white metal plate. The metal plate was in turn illuminated and constituted the background. A scanning mirror was placed in the light path in order to provide a moving stimulus to the observer. The observer was positioned on a chin rest and inspected the display through a 2 mm artificial pupil providing a 10 deg field of view.

Three light sources were utilized in order to provide light for the stimulus (lamp #1), for the background (lamp #2), and finally for a luminous fixation point (lamp #3) that was used only for a dark background condition. Light for the stimulus was generated using a 100-W DC-powered tungsten-halogen lamp (lamp #1). The background light was generated using a 300-W halogen lamp (lamp #2). Finally, the luminous fixation point channel was generated using a DC-powered halogen lamp (lamp #3). A pellicle beamsplitter (Rolyn Optics Co.) was positioned in the light path in order to combine the common channel and the luminous fixation point channel.

The moving stimulus was a 4 min. by 2 deg vertical slit drilled into the background plate. This configuration permitted independent manipulation of the stimulus and background luminances and chromaticities. Neutral density filters were used to vary the luminances of the stimulus and the background. A color wheel attached to a variable speed brushless DC motor (Bodine model 22B4B-EBL) provided the sequential presentation of primary colors (Fig 1). The motor was connected to a motor control unit (Bodine model ABL-3921C) which allowed, via a ten turn potentiometer, adjustment of the speed of the motor. In order to register field rates, an infrared LED and a photocell

were placed on opposite sides of the color wheel. Several holes were drilled through the wheel with the photocell and infrared LED positioned in registration with the holes. The signal from the photocell was monitored and field rates were displayed on a universal counter (225-MHz Hewlett Packard model HP53131A/132A). Several wheels were produced differing in the number of RGB triplets or frames they possessed. (This allowed for greater field rate flexibility since the number of frames per revolution could be varied). For conditions requiring low field rates (i.e. stationary stimulus), a wheel containing one RGB frame was utilized. For most other conditions, a wheel containing 6 frames was used. In cases where extremely high field rates were required, a wheel containing 12 frames was used. With the 12 RGB-frame wheel, a maximum field rate of 5.3 KHz was possible. The wheels were all produced printing them as a viewgraph transparency on a dye-sublimation printer (Kodak model XLT 7720). Because the primary fields were immediately adjacent to each other on the wheel, the apparatus did not simulate the blanking used in practical displays to change the image between fields. Thus, the apparatus produced an ideal field sequential display.

In order to present stimuli moving at various velocities, a scanning mirror (General Scanning Inc. model E10-082694) was positioned in the path of the common channel (Fig 1). The mirror was attached to a closed-loop galvanometer (GSI model G120DT) driven by a GSI model AE1000 controller. The mirror system swept the target stimulus horizontally across the field of view. The AE1000 was driven by a digital-to-analog converter (DAC), installed in a desktop computer, and the DAC was controlled by a computer program. The program caused the galvanometer to perform constant-velocity sweeps that started and ended outside of the field of view. The sweeps alternated between left-to-right and right-to-left, with a 1-s pause between each sweep to allow the afterimage to fade before the next sweep. Observers viewed the display, which subtended 10 deg of visual angle, through an artificial pupil.

The CIE chromaticity coordinates of the RGB fields were chosen to match the RGB primaries of a typical color CRT. Furthermore, the fields were made approximately isoluminant. The coordinates and achievement of isoluminance were confirmed by installing the wheels in the apparatus and measuring the fields at the system's exit pupil with a Photo Research model PR-703 spectroradiometer. Numerous iterations with the dye-sublimation printer were required to produce wheels having the desired chromaticity coordinates. The CIE 1976 coordinates for the red, green, and blue fields of the wheels were as follows: red (.43, .53), green: (.12, .56), and blue (.20, .17). The chromaticity of the spinning wheel was (.22, .32). Finally, the background chromaticity was (.18, .51). Luminance and contrast calibrations were done following the procedures described in Post, Monnier, and Calhoun (1997).

Procedure

The experimental design was completely within subjects. Viewing conditions included 5 levels of background luminance (0, 5, 49, 468, and 2223 cd/m^2), 5 levels of stimulus luminance modulation (0.05, 0.16, 0.32, 0.56 and 0.89), and 5 retinal target-velocities (0, 6, 34, 85, and 200 degrees/s). Target luminances of 11, 25, 86, 102, and 875 cd/m^2 were tested against the dark background at all 5 retinal velocities. The luminance modulation, M, of the stimulus is a measure of contrast that is defined as

$$M = (L_{max} - L_{min}) / (L_{max} + L_{min}) \qquad (2)$$

where, in the present case, L_{max} is the stimulus luminance and L_{min} is the background luminance.

Trials cycled first through the retinal velocities, then the target modulations, and finally through the background luminances. The background luminance levels were chosen randomly for each observer. Thus, background luminance varied the least often and the participant's level of light adaptation was kept stable. Typically, the participants completed two or three background luminances in a session, which lasted 1 to 1.5 hours. Participants were permitted rest pauses on an as-needed basis and were also allowed to terminate sessions early if they felt they were becoming fatigued. Two replications were performed with each participant so we could evaluate the consistency of their thresholds. We found that the replications for a given participant were typically within 10-20% of each other.

The room in which the experiments were conducted was dark, except for a small amount of light that spilled from baffles around the lamps and light emitted by equipment such as the computer's CRT monitor. The experimenter met momentary needs for illumination with a miniature flashlight. At the start of each session, the experimenter seated the participant at the apparatus and installed the appropriate neutral-density filters for the first trial. Then, the participant donned an eye patch over his or her non-dominant eye and adjusted a chin rest to position the dominant eye within the optical system's exit pupil, using the fixation point as a reference. 5 minutes were allowed for the participant's eye to adapt to the background luminance.

For each trial, the experimenter commanded the computer to produce a specific retinal velocity for the target. The participant foveated the fixation point, observed sweeps of the target, and adjusted the potentiometer until color breakup in the target was just invisible. The experimenter read the wheel's field rate from the counter. Next, the observer spun the potentiometer's knob to a higher, random position and then adjusted the knob until color breakup was just visible, at which point the experimenter recorded the new field rate threshold. The average of the two field

rate settings was taken as the observer's threshold. Under some viewing conditions, the participant was unable to see the stimulus sufficiently to produce a setting; in these cases, the condition was skipped and no data were recorded.

Results

Examples of raw data are shown in Fig. 2. The mean field rate set by the observer is plotted as a function of the luminance modulation of the stimulus with stimulus velocity as a parameter. Error bars indicate one standard deviation of the mean. Each panel shows data for one observer. The left panel shows results from observer PM on the 5 cd/m^2 background and the right panel shows results for observer ALN on the 468 cd/m^2 background. Such plots were made for each of the 5 observers and each of the 5 background levels. The results shown are typical. At each velocity the field rate needed to prevent color breakup increases with the luminance modulation of the stimulus. Field rate also increases with the velocity of the stimulus. The results are consistent across all observers and all background levels.

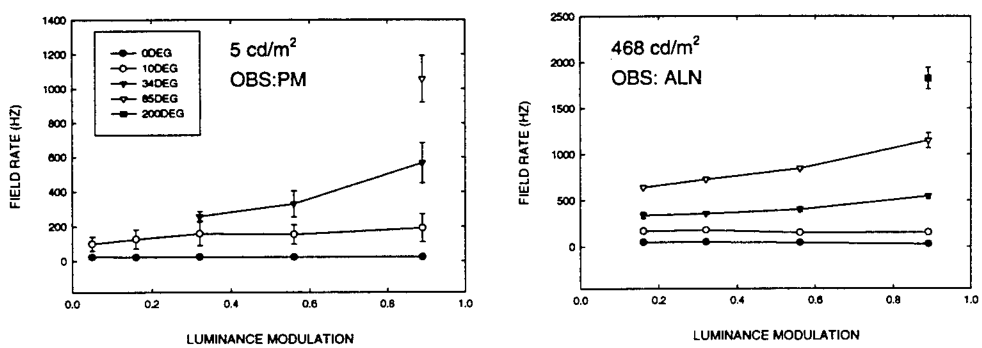

Figure 2. Field rates set by two different observers under two different adapting conditions

In order to compare the results for different backgrounds and velocities with the hypothesis that color breakup is mediated by the spatial and temporal properties of the color coding mechanisms the independent and dependent variables in the raw data were transformed. Since we reasoned that the color signals generated in the two color opponent mechanisms were responsible for the detection of color breakup, we calculated the cone contrast signals input into each color mechanism for each primary and for each level of the independent variable luminance modulation. This was done by converting the chromaticies of the background and the stimulus primaries into cone

excitations. The chromaticities of the background and stimulus primaries were first converted to Judd tristimulus values (See Vos, 1978). The tristimulus values were converted into cone excitations with the transformation (from Appendix I, in Boynton, 1992) shown in equation 3 with one change. The coefficient for Z in the equation for S was changed from 0.001608 to 1 so as to scale S excitation such that the S chromaticity (S/(L+M)) was approximately 1 at equal energy white rather than at 400 nm.

$$
\begin{aligned}
L &= +\,0.15514\,X + 0.54312\,Y - 0.03286\,Z \\
M &= -\,0.15514\,X + 0.45684\,Y + 0.03286\,Z \\
S &= Z
\end{aligned}
\tag{3}
$$

Then the cone contrast ratios (e.g. $\Delta L/L$) were calculated by taking the difference between the cone excitations generated by a stimulus primary and the background and dividing this difference by the excitation generated by the background. The contrast ratios were calculated for each stimulus primary and each of the cone mechanisms. Stromeyer et al. (1983) have shown that the weightings of these cone contrasts into the color opponent mechanisms are constant over a wide variety of conditions. Therefore cone contrasts are a convenient way of representing color contrast. In order to calculate the color contrast within each of the two color opponent mechanisms, sums and differences of the individual cone contrasts were calculated for each test stimulus primary. For the long wavelength color opponent mechanism, the difference between the contrasts in the long and middle wavelength cone mechanisms (L-M) was calculated. For the short wavelength color opponent mechanism the sum of the long and middle wavelength cone contrasts was subtracted from the short wavelength cone contrast [S-(L+M)]. These two contrast signals were taken as estimates of the input signals for each of the color opponent mechanisms. The magnitudes of these two contrast signals were calculated for each level of luminance modulation of the test stimulus.

The color contrast signals generated by the test stimulus primaries at a luminance modulation of 0.05 are shown in Figure 3. As the luminance modulation is increased the opponent color contrast signals increase proportionally. Contrasts generated in the long-wavelength opponent mechanism are shown in the left panel and those generated in the short wavelength color opponent mechanism are shown in the right panel. The left panel shows that the red primary generates a substantial color contrast signal in the reddish direction while the green and blue primaries generate somewhat smaller, and similar, contrast signals in the greenish direction. For the short wavelength color

opponent mechanism the blue primary generates a very large contrast signal in the bluish direction while the red and green primaries generate very small contrast signals in the yellowish direction.

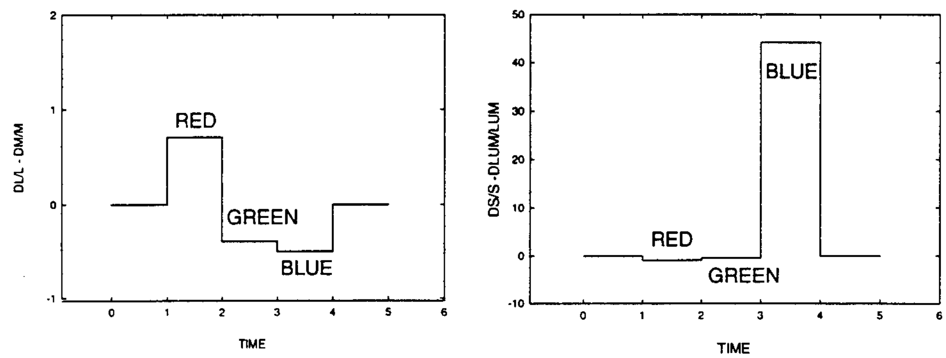

Figure 3. Color contrast signals generated in the color opponent mechanisms by the stimulus primaries.

These contrast signals are consistent with the appearance of the stimulus under varying contrast levels and velocities. The blue primary was often the most visible component of the test stimulus. The red primary was the next most visible component of the stimulus. The green primary was only visible under a limited range of conditions and none of the stimulus components ever appeared yellowish relative to the background. At or near the threshold for color breakup, bluish and reddish components of the stimulus were visible at different spatial locations with the bluish component being more prominent. We assumed that the bluish signal in the short wavelength color opponent mechanism was above threshold under these conditions and threshold for color breakup was exceeded when the reddish signal in the long-wavelength color opponent mechanism became visible. Therefore we reasoned that thresholds for color breakup were determined by the contrast in the long wavelength color opponent mechanism.

As the velocity of the stimulus was increased the appearance of the stimulus clearly changed. At higher velocities the perceived contrast of the stimulus relative to the background decreased and its shape or form became less distinct. At the very highest velocities the stimulus had little form, the direction of movement was difficult to discriminate, and the perceived contrast was very low. In order to incorporate these effects into the contrast measures we made an initial simplifying assumption. We assumed that the effect of velocity was simply to reduce the effective contrast. This assumption was based on the fact that the color and luminance coding mechanisms integrate signals

over time and space. As the stimulus moves across the receptive field of a color opponent or achromatic coding unit in the visual system, it generates a contrast signal relative to the background. The size of the signal generated by the test stimulus depends not only on its physical contrast, but also on the portion of the receptive field it occupies and the length of time it spends in the receptive field. Since the size and shape of the stimulus were fixed throughout the experiment the portion of the receptive field occupied by the stimulus was fixed. However, as the velocity of the stimulus increased the length of time spent in the receptive field of any color or luminance coding unit decreased. Therefore we assumed that the effective contrast of the stimulus was inversely proportional to its velocity. The color contrasts calculated for each stimulus primary at each luminance level were weighted by the velocity of the moving stimulus. We assumed that the weighting factor was 1 at 6 deg/sec and weighted contrasts for other velocities relative to this velocity. (For a unit that integrates signals over an area 0.5 degrees in diameter, this is equivalent to assuming that the interval of complete temporal summation for the unit is 83 msec in duration. This is probably a relatively safe assumption for color coding units, since previous research suggests that complete temporal summation occurs over an interval of 200 to 400 msec in the color mechanisms.) For example, at 34 deg/sec we assumed that the effective contrast of the stimulus was 6/34 times the effective contrast at 6 deg/sec. This assumption is equivalent to assuming that velocity has no effect on detecting color breakup other than through its effect on the magnitude of the color contrast signals generated by the stimulus.

The dependent variable was the field rate set by the observer at the threshold for color breakup. As the stimulus moves across the retina it paints an image that resembles a chromatic grating. The bars in this grating consist of the red, green, and blue primaries that are presented in succession. At a fixed velocity, the width of the bars in the grating is determined by the field rate or the rate of alternation of the primaries. At low field rates the bars are wide, while at high field rates the bars are narrow. We reasoned that the detection of color breakup was similar to the detection of chromatic modulation in stationary grating patterns. The observer's task was to adjust the field rate so that the chromatic modulation of the grating was at threshold. This is equivalent to adjusting the spatial frequency of a stationary chromatic grating so that the chromatic modulation is at threshold. The spatial frequency of the resulting grating can be calculated from equation 1 (Post, Monnier, and Calhoun; 1997). Therefore all of the field rates set by observers were transformed into spatial frequencies in this way.

Figure 4 shows an example of transforming the independent and dependent variables as described above. The results for one background level are shown for each of the 6 observers in separate panels. Spatial frequency, the transformation of the dependent variable, is shown on the vertical axis of each panel. The effective chromatic

contrast, the transformed independent variable, in the reddish direction for the long wavelength color opponent mechanism is plotted along the horizontal axis. Different stimulus velocities and luminance modulation levels are collapsed into this one variable by the transformation described above. Results are shown for the 49 cd/m^2 background. Similar plots (not shown) were made for the other 4 background levels. In all cases the results were similar. The threshold for color breakup, expressed as a spatial frequency, increases with the effective contrast generated in the long wavelength color opponent mechanism. Points for different stimulus velocities in general tend to fall on the same curve. The spatial frequency at threshold increases from approximately 1 to 2 cycles/deg. at the lowest effective contrasts at which color breakup could be seen to approximately 4 to 8 cycles/deg. at high contrasts. Spatial frequency increases approximately linearly with effective contrast up to high contrasts where the threshold appears to become approximately constant. The threshold appears to become approximately constant at a spatial frequency of something like 4 to 8 cycles per degree for very high chromatic contrast signals.

The results shown in Figure 4 suggest that the simplifying assumption about the effect of velocity on contrast and the threshold for color breakup was a reasonable one. Results are consistent with the idea that the only effect of varying velocity is to vary the effective contrast of the stimulus. For the most part, data points obtained at different velocities tend to fall on the same curve. The curves fit to the data are hyperbolic functions with two parameters. One parameter represents the spatial frequency at which the curve flattens out or saturates. The other parameter represents the contrast level at which the curve reaches half of its maximum height or saturation level.

Hyperbolic functions were fit to each data set for each observer at each background level. On the average the curves explain approximately 80% of the variance (low of 43%; high of 98%) in the individual data and provide a good characterization of the results. The parameters for each curve fit are plotted as a function of background level in Figure 5. The parameter A, the maximum spatial frequency at high contrasts, is plotted in the left panel, while B, the contrast level at half the maximum spatial frequency is plotted in the right panel. The plot of parameter A indicates that the maximum spatial frequency increases with background adaptation level from approximately 7 c/deg on a dark background to approximately 10 c/deg on the brightest background. Most of the increase occurs above 100 cd/m^2. Individual differences in this parameter are apparent. The maximum spatial frequency varies by a factor of nearly 2 depending on the observer. Below approximately 100 cd/m^2, the parameter B decreases with increasing background level. Above 100 cd/m^2 the parameter B appears to be approximately

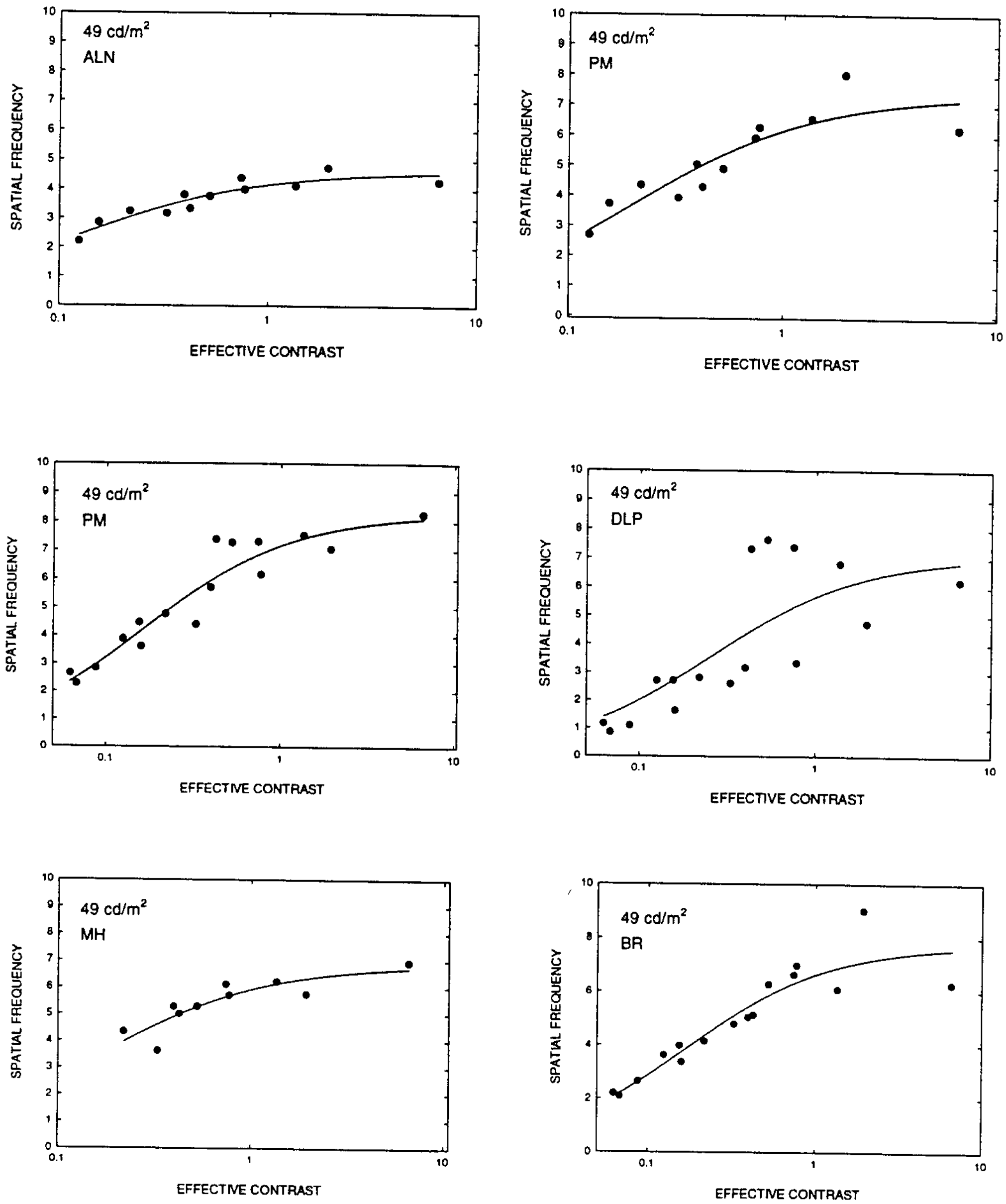

Figure 4. Spatial frequency plotted as a function of effect chromatic contrast for the 49 cd/m^2 background.

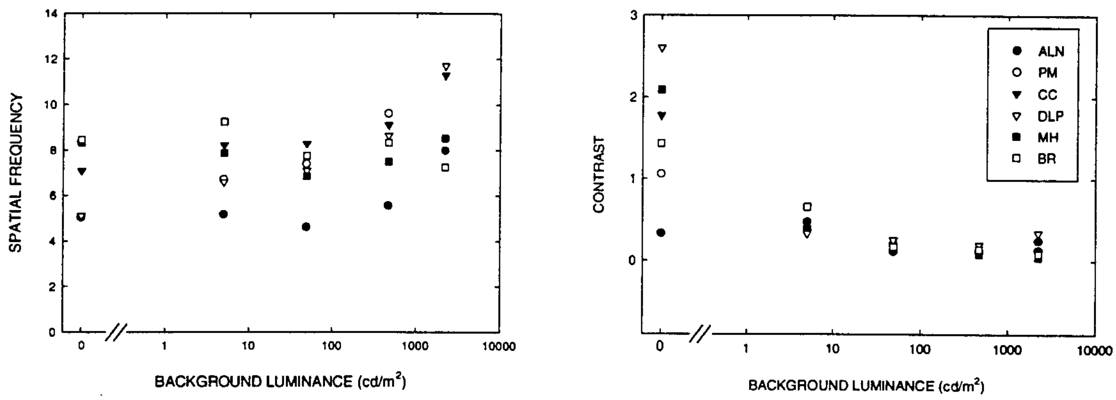

Figure 5. Parameters for fits of hyperbolic function to individual data.

constant. Though there is a large variation in this parameter for the dark background, at the other background levels the value of the parameter is quite similar for all observers.

Figure 6 summarizes the results obtained from all 6 observers on all 5 background levels. Spatial frequency is again plotted as a function of effective red/green contrast. Data from all 6 observers have been pooled within each panel with each panel representing a different background level. Hyperbolic functions again have been fit to the pooled data. The curves account for 60% of the variance in the pooled results on average (low of 52%; high of 66%) and provide a good characterization of the data. The parameter A (maximum spatial frequency) increases from 7.0 on the dark background to 8.9 on the brightest background. Again the maximum spatial frequency is approximately constant below a background level of approximately 100 cd/m^2. The parameter B (contrast at half maximum spatial frequency) decreases from a high of 1.35 on the dark background to 0.12 on the brightest background. It is similar at the two highest background levels again suggesting that it would not change with further increases in background level.

Conclusions

Results of the experiments described above are consistent with hypothesis that the detection of color breakup is limited by the spatiotemporal properties of the color opponent mechanisms. Color breakup was detectable only when the spatial frequency of the chromatic pattern generated on the retina was less than approximately 11

cycles/deg. This result agrees with the work of Mullen (1985) on chromatic gratings and was true even for very high contrast stimuli that generated very large color contrast signals in the color opponent mechanisms.

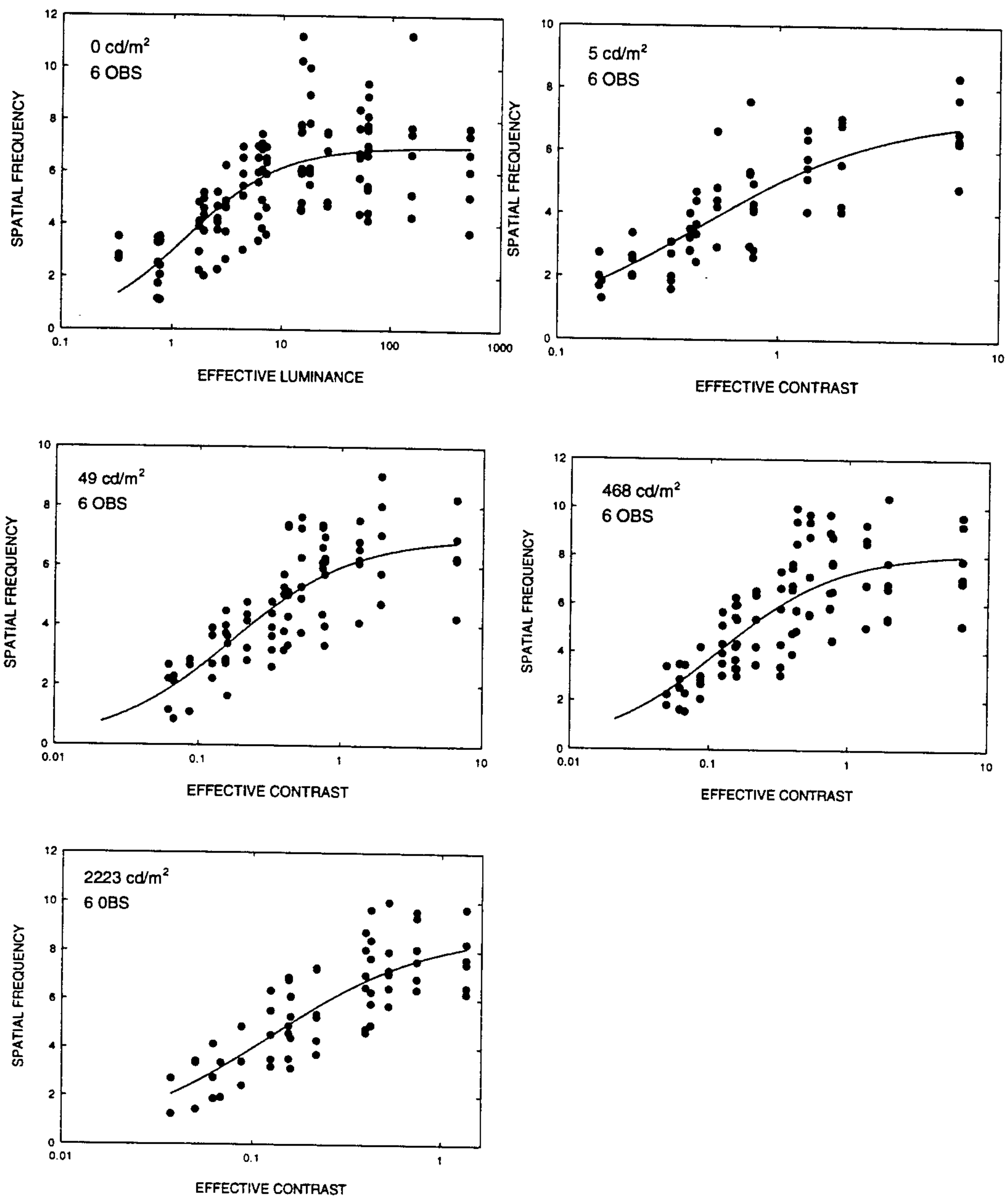

Figure 6. Pooled results from all 6 observers at each of the 5 background levels with further increases in background level.

Furthermore, the assumption concerning the effect of stimulus velocity is well supported by the data. The results are consistent with the idea that the only effect of velocity can be characterized as an effect on the contrast signals generated within the color mechanisms by the stimulus. As a result of temporal summation within the color mechanisms, the effect of increasing velocity was to reduce the contrast signal generated within the color mechanisms.

The results are also consistent with the notion that color breakup is mediated by signals in the two color opponent mechanisms independently of activity in the achromatic or luminance coding mechanism. This assertion requires more rigorous testing but was supported by the fact that the results obtained with a wide range of luminance contrasts between the test stimulus and the background are consistent with Mullen's work, which was obtained under equiluminant conditions. This result strongly suggests that luminance contrast signals in the achromatic mechanisms have little effect on the detection of color breakup. The detection of color breakup appears to be mediated by the color opponent mechanisms.

Results at different background or adaptation levels are very similar suggesting that adaptive state has only a minor effect on the detection of color breakup. These effects can be characterized by changes in the parameters of the hyperbolic functions fit to the data. The contrast level at which spatial frequency reaches half its maximum, characterized by parameter B, decreases slightly with increasing adaptation level up to approximately 100 cd/m2. The maximum spatial frequency at which color breakup was detected, characterized by parameter A, increased slightly with increasing background level above approximately 100 cd/m^2. This result is, perhaps, not surprising since it is well known that the spatial resolution of the visual system in general tends to improve at higher light levels. Whether this is true for chromatic patterns does not appear to have been previously investigated. Most previous studies of chromatic spatial resolution have been conducted at one luminance level. Mullen's (1985) data were collected at a luminance level of 15 cd/m^2, a level between the two lowest illuminated background levels used in this experiment. At this adaptation level the maximum spatial frequency at which color breakup could be detected was approximately 7 c/deg.

The comparison with Mullen's data raised a question as to why color breakup in our experiment could be detected at spatial frequencies only half as high as those detectable in chromatic gratings at moderately low adaptation levels. There are several possible explanations. First of all the gratings in Mullen's study were presented for an extended period of time and covered a much larger spatial extent than the stimulus used in the experiments reported here. Spatial and temporal summation were therefore likely to be much more extensive in the grating study, resulting in higher sensitivity. Second of all, the stimulus used in the study reported here was 4 minutes wide. Calculations

show that as the spatial frequency of the pattern painted on the retina was increased above 5 cycles per degree each region of the retina was stimulated by at least two primaries. If the spatial frequency was increased above 10 cycles/degree each region of the retina was stimulated to some extent by all three primaries. Further calculations showed that the effect of stimulation by more than one primary was to reduce the effective color contrast of the grating produced on the retina though the spatial frequency of the pattern was unaffected. As a result the very highest contrast levels could not be produced at the very highest spatial frequencies. Here we have not tried to correct our estimates of the effective contrast of the stimulus for this effect. This problem could be avoided and a better comparison with Mullen's (1985) grating data could be obtained by repeating some of the experiments using a smaller slit width. It is possible that under these conditions the visibility of color breakup would agree quite well with Mullen's data on gratings. This problem, however, also points the way to generalizing the results presented here to other stimulus configurations. Wider stimuli would tend to breakup only at lower spatial frequencies as a consequence of the stimulation of each retinal area by more than one primary. Thus lower field rates would be required to prevent color breakup with wider stimuli. The effective reduction in contrast could be calculated for wider stimuli and the field rate required to prevent color breakup could then be predicted based on the results presented here.

The data and modeling presented here can be regarded as a start toward predicting the field rate required to prevent color breakup under a wide variety of viewing conditions from the basic spatiotemporal properties of the color coding mechanisms. The model could be used to evaluate design tradeoffs and limitations for such parameters as field rate, contrast level, primary chromaticities, adaptation level, and stimulus velocity in the development of usable sequential color displays. The variables entered into the model are the color contrasts produced by the primaries of the display against the prevailing background field, the luminance contrasts of test stimuli against the background, the velocity of moving stimuli to be presented in the display, and the width of the stimuli to be used. If these variables are known then the field rates required to prevent color breakup should be predictable. There are two parameters in the model that are experimentally determined. These are the parameters A, the maximum spatial frequency, and B the effective contrast level at which half the maximum spatial frequency is reached. The values of these parameters are dependent on adaptation level. Parameter A increases with adaptation level, while parameter B decreases with adaptation level. There are also individual differences among observers in the parameters. It appears that most of the individual differences between observers can be captured in these two parameters. It would be

worthwhile to explore this assertion more fully and to obtain estimates of the two parameters in a larger sample of individuals so that reasonable estimates of population variability could be obtained.

In order to generalize the model to a broad range of conditions further work needs to be done. First it is important to determine that the model works with other combinations of stimulus primaries, that is other chromaticities and other luminance ratios between these primaries. The results obtained here were obtained with one set of primary chromaticities set in a fixed luminance ratio so that the test stimulus always had the same chromaticity. Also, only one background chromaticity was used. While there is no reason to believe that the model would not extend to different primary chromaticies, different test stimulus chromaticities, and different background chromaticities, this needs to be verified. Second, since interest in sequential color displays has been generated largely by the need for color displays with high spatial resolution, one of the most important points would be to do further work with even narrower stimuli. This would make it possible to determine the highest spatial frequencies that could be detected by the color mechanisms in sequential color displays. While it seems likely that the results of these experiments will show at least approximate agreement with Mullen's (1985) experiments, this result still needs to be determined. Also measures of the spatial contrast sensitivity of the color mechanisms (reviewed in Mullen, 1985) have been obtained only under a very limited set of adapting conditions. Further work on color breakup would be useful in extending this work to a broader range of adapting conditions and describing how the spatial contrast sensitivity of the color mechanisms varies with adaptation level. Finally, it remains to be determined whether the model can be extended to the case in which the test stimulus is stationary and the observer makes eye movements. It is well known that color breakup occurs under these conditions, and some means of predicting when it will occur are required. It is not known whether color breakup is equally visible whether the test stimulus is moved across the retina, as in the experiments reported here, or the eye is moved to sweep the stimulus across the retina. If these two conditions produce similar results, the model should work for either type of situation. Previous work suggests that some visual signals are suppressed during eye movements. Thus it might be expected that color breakup is less visible during eye movements. In that case the moving stimulus condition would be the situation that limits the design of sequential color displays.

References

Arend, L., Lubin, J., Gille, J., and Larimer, J. (1994) Color breakup in sequentially scanned LCD's. Society for Information Display International Symposium Digest of Technical Papers. 25, 201-204, Society for Information Display. Playa Del Ray, 1994.

Boynton, R.M. (1992) Human Color Vision. Optical Society of America. Washington, D.C.

Mullen, K.T. (1985) The contrast sensitivity of human colour vision to red-green and blue-yellow chromatic gratings. J. Physiol. (London) 359, 381-400.

Post, D.L., Monnier, P., and Calhoun, C.S. (1997) Predicting color breakup on field-sequential displays. Proceedings of SPIE, 3058, 57-65.

Stromeyer, C.F., Kronauer, R.E., and Cole, G.R. (1983) Adaptive mechanisms controlling sensitivity to red-green chromatic flashes. In Color Vision. Ed by J.D. Mollon and L.T. Sharpe, Academic Press, New York, 313-330.

Vos, J.J. (1978) Colorimetric and photometric properties of a 2 deg fundamental observer. Color Res. and Appl., 3, 125-128.

RAPID PCR DETECTION OF VANCOMYCIN RESISTANCE OF *ENTEROCCUS* SPECIES IN INFECTED URINE AND BLOOD

Brent L. Nielsen
Associate Professor
Department of Botany & Microbiology

Auburn University
101 Life Sciences Building
Auburn, AL 36849

Final Report for:
Summer Faculty Research Program
Armstrong Laboratory

Sponsored by:
Air Force Office of Scientific Research
Bolling Air Force Base, DC

and

Armstrong Laboratory

September 1997

RAPID PCR DETECTION OF VANCOMYCIN RESISTANCE OF *ENTEROCCUS* SPECIES IN INFECTED URINE AND BLOOD

Brent L. Nielsen
Associate Professor
Department of Botany & Microbiology
Auburn University

Abstract

Resistance of pathogenic bacteria to antibiotics is a rapidly growing problem in the U.S. and around the world. Several species of bacteria are developing resistance to many of the previously effective antibiotics, including vancomycin. This is especially a problem with *Enterococcus* species, which cause blood and urinary tract infections. In this study, a rapid method for recovery of bacterial DNA from urine or blood samples, coupled with the polymerase chain reaction (PCR) and analysis of the presence of vancomycin resistance genes by Gene Comb™ technology was optimized. This method could also be used to distinguish between *E. faecium* and *E. faecalis* in blood and urine samples, as well as provide rapid determination of the presence of either of these species and/or vancomycin resistance in less than 6 hours. It is also possible to determine the individual presence of *van*A, *van*B, *van*C-1, *van*C-2 or *van*C-3 genes in samples, an ability which may be applicable to other pathogenic organisms such as *Staphylococcus aureus*. Traditional clinical laboratory identification of *Enterococcus* species and vancomycin resistance typically requires several days. In serious infections this time factor may be very critical for patients, and thus this new method has great potential for assisting in the prompt and proper treatment of these bacterial infections.

RAPID PCR DETECTION OF VANCOMYCIN RESISTANCE OF *ENTEROCOCCUS* SPECIES IN INFECTED URINE AND BLOOD

Brent L. Nielsen

Introduction and Discussion of Problem

Bacteria from the genus *Enterococcus* are among the increasing number of pathogenic microorganisms that have developed resistance to antibiotics used to treat infections (10). These drug-resistant bacteria are a growing problem especially among hospitalized patients whose bodies are weakened by cancer or other illnesses. While in hospitals patients are more likely to come in contact with drug-resistant organisms from other patients (5,11,13,26). In addition, there is growing evidence of community-acquired infections (2,15). In some European countries avoparcin, an antibiotic related to vancomycin, has been used as a growth promoter in farm animals and has been linked with an increased incidence of vancomycin-resistant enterococci (2). Vancomycin has been an effective antibiotic for the treatment of *Enteroccus* infections for a number of years. This antibiotic disrupts bacterial cell wall synthesis in gram positive microorganisms, by a mechanism different from penicillin and its derivatives. In recent years vancomycin-resistant *Enterococcus* isolates have increased in prevalence, from 0.3% of all nosocomial (hospital-acquired) infections in 1989 to 7.9% in 1993 (5). The two most common species of *Enterococcus* associated with nosocomial infections are *E. faecium* and *E. faecalis*, although several other species are known (10). This increase in vancomycin resistance is especially alarming when it is considered that this antibiotic is also used to treat infections caused by *Streptococcus* spp. and *Staphylococcus aureus* (3,4,18), which are also serious pathogens. Mechanisms for the transfer of resistance genes between gram positive bacteria have been well studied and this transfer is a serious problem. Fortunately most streptococcal

infections remain treatable by penicillin derivatives, and vancomycin-resistant strains have only very recently been reported in isolated cases. *S. aureus* has developed resistance to most of the antibiotics used to treat it, and vancomycin has been essentially the only effective antibiotic for treatment of infections caused by this organism (3). However, there are recent reports from Japan and the U.S. of intermediate levels of vancomycin resistance in *S. aureus*, which will be a major problem if it speads (3,4).

Vancomycin is a glycopeptide that binds to the D-alanine-D-alanine portion of UDP-muramyl-pentapeptide, a precursor in peptidoglycan synthesis, thus preventing bacterial cell wall synthesis (22). The mechanism for resistance to vancomycin is not fully understood, but involves proteins (ligases) that substitute D-alanine-D-lactate or other derivatives termed depsipeptides in place of D-alanine-D-alanine into the UDP-muramyl-pentapeptide (8,14). The alternate depsipeptide forms are not bound by vancomycin and are incorporated during peptidoglycan synthesis, allowing bacterial cell wall synthesis in the presence of the antibiotic.

Several genes involved in vancomycin resistance have been isolated and characterized. Both *van*A and *van*B are involved in acquired inducible resistance, and encode ligases of broad substrate specificity which are responsible for the synthesis of depsipeptides which do not bind vancomycin (8,21). These genes are most likely spread by plasmid or transposon transfer from a resistant organism, and a transposable element carrying vancomycin resistance genes has been characterized (1,12,21). The *van*C-1, *van*C-2 and *van*C-3 genes are associated with constitutive low-level resistance to vancomycin, and the clinical significance of these genes is not known (9,17). The *van*C genes are found in *E. gallinarum*, *E. casseliflavus* and *E. flavescens*. The *van*B gene has been found mostly in *E. faecium* and *E. faecalis*, while *van*A is found in most *Enteroccus* species, including those already mentioned that may carry *van*B and *van*C.

Enterococcus species are a major cause of blood and urinary tract infections, and as such are difficult pathogens to treat if they become antibiotic resistant (26). It typically takes several days to isolate these species from urine or blood samples and to determine their resistance to vancomycin. If the infection is not promptly treated with an effective antibiotic, it may rapidly spread and may lead to death. The development of a rapid method to identify the bacteria and vancomycin resistance would greatly help in the proper treatment of infections. The vancomycin resistance genes have been sequenced and primers for PCR have been designed and used to identify the presence of these genes in DNA from clinical isolates (7,16,19,20,23). However, there is still the need to isolate DNA from bacterial cells, which is typically done from isolated colonies on agar plates, in order to provide the template for PCR. The analysis of PCR products in agarose gels requires additional time. This PCR approach may allow correct diagnosis in two days, which is a considerable improvement over traditional methods. The ability to identify the organism and vancomycin resistance directly from urine or blood samples would represent another significant advance, further reducing the time needed for diagnosis. The work described herein presents a method which couples a rapid DNA isolation method, PCR and Gene Comb™ technology to allow complete diagnosis of vancomycin-resistant *Enterococcus* species from urine or blood samples within 6 hours. This approach has the potential to impact the lives of many patients.

Methodology

Various *Enterococcus* strains were obtained from clinical isolates, and are shown in Table 1. For isolation of DNA for PCR, strains were inoculated into 3 ml BHI broth and incubated overnight at 37°C with shaking. Serial dilutions (1:10 to 1:10,000) of each culture were made in sterile phosphate buffered saline (PBS).

Isolation of bacterial DNA from urine samples Dilutions were combined with urine by adding 100 μl of the dilution to 900 μl of urine. After thorough mixing, the samples were centrifuged at full speed for 1 min in a microfuge to recover bacteria. The supernatant was carefully removed, and 200 μl of Insta-Gene matrix (BioRad) was added to each pellet. Samples were then incubated for 30 min at 56°C, followed by high speed vortexing for 10 sec and incubation at 100°C for 8 min. Samples were vortexed again and centrifuged at 12,000 rpm for 2.5 min. The resulting supernatant was used directly for PCR (20 μl) and the remaining Insta-Gene preparation was stored at -20°C for future use.

Isolation of bacterial DNA from blood samples Dilutions of overnight cultures in PBS (1:10 or 1:1000) were thoroughly mixed with freshly drawn human blood (5 μl into 45 μl blood). From each sample, 10 μl was immediately transfered into 1 ml sterile water. These samples were then mixed and incubated at room temperature for 20 min, followed by centrifugation at 12,000 rpm for 2.5 min. After removal of the supernatant, 200 μl Insta-Gene matrix was added to the pellet, and the remaining steps were carried out exactly as for the urine samples.

PCR detection of vancomycin-resistant genes Using the isolated DNA, PCR was carried out using species-specific or vancomycin resistance gene-specific primers as shown in Table 2. For each primer pair, one primer has a 5' biotinylated tag to facilitate detection by the respective capture probe, which is designed from the strand complementary to the biotinylated primer. PCR reaction conditions were the same for *van*A, *van*B, *van*C-1 and *van*C-2/3, and are as follows: 1X PCR buffer II (Perkin-Elmer, 1X contains 10 mM Tris, pH 8.3 and 50 mM KCl), 1.5 mM $MgCl_2$, 0.2 mM each dNTP, 50 pmole each primer, 1.5 units Taq DNA polymerase, and 20 μl DNA in a total reaction volume of 50 μl. Thermocycler (Perkin-Elmer model 9600)

conditions were 4 min at 94°C, then 30 cycles of 1 min at 94°C, 1 min at 55°C, and 1 min at 72°C. After the 30 cycles, reactions were incubated for 8 min at 72°C and then indefinitely at 4°C. PCR products were analyzed in agarose gels or directly by the GeneComb™.

For *E. faecium*-specific PCR (6), the reaction conditions were: 1X PCR buffer 4 (Stratagene, 1X contains 10 mM Tris, pH 8.3, 3.5 mM $MgCl_2$ and 75 mM KCl), 0.2 mM dNTPs, 25 pmole each primer, 1.25 units Taq polymerase, and 10 µl DNA in a reaction volume of 25 µl. Thermocycler conditions were 4 min at 94°C, and 30 cycles of 1 min at 94°C, 1 min at 72°C, followed by 8 min at 72°C and at 4°C indefinitely.

For *E. faecalis*-specific PCR, reaction conditions were: 1X PCR buffer 4 (Stratagene), 0.2 mM dNTPs, 50 pmole each primer, 1.5 units Taq polymerase, and 20 µl DNA in a reaction volume of 50 µl. Thermocycler conditions were 4 min at 94°C, 30 cycles of 1 min at 94°C, 1 min at 62°C, and 1 min at 72°C, followed by 8 min at 72°C and then held at 4°C.

<u>Gene Comb™ analysis of PCR products</u> Each capture probe was diluted 1:10 in freshly prepared binding buffer (BioRad) to a concentration of 100 ng/µl. From these dilutions 0.5 µl (50 ng) was spotted carefully onto individual teeth of the Gene Comb, following the manufacturer's directions (BioRad, ref. 24). In most cases two capture probes were spotted diagonally onto each tooth, with one serving as a negative control. After absorption of the liquid, the comb was exposed to ultraviolet light (high intensity on a BioRad mini-transilluminator) for 3 min. Denaturation solution (2 µl) was added to 10 µl of each PCR product to be analyzed and the samples incubated at room temperature for 5 min. HybriRun neutralization buffer (50 µl) was added to each sample and 50 µl was transferred to wells in the first row of a micro-titer plate. The GeneComb was inserted into this row of wells, incubated for 15 min at 37°C, and

transferred successively to the second row containing streptavidin/alkaline phosphatase conjugate for 5 min at room temperature, the third row containing chromogenic substrate for 7 min at room temperature, and the fourth row containing stop solution for 3 min. The comb was allowed to dry and then photographed using the Gel-Doc system (BioRad).

Results

PCR products from bacterial DNA isolated from urine or blood spiked with *Enterococcus* cultures were analyzed by agarose gel electrophoresis, and the results are shown in Figures 1-4. The numbers of colony forming units (CFU) per ml or per sample are given in the figure legends. While not every sample resulted in a detectable band after PCR, in several cases very low numbers of CFU gave rise to faint but detectable bands (Fig. 1 lanes 3,4,7 and 10; Fig. 2 lanes 4,9 and 11). The bands observed were of the expected size for each primer pair. There is an extra, unexplained band in Fig. 2 lane 9. In each experiment negative controls were included and no PCR products were detected for the controls. For urine samples, detectable *van* gene products were obtained with as few as 76,000 CFU/ml (Fig. 2 lane 4). With blood samples, as few as 100,000 CFU/ml blood could be detected (Fig. 2 lane 11), but since only 10 μl blood is used for bacterial DNA isolation, this means that 1000 CFU provided sufficient DNA for PCR amplification. Similar sensitivities were obtained with the species-specific primers (Fig. 3 and 4). The GeneComb (Fig. 5) provided a lower level of sensitivity as compared to the agarose gel analysis of amplicons. Only faint spots were observed with most amplicons from blood and urine samples (Fig. 5B). This may be due to lower sensitivity with some sequences such as those used in this study, or to other factors related to the kit itself.

Table 1. *Enterococcus* strains used in this study

Strain No.	Species	Resistance Gene	Source
E1	*E. faecium*	*van*A	Univ. Scranton
E2	*E. faecium*	*vanB*	Univ. Scranton
E3	*E. faecium*	*van*A	Brooks AFB
E4	*E. faecium*	*van*B	Brooks AFB
E5	*E. faecalis*	*van* sensitive	Brooks AFB
E6	*E. faecium*	*van*A	Univ. Scranton
E7	*E. faecium*	*van*B	Univ. Scranton
E8	*E. faecium*	*van*B	Univ. Scranton
E9	*E. casseliflavus*	*van*C_2	Univ. Scranton
E10	*E. casseliflavus*	*van*C_2	Univ. Scranton
E11	*E. gallinarum*	*van*C_1	Univ. Scranton
E12	*E. gallinarum*	*van*C_1	Univ. Scranton
E13	*E. faecalis*	*van*B	Brooks AFB
E14	*E. faecalis*	*van*A	Brooks AFB
E15	*E. faecalis*	*van* sensitive	Brooks AFB
E16	*E. faecalis*	*van*A	Univ. Scranton
E17	*E. faecalis*	*van*B	Univ. Scranton
E18	*E. faecalis*	*van*B	Univ. Scranton
E19	*E. faecalis*	*van*B	Univ. Scranton

Table 2. PCR primers and capture probes used in this study

Name of oligonucleotide	Sequence
*van*A forward primer	5'(Bio)CATGACGTATCGGTAAAAC3'
*van*A and *van*B reverse primer	5'ACCGGGCAGRGTATTGAC3'
*van*B forward primer	5'(Bio)CATGATGTGTCGGTAAAATC3'
*van*C forward primer	5'GATGGCWGTATCCAAGGA3'
vanC_1 reverse primer	5'(Bio)GTGATCGTGGCGCTG3'
vanC_2 reverse primer	5'(Bio)ATCGAAAAAGCCGTCTAC3'
E. faecium forward primer	5'(Bio)TTGAGGCAGACCAGATTGACG
E. faecium reverse primer	5'TATGACAGCGACTCCGATTCC3'
E. faecalis forward primer	5'(Bio)AAGTGCTGATTATCCTAGACC
E. faecalis reverse primer	5'TTATCCAATGCCAAATAGAC3'
*van*A capture probe	5'CCTCGCTCCTCTGCTGAAAG3'
*van*B capture probe	5'CGACAATCAAATCATCCTCG3'
vanC_1 capture probe	5'CCGCTATGAAAACGATCCTG3'
vanC_2/C_3 capture probe	5'CACCTGCGTTGAAGAAATCG3'
E. faecium capture probe	5'GGAAGTGATGCTTCCTACTG3'
E. faecalis capture probe	5'CCGCGTTCTCTCTCTAAATC3'

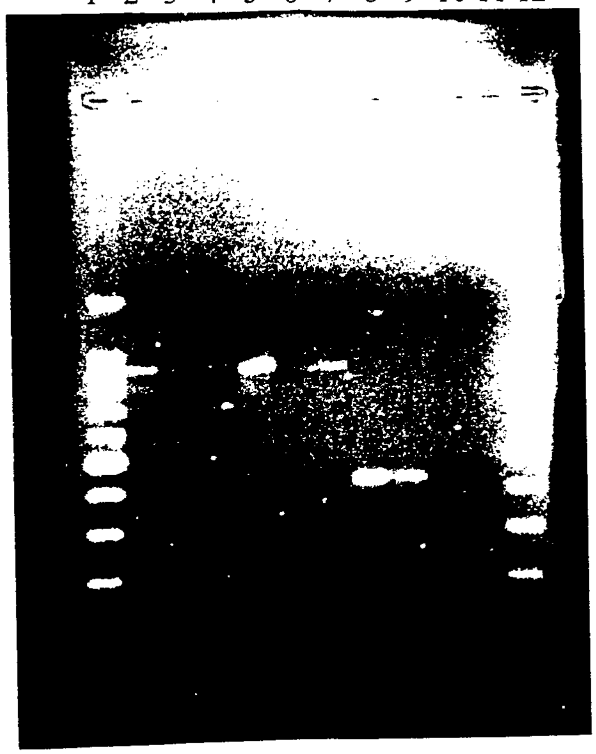

Figure 1. Ethidium bromide-stained gel of PCR products from urine samples. The samples were loaded into a 50 ml 1.1% agarose gel in 0.5X TBE buffer, and the gel (Hoefer mini-gel) was electrophoresed for 75 min at 80 V. The gel was then photographed and also analyzed by the GelDoc system (BioRad). Lanes 1 and 12, 100 bp molecular weight markers (Promega). Lanes 2-4, PCR products of DNA from strain E1 using *van*A primers, from 1×10^7 CFU/ml urine for lane 2, 1×10^6 CFU/ml for lane 3, and 1×10^5 CFU/ml for lane 4. Lanes 5-7, PCR products of DNA from strain E2 using *van*B primers, from 1.1×10^7 CFU/ml urine for lane 5, 1.1×10^6 CFU/ml for lane 6, and 1.1×10^5 CFU/ml for lane 7. Lanes 8-10, PCR products of DNA from strain E9 using *van*C_2 primers, from 8×10^6 CFU/ml urine for lane 8, 8×10^5 CFU/ml for lane 9, and 8×10^4 CFU/ml for lane 10. Lane 11, PCR products from strain E15 (vancomycin sensitive control) using *van*C_2 primers, from 2×10^5 CFU/ml urine.

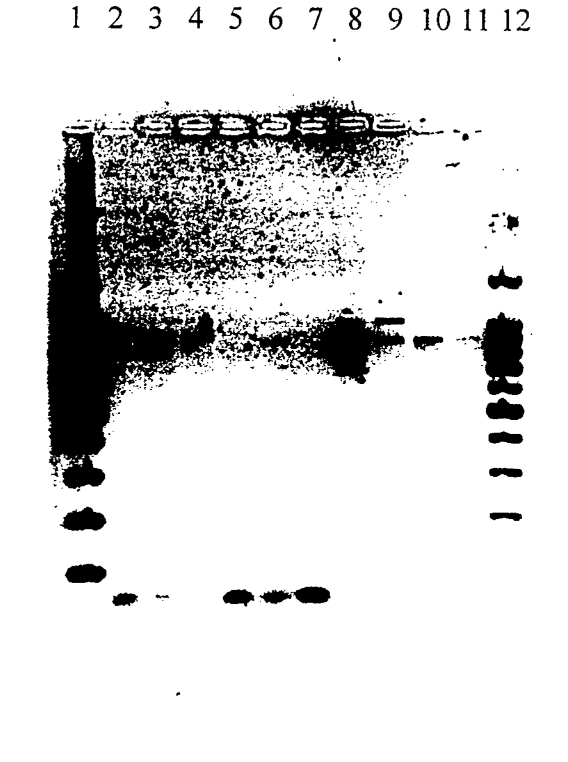

Figure 2. Ethidium bromide-stained gel of PCR products from urine and blood samples. Samples were analyzed as described in the legend to Fig. 1. Lanes 1 and 12, 100 bp molecular weight markers (Promega). Lanes 2-7, bacterial DNA isolated from urine samples, lanes 8-11, DNA isolated from blood samples. Lanes 2-4, PCR products of DNA from strain E1 using *van*A primers, from 7.6 x 10^3 CFU/ml urine for lane 2, 7.6 x 10^5 CFU/ml for lane 3, 7.6 x 10^4 CFU/ml for lane 4. Lanes 5-7, PCR products of DNA from strain E2 using *van*B primers, from 1 x 10^4 CFU/ml urine for lane 5, 1 x 10^6 CFU/ml for lane 6, and 1 x 10^5 CFU/ml for lane 7. Lanes 8-9, PCR products of DNA from strain E1 using *van*A primers, from 7.6 x 10^6 CFU/ml blood for lane 8 and from 7.6 x 10^4 CFU/ml for lane 9. Lanes 10-11, PCR products of DNA from strain E2 using *van*B primers, from 1 x 10^7 CFU/ml blood for lane 10 and from 1 x 10^5 CFU/ml for lane 11.

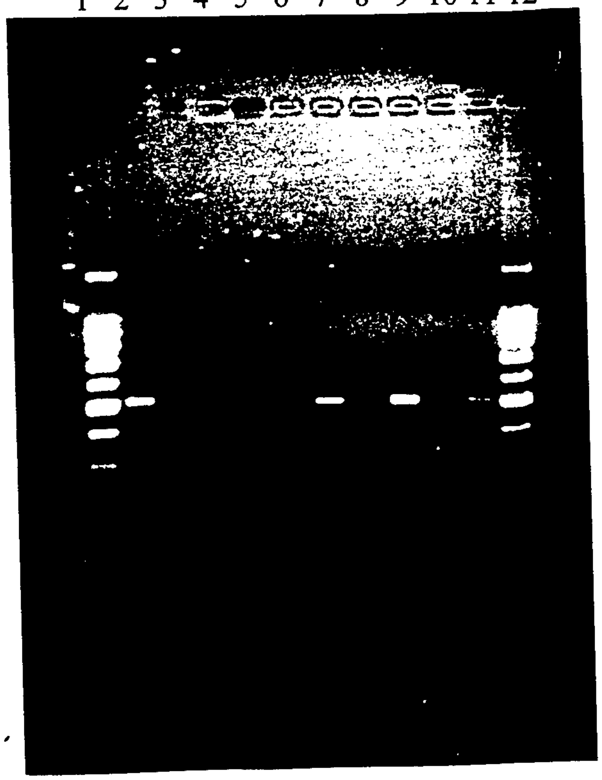

Figure 3. Ethidium bromide-stained gel of *E. faecalis*-specific PCR products from urine and blood samples. Samples were analyzed as described in the legend to Fig. 1. All PCR reactions were carried out with the *E. faecalis*-specific primers (Table 2). Lanes 1 and 12, 100 bp molecular weight markers. Lane 2, DNA from 152,000 CFU of strain E15 in blood. Lane 3, DNA from 1520 CFU of strain E15 in blood. Lane 4, DNA from 6080 CFU of strain E15 in blood. Lane 5, DNA from 76,000 CFU of strain E2 in blood. Lane 6, DNA from 76,000 CFU of strain E1 in blood. Lanes 5 and 6 are from *E. faecium* controls. Lane 7, DNA from 78,000 CFU of strain E15 in urine. Lane 8, DNA from 7800 CFU of strain E15 in urine. Lane 9, DNA from 203,000 CFU of strain E15 in urine. Lane 10, DNA from 7800 CFU of strain E15 in urine. Lane 11, DNA from 78,000 CFU of strain E15 in urine.

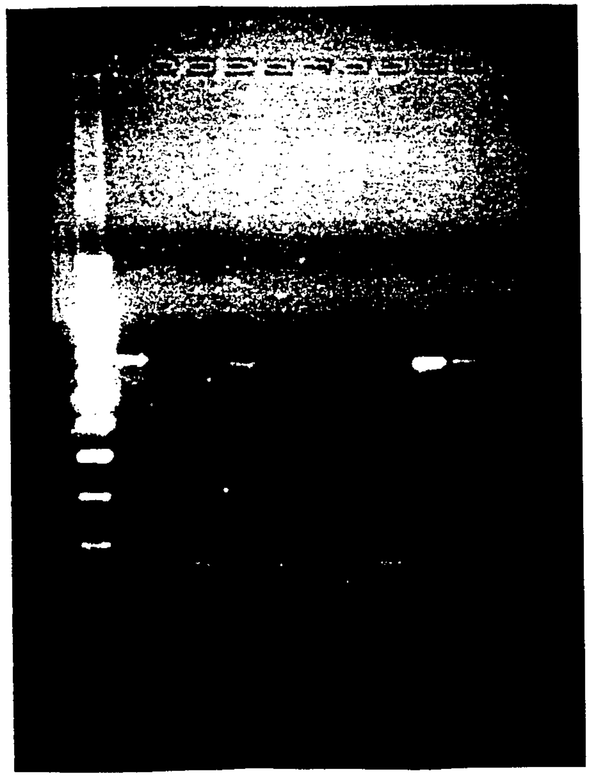

Figure 4. Ethidium bromide-stained gel of *E. faecium*-specific PCR products from urine and blood samples. Samples were analyzed as described in the legend to Fig. 1. All reactions were carried out using the *E. faecium*-specific primers (Table 2). Lane 1, 100 bp molecular weight markers. Lane 2, DNA from 76,000 CFU of strain E1 in blood. Lane 3, DNA from 760 CFU of strain E1 in blood. Lane 4, DNA from 9800 CFU of strain E2 in urine. Lane 5, DNA from 98,000 CFU of strain E2 in urine. Lane 6, DNA from 9800 CFU of strain E2 in urine. Lane 7, DNA from 110,000 CFU of strain E1 in urine. Lane 8, DNA from 170,000 CFU of strain E7 in urine. Lane 9, DNA from 7800 CFU of strain E15 (*E. faecalis* control) in urine. Lane 10, DNA from 2,000,000 CFU of strain E6 in urine. Lane 11, DNA from 200,000 CFU of strain E6 in urine. Lane 12, DNA from 1,700,000 CFU of strain E7 in urine.

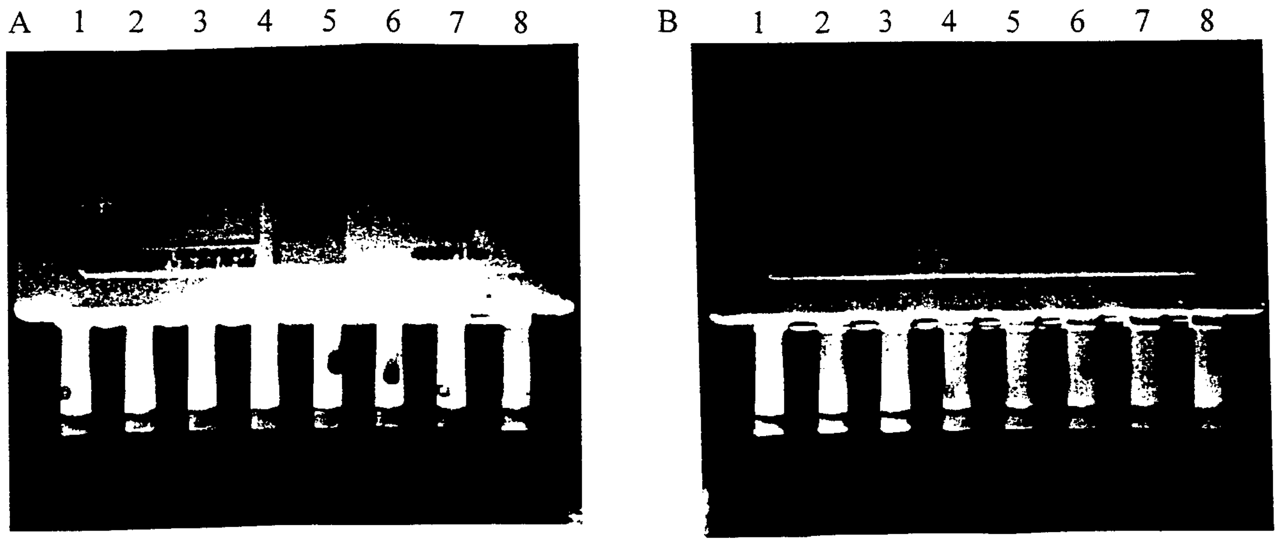

Figure 5. GeneComb analysis of PCR amplicons. Aliquots of selected PCR amplicons were analyzed on GeneCombs as described in the text. After development, the combs were photographed using the GelDoc system. Panel A, PCR products using purified DNA from bacterial cultures. For wells 1-4, *van*A, *van*B and *van*C_1 were used as capture probes, loaded in a diagonal from bottom left to top right, respectively. For wells 5 and 6, *van*A, *van*C_1, and *van* C_2 were used as capture probes, loaded as described. For well 7, *E. faecalis* and *E. faecium* capture probes were used. Well 1, E1 DNA; well 2, E5 DNA; well 3, E4 DNA; well 4, E4 DNA; well 5, E9 DNA; well 6, E11 DNA; well 7, E5 DNA; well 8, kit control. Panel B, PCR products using bacterial DNA recovered from urine. For wells 1-4, *van*A and *van*B capture probes were used (left to right); for wells 5-7, *van*C_1 and *van*C_2 capture probes were used. Well 1, E1 DNA from 1 x 10^7 CFU/ml urine; well 2, E1 DNA from 1 x 10^5 CFU/ml urine. Well 3, E2 DNA from 1.1 x 10^7 CFU/ml urine; well 4, E2 DNA from 1.1 x 10^5 CFU/ml urine. Well 5, E9 DNA from 7.9 x 10^6 CFU/ml; well 6, E9 DNA from 7.9 x 10^4 CFU/ml urine. Well 7, E11 DNA from 1.7 x 10^6 CFU/ml urine. Well 8, kit control which should only give a spot at the upper right, as observed.

Conclusion

This report describes a method for rapid isolation of *Enterococcus* DNA from urine or blood samples, with DNA ready for PCR in about 1 hour without the need for time-consuming extractions and precipitation. We have used DNA recovered by this method to identify by PCR the presence of *van*A, *van*B and *van*C_2 genes in various isolates, and to distinguish between *E. faecalis* and *E. faecium* species. The PCR reactions require about 3 hours, and agarose gel electrophoresis requires an additional 1.5 hours. Thus the total time for diagnosis of the presence of one of these two species and/or *van* genes is less than 6 hours. As only 10 μl of blood is transferred into 1 ml water for isolation of bacterial DNA, this results in a further dilution of 1:100, meaning that PCR products are obtained from a blood sample (10 μl) containing 760 CFU for E1 or 1000 CFU for E2. This illustrates the usefulness of the InstaGene method for preparation of template DNA and the sensitivity of the PCR. However, not all strains gave equally good results, and additional work needs to be done to standardize this procedure in order to get more consistent results. PCR products were also analyzed by the GeneComb™ (24), but the level of sensitivity was less than observed in agarose gels. In most cases only faint spots appeared on the combs. There appears to be some difference in sensitivity depending on the capture probe used, as the *van*C capture probes generally gave much stronger signals although there was less noticeable difference when the PCR products were analyzed in agarose gels. Further efforts may be warranted to determine whether the sensitivity of the GeneComb can be increased. This would allow rapid non-gel detection of the PCR amplicons. Alternatively, PCR amplification using the Idaho Technologies Light Cycler™ using DNA purified by the InstaGene method would allow very rapid determination of the presence of these sequences in blood or

urine samples. The ability to very rapidly identify the presence of *Enterococcus* species and vancomycin resistance genes should provide doctors the information they need to select specific therapy for bacterial infections, and prevent the use of vancomycin for the treatment of resistant bacteria, which contributes to the spread of these resistant organisms. This same approach may also be applicable to other antibiotic resistance genes in other species of pathogens.

References

1. Arthur, M., Molinas, C., Depardieu, F., Courvalin, P. 1993. Characterization of Tn*1546*, a Tn*3*-related transposon conferring glycopeptide resistance by synthesis of depsipeptide peptidoglycan precursors in *Enterococcus faecium* BM4147. J. Bact. 175:117-127.

2. Bager, F., Madsen, M., Christensen, J., Aarestrup, F.M. 1997. Avoparcin used as a growth promoter is associated with the occurrence of vancomycin-resistant *Enterococcus faecium* on Danish poultry and pig farms. Prev. Vet. Med. 31:95-112.

3. Centers for Disease Control and Prevention. 1997. Reduced susceptibility of *Staphyloccus aureus* to vancomycin-Japan, 1996. Morbid. Mortal. Weekly Rep. 46:624-626.

4. Centers for Disease Control and Prevention. 1997. *Staphylococcus aureus* with reduced susceptibility to vancomycin-United States, 1997. Morbid. Mortal. Weekly Rep. 46:765-766.

5. Centers for Disease Control and Prevention. 1993. Nosocomial enterococci resistant to vancomycin-United States, 1989-1993. Morbid. Mortal. Weekly Rep. 42:597-599.

6. Cheng, S., McCleskey, F.K., Gress, M.J., Petroziello, J.M., Liu, R., Namdari, H., Beninga, K., Salmen, A., delVecchio, V.G. 1997. A PCR assay for identification of *Enterococcus faecium*. J. Clin. Microbiol. 35:1248-1250.

7. Dutka-Malen, S., Evers, S., Courvalin, P. 1995. Detection of glycopeptide resistance genotypes and identification to the species level of clinically relevant enterococci by PCR. J. Clin. Microbiol.33:24-27.

8. Dutka-Malen, S., Molinas, C., Arthuir, M., Courvalin, P. 1990. The VanA glycopeptide resistance protein is related to D-alanyl-D-alanine ligase cell wall biosynthesis enzymes. Mol. Gen. Genet. 224:364-372.

9. Dutka-Malen, S., Molinas, C., Arthur, M., Courvalin, P. 1992. Sequence of the vanC gene of *Enterococcus gallinarum* BM4174 encoding a D-alanine:D-alanine ligase-related protein necessary for vancomycin resistance. Gene 112:53-58.

10. Gordon, S., Swenson, J.M., Hill, B.C., Pigott, N.E., Facklam, R.R., Cooksey, R.C., Thornsberry, C., Enterococcal Study Group, Jarvis, W.R., Tenover, F.C. 1992. Antimicrobial susceptibility patterns of common and unusual species of enterococci causing infections in the United States. J. Clin. Microbiol. 30:2373-2378.

11. Gray, J.W., Steward, D., Pedler, S.J. 1991. Species identification and antibiotic susceptibility testing of enterococci isolated from hospitalized patients. Antimicrob. Agents Chemother. 35:1943-1945.

12. Leclercq, R., Derlot, E., Duval, J., Courvalin,P. 1988. Plasmid-mediated resistance to vancomycin and teicoplanin in *Enterococcus faecium*. N. Engl. J. Med. 319:157-161.

13. Livornese, L.L.Jr., Dias, S., Samel, C., Romanowski, B., Taylor, S., May, P., Pitsakis, P., Woods, G., Kaye, D., Levinson, M.E., Johnson, C.C. 1992. Hospital-acquired infection with vancomycin-resistant *Enterococcus faecium* transmitted by electronic thermometers. Ann. Intern. Med. 117:112-116.

14. Marshall, C.G., Broadhead, G., Leskiw, B.K., Wright, G.D. 1997. D-ala-D-ala ligases from glycopeptide antibiotic-producing organisms are highly homologous to the enterococcal vancomycin-resistance ligases VanA and VanB. Proc. Natl. Acad. Sci. USA 94:6480-6483.

15. McDonald, L.C., Kuehnert, M.J., Tenover, F.C., Jarvis, W.R. 1997. Vancomycin-resistant enterococci outside the health-care setting: Prevalence, sources, and public health implications. Emerg. Infect. Dis. 3:311-317.

16. Miele, A., Bandera, M., Goldstein, B.P. 1995. Use of primers selective for vancomycin resistance genes to determine van genotype in enterococci and to study gene organization in vanA isolates. Antimicrob. Agents Chemother. 39:1772-1778.

17. Navarro,F., Courvalin, P. 1994. Analysis of genes encoding D-alanine-D-alanine ligase-related enzymes in *Enterococcus casseliflavus* and *Enterococcus flavescens*. Antimicrob. Agents Chemother. 38:1788-1793.

18. Noble, W.C. 1997. Antibiotic resistance in the staphylococci. Science Progress 80:5-20.

19. Noskin, G.A. 1997. Vancomycin-resistant enterococci: clinical, microbiologic, and epidemiologic features. J. Lab. Clin. Med. 130:14-20.

20. Patel, R., Uhl, J.R., Kohner, P., Hopkins, M.K., Cockerill III, F.R. 1997. Multiplex PCR detection of *van*A, *van*B, *van*C-1, and *van*C-2/3 genes in Enterococci. J. Clin. Microbiol. 35:703-707.

21. Quintiliani, R., Evers, S., Courvalin, P. 1993. The *van*B gene confers various levels of self-tranferable resistance to vancomycin in enterococci. J. Infect. Dis. 167:1220-1223.

22. Salyers, A.A., Whitt, D.D. 1994. Bacterial Pathogenesis: a Molecular Approach. American Society for Microbiology Press, Washington, D.C., pp. 97-109.

23. Satake, S., Clark, N., Rimland, D., Nolte, F.S., Tenover, F.C. 1997. Detection of vancomycin-resistant enterococci in fecal samples by PCR. J. Clin. Micro. 35:2325-2330.

24. Shaw, J.J., Ramaika, C.A., Hawkins, L.K., Wu, S.J., Beninga, K., McCleskey, F., DelVecchio, V. 1997. Non-gel detection of PCR amplicons diagnostic of *E. coli* O157:H7. Molecular Diagnostics Newsletter (BioRad) 2:1,5-7.

25. Shay, D.K., Maloney, S.A., Montecalvo, M., Banerjee, S., Wormser, G.P., Arduino, M.J., Bland, L.A., Jarvis, W.R. 1995. Epidemiology and mortality risk of vancomycin-resistant enterococcal bloodstream infections. J. Infect. Dis. 172:993-1000.

26. Uttley, A.H., George, R.C., Naidoo, J., Woodford, N., Johnson, A.P., Collins, C.H., Gilfillan, A.J., Fitch, L.E., Heptonstall, J. 1989. High-level vancomycin-resistant enterococci causing hospital infections. Epidemiol. Infect. 103:173-181.

GROUP DIFFERENCES IN PERCEIVED IMPORTANCE OF SWAT WORKLOAD DIMENSIONS: EFFECTS ON JUDGMENT AND PERFORMANCE IN A VIRTUAL HIGH WORKLOAD ENVIRONMENT

Thomas E. Nygren
Associate Professor
Department of Psychology

Ohio State University
1885 Neil Avenue Mall
Columbus, OH 43210

Final Report for:
Summer Faculty Research Program
Armstrong Laboratory

Sponsored by:
Air Force Office of Scientific Research
Bolling Air Force Base, DC

and

Armstrong Laboratory

August 1997

GROUP DIFFERENCES IN PERCEIVED IMPORTANCE OF SWAT WORKLOAD DIMENSIONS: EFFECTS ON JUDGMENT AND PERFORMANCE IN A VIRTUAL HIGH WORKLOAD ENVIRONMENT

Thomas E. Nygren
Associate Professor
Department of Psychology
Ohio State University

Abstract

The Subjective Workload Assessment Technique (SWAT) is a numerical conjoint scaling procedure that is used to construct estimates of workload scales for individuals or groups and importance estimates of time load, effort load, and stress load in determining workload. SWAT scales were constructed for 124 individuals who were found to fit one of six "workload prototype" groups on the basis of a cluster analysis of their importance weights. Individuals were then placed into three different virtual environment scenarios for which the task had either a high time, high mental effort, or high stress load component, respectively. Workload judgments and performance scores were obtained for each scenario. Results indicated that how individuals weighted the dimensions of workload (i.e., what prototype groups they were associated with) affected different reactions to each scenario on both their judged workload for the scenarios and on their performance measures. Implications for the use of separate workload prototype groups in workload research are discussed.

GROUP DIFFERENCES IN PERCEIVED IMPORTANCE OF SWAT WORKLOAD DIMENSIONS: EFFECTS ON JUDGMENT AND PERFORMANCE IN A VIRTUAL HIGH WORKLOAD ENVIRONMENT

Thomas E. Nygren

Introduction

Cognitive engineering research, particularly in the field of aviation, has rendered cognitive workload an important psychological concept. A better understanding of the modern concept of mental workload developed as an outgrowth of a significant increase in the use of technology in work environments, especially computer-based systems, and the demands this technology places on users of these systems. As mental tasks required of a human operator increase, the workload experienced to maintain an acceptable level of performance also increases. However, the outward appearance of an increase in workload is difficult to assess because the individual works harder to maintain acceptable performance levels (Gopher & Donchin, 1986). From a performance perspective although it may appear that everything is fine, the individual may be working at his or her limit. A number of measures of workload including subjective measures have been proposed in recent years to assess the practical implications of this issue (see Hancock & Meshkati, 1988).

Because of their ease of implementation, non-intrusiveness, and sensitivity, subjective workload measures have been used extensively to assess operator workload (Moray, 1982; Hancock & Meshkati, 1988). One such measure based on formal conjoint measurement theory is the Subjective Workload Assessment Technique (SWAT) which was developed to measure perceived workload as a multidimensional construct (Reid & Nygren, 1988). In the application of SWAT, mental workload is composed of three psychologically independent components: perceived Time load, Mental Effort load, and Psychological Stress load with constructed levels of each factor corresponding approximately to low, medium, or high demand. In forming an overall mental workload

scale based on SWAT, raters first provide an ordinal ranking (i.e., a card sort) to twenty-seven combinations formed from the 3x3x3, Time load x Effort load x Stress load design. In the model/measurement validation phase of the SWAT procedure, individual or group rank order data from these twenty-seven combinations are submitted to five axiom tests that are necessary for an additive conjoint scale, the most diagnostic of which are single-factor and joint-factor independence (see Nygren, 1985). If the conditions of additive conjoint measurement are met, the nonmetric conjoint scaling phase of SWAT can then be used to simultaneously obtain scale values for the levels of each factor and for the overall additive workload scale. Once this scale has been obtained, subsequent applications of SWAT can be done where component ratings are given to a task or set of tasks (labeled "event scoring"), and an overall workload score can be found using the derived one-dimensional scale (Reid & Nygren, 1988). As a partial validation of the SWAT methodology, past research has shown that Time load, Mental Effort load, and Psychological Stress load do not significantly co-vary and can be viewed as three independent dimensions of workload (Hart, Sellers, & Guthart, 1984).

SWAT, then, requires that people act as their own "workload meters" by indicating the amount of work they are experiencing during a task. This suggests that individual differences are not only accommodated by the model but are expected. In fact, the scale construction phase in SWAT is not only used to obtain an individual's overall workload scale but also to indirectly estimate how that person weights each dimension as contributing to overall workload.

Although in applications of SWAT the conjoint analysis procedure allows for a separate SWAT scale to be used for each individual, this method is rarely employed for several reasons. No significant data reduction is afforded by constructing individual scales, and, in practice, individual scaling solutions do not necessarily fit the model better than a group scaling solution based on a homogeneous group of individuals. This is because it is difficult to expect individuals to give rankings that perfectly conform to an additive model, but a group scaling solution from a homogeneous group of individuals will tend to average out minor deviations from additivity. However, there is a potential

practical tradeoff in that an overall group scaling solution that is too global or heterogeneous will tend to obscure individual or subgroup differences in the weightings of the dimensions and will produce a workload scale that may be representative of no one.

Group Prototyping

In order to gain the strength and stability of group scales and to minimize potential weaknesses of individual scales, six general SWAT "prototype groups" which represent perfect data with consistent weightings on the time, effort and stress dimensions were originally suggested by Reid, Eggemeier, and Nygren (1982). These six prototype groups were formed by considering the SWAT dimensions to be arranged in a dominant manner where one component of workload is always perceived as the most important contributor, a second component as the next largest contributor, and the last component as consistently contributing the least to overall workload. The six natural Time-Effort-Stress prototype groups suggested by Reid et al. (1982) as a means of classification were $T > E > S$, $T > S > E$, $E > T > S$, $E > S > T$, $S > E > T$, and $S > T > E$.

In the current version of SWAT individuals can be placed into these prototype groups on the basis of the maximum correlation between their actual rank order data and the rank order of each prototype. Reid et al. (1982) argued that using scales from these prototype groups instead of a scale from an overall averaged sample should provide better detection of small changes in workload.

There are, however, other unexplored natural possibilities for grouping individuals than the six ordered prototype groups suggested by Reid et al. (1982). These six assume that the rankings will be strictly hierarchical, but this may not accurately represent how some people view workload. It is possible that two dimensions of workload could be seen as essentially equal with the third dimension being much higher or lower ($T \approx E > S$, $T \approx S > E$, $E \approx S > T$, $T > E \approx S$, $E > T \approx S$, $S > T \approx E$), or that each dimension is viewed as equally contributing to overall workload ($T \approx E \approx S$). An initial goal of this study was to first see if individuals do fall into any of these natural groupings making prototyping a useful data reduction technique.

However, even if homogeneous prototype groups were to be found there is still the question of whether there is a practical usefulness to identifying and separating out groups who might perceive and react to workload quite differently. Although prototyping, much like market segmentation in consumer research, seems intuitively reasonable it has not been specifically examined in the workload literature. In predicting workload for a task, does it really matter how individuals actually weight the component dimensions? For example, it seems plausible but has not been demonstrated that persons who emphasize time demands in assessing overall workload would either assess workload differently or would perform differently in a high time load environment than would persons who emphasize either mental effort or psychological stress in their workload evaluations. The present study was designed to examine this issue by creating three distinct virtual workload environments that had either a high time load, a high mental effort load, or a high psychological stress load component, respectively. Then, in conjunction with the prototyping information, individuals whom we hoped to identify as placing differential weights on the three dimensions of workload were placed in each of these virtual environments and their performance observed.

Workload Prototypes and Performance

Surprisingly, workload prototype groups have also not been used previously in workload research to assess performance differences across individuals even though there are clear theoretical and practical relationships between overall workload and performance. The strength of the workload/performance relationship is known to vary in accordance with the amount of operator workload that is required and this relationship had been proposed as shown in Figure 1. At a low to moderate level of operator workload, acceptable performance levels can be maintained because the individual has spare information-processing capacity. In looking for potential overload in this region, subjective workload measures are often more sensitive than are performance measures. As workload increases, however, the ability to compensate is eventually exceeded and performance degradation begins to occur, gradually at first but increasing dramatically after this initial stage. The complex, non-linear functional relationship shown in Figure 1

is often cited as a major reason for observed dissociation between workload and performance measures. The thick vertical line in the top part of Figure 1 represents what Reid and Colle (1988) have labeled the "red line" -- the point at which workload is sufficient to begin to degrade performance. In their review of a number of studies where both SWAT and performance measures were obtained, they found that a SWAT score region of 40 ± 10 describes this red line in many applications. As Figure 1 illustrates, we attempted in this study to develop three virtual environments where the levels of time demands, mental effort demands, and stress demands, respectively, were sufficient to place workload levels just above this region, but not so far as to completely degrade performance.

Figure 1 clearly indicates why a consistent observable linear association between workload and performance is not always expected to exist. We hypothesize, however, that individual and group differences in the perceived importance of workload dimensions lead to another factor that may enhance or degrade the strength of association between perceived workload and performance. We suggest that the extent to which the time, mental effort, and stress load components of a workload environment conform with the individual's or group's own perception of the importance of these dimensions may relate to how perceived workload and performance associate. That is, suppose that two individuals' SWAT judgments of workload indicate that they fit two very different workload prototypes -- one individual weights Time load as very important and the other gives it very little weight. Suppose further that each individual is placed in an environment with high but not excessive time demands. If, in fact, the way an individual thinks about and orders the components of workload is relevant to performance in the environment (i.e., some kind of prototyping of individuals is meaningful), then the following implications are offered. For individuals who are placed in an environment where the workload components are consistent with the way they view workload (e.g., a time-important person is placed on a high time demand task), then we might expect these individuals to be more compatible with this environment and more easily able to compensate for increased time demands. Thus degradations in performance due to

increased time demands might not be reflected by comparable increases in evaluations of workload. For these individuals the dissociation between perceived workload and performance would be expected to be enhanced. For an individual whose view of workload is more inconsistent with the actual component workload levels of the environment, however, attempting to maintain performance levels on the task may be more difficult and the individual would be more cognizant of increases in perceived workload, and a greater association between workload and performance would be expected.

In order to test this hypothesis as a partial explanation of the dissociation between workload and performance measures, we needed to use a "real-world" multidimensional task where time load, mental effort load, and psychological stress load demands could be independently manipulated in a satisfactory way. At the same time we wanted to minimize any requirement of extensive training associated with such a "real world" task. A virtual environment computer program called 3D-World (3D-World, 1997) presents one such opportunity for examining workload effects in such a "real world" environment and requires little training. Three multidimensional tasks situated in virtual environments in 3D-World were designed to independently manipulate time, mental effort, and stress load. Subjects performed the 3D-World task in each environment and their perceived workload judgments and performance scores on a series of tasks in these environments were used to examine our hypotheses that different prototype groups would, in fact, perform in and evaluate the three workload environments differently.

Method

Participants. One hundred twenty-four introductory psychology students (73 females and 51 males) agreed to participate in partial fulfillment of a class requirement. Data from all 124 participants were used, but because of a problem in the stopping mechanism of the 3D-World program, only n = 120 had complete data in the time scenario, n = 114 in the effort scenario, and n = 110 in the stress scenario. All 124 participants, however, completed at least two of the three scenarios.

3D-World. The 3D-World computer program provided the virtual environment to manipulate workload. 3D-World is a computer program developed in the Cognitive Assessment Laboratory at Wright-Patterson Air Force Base to create virtual task environments which include hallways and rooms where an individual can virtually "walk". It has the capability of using sound and pop-up windows for giving additional information and instructions.

Any type of environment can be created in 3D-World; the basic environment created for this experiment simulated an office building. Offices and hallways were available for participants' exploration. The environments contained many familiar items associated with an office building, for example, a copy machine, filing cabinets, and desks. Each experimental environment had the same floor plan, however, rooms were not found in the same place between environments.

Procedure. The Subjective Workload Assessment Technique (SWAT) was used for workload scale development, to place people into workload prototype groups, and to rate the environments for subjective workload. (For a complete description of SWAT, see Reid & Nygren, 1988.) The card sort of the twenty-seven SWAT combinations was first completed to construct the individuals' workload scales. After completing the card sort, each student was seated at a computer and instructed to begin the experiment using 3D-World. Upon completion of the computer portion of the experiment, participants were given several inventories to complete and a questionnaire asking their opinions of the 3D-World task, and were then debriefed.

For the experiment, four scenarios were created: a training environment, and three environments to selectively emphasize each of the three SWAT workload dimensions. All participants received the same four scenarios within 3D-World with instructions simultaneously presented visually (on screen) and acoustically (through headphones). The training scenario was always presented first, the other three were randomly ordered. Participants were told that the training scenario was being completed so they could learn how to maneuver and how to complete the sub-tasks of making phone calls, scheduling appointments, making copies, retrieving files, and ordering from a menu.

For the three test scenarios participants were given the pretense that they were working for a temporary agency and would be working for a different company each "day" where a day corresponded to an experimental scenario. In the time-manipulated scenario (presented in the context of a doctor's office) participants were given less time to complete the tasks and were always informed of the amount of time they had to complete each subtask. In the effort-manipulated scenario (a lawyer's office), the information given to participants was more complex than the information given in the other scenarios. In the stress-manipulated scenario (a college advising office) computer malfunctions were inserted: The computer was programmed to freeze for a specified amount of time, and the computer took control of the person by turning them around or backing them up. Additionally, the people speaking to the participant within the scenario were not polite, and the items the participant had to retrieve (e.g. particular food from a menu or files from the filing room) were not necessarily available. In each scenario a counter was always present in the corner of the computer screen that indicated the number of seconds remaining for task completion. All of the subtasks (filing, phone calls, ordering from menu) were completed in every scenario, however the order of presentation and the difficulty varied between scenarios.

Results

In the 3x3x3 version of SWAT there are 324 individual axiom tests that can be examined for each of the critical single-factor and joint-factor independence axioms associated with the fundamental additivity assumption of the time, effort, and stress dimensions (108 tests for each factor, respectively). These initial axiom tests revealed that across the 124 subjects, additivity in the workload rankings was clearly supported. The median proportions of errors on the single-factor independence axiom were .074, .037, and .000 for the time, effort, and stress factors, respectively. Median proportions of errors on the joint-factor independence axiom were equally low, being .074 in each case for all three pairs of factors. These values are more impressive when one considers the fact that because each of the twenty-seven workload combinations is involved in multiple

independence tests for each factor or factor pair, a single simple reversal in the rank ordering will usually lead to a proportion of 8/108 = .074 errors. Although a formal hypothesis test of the difference between the observed error proportions and perfect additivity is neither possible nor meaningful, these values suggest that the median number of rank reversals in the subjects' workload data was approximately one, a value arguably well within a tolerance range for error.

Given this support for the additive SWAT model, we next wanted to ensure that our three 3D-World generated scenarios did manipulate time, effort, and stress demands respectively. Manipulation checks were made by examining overall workload judgments given to each of the three 3D-World scenarios. Wilcoxon signed rank tests revealed that raw SWAT ratings for the time, effort, and stress dimensions (e.g., a "1-2-2" or "3-2-3" for T-E-S, etc.) given by participants to the time-manipulated scenario were indeed significantly higher for time ratings than for both the effort ratings ($z = 4.738$, $p < 0.001$) and the stress ratings ($z = 1.870$, $p = 0.031$). Additional tests for the effort-manipulated and stress-manipulated scenarios revealed comparable successful manipulations; across participants in the effort scenario, effort ratings were significantly higher than both time ratings ($z = 5.509$, $p < 0.001$) and stress ratings ($z = 2.126$, $p = .017$), and in the stress scenario stress ratings were significantly higher than both time ratings ($z = 5.484$, $p < 0.001$) and effort ratings ($z = 5.779$, $p < 0.001$).

Derived SWAT workload scales with estimates of the weight or importance of each dimension were obtained for all 124 participants. As a further check of the validity of the three-dimensional additive model and the reliability of the dimension weights, a separate scaling with independent estimates of the weights was also obtained using Carroll's (1972) nonmetric multidimensional scaling procedure, MDPREF. Unlike the conjoint scaling algorithm in SWAT which attempts to fit an additive model to a known three-dimensional structure, MDPREF attempts to find the best fitting common solution in an n-dimensional space.

Three MDPREF dimensions were clearly indicated, accounting for 91.9% of the variance in the subjects' data; a fourth dimension improved the fit by only 1.4%. When

the MDPREF scaling solution was orthogonally rotated to congruity with the SWAT solution, very similar subject weights emerged from the separate analyses. Correlations between the two sets of weights suggest stability in the estimates, being .957, .955, and .964 for the time, effort, and stress dimensions, respectively. Both sets of weight estimates were independently used as input to several different clustering procedures including a hierarchical clustering algorithm based on Ward's method. In each case six clearly defined common clusters of subjects emerged. Table 1 shows these six clusters, our labels, and the respective mean weight estimates on the time, effort, and stress dimensions for both the SWAT and MDPREF scaling solutions. These six groups differ from the six generated prototypes of Reid et al. (1988) in that three groups are composed of individuals who heavily weight one of the dimensions and the other three have two or all three dimensions about equally weighted.

Table 1

Mean Estimated Weights on Time, Mental Effort, and Stress Dimensions from SWAT Scaling and MDPREF Scaling of Workload Rank Judgments

			SWAT Weights			MDPREF Weights		
Cluster Group	Label	N	Time	Effort	Stress	Time	Effort	Stress
Effort	E	15	.173	.601	.226	.249	.881	.338
Stress = Time	ST	17	.346	.252	.402	.604	.391	.674
Time > (Effort = Stress)	T*	21	.368	.322	.310	.652	.528	.523
Effort = Stress	ES	23	.268	.373	.359	.431	.636	.620
Stress	S	26	.213	.222	.565	.315	.326	.858
Time	T	22	.667	.216	.116	.921	.317	.170

Note: SWAT weights and MDPREF weights are not on the same scale and cannot be directly compared. SWAT weights are normalized to sum to 1.0; *squared* MDPREF weights are normalized to sum to 1.0.

Group Differences and SWAT Judgments. The SWAT event scores given by each participant to each scenario (e.g., 2-1-3) were converted to SWAT ratings (e.g., 72.2 on the 0.0 to 100.0 scale) based on either their own unique SWAT scaling solution (ISWAT), a common scaling solution for their cluster from Table 1 (CSWAT), or a common scaling solution based on their placement into either a simple time, effort, or stress-dominant prototype (PSWAT). Skewness and kurtosis values for these distributions of scores indicated rather severe deviations from normality and homogeneity of variance assumptions; hence, a nonparametric alternative to a mixed ANOVA design was deemed a more powerful and appropriate test for examining group differences.

For each of the three scenarios a separate K-sample median test was used to test our hypothesis that our cluster groups in Table 1 who weighted the workload dimensions very differently would subsequently judge the perceived workload in the three scenarios differently. For the time-manipulated scenario this was not the case; no group differences were found for either the ISWAT, PSWAT, or CSWAT ratings ($p > .20$ in each case). However, the overall median CSWAT rating for the time scenario was only 44.2 and ranged from just 32.9 to 52.9 for the six groups, suggesting with respect to the Reid and Colle (1988) "redline" in Figure 1 that the time manipulation may have been too weak. For the effort scenario the median rating was significantly higher than for the time scenario (58.1 with a range for groups of 45.4 to 69.7) and group differences were found for the CSWAT ratings ($\chi^2 = 10.981$, df=5, n=114, $p = .052$) but not for ISWAT or PSWAT ($p > .20$). Subjects in the Effort (E) cluster did have the highest median CSWAT rating for the effort scenario (69.7); subjects in the ES and T clusters had the lowest median ratings (45.4 and 51.2). For the stress scenario the median rating was 72.2 (group range of 65.2 to 90.2). Group differences were again found for the CSWAT ratings ($\chi^2 = 13.030$, df=5, n=110, $p = .023$) but not for ISWAT or PSWAT ($p > .20$). Subjects in the T and S clusters had the highest median CSWAT ratings (90.2 and 80.3); subjects in the ES cluster had the lowest median ratings (65.2).

Group Differences and Performance. Two performance measures were obtained from each scenario – the composite amount of time it took a subject to complete the relevant segments of each scenario, and the proportion of errors made by the subject in component subtasks of the scenarios. The error proportion score was a weighted average of error responses to several subtasks including the menu ordering task, the phone task, and the filing task. Because the scenarios has somewhat different subtasks of different durations, neither dependent measure could be meaningfully and directly compared across scenarios. Thus, group analyses were done on the measures for each scenario separately.

With respect to actual performance scores, no significant differences were found among the cluster groups in any of the three scenarios either for the time variable or the %-error measure. How individuals thought about workload dimensions did not affect their observed performance per se. However, Table 2 does show an important effect with respect to performance. Table 2 presents for each scenario the correlations between subjects' workload judgments and their performance scores for the two measures. SWAT judgments came from either CSWAT, ISWAT, or PSWAT estimates. Because the sample sizes in each cluster were too small to obtain stable correlation values for the analysis of each scenario, clusters were combined for these analyses such that subjects who placed either low or high weight on the comparable SWAT dimension were grouped together. For the time-manipulated scenario the E, ES, and S clusters were grouped as "low time-important" (n=62) and T, TS, and T* were grouped as high (n=58). For the effort scenario analysis the comparable low and high groups consisted of (TS, T*, T, S; n=79) and (E, ES; n=35) clusters. For the stress scenario they were (E, T*, T; n=50) and (TS, ES, S; n=60).

A similar pattern can be seen in Table 2 for all three scenarios and derived SWAT ratings, although the individual ISWAT data is weaker. For both the time and error measures there is typically a significant correlation between loss of performance and perceived increased workload for those individuals who place *low* importance on the dimension that corresponds to the one having high demand in the scenario.

Table 2

Correlations Between Workload Judgments and Performance Measures in Each Scenario for Those Who Weighted Time, Effort, and Stress Factors as Low or High in Importance

	Cluster SWAT Importance Group Low	Cluster SWAT Importance Group High	Individual SWAT Importance Group Low	Individual SWAT Importance Group High	Prototype SWAT Importance Group Low	Prototype SWAT Importance Group High
			Time Scenario			
Time on Task	0.253**	0.156	0.234*	0.129	0.279**	0.122
% Error	0.177	0.024	0.155	0.006	0.168	0.028
			Effort Scenario			
Time on Task	0.280**	0.186	0.220*	0.081	0.260**	0.149
% Error	0.234**	0.117	0.187	0.131	0.249**	0.120
			Stress Scenario			
Time on Task	0.269*	-0.260*	0.223*	-0.273**	0.306**	-0.267**
% Error	0.026	-0.057	0.070	-0.049	0.030	-0.041

Note: For "Time on Task" and "% Error" a positive correlation indicates that a high SWAT workload rating is associated with poorer performance.
$p < 0.10$, ** $p < 0.05$.

For example, in the scenario where effort demand is high there is a positive association between the low effort-important subjects' poorer performance and increased perceived workload. Individuals who weighted the corresponding dimension as high in importance do not show this trend; there is more of a dissociation between high perceived workload and poorer performance. In fact, in the stress scenario (where overall workload was rated highest of the three scenarios) high stress-important individuals actually tended to give lower workload ratings when they took more time to complete the task. Finally, it is interesting to note that the pattern for the %-error data was strongest in the effort scenario and weakest in the stress scenario. This is consistent in the sense that the subtasks where the error data were recorded were very mentally demanding in the effort scenario (e.g., remembering of items was required) but not at all demanding in the stress scenario.

Discussion

Although the SWAT workload scaling technique has been used extensively in applied research, the underlying additive model is usually assumed, not tested. The results from this study are encouraging in that they support the validation of the additive model in several respects. First, the very small number of independence violations in most subjects data suggests that the psychological independence of time, effort, and stress load in forming judgments of workload is substantiated. Second, this appears to be true regardless of large individual differences that were found in the weights that individuals place on the workload dimensions. Third, the consistency found in workload estimates and weights when comparing the derived scales obtained from the SWAT algorithm and the very different MDPREF nonmetric algorithm lends some support to the stability of these estimates.

One of the advantages that has often been stated for SWAT over other applied workload measures is that individual differences in the importance of the dimensions can be assessed and are meaningful. Much as applied marketing researchers have very successfully used other scaling techniques to identify and cluster consumers into market segments and have used this information to predict consumer preferences and choices, it has always been implicitly assumed, though untested, that SWAT has the capability to do the same for predicting performance behavior for workload prototype groups in complex workload environments. The results from this study lend at least some encouragement and credibility for this idea. Group differences from both the ratings analyses and the performance data suggest that a "segment identification" or prototyping of subjects has both theoretical and practical implications.

The different subjective workload estimates given to the three scenarios by individuals in the six clusters suggests that how an individual assesses workload may have a significant influence on workload judgments given in different environments. Our results suggest that individuals who weight a particular dimension as very important in determining overall workload are more likely to give a higher estimate of workload to a task or environment that is high on that same component of workload than are those who treat that dimension as less important. We found this relationship in the effort and stress scenarios,

but not in the time scenario. However, the time scenario was the one scenario for which we were least successful in manipulating a high workload level. It is quite possible that our time scenario was perceived as being uniformly low in workload for all subject groups, regardless of how they assessed it.

Our performance data has equally interesting implications. Our hypothesis that there is more likely to be a dissociation between perceived workload and performance by those whose view of workload is highly compatible with the actual level of the workload components in the environment was supported. When placed in an environment where the defining workload characteristics are similar to how they actually perceive workload (e.g., effort-important individuals in a high mental effort load environment), these individuals appear to be less likely to give workload judgments that are related to their actual performance. Individuals for whom there is an incompatibility between their view of workload and the workload environment appear to be more likely to give workload estimates that are consistent with their actual performance.

Finally, despite being a first attempt, the successful manipulation of the component dimensions of workload in the 3D-World environment suggests that this type of virtual environment simulation can be a very powerful tool in applied workload research. An issue with laboratory research has always been whether rigorous face-valid tasks can be constructed for which the time, mental effort, and psychological stress components of workload can be meaningfully and independently manipulated. Our work with the 3D-World environment suggests that they can and that they can lead to important insights into how actual workload levels, peoples' subjective evaluations of workload, and their performance are related.

Acknowledgments

Data for this study were collected by Susan Schnipke while she was a participant in the 1996-1997 Student Practicum Program at the Fitts Laboratory. The author is also indebted to Annette McCoy and Brian Porter for technical assistance with the 3D-World program.

References

3D-World [Computer software]. (1997). Dayton, Ohio: The Cognitive Assessment Laboratory, Wright-Patterson Air Force Base.

Carroll, J. D. (1972). Individual differences and multidimensional scaling. In: R. N. Shepard, A. K. Romney & S. Nerlove (Eds), *Multidimensional scaling: Theory and applications to the behavioral sciences, Vol. I.* New York: Academic Press.

Gopher, D., & Donchin, E. (1986). Workload - An examination of the concept. In K. R. Boff, L. Kaufman, & J. P. Thomas (Eds.), *Handbook of Perception and Human Performance.* New York: John Wiley and Sons.

Hancock, P., & Meshkati, N. (1988). *Human Mental Workload.* Amsterdam, The Netherlands: North Holland.

Hart, S. G., Sellers, J. J., & Guthart, G. (1984). The impact of response selection and response execution difficulty on the subjective experience of workload. *Proceedings of the Human Factors Society 28th Annual Meeting.* Pp. 732-736.

Moray, N. (1982). Subjective mental workload. *Human Factors, 24,* 25-40.

Nygren, T. E. (1985). An examination of conditional violations of axioms for additive conjoint measurement. *Applied Psychological Measurement, 9,* 249-264.

Reid, G. B., & Colle H. A. (1988). Critical SWAT values for predicting operator overload. *Proceedings of the Human Factors Society 32nd Annual Meeting.* Pp. 1414-1418.

Reid, G. B., Eggemeier, F. T., & Nygren, T. E. (1982). An individual differences approach to SWAT scale development. *Proceedings of the Human Factors Society 26th Annual Meeting.* Pp. 639-642.

Reid, G. B., & Nygren, T. E. (1988). The subjective workload assessment technique: a scaling procedure for measuring mental workload. In P. Hancock & N. Meshkati (Eds.), *Human Mental Workload.* Amsterdam, The Netherlands: North Holland.

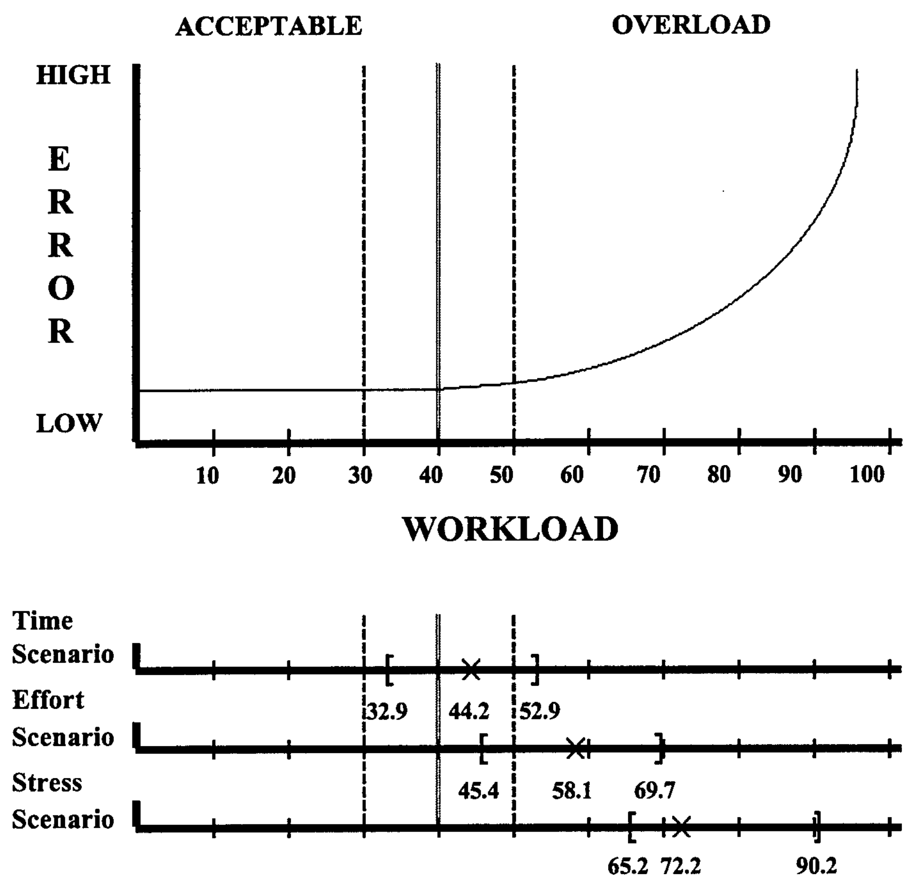

Figure 1. Theoretical relationship between SWAT workload judgments and performance with "redline" region suggested by Reid and Colle (1988). Ranges and overall median values of SWAT judgments across the six prototype cluster groups are shown for each scenario at the bottom of the figure.

Associate did not participate in the program.

ACCUMLATION OF STRONTIUM AND CALCIUM BY DIDEMNUM CONCHYLIATUM

Judy Ratliff
Associate Professor
Department of Chemistry

Murray State University
P. O. Box 9
Murray, KY 42071

Final Report for:
Summer Research Program
Armstrong Laboratory

Sponsored by:
Air Force Office of Scientific Research
Bolling Air Force Base, Washington, DC

And

Armstrong Laboratory

August 1997

ACCUMULATION OF STRONTIUM AND CALCIUM BY *DIDEMNUM CONCHYLIATUM*

Judy Ratliff
Assistant Professor
Department of Chemistry
Murray State University

Abstract

The average concentration of strontium in the ascidian *D. conchyliatum* was found to be greater than 4000 ppm having a calcium concentration around 250,000 ppm. The average ratio of calcium to strontium in this didemnid was 58:1. This ratio was smaller than any of the other samples analyzed. Other samples analyzed included varieties of shellfish, corals, sponges, solitary and colonial tunicates, echinoderms, etc. Since the samples analyzed were from the same area, all were presumably exposed to the same concentrations of strontium and calcium, the same temperature effects, and the same overall environmental conditions. From all of the samples analyzed, the dry weight concentration of strontium in this didemnid was always greater than that found in almost all of the other samples.

The samples which showed accumulated strontium concentrations closest to *D. conchyliatum* were barnacles whose concentrations were in the upper 3000 ppm's and a coral whose concentration of strontium was greater than 8000 ppm. The calcium concentration of the barnacles, similar to the strontium concentration, was equally large; 440,000 ppm. The average ratio of calcium to strontium for the barnacle was almost double that for *D. conchyliatum*, 116:1. The calcium concentration in the coral was also quite large, 579,872 ppm. The ratio of calcium to strontium for the coral was 71:1 which is higher than that measured for the didemnid being examined.

ACCUMULATION OF STRONTIUM AND CALCIUM BY *DIDEMNUM CONCHYLIATUM*

Judy Ratliff

Introduction

Previous studies involving tunicates collected off the coast of west Florida identified a tunicate, *Didemnum conchyliatum*, that is rich in strontium and calcium.[1] The aim of this study was to examine the strontium to calcium ratios of *D. conchyliatum* compared to those present in sea water, sea flora, and other calciferous species. Strontium is a coprecipitant with aragonite in skeletal or shelly materials since it has a similar ionic radius and valence compared to that of calcium (Calcium: 0.99 Å, Strontium: 1.13 Å). It is well known that in humans, strontium in both its stable and radioactive forms, is a bone seeking ion that readily exchanges for calcium in the apatite lattice of bones.[2] Increased strontium in the diet has been used to remineralize bone lesions or augment bone mass and has been found to provide a resistivity to dental caries.[3,4] Excessive amounts of strontium, however, can produce rickets.[5] Radioactive and stable strontium behave similarly in food chains.[6] Most plants indiscriminantly absorb strontium and other alkaline earth metals - calcium, barium, and magnesium - from the soil.[7,8] Terrestrial vertebrates discriminate against strontium in favor of calcium, since the proteins necessary for the transfer of ions across the intestinal mucosa have a lower affinity for strontium than for calcium.[9,10] This may indicate the fact that calcium is a more essential nutrient in vertebrate metabolism than strontium.[11,12,13] The essentialness of strontium in vertebrate metabolism is controversial. Although most investigators contend that strontium has no known independent metabolic function some argue that like calcium it aids in the formation and maintenance of bones, enamel, and dentin. It has been suggested that strontium is absorbed to the hydroxyapatite matrix of bone or is chemically incorporated into the mineral phase as a non-diffusible phosphate. Strontium deficiencies are reported to result in depressed growth, impaired mineralization of bones and teeth and high incidence of dental caries.[7,14]

Most authors in the literature reviewed believed that strontium to calcium (Sr/Ca) ratios decrease as one moves up the food chain. This makes sense since herbivores absorb only a small amount of the strontium available to them in the plants they consume. Carnivores incorporate even less strontium than herbivores because of both continued discrimination and reduced amounts of strontium in their diets.

Ascidians have been of interest to scientists for more than one hundred years because they were found to accumulate various metals at levels far above what is toxic to humans and most other species. The tunicate being studied lives in sea water, therefore, routes of uptake for calcium and strontium include uptake from solution and uptake from food. Average global ocean concentrations of strontium and calcium are, respectively, 6-8 ppm and 400 ppm in sea water. [15] Previous analysis of the ascidian *Didemnum conchyliatum* using inductively coupled plasma atomic emission spectrometry (ICP-AES) had indicated a concentration of strontium greater than 4000 ppm and a calcium concentration greater than 250,000 ppm. An ICP-AES scan of emission intensities for 72 elements in the tunicate sample compared to that of sea water indicated that the ascidian was accumulating vasts amounts of these two elements. Figure 1 shows the plot of the emission intensities for the elements scaned and is discussed later.

This project then focused on the source of the elevated concentrations of the Group IIA elements and how the ratio of calcium to strontium in this ascidian compares to that of other species. The Ca/Sr ratio is given throughout this study instead of the traditional Sr/Ca ratio since it provides the largest number due to the large concentrations of calcium and strontium being sampled.

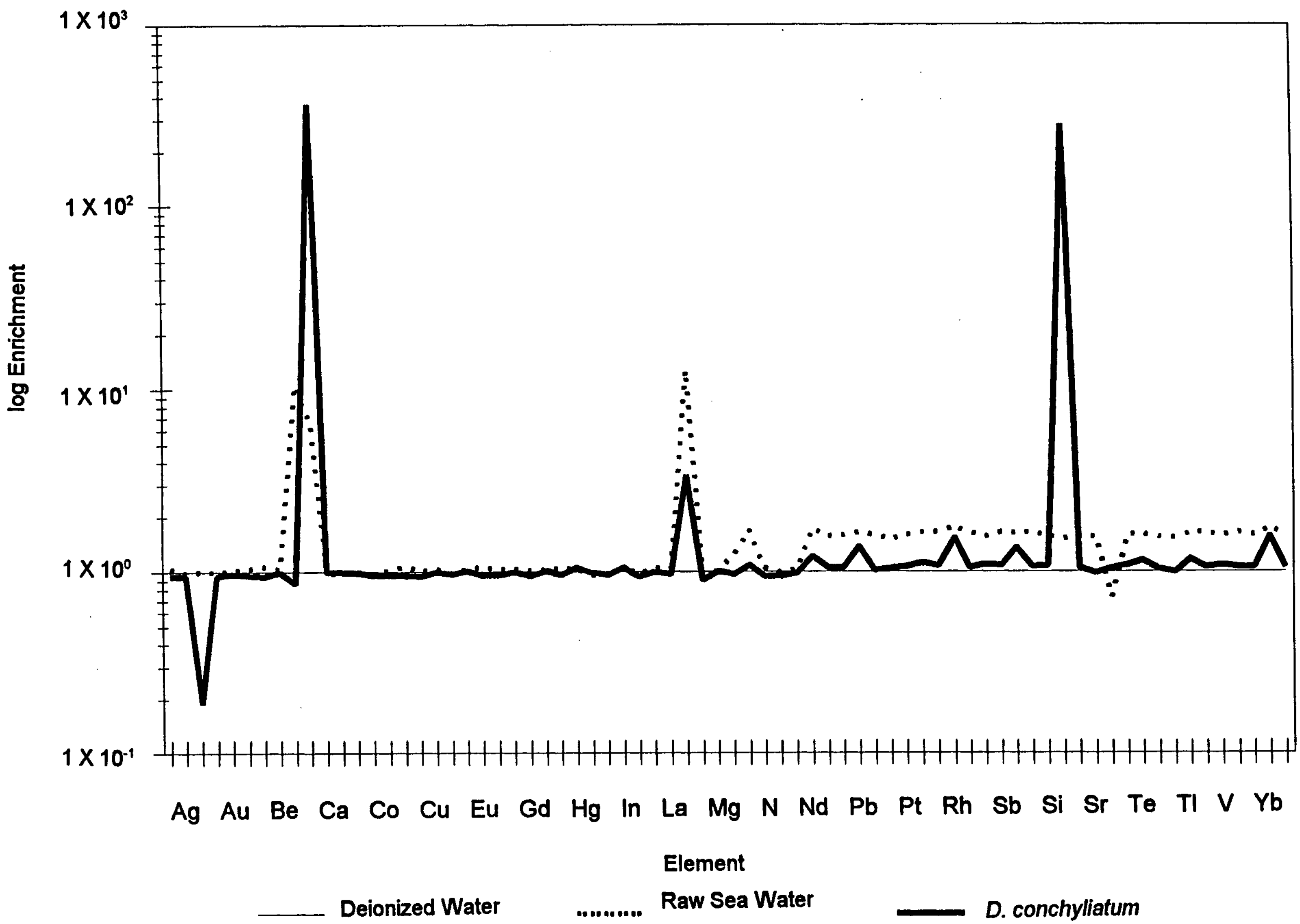

Figure 1: Emission intensities for species in the didemnid, *Didemnum conchyliatum*, compared to sea water and distilled/deionized water

Methodology

All samples analyzed were taken off the coast of west Florida from the Gulf of Mexico, St. Andrew Sound, and Wild Goose Lagoon. The shells were identified then analyzed on a Varian SpectrAA 600 (Varian Australia Pty. Ltd., Mulgrave Victoria, Australia).[16, 17] Standards were made from 1000 ppm stock solutions purchased from Fisher (Fisher Scientific, Fair Lawn, NJ).

As an improvement over the digestion technique used for tunicates previously (see AFOSR Summer 1996 Report by Ratliff) a microwave digestion was used. The microwave used was an Emerson (Model MW8665W) purchased from Wal-Mart. The digestion bombs were Parr Model 4781 Microwave Digestion Bombs (Parr Instrument Co., Moline, IL).[18] The new digestion technique used considerably fewer reagents, (2.5 mL of concentrated, trace metal grade nitric acid per sample) and did not damage the fume hood as refluxing in concentrated nitric and hydrochloric acids do. The procedure for digesting the tunicates is given on the next page.

Proper safety equipment and procedures should be followed throughout the use of the microwave digestion procedure. If a bomb is overloaded (contains more than 0.1 g of sample) the bomb will 'blow-up'. When the bomb blows up, the Teflon o-ring is simply blown out of the cap. The assembly itself will not disintegrate. When the o-ring blows out, it will quickly release pressure from the holes in the screw cap, generally this is directional and the sudden escape of gases will topple the bomb assembly and blow the door to the microwave open. Observers will hear a 'boom' and will observe a brown gas containing a variety of nitrogen oxides emanating from the microwave. If an explosion should occur, evacuate the immediate area for 10 minutes, if the microwave is being used in a hood - which is recommended, cleanup can begin immediately. The acid, some of which will have leaked out into the glass microwave turntable, should be neutralized and disposed of. The interior of the microwave should be neutralized, washed down, then dried. The bomb should be carefully opened and any spilled nitric acid on the bomb or Teflon liner neutralized and discarded. Clean the bomb assembly as specified in the operating instructions on the next page. Keep in mind that the bomb contains only 2.5 mL of concentrated acid so there will not be a tremendous amount of acid to clean up. As soon as you have properly cleaned up the spill, digestion of additional samples can resume.

Digestion of Tunicates Using Microwave Digestion Bombs:

1. Check the bomb and Teflon cup for damage. If either is damaged -DO NOT USE THEM. If the bomb or cup should become damaged it should be discarded.

2. Dry the tunicate samples at less than 100°C for 24 hours then cool for 1 hour in a desiccator.

3. Weigh out less than 0.1 g of the dry sample and place it into the Teflon cup.

4. Add 2.5 mL of concentrated, trace metal grade nitric acid to the Teflon cup.

5. Once all visible reactions have stopped in the cup between the sample and the acid, place the Teflon cap equipped with an O-ring on the Teflon cup.

6. Make sure the bottom disc is in the bomb with the flat side up then place the Teflon cup inside.

7. Put the bomb screw cap on and twist till it fits against the top of the Teflon cup then give it about 1/8 a turn more. Do not over tighten the bomb.

8. Heat the bomb in the microwave for 25 seconds then allow to cool in a hood for 30 minutes.

9. Once the bomb is cooled, carefully unscrew the top. This slowly releases any pressure that may have built up gradually. The Teflon cup can then be removed by placing a finger in the bottom hole of the bomb and pressing the bottom plate upward. Keep a finger on top of the cup cap, as this is done, to prevent pressure from blowing the cap off. If the cup is difficult to remove, it has not cooled sufficiently and should be allowed to cool 10 minutes more.

10. The sample is now ready to be diluted.

11. Rinse the Teflon cup and cap and the bomb after use but make sure all water has been removed before placing in the microwave again. If the bomb assembly needs to be cleaned, mild soap and water can be used but this must be rinsed with copious amounts of water and should be completely dry before it is used again.

Results

The Inductively Coupled Plasma (ICP) Scans provide a quick qualitative look at any sample examined. The scan simply records the emission intensity of each sample at the primary analytical wavelength for 72 elements. The initial ICP scan in Figure 1 shows increased emission intensity, indicating elevated concentrations, primarily from carbon, calcium, and magnesium in raw sea water. The emission intensities were compared by collecting raw signals from each sample than dividing each sample scan by the scan for the distilled-deionized water. The scan of the didemnid shows elevated concentrations of calcium, magnesium, and strontium. Interestingly, the calcium and strontium concentrations in the didemnid were greater than that of sea water but the magnesium concentration actually appeared to be depressed in the didemnid compared to sea water. This indicates that the didemnid, *Didemnum conchyliatum*, is selectively concentrating these two Group IIA metals. Subsequent quantitation of the Alkaline Earth metals in the didemnid confirmed that strontium and calcium are accumulated but magnesium and barium appear at lower concentrations than in sea water. Beryllium is typically present at 5.6×10^{-6} ppm in sea water, a concentration below the detection limits of the instruments being used in the analyses, so it was not examined. The depression of the arsenic in the didemnid as well as the depression of tellurium in the sea water is an artifact of the low emission signal detected for these elements at the wavelengths monitored. The variation in the background signal is being magnified to produce a signal since there was no detectable amount of either element present . A complete discussion of *D. conchyliatum* can be found in Ch. 10.[19]

To determine if the elevated levels of calcium and strontium originated in the tunic or the spicules of the tunicate, *D. conchyliatum*, an additional test was completed. Literature suggests that these spicules are composed entirely of calcium carbonate.[20] The tunic and the spicules were singled out as possible sources of the Group IIA metals because when the didemnid was placed in nitric acid, an immediate reaction occurred. The spicules were dissolved upon contact with the acid accompanied by profuse fizzing; spicules near the surface disappeared instantly whereas those imbedded deeper into the tunic dissolved more slowly and only upon prolonged contact with the acid. The tunic and the spicules could thus be separated easily. Electron micrographs of spicules present on *D. conchyliatum* found in the water systems surveyed are shown in Figure 2. These spicules are similar to those reported by Monniot *et al.*[20]

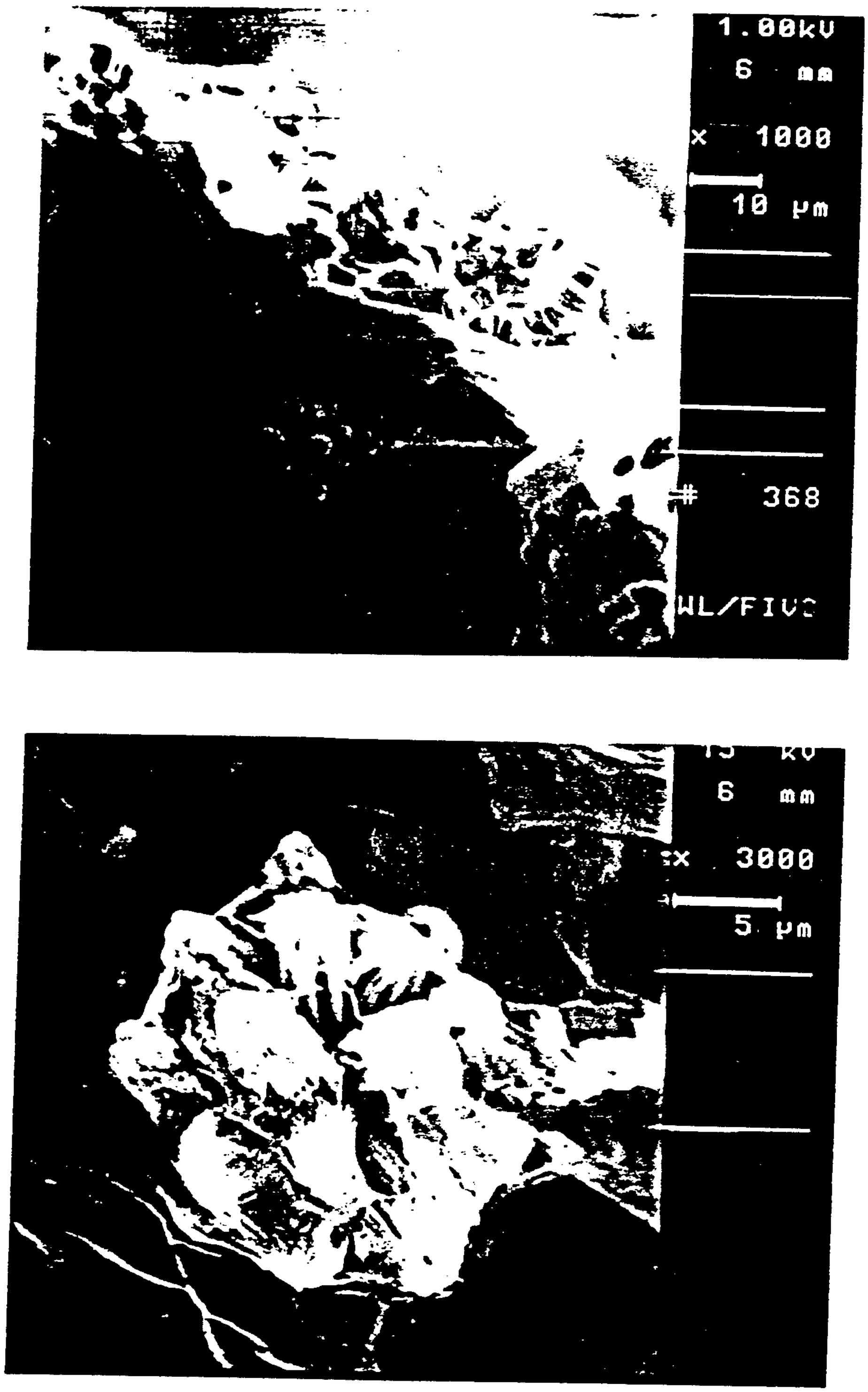

Figure 2: Electron micrographs of spicules from *Didemnum conchyliatum*. Courtesy of Dr. Bill Wallace, Applied Research Associates, Tyndall AFB, Panama City, FL.

In 1925 French biologist M. Pregnant suggested that spicules arise when $CaCO_3$ precipitates during a reaction of sea water with the serum of ascidian blood in the tunic.[20] He was successful in producing spicules in a test tube that contained a solid agar between two solutions of calcium and sodium salts. This experiment was duplicated and the results confirmed in 1970 by Monniot, Monniot, and Laboute.[20] The spicules produced were examined with an electron microscope and had shapes and sizes similar to *Didemnum* sp. spicules. These researchers then suggested the formation of the spicules occurred when blood serum 'leaked' out of the mantle and into the tunic.[20] After the spicules have begun to grow, further precipitation occurs. As the tunic grows spicules migrate throughout the tunic.[20]

A test was then designed to compare *D. conchyliatum* , which had a wealth of spicules, with an aspiculate didemnid, *Diplosoma macdonaldi*. Since *D. macdonaldi* had no spicules it was expected that the calcium and strontium concentrations in this sample would be nominal if indeed the Group IIA metals were concentrated in the spicules. The results of this analysis are shown in Table 1.

Sample	**[Sr] (ppm)**	**CV**	**[Ca] (ppm)**	**CV**	**Ca/Sr**
Sea Water, St. Andrew Bay	6.0	0.9	434.9	1.6	72
Didemnum conchyliatum	4504	1.2	264,805	1.6	59
Didemnum conchyliatum	4968	1.3	294,796	0.5	59
Diplosoma macdonaldi	16	14.8	20,695	1.8	1334
Diplosoma macdonaldi	13	12.6	13,595	2.9	1052

Table 1: Analysis of two different didemnids; one with spicules, *D. conchyliatum*, and one without, *D. macdonaldi*.

It can be clearly seen in Table 1 that the concentration of strontium and calcium in the didemnid that contains spicules is much greater than the aspiculate didemnid. Both didemnids exhibit greater concentrations of strontium and calcium than sea water. *D. macdonaldi* has only a slightly higher

concentration of strontium than sea water (approximately double what is typical of sea water in this area) but has a calcium concentration that is almost 50 times greater than sea water. *D. conchyliatum* has a strontium concentration that is about 800 times greater than sea water and a calcium concentration that is almost 800 times the concentration of sea water. Both tunicates were taken from St. Andrew Sound so they were probably exposed to the same environmental conditions as well as concentrations of calcium and strontium. This then suggests that the calcium and strontium are located primarily in the spicules of *D. conchyliatum.* An interesting observation here is that *D. macdonaldi* does appear to be accumulating calcium but not strontium.

To determine the variability of calcium and strontium in the didemnid, as well as determine the most efficient digestion time, several samples were analyzed and that data is summarized in Table 2. The average concentration of strontium was 4372 ± 350 and that of calcium was 254,871 ± 18,505. The coefficient of variation for the strontium and calcium are 8.00 and 7.26 respectively. This is actually quite good since the spicules are not regularly spaced within the tunic and once their growth has begun, they continue to grow as they migrate further from their points of origin. The spicules vary in size, indicative of their age and possibly other factors; this variation may account for the observed concentration variations.

Sample #	[Sr] ppm Dry Wt.	CV	[Ca] ppm Dry Wt.	CV	Digestion Time (s)	Ca/Sr
CIS 141 E1	4504.44	1.2	264804.72	1.6	50	58.78
CIS 141 E2	4968.24	1.3	294796.03	0.5	75	59.34
CIS 141 E3	4338.46	0.9	255399.00	1.1	75	58.87
CIS 141 E4	4921.53	0.8	276507.16	1.9	75	56.18
CIS 141 F2	4853.39	0.4	268756.30	1.1	75	55.37
CIS 141 F3	4276.16	1.2	242030.93	1.0	75	56.6
CIS 141 F4	4018.47	0.8	227245.29	1.0	75	56.55
CIS 141 H1	4023.45	0.2	237811.23	0.9	75	59.11
CIS 141 H2	4172.55	0.8	248151.14	1.0	75	59.47
CIS 141 H3	4189.43	1.2	254287.63	1.7	75	60.7
CIS 141 H4	4479.23	1.2	263132.01	0.7	75	58.74
CIS 141 H5	3789.24	1.0	227264.63	1.9	25	59.98
CIS 141 H6	4310.91	1.8	253139.57	1.7	25	58.72

Table 2: *Didemnum conchyliatum* samples analyzed for variability as well as digestion efficiency.

The most efficient digestion time for *D. conchyliatum*, using the Parr microwave digestion bombs appears to be one digestion cycle or 25 seconds. Each digestion period was followed by a thirty minute cooling period to allow pressures inside the bomb to subside to a safe handling level so the actual analysis time per sample is 30 minutes and 25 seconds. The lowest concentration of strontium was produced by one of the 25 second sample groups but was not repeated by the second sample group microwaved for that length of time. In fact, one of the 25 second sample groups reported a higher concentration of strontium than five of the 75 second sample groups. The lowest calcium concentration was reported by one of the 75 second sample groups, and the 25 second sample groups yielded calcium concentrations similar to those reported by the 50 and 75 second sample groups.

When comparing calcium concentration from a didemnid digested for 25 seconds to one digested for 75 seconds, Student's t of 2.56 was obtained, for 2 degrees of freedom, t-tabulated at the 95% confidence level is 4.303. Since the calculated t is less than the tabulated t at the 95% confidence level, the 2 results are considered to be the same. Student's t for samples digested for 50 seconds compared to 75 seconds was 2.68 which for 2 degrees of freedom is still less than the tabulated t so there was no significant difference here either. For strontium, Student's t for 25 and 50 seconds compared to 75 seconds was 0.45, once again, this is smaller than the tabulated t at the 95% confidence level so the different digestion times made no difference to the concentration of strontium or calcium detected.

The only visual difference between the digestion times was that after 25 seconds only the spicules seemed to be dissolved. After 50 seconds the tunic had been partially digested but there were still solid bits of tunic evident in the digestate. After 75 seconds, the digestate was completely clear and contained only occasionally a few sand grains which had apparently become embedded or incorporated into the tunic. Since the calcium and strontium concentrations were of primary interest here, and there was no significant difference, statistically, between 25 or 75 second digestion times, the most efficient procedure would digest for only 25 seconds. This also supports the theory that the strontium and calcium are located primarily in the spicules of *D. conchyliatum*.

The variation in the strontium and calcium concentrations is quite small as indicated by their coefficients of variation, both around 8.00. For biological samples, each having different numbers and sizes

of spicules, the agreement is actually quite remarkable. The calcium to strontium ratio for all ranged between 55-60. However, all of these samples were collected on the same day from the same general location and were probably part of the same colony. Samples were analyzed that had been collected then frozen from previous years which do differ slightly but all still contain high calcium and strontium concentrations and generally have calcium to strontium ratios less than 70.

Multiple bombs can be used, such as was employed in this study, to decrease sample analysis times. With two bombs, only 4 samples could be digested per hour but this is a great improvement compared to previous work.[1] With more bombs, 144 samples per hour could be digested. Since one sample can be digested every 25 seconds and there are 3600 seconds in one hour, 144 samples could be digested per hour if the appropriate number of digestion bombs were available.

Once the analysis of the didemnid was complete, the focus of the study then shifted to other calcium containing species living in the same water system as *D. conchyliatum.* Since shellfish and other species are known to accumulate calcium to form their shells or body structures, it seems reasonable to expect them to be accumulating strontium too. Analysis of a variety of clams, crabs, barnacles, sea urchins, and sea stars in and near St. Andrew Sound was carried out to determine the extent to which calcium and strontium are taken up by animals known to have calciferous skeletal elements as shown in Table 3. The dry weight concentration of strontium in the shellfish ranged from 842 to 3035 ppm. The dry weight calcium concentration ranged from 499,231 to 581,034 ppm. Typical Ca/Sr ratios were 300:1. Though few of the Sr concentrations came close to those of the didemnid, most of the shellfish had calcium concentrations essentially equal to that of *D. conchyliatum*. This paucity in strontium in the shellfish indicates that *D. conchyliatum* is preferentially accumulating strontium instead of calcium to form the spicules that are embedded throughout its tunic.

The average concentration of strontium in the ascidian *D. conchyliatum* was found to be greater than 4000 ppm having a calcium concentration around 250,000 ppm. The average Ca/Sr ratio in this didemnid was 58:1. This ratio was smaller than any of the other samples analyzed. Since the samples analyzed were from the same area, all were presumably exposed to the same concentrations of strontium and calcium, the same temperature effects, and the same overall environmental conditions. From all of the

samples analyzed, the dry weight concentration of strontium in this didemnid was always greater than that found in almost all of the other samples.

The samples which showed accumulated strontium concentrations closest to *D. conchyliatum* were barnacles whose concentrations were in the upper 3000 ppm's and a coral whose concentration of strontium was greater than 8000 ppm. The calcium concentration of the barnacles, similar to the strontium concentration, was equally large; 440,000 ppm. The average Ca/Sr ratio for the barnacle was almost double that for *D. conchyliatum*, 116:1. The calcium concentration in the coral was also quite large, 579,872 ppm. The ratio of Ca/Sr for the coral was 71:1 which is higher than *D. conchyliatum*.

Scientific Name	Common Name	Sr (ppm)	CV	Ca (ppm)	CV	Ca/Sr
Acanthochitona pygmaea	Dwarf Glass-haired Chiton	5510	1.2	461013	0.8	83.66
Anodontia alba	Buttercup Lucine	1964	0.6	586592	0.1	298.72
Anomia simplex	Jingle Shell	1022	0.5	559735	0.4	547.86
Arcinella cornuta	Florida Spiny Jewel Box	1564	0.6	499231	0.6	319.29
Argopecten irradians	Scallop	1135	1.0	581330	0.2	512.00
Atrina rigida	Stiff Pen Shell	1048	1.9	539781	0.7	514.88
Atrina seminuda	Half-Naked Pen Shell	1430	0.9	586323	1.2	409.87
Balanus eburneus	St. Andrew Sound Barnacle	3809	0.3	441825	0.5	116.00
Bulla striata	Striate Bubble	1452	0.4	553707	0.6	381.25
Busycon contrarium	Lightning Whelk	2289	1.2	563325	0.9	246.07
Busycon spiratum	Fig Whelk	2322	0.9	506477	0.2	218.14
Callinectes sapidus	Blue Crab Claw	2535	0.4	404421	0.6	159.54
Carditamera gracilis	West Indian Cardita	2916	0.6	642500	0.3	220.36
Cerithium muscarum	Dotted Horn Shell	1372	0.8	528263	0.3	385.17
Chione cancellata	Cross-barred Chione	1112	0.9	556400	0.4	500.54
Cliona intestinalis	Sponge	101	3.4	12534	3.9	124.29
Crepidula fornicata	Common Atlantic Slipper Shell	2184	0.9	580016	0.3	265.59
Crepidula maculosa	Spotted Slipper Shell	2284	0.3	547317	1.4	239.60
Crepidula plana	Eastern White Slipper Shell	1770	0.7	505972	1.0	285.89
Cyrtopleura costata	Angel Wing	2370	0.7	622727	1.0	262.73
Dinocardium robustum	Giant Atlantic Cockle	2097	1.0	548466	0.5	261.51
Divaricella quadrisulcata	Crosshatched Lucine	1396	1.7	546900	1.2	391.80
Donax variabilis	Coquina	1484	1.9	556950	1.0	375.33
Dosinia discus	Disk Shell	1275	1.4	560265	0.8	439.37
Echinaster spinulosus	Sea Star	871	1.3	297762	1.5	341.79
Fasciolaria hunteria	Banded Tulip Shell	1668	0.7	576898	0.9	345.96
Laevicardium laevigatum	Common Egg Cockle	2479	1.8	534363	1.2	215.54
Littorina irrorata	Marsh Periwinkle	1778	0.9	644541	1.1	362.53

Lucinoma filosa	Northeast Lucinia	1782	1.3	516430	0.8	289.87
Lytechnius variegatus	Sea Urchin Test	1238	1.3	468032	0.6	378.12
Macrocallista nimbosa	Sunray Shell	1572	0.7	558117	0.2	355.09
Mellita quinquiesperferota	Five-Holed Keyhole Urchin	1865	0.7	492664	1.5	264.15
Melongena corona	Crown Conch	1751	0.5	558333	1.2	318.90
Mercenaria campechiensis	Southern Quahog	2335	0.5	611975	0.8	262.14
Modiolus americanus	Tulip Mussel	1468	0.6	591818	1.2	403.27
Modiolus demissus	Ribbed Mussel	1373	0.6	530893	1.5	386.72
Molgula occidentalis	Tunicate Tunic	22	6.7	11174	1.3	496.95
Noetia ponderosa	Ponderous Ark	1084	0.9	520234	1.2	479.74
Oculina diffusa	Ivory Bush Coral	8167	0.7	579872	0.5	71.00
Oliva sayana	Lettered Olive	1677	0.8	576047	0.6	343.47
Ostrea equestris	Crested Oyster	842	1.4	576116	0.6	683.94
Petrolisthes sp.	Crab	1421	0.6	245124	0.6	172.49
Phalium granulatum	Scotch Bonnet	1746	0.8	568556	1.0	325.65
Polinices duplicatus	Southern Moon Snail	1558	0.5	531787	0.8	341.23
Psammotreta intastriata	Atlantic Grooved Macoma	1851	0.5	548091	0.8	296.14
Sinum perspectivum	Common Baby's Ear	2554	0.9	533613	1.7	208.93
Spisula solidissima	Atlantic Surf Clam	1436	0.3	581034	1.0	404.76
Strombus alatus	Florida Fighting Conch	1984	1.8	575306	1.2	289.94
Tagelus divisus	Purplish Tagelus	3035	0.3	576639	0.2	189.98
Terebra salleana	Salle's Auger	1466	0.4	521240	0.6	355.45
Thalassia testudinum	Turtle Grass	119	1.5	38426	2.2	322.54
Trachycardium egmontianum	Prickly Cockle	1920	1.4	531050	0.5	276.59
Turbo castaneus	Chestnut Turban	1619	1.1	567778	0.7	350.60

Table 3: Strontium and calcium concentrations of a variety of sea animals found in St. Andrew Sound, Wild Goose Lagoon, the East Bay of the Gulf of Mexico, and along the shore of Crooked Island where they wash up from the Gulf of Mexico.

Conclusion

The major finding in this study was the preferential accumulation of strontium by the didemnid *Didemnum conchyliatum*. Suggested studies which could be completed to better understand the accumulation of strontium by *D. conchyliatum* are outlined below.

The samples of the strontium rich tunicate were all collected from the same area of St. Andrew Sound. Since this water system is somewhat cut off from the Gulf of Mexico, the conditions in this area tend to be more constant in pH, temperature, salinity, calcium, and strontium concentrations. Though a few dives were made into other water systems, no *D. conchyliatum* were found. A more extensive search for *D. conchyliatum* in different water systems needs to be completed. Searches in St. Joe Bay as well selected sites in the Gulf of Mexico, and a more extensive search of St. Andrew Sound would provide a better understanding of the abundance of *D. conchyliatum* in this area. Ideally, if samples of the tunicate and sea water from world oceans were to be collected and analyzed, would a different Ca/Sr ratio be found? This remains a subject for further study.

What is the rate at which strontium and calcium are taken up by this tunicate? What factors affect the rate at which these metals are taken up? It has been shown experimentally that the amount of strontium incorporated in inorganic aragonite is temperature dependant.[21, 22, 23] Strontium to calcium ratios have been reported to provide information on temperature changes experienced by fish seasonally and during migration but Sr/Ca ratios in molluscs shells were unaffected by variations in temperature.[24, 25, 26] Could this tunicate be used as bioremediator? Can the Ca/Sr ratio be altered? Other researchers have found that exposure to elevated levels of Sr has increased the Sr content in human and animal bone and teeth.[26] These tunicates should be cultured in an aquarium where the Ca/Sr ratios as well as environmental conditions can be manipulated and monitored.

Since this tunicate is accumulating Sr, what portion of this is Sr-90? Strontium-90 is widely used in medical and research establishments and is produced as a by-product of nuclear fission, two to five atoms of Sr-90 are produced for every 100 nuclei undergoing fission.[27] Of the six strontium isotopes produced by nuclear fission, Sr-90 is the most important and the most prevalent. It is also the most persistent source of

Sr radiation to man since it has a half-life of 28 years. How does the Sr/Sr-90 ratio in the didemnid compare to shellfish and other calcium containing species? A practical method for analyzing for Sr-90 in calcium-rich samples was outlined by Bunzl and Kracke.[28] This method is based on the different solubilities of the oxalates of strontium and calcium in the presence of a large excess of calcium. The sample is dissolved and impurities are removed then Y-90 crystals are allowed to grow in the solution for two to three weeks and are then counted using a scintillation counter. Y-90 is a daughter produced by the decay of Sr-90. This technique seems simple enough that it could be carried out in any lab. Since Sr/Sr-90 is ubiquitous, you are not elevating the concentration of any radioactive material that is already present. Both Sr-90 and Y-90 are beta emitters.

Though progress has been made in the understanding of the chemistry of D. conchyliatum, much more work needs to be completed.

References

1. Ratilff, J.; Final Report to Air Force Office of Summer Research, Summer 1996.

2. Grynpas, M. D. and Marie, P. J.; Bone, 1990, 11, 313-319.

3. Curzon, M. E. J. and Spector, P. C. Handbook of Stable Strontium, pp. 581-591, Plenum Press, 1981, New York, NY.

4. Skoryna, S. C. Can. Med. Assoc. J., 1984, 125, 703-712.

5. Matsumoto, A. Jap. J. Pharmacol, 1976, 26, 675-681.

6. Comar, C. L. The Transfer of Calcium and Strontium Across Biological Membranes, pp. 405-418, Academic Press, 1963, New York, NY.

7. Hitchin, M. E. and Vaughan, B. E. Plant Physiol, 1968, 43, 1913-1918.

8. Sanzharova, N. I. Mosc. Univ. Soil Sci. Bull, 1978, 33, 42-43.

9. Ingersoll, R. J. and Wasserman, R. H., J. Biol. Chem, 1971; 246, 2808-2814.

10. Menezel, J. and Mor, E., Proc. of the 2nd International Symposium on Strontium Metabolism, Glasgow, Scotland, 1972.

11. Comar, C. L. and Wasserman, R. H., Mineral Metabolism. Volume 2., Academic Press, New York, NY.1964.

12. Schroeder, H. A., Tipton, J. H., and Nason, A. P. J. Chronic Dis., 1972; 56, 547-571.

13. Spencer , H., Warren, J. M., Kramer, L., and Samaschson, J. J. Clin. Orthop. Rel. Res., 1973, 91, 225-234.

14. Underwood, E. J. Trace Elements in Human and Animal Nutrition, 4th ed.,1977, New York, NY.

15. Brown, J. Seawater: Its Composition, Properties and Behavior, Pergamon Press, 1989, New York, NY.

16. Abbott, R. T. American Seashells, Van Nostrand Reinhold Co., 1974, New York, NY.

17. Morris, P. A. A Field Guide to Shells of the Atlantic and Gulf Coasts and the West Indies, The Peterson Field Guide Series, Haughton Mifflin Co., 1973, Boston, MA.

18. Operating Instructions for Parr Microwave Acid Digestion Bombs, U.S. Pat. No. 4882128, Circular No. 243M, Parr Instrument Company, Moline, IL.

19. Collard, S. B. Suitability of Ascidians as Trace Metal Biosensors-Biomonitors in Marine Environments: An Assessment. AFOSR Final Report. Chapter 10, Summer 1997.

20. Monniot, C.; Monniot, F.; Laboute, P.; Coral Reef Ascidians of New Caledonia, pp. 69-75, Institute Français De Recherche Scientific Pour le Développement en Coopération, Paris, France, 1991.

21. Kinsman, D. J. J. and Holland, H. D. Geochimica et Cosmochimica Acta, 1969, 33 1-17.

22. Radtke, R. L. Coral Reefs, 1987, 6, 19-25.

23. Townsend, D. W.; Radtke, R. L.; Morrison, M. A.; and Folsom, S. D. Marine Ecology Progress Series, 1989, 55, 1-13.

24. Radtke, R. L. and Targett, T. E. Polar Biology, 1984, 31, 203-210.

25. Buchardt, B. and Fritz, P. Science, 1978, 199, 291-292.

26. Lorens, R. B. and Bender, M. L. Geochimica et Cosmochimica Acta, 1980, 44, 1265-1278.

27. Smith, G. L.; Rees, S. B.; and Williams, D. R. Polyhedron, 1985, 4, 713-716.

28. Bunzel, K. and Kracke, W. Journal of Radioanalytical and Nuclear Chemistry, 1991, 148, 115-119.

THE EFFECTS OF INDIVIDUAL DIFFERENCES AND TEAM PROCESSES ON TEAM MEMBER SCHEMA SIMILARITY AND TASK PERFORMANCE

Joan R. Rentsch
Associate Professor
Department of Psychology

Wright State University
Dayton, Ohio 45435

Final Report for:
Summer Faculty Research Program
Armstrong Laboratory

Sponsored by:
Air Force Office of Scientific Research
Bolling Air Force Base, DC

And

Armstrong Laboratory

August, 1997

THE EFFECTS OF INDIVIDUAL DIFFERENCES AND TEAM PROCESSES ON TEAM MEMBER SCHEMA SIMILARITY AND TASK PERFORMANCE

Joan R. Rentsch
Associate Professor of Psychology
Department of Psychology, Wright State University

Michael D. McNeese
Research Scientist
CFHI, Armstrong Laboratory

Dawn D. Burnett
Graduate Student
Department of Psychology, Wright State University

Kristen R. Bonnema
High School Student
Wayne High School

Abstract

The research reported here examined team member schema similarity, its predictors, and its relationship to team performance. This research has implications for applied Air Force problems such as UCAV (Unmanned Combat Air Vehicle) operation, transport command centers, information warfare, battlefield management, C^3I, and joint collaborative systems such as data walls, avatars, intelligent agents, and knowledge rooms.

One purpose of the present study was to test a portion of the Team Member Schema Similarity Model with modifications. It was hypothesized that team member individual differences would predict team process variables (team interaction process variables and group process variables) and team member schema similarity (TMSS). Team process variables and TMSS were hypothesized to predict team performance.

Data were collected in a laboratory setting. Forty-five two member teams attempted to solve a complex, ill-defined problem. Team members completed individual difference measures before working on the problem. After solving the problem, team members completed teamwork schema measures. TMSS was operationalized as schema agreement and schema accuracy. Team performance and team interaction processes were coded by raters. Preliminary results are reported that indicate some support for portions of the modified model. Future research and potential applications are discussed.

THE EFFECTS OF INDIVIDUAL DIFFERENCES AND TEAM PROCESSES ON TEAM MEMBER SCHEMA SIMILARITY AND TASK PERFORMANCE

Joan R. Rentsch
Michael D. McNeese
Dawn D. Burnett
Kristen R. Bonnema

Teams, crews, multi-operator units, and collaborative systems abound in the Air Force. Dr. Michael McNeese has developed a research program to study the socio-cognitive variables operating within these multi-person units. Because Air Force teams operate in environments that are characterized by ill-defined and emergent situations, McNeese's research program has incorporated theories of situational awareness, crew schemata, shared cognition, social construction of knowledge, and interpersonal interaction to understand the development of meanings necessary for effective functioning in these environments (e.g., Brown, Whitaker, Selvaraj, & McNeese, 1995; McNeese, Zaff, Citera, Brown, & Whitaker, 1995; McNeese, 1993; Nosek & McNeese, 1997; Wellens & McNeese, 1987; Young & McNeese, 1995). This type of research will produce knowledge that will be applicable to the development of joint collaborative systems technology within the Air Force. The research study reported in this document is part of this research program.

The research reported below focused on cognitive processes within teams. Specifically, the research examined team member schema similarity, its predictors, and its relationship to team performance. This research is relevant to co-located or distributed teams. It also has implications for applied Air Force problems such as UCAV (Unmanned Combat Air Vehicle) operation, transport command centers, information warfare, battlefield management, C^3I, and joint collaborative systems such as data walls, avatars (Wells & Hoffman, 1996), intelligent agents, and knowledge rooms.

For example, UAV operation requires that pilots coordinate with field controllers, tower personnel, and manned air vehicles in complex, dynamic, ill-defined situations. During the chaos of combat, the UCAV crew must be able to construct meaning quickly in these ambiguous situations. UAV crew members must be able to

understand each other and they must have shared situational awareness. This ability to understand one another and to develop shared situational awareness is developed, in part, through team member schema similarity. Thus, team member schema similarity (TMSS) will enhance the performance of these types of teams.

Below, the conceptual model used to guide the current research is described, relevant past research is reviewed, and a modified version of the model is presented. Then the present study is described.

Team Member Schema Similarity Model

The Team Member Schema Similarity Model (Rentsch & Hall, 1994) is shown in Figure 1. The critical variable in the model is team member schema similarity (TMSS). Team member schema similarity (TMSS) refers to the degree to which team members have similar team-related schemas. A schema is a complex knowledge structure that organizes new information and facilitates understanding (Poole, Gray, & Gioia, 1990).

Although team members may develop many team-related schemas (e.g., schemas of team members, schemas of the task), the focus of the present study is on teamwork schemas (Cannon-Bowers & Salas, 1990). Teamwork schemas contain knowledge and information regarding communicating about, evaluating, and compensating for teammates' performance (Cannon-Bowers & Salas, 1990). Teamwork schemas will guide team members' assumptions, expectations, and behavior regarding teamwork.

Rentsch and Hall (1994) extended the concept of coorientation (Poole & McPhee, 1983), which is typically studied with respect to attitudes, to the study of teamwork schemas. They suggested that TMSS refers to schema accuracy as well as schema agreement. Schema agreement among individuals exists when individuals have similar schemas. This type of schema similarity has received research attention in the past (e.g., Walsh, Henderson, & Deighton, 1988). Schema accuracy exists when individuals are able to describe another individuals' schema accurately. This type of schema similarity has received very little research attention. A critical or optimal level of TMSS, in terms of both accuracy and agreement, is hypothesized to enhance team effectiveness. Empirical research has revealed some support for this hypothesis (Rentsch, Pape, & Brickman, 1997; Rentsch, 1993).

Team members who have schema similarity have similar knowledge about teamwork and they organize this information in a similar way. Teamwork schema similarity is hypothesized to enhance team effectiveness

because similar teamwork schemas in terms of agreement and accuracy among team members will allow team members to interact efficiently and effectively. Team members with high TMSS will be able to anticipate, to facilitate, and to compensate for one another's behavior.

Communication among team members is also likely to be enhanced as team members' teamwork schemas become increasingly similar. Team members may be aware of the information required by each other and fully understand the information that is being communicated to each other. Moreover, team members are likely to anticipate and understand each other's actions due to teamwork schema similarity.

Researchers in the military realm have studied team cognitions as team mental models. They have examined the relationship between team cognitions and team performance (e.g., Cannon-Bowers, Salas, & Converse, 1993). Much of this research provides indirect evidence that team mental models predict team performance (Cannon-Bowers et al., 1993).

Most researchers have conceptualized team cognitions in terms of schema agreement. The accuracy component of TMSS has not been explored extensively to the authors' knowledge. Thus, one purpose of the present study was to test the roles of team member schema accuracy and agreement in the prediction of team effectiveness. Rentsch, Pape, and Brickman (1997) examined TMSS conceptualized as schema agreement and schema accuracy. Their results revealed that agreement and accuracy predicted team effectiveness significantly. They suggested that schema accuracy may be more important in predicting team effectiveness than schema agreement. They suggested that future research examine these relationships in detail.

<u>Antecedents of TMSS</u>. As shown in Figure 1, two antecedents of team-related schema similarity are team membership influences, such as person-environment fit, and schema related communications, such as communication that occurs during socialization processes. These antecedents are expected to regulate the degree of schema similarity among team members to an optimal level. It is assumed that an optimal level of schema similarity exists for any given team and that when schema content is of high quality, the optimal level of schema similarity will enhance team effectiveness maximally.

In the present study, we focused on a subset of team membership influences and a subset of schema related communications as predictors of TMSS. The team membership influences we examined were individual differences. The schema related communications in our study were team interaction process variables. Below, we elaborate these portions of the model.

Team membership influences as individual differences. Schneider (1987) hypothesized that individuals are attracted to organizations containing people who are similar to themselves (Attraction), organizations select individuals who are similar to others already in the organization (Selection), and individuals who gain entry into the organization, but who are significantly different from those already in the organization are predicted to leave the organization (Attrition). One outcome of the ASA process is excessive similarity among organizational members. In the extreme, Schneider hypothesized, organizations may fail due to excessive homogeneity among organizational members, because too much homogeneity among organizational members would limit organizational creativity.

Thus, this organizational theorist predicted that similarity among organizational members will be associated with organizational members thinking similarly. In other words, individuals who are similar in terms of individual difference characteristics are likely to have similar schemas. Extending this logic to teams implies that similarity among team members' individual difference characteristics may enhance TMSS. Thus, an optimal level of TMSS may be due, in part, to similarities among team members' individual difference characteristics (Rentsch & Hall, 1994).

Although similarity among team member individual differences characteristics may be related to TMSS, it may also be the case that the level of the individual difference characteristics existing within the team may also be related to TMSS. Pape (1997) hypothesized that high levels of teamwork schema accuracy and agreement would exist when perceivers were high on trust and perspective taking, and when targets were high on private self-consciousness[1]. She hypothesized that targets high on self-monitoring would have low levels of accuracy and agreement. Team members who are high and similar in terms of several individual difference variables, such as perspective taking, trust, and private self-consciousness, and who are low and similar on self-monitoring are likely to experience high TMSS. These variables were investigated in the present study.

Schema related communications as team interaction processes. Schema related communication processes include communication that occurs during training, team member socialization, and team member interactions. In the present study we examined schema communication processes that occur while team members interact to complete a task. Within the team context, there is evidence that team member interaction is a primary cause of schema similarity among team members (Bettenhausen & Murnighan, 1991; Gersick, 1989; Walsh, Henderson, & Deighton, 1988). Many researchers agree that groups require social construction of knowledge and metacognitive processes to solve problems successfully (e.g., Young & McNeese, 1995). However, the research has not addressed the nature of the interactions leading to socially constructed meaning. No definitive theory for studying these interaction processes has been developed. Therefore, another purpose of the present study was to determine team interaction process variables that predict TMSS and team performance. We drew upon the group communication and crew coordination literatures. Our summary of this literature is presented next.

Team Interaction Processes

As Tower and Elliott (1996) note, although team member communication and coordination are hypothesized to be related to team performance, very little empirical research has been conducted to test the nature of these linkages. However, according to Tannenbaum, Beard, and Salas (1992), existing research evidence tends to support communication processes, coordination processes, and decision making processes as predictors of team performance.

For example, Hakel, Weil, and Hakel (1988) reported that intrateam communication patterns differentiated high from low performing teams. Among other findings, Kimble and McNeese (1987), found that teams that talked in longer utterances performed better than teams that spoke in shorter utterances.

Team interaction processes and TMSS are likely to have a reciprocal relationship. Team member communication is important because it is critical to developing similar understandings, and similar understandings, in turn, imbue communication with meaning (Fischer, 1996). Again, the research evidence is indirect. For example, Dyer (1984) reported research by Obermayer and colleagues revealing that experienced aircrews communicated more frequently during nonroutine missions than during routine missions compared to less

experienced crews. This suggests that experienced aircrews might have had TMSS for routine situations and, therefore, did not require high levels of communication for these situations.

Although there are many approaches for studying team interaction processes, there is none that specifically addresses the sense-making, or socially constructed aspect of interaction. Interaction seems to enhance performance and it seems to be related to TMSS. Yet, there exists a need for additional study of interactions and communication within teams (Duffy, 1993).

Team Interaction Process Variables

We developed a coding scheme to record the nature of the interactions occurring among team members. In particular, we focused on the degree to which team members tended to share interpretive information with one another. We assessed: depth of meaning of informing oriented communication, depth of meaning of learning oriented communication, quality of exchange, consensus evaluation communication, openness and acceptance of communication, and egocentricity versus mutuality of interaction. We also included group process variables in the present study. The group process variables were team cohesion, task motivation, and team metacognition.

The Present Study

The primary purpose of the present study was to test a portion of the TMSS model with modifications. The variables explored in the present study are presented in Figure 2. It was hypothesized that team member individual differences will predict team process variables (team interaction process variables and group process variables) and TMSS. Team process variables and TMSS are hypothesized to predict team performance.

Method

Participants

The participants were 90 undergraduate students who comprised 45 two member same-sex teams. There were 20 male teams and 25 female teams.

Task

The task used for the present study was *The Adventures of Jasper Woodbury: Rescue at Boone's Meadow.* The Jasper task is a complex, ill-defined task that requires problem solvers to identify the problem and the

subproblems needed to solve the problem, to distinguish between relevant and ill-relevant information, to coordinate relevant information, and to evaluate alternative possible solutions. Middle-school level mathematics are required to solve the problem (McNeese, 1993; Vye, Goldman, Voss, Hmelo, & Williams, undated).

The Jasper task is presented on laser video disc. A story problem is presented in which an injured eagle must be rescued from a remote location. Alternative routes, modes of transportation, and individuals are available for rescuing the eagle. Two problems are to be solved: (1) What is the quickest way to move the eagle? (2) How long will that take?

When solving the problem, team members could refer back to the video disc by using a Macintosh computer system. They were to record their answer and any information used to arrive at their answer in writing. The teams were videotaped as they attempted to solve the problem. They were stopped after 60 minutes, if they had not reached a solution. Only three teams were stopped. All other teams reached a solution in 12 to 56 minutes.

<u>Measures</u>

<u>Individual differences</u>. Traditional individual difference measures were used. The Interpersonal Trust Scale (Rotter, 1967) was used to assess trust. It had an internal consistency reliability estimate of .63 in the present study. In past research internal consistency reliability has been estimated at .76 (Rotter, 1967). Perspective taking was measured using the Interpersonal Reactivity Index (Davis, 1980), which is a 7 item measure. The internal consistency reliability estimate obtained in the present study was .77, which is consistent with past research findings (Davis, 1980). The Self Monitoring Scale (Snyder & Gangestad, 1986) was used to evaluate self-monitoring. An internal consistency reliability estimate of .70 is typical in past research (Snyder & Gangestad, 1986) and it was .69 in the present sample. Private and public self-consciousness were measured by the Self-Consciousness Scale (Fenigstein, Scheier, & Buss, 1975). The public self-consciousness scale contains seven items and had an internal consistency reliability estimate of .76. The private self-consciousness scale consists of 10 items and had an internal consistency reliability estimate of .54 in the present study.

<u>Teamwork schema similarity</u>. Teamwork schema similarity was assessed using a measure developed for this study based on pilot research (Pape, 1997). The measure was developed using the procedure advanced by

Rentsch (1993). The measure consisted of 15 items that assessed teamwork schema. Each team member rated the 15 items for how important they were to his or her concept of teamwork. Then each team member completed the items as he or she believed his or her teammate would rate them.

Team Performance. Eight aspects of team performance were coded: problem space identification, constraint violations, misconceptions, confusions, math errors, speed, accuracy, corrections, and solution quality. Similar types of performance measures for the employed task have precedence in the research literature (e.g., McNeese, 1993; Vye, Goldman, Voss, Hmelo, & Williams, undated). Two raters coded performance independently by reviewing each team's written work and the videotape of the team. Interrater reliability was 93% agreement. The raters resolved any discrepancies in ratings through consensus.

Team processes. Team processes were coded using a coding scheme developed for this study. Two categories of team processes were assessed: team interaction processes and group processes. Team interaction processes included: depth of meaning in informing oriented communication, depth of meaning in learning oriented communication, quality of exchange, consensus evaluation communication, egocentricity versus mutuality, openness and acceptance of communication. Group processes were: group cohesion, task motivation, and team metacognition.

The total time during which the team worked was divided into quarters. Each process variable was rated for each quarter. The team received a rating for depth of meaning in informing oriented communication, depth of meaning in learning oriented communication, quality of exchange, consensus evaluation communication, egocentricity versus mutuality, group cohesion, and team metacognition for each quarter. Each team member was rated on depth of meaning in informing oriented communication, depth of meaning in learning oriented communication, consensus evaluation communication, openness and acceptance of communication, task motivation and team metacognition for each quarter.

Each variable was rated by two raters. One rater prepared a transcript of the videotape and then reviewed the videotape using the transcript to rate the team members and the team on the process measures. The other rater

used the transcripts when reviewing the videotape to make the ratings. The raters achieved interrater reliability of 77% agreement on all of the ratings. All discrepancies were resolved through consensus.

Preliminary Results

Variables

The results reported here are very preliminary. The similarity among team members on the individual difference measures was assessed using the within team standard deviations on each variable. Team level on the individual difference measures was assessed using the within team level mean for each variable. Two forms of TMSS accuracy and agreement were calculated. One form was based on absolute difference scores. Using the absolute difference score method, TMSS agreement was calculated as the average of the summed absolute difference scores between members' ratings on each teamwork schema item. TMSS accuracy scores were calculated as the average of the summed absolute differences scores between each member's ratings of the other member's schema and the other member's actual schema ratings. Stated differently, the absolute difference was calculated for each item, then summed for each team member, and the sums were averaged for the team level accuracy measure. The second form of TMSS was calculated using the square root of the sum of the squared difference scores. Both forms of TMSS produced similar results, therefore, the results from the absolute difference form are presented.

Each process variable was aggregated across quarters for a total score. An aggregated team level score was computed for those variables on which each team member was assessed. All analyses involving process variables are based on a sample size of 30. All other analyses are based on a sample size of 45.

Individual Differences as Predictors of TMSS

The similarity and level of the individual difference scores were correlated with TMSS accuracy and agreement scores. The bivariate correlations revealed no statistically significant relationships. Regression analyses were conducted using a backward stepwise strategy. These results revealed that TMSS Accuracy was predicted by team member similarity on trust and on public self-consciousness ($\underline{R} = .37$, $\underline{p} < .05$; $\beta = .24, .28$, respectively, $\underline{p} > .05$). TMSS Agreement was predicted by team level on team experience, trust, public self-consciousness, and

private self-consciousness ($R = .45$, $p < .05$; $\beta = -.24, .26, .28, -.38$ respectively). Private self-consciousness and team experience had negative beta weights. These are unexpected results. Additional analyses are required to test for suppression effects.

Team Interaction Processes as Predictors of TMSS

The only team interaction process variable that predicted TMSS was the aggregated team level openness variable. This variable predicted both TMSS Accuracy and Agreement with correlations of .44 ($p < .05$). This result was unexpected, because it was in the opposite direction of the prediction. Remember a low value indicates high TMSS. Therefore, the positive correlations suggest that low TMSS is related to a high level of openness. After reviewing this result, the process coders suggested that perhaps, the measure of openness was assessing some other variable such as acquiescence or passivity. They believed that this may be the case, because team members were given high ratings on openness and acceptance when they were willing to consider the other team members' input. A high degree of openness and acceptance was characterized by immediate discussion of another's input. The more persuasion required before input is considered or discussed, the lower the level of openness and acceptance. These behaviors might also characterize high levels of acquiescence or passivity. If this is true, then these correlations may make sense.

TMSS Accuracy and Agreement as Predictors of Team Performance

TMSS Accuracy correlated significantly with how completely teams identified the problem space, with the solution rating, and with making a constraint violation ($r = -.33, -.30, .36$, $p < .05$). Higher TMSS accuracy was related to better problem identification and a higher solution rating. However, it was an unexpected finding that high TMSS Accuracy was related to making more constraint violations.

Simultaneous regression equations were computed in which TMSS accuracy and agreement were entered as predictors of team performance. Significant results were obtained for a constraint violation and for problem space identification. In both cases TMSS Accuracy had a significant beta weight and TMSS Agreement did not. Furthermore, in both cases, the multiple R was .39. Although an additional hierarchical regression analysis is required, it appears that TMSS Accuracy alone predicts as well as TMSS Accuracy and Agreement combined.

Team Interaction Processes as Predictors of Team Performance

Correlational analyses have been conducted to provide preliminary results regarding the nature of the relationship between team interaction processes and team performance. Problem space identification was correlated significantly with aggregated team level openness, team depth of informing oriented communication, and team learning oriented communication, and team cohesion (r = -.39, .42, .36, -.51, respectively, p < .05). Team cohesion and team level openness were related negatively to team performance. Again, this pattern of results may indicate that the openness measure really assessed acquiescence. It might also suggest that highly cohesive teams suffered from a bit of groupthink causing them to ignore some information.

Aggregated team openness, team cohesion, and quality of exchange were correlated significantly with constraint violations (r = .41, .38, .47, respectively, p < .05). All of these correlations were in the direction opposite of that predicted. Again, the acquiescence and groupthink hypotheses may explain these results.

Egocentricity versus mutuality and team depth of meaning in informing oriented communication predicted corrections (r = -.37, .40, respectively, p < .05). Egocentricity also predicted misconceptions (r = -.47, p < .05). Solution rating was predicted significantly by team depth of information processing (r = .38, p < .05).

Discussion Based on Preliminary Results

We would like to remind the reader that these results are preliminary for several reasons. First, the analyses involving the process variables were based on a sample size of 30. Data from all 45 teams will be analyzed in the near future. Second, additional analyses are required to further explore the nature of the predicted relationships and the nature of the unexpected results. Some of the analyses to be conducted were mentioned in the results section. Third, our dataset contains variables that may serve as control variables (e.g., time to solution, demographic characteristics). These variables have not yet been analyzed. Therefore, due to the preliminary nature of the data analysis, our discussion of these results is presented tentatively and cautiously.

In this study we tested a model of team member schema similarity (TMSS) that included individual difference and team process variables as predictors of TMSS, and TMSS and team process variables as predictors of team performance. The results revealed that the individual difference variables predicted TMSS in combination

only. In addition, similarity of individual differences predicted TMSS Accuracy and level of individual differences predicted Agreement. These results reflect the complex nature of personality. Also, we suggest that future research include the Armstrong Laboratory Aviation Personality Survey (ALAPS; Retzlaff, King, McGlohn, Callister, 1996) as a measure of individual differences related to teams and collaborative work. The variables on the ALAPS may be related more strongly to TMSS than the individual difference variables assessed in the present study.

The process variable related to openness or acquiescence predicted TMSS. This relationship requires additional study. However, we hesitate to interpret any of the process correlations in depth due to the preliminary sample size.

In past research, team effectiveness has often been assessed by the teams rating their own performance. This practice is common (Tannenbaum, Beard, & Salas, 1992). However, Tannenbaum et al. (1992) advocate the use of objective measures. In the present study, we employed objective performance measures. TMSS was not a strong predictor of these performance measures. Interestingly, included on the background survey was a single item on which team members rated their satisfaction with the teamwork that had occurred on their team. This item correlated significantly with TMSS accuracy and agreement ($\underline{r}$ = -.37, -.35, respectively).

Although based on only part of the dataset, it appears that team processes have weak relationships to TMSS. However, team processes do predict team performance. The nature of these relationships requires additional analyses.

This study has revealed that TMSS Accuracy and Agreement predict team performance differently and are related differentially to individual differences. TMSS Accuracy deserves additional investigation.

<u>Future Research</u>

The next step in this line of research is to test the TMSS model within the context of an ecologically valid synthetic task environment, such as the VIPER/VECTOR tasks (McNeese, personal communication) that were developed in Armstrong Laboratory, or such as the TRAP task (Wilson, McNeese, Brown, & Wellens, 1987) modified to realistically portray the UCAV or the command-post environment. This research will contribute to the

Collaborative Systems Technology Lab at The Fitts Human Factors Engineering Laboratory at the Collaborative Systems Technology Branch of Armstrong Labs at Wright Patterson AFB.

Baker and Salas (1992) suggest that teamwork may evolve, therefore researchers need to develop teamwork measures that are generalizable to teams in many settings and different team tasks. Our efforts to develop team interaction process measures are in line with this objective. Our measures will be useful in understanding the development of teamwork behaviors and the development of TMSS. We wish to pursue future research in which we will use these measures to study the development of teamwork and TMSS.

Future Applications

The theoretical constructs and the measures that we have developed as part of the Air Force Office of Scientific Research Summer Faculty Research Program applied within the ecologically valid synthetic task environment will provide the foundation for future research on Joint Cognitive Systems. As we acquire knowledge of team member schema similarity and its relation to shared responsibility and team performance, we can pursue research relating these variables to collaborative systems technologies such as datawalls or knowledge rooms. Understanding how team members interact will facilitate the design and development of human-machine communication (Wellens & McNeese, 1987).

We know that the *New World Vistas Air and Space Power for the 21st Century* publication indicates that collaborative computing is a high priority. Collaborative computing may take the form of advanced "groupware," which may be used to facilitate group interaction and decision making among co-located or distributed group members, and human-machine interaction. Clearly, understanding the effects of the joint cognitive system designs on TMSS will enhance the utility of these technologies. MUDs, or Multiple User Dimensions, are described as "....in effect social virtual realities"...."to manage the details of the social interaction... (NWV, p. 100)." The New World Vistas report goes so far as to suggest that a "virtual Pentagon (p. 101)" may become a reality. These innovations require extensive knowledge of socio-cognitive processes and their relationships to technology.

Footnotes

1. Perceiver refers to the individual who is asked to rate another person. The person being rated is referred to as the target.

References

Baker, D. P., & Salas, E. (1992). Principles for measuring teamwork skills. Human Factors, 34(4), 469-475.

Bettenhausen, K. L. & Murnighan, J. K. (1991). The development of an intragroup norm and the effects of interpersonal and structural challenges. Administrative Science Quarterly, 36, 20-35.

Brown, C. E., Whitaker, R. D., Selvaraj, J. A., & McNeese, M. D. (1995). The development of trace: An integrative bargaining paradigm for investigating multidisciplinary design tradeoffs. Air Force Material Command, Wright-Patterson Air Force Base, Ohio. (AI/CF-TR-1995-0073).

Cannon-Bowers, J. & Salas, E. (1990, April). Cognitive psychology and team training: Shared mental models in complex systems. Paper presented to the Meeting of the Society for Industrial/Organizational Psychology, Miami Beach, Florida.

Cannon-Bowers, J. A., Salas, E., & Converse, S. (1993). Shared mental models in expert team decision making. In N. J. Castellan (Ed.), Individual and group decision making (pp. 221-246). Hillsdale: Lawrence Erblaum Associates.

Davis, M. H. (1980). A multidimensional approach to individual differences in empathy. JSAS: Catalog of Selected Documents in Psychology, 10, 85.

Duffy, L. (1993). Team decision making and technology. In N. J. Castellan (Ed.), Individual and group decision making (pp. 247-265). Hillsdale: Lawrence Erblaum Associates.

Dyer, J. L. (1984). Team research and team training: A state of the art review. In F. A. Muckler (Ed.), Human factors review (pp. 285-323). Santa Monica: Human Factors Society.

Fenigstein, A., Scheier, M. F., & Buss, A. H. (1975). Public and private self-consciousness: Assessment and theory. Journal of Consulting and Clinical Psychology, 43(4), 522-527.

Fischer, U. M. (1996). Methods for analyzing group problem solving decision making. United States Army Research Institute for the Behavioral and Social Sciences. (ARI Research Note 96-64).

Gersick, C. (1989). Marking time: Predictable transitions in task groups. Academy of Management Journal, 32, 274-309.

Hakel, M. D., Weil, E. K., & Hakel, L. (1988). The analysis and clustering of navy ratings based on social interaction characteristics: A literature review and conceptual model. Naval Personnel Research and Development Center, San Diego, California. (TR-88-46).

Kimble, C. E., & McNeese, M. D. (1987). Emergent leadership and team effectiveness on a team resource allocation task. Harry G. Armstrong Aerospace Medical Research Lab, Wright-Patterson Air Force Base, Ohio. (AD-A192-105).

McNeese, M. D. (1993). Putting knowledge to use: The acquisition and transfer of knowledge in situated problem solving environments. Dayton, OH: Wright-Patterson Air Force Base, Armstrong Laboratory. (NTIS No. AL/CF-TR-1993-0052).

McNeese, M. D., Zaff, B. S., Citera, M., Brown, C. E., & Whitaker, R. (1995). AKADAM: Eliciting user knowledge to support participatory ergonomics. The International Journal of Industrial Ergonomics, 15(5), 345-363.

New World Vistas: Air and Space Power for the 21st Century. Information Technology Volume. Department of the Air Force. USAF Scientific Advisory Board.

Nosek, J. T., & McNeese, M. D. (1997). Issues for knowledge management from experiences in supporting group knowledge elicitation and creation in ill-defined, emerging situations. Paper presented to the AAAI Spring Symposia: Knowledge Management, Standford University, March.

Pape, L. J. (1997). The effect of personality characteristics on team member schema similarity. Unpublished master's thesis proposal. Wright State University, Dayton, Ohio.

Poole, M. S., Gray, B. & Gioia, D. A. (1990). Organizational script development through interactive accommodation. Group and Organization Studies, 15(2), 212-232.

Poole, M. S. & McPhee, R. D. (1983). A structural analysis of organizational climate. In L. L. Putnam & M. E. Pacanowsky (Eds.), Communication and organizations: An interpretive approach (pp. 195-219). Beverly Hills, CA: Sage Publications.

Rentsch, J. R. (1993, August). Predicting team effectiveness from teamwork schema similarity. Paper presented at the Academy of Management Meetings, Atlanta, Georgia.

Rentsch, J. R., & Hall, R. J. (1994). Members of great teams think alike: A model of team effectiveness and schema similarity among team members. In M. M. Beyerlein & D. A. Johnson (Eds.), Advances in interdisciplinary studies of work teams. Vol. 1. Series on self-managed work teams (pp. 223-262). Greenwich, CT: JAI Press.

Rentsch, J. R., Pape, L. P., & Brickman, N. M. (1997). Team member schema similarity: Exploring individual differences predictors. Unpublished manuscript. Wright State University.

Retzlaff, P. D. King, R. E., McGlohn, S. E., & Callister, J. D. (1996). The development of the Armstrong Laboratory Aviation Personality Survey (ALAPS). Air Force Material Command, Brooks Air Force Base, Texas. (AL/AO-TR-1996-0108).

Rotter, J. B. (1967). A new scale for the measurement of interpersonal trust. Journal of Personality, 35, 651-665.

Schneider, B. (1987). People make the place. Personnel Psychology, 40, 437-453.

Snyder, M., & Gangestad, S. (1986). On the nature of self-monitoring: Matters of assessment, matters of validity. Journal of Personality and Social Psychology, 51(1), 125-139.

Tannenbaum, S.I., Beard, R.L., & Salas, E. (1992). Team building and its influence on team effectiveness: an examination of conceptual and empirical developments. In K. Kelley (Ed.), Issues, theory, and research in industrial/organizational psychology (pp. 117-153). North-Holland: Elsvier.

Tower, S. L., & Elliott, L. R. (1996). The role of communication efficiency in teams with distributed expertise: Application of the multi-level theory. Proceedings of the International Association of Management Conference, Toronto, Canada.

Vye, N. J., Goldman, S. R., Voss, J. F., Hmelo, C., Williams, S., & Cognition and Technology Group at Vanderbilt. (undated). Complex Mathematical Problem Solving by Individuals and Dyads. Unpublished manuscript. Vanderbilt University, Nashville, Tennessee.

Walsh, J. P., Henderson, C. M, & Deighton, J. (1988). Negotiated belief structures and decision performance: An empirical investigation. Organizational Behavior and Human Decision Processes, 42, 194-216.

Wellens, A. R., & McNeese, M. D. (1987). A research agenda for the social psychology of intelligent machines. IEEE Systems, Man, and Cybernetics.

Wells, M. J., & Hoffman, H. G. (1996). The virtual crewmember. Paper presented to the Human Factors and Ergonomics Society, Philadelphia, September 2-6.

Wilson, D. L., McNeese, M. D., Brown, C. E., & Wellens, A. R. (1987). Utility of shared versus isolated work setting for dynamic team decision-making. Armstrong Aerospace Medical Research Laboratory, Wright-Patterson Air Force Base, Ohio. (AD-A192-434).

Young, M. F., & McNeese, M. D. (1995). A situated cognition approach to problem solving. In Hancock, P., Flach, J., Caird, J., & Vincente, K. (Eds.), Local applications of the ecological approach to human-machine systems. Hillsdale: Lawrence Erblaum Associates.

Figure 1: Team Member Schema Similarity Model
(Rentsch & Hall, 1994)

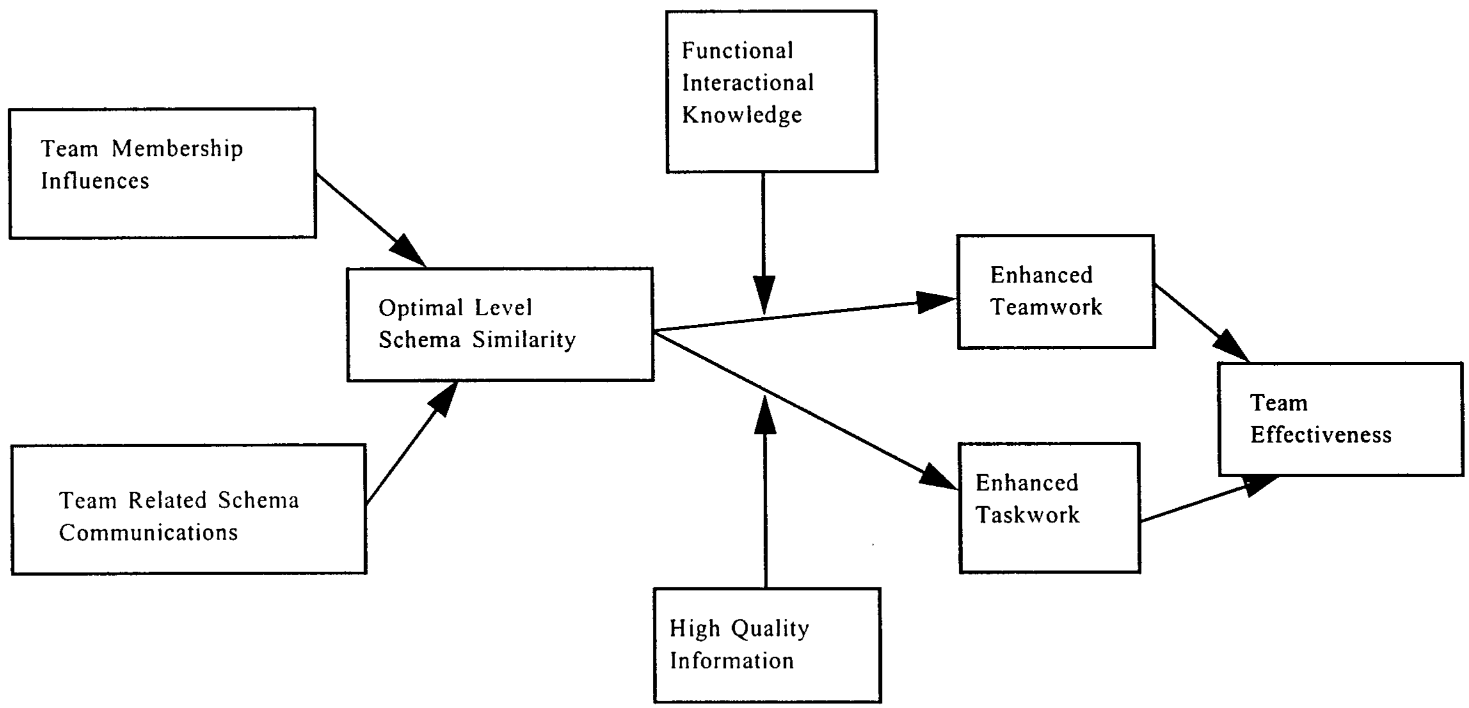

Figure 2: Model Modifications

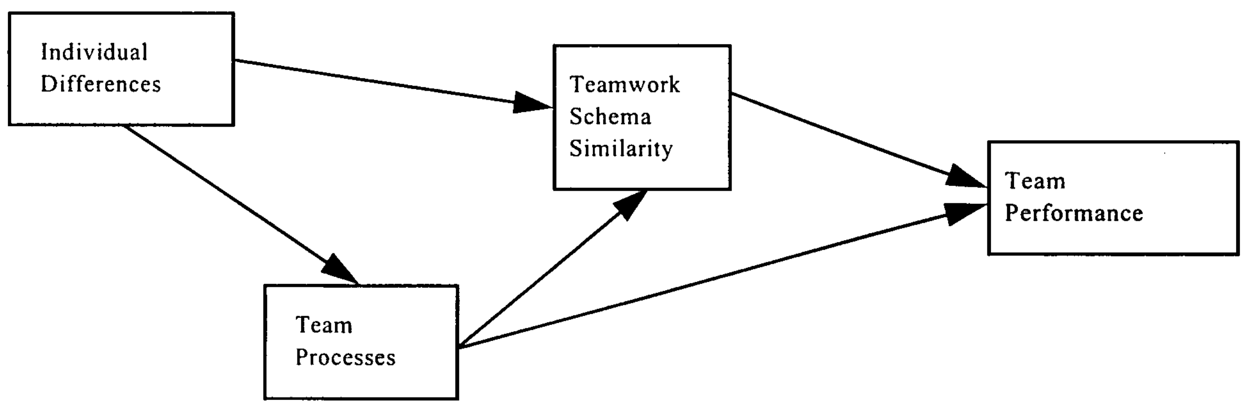

THE ARMSTRONG LABORATORY AVIATATION PERSONALITY SURVEY (ALAPS): NORMING AND CROSS-VALIDATION

Paul D. Retzlaff
Professor of Psychology
Department of Psychology

University of Northern Colorado
Greeley, CO 80639

Final Report for:
Summer Faculty Research Program
Armstrong Laboratory

Sponsored by:
Air Force Office of Scientific Research
Bolling Air Force Base, DC

And

Armstrong Laboratory

July, 1997

The Armstrong Laboratory Aviation Personality Survey (ALAPS): Norming and Cross-validation.

Paul D. Retzlaff
Professor
Department of Psychology
University of Northern Colorado

Abstract

The Armstrong Laboratory Aviation Personality Survey (ALAPS) was developed to better psychologically assess aircrew. The 15 scales cover personality, psychopathology, and crew interaction styles. This work provides additional psychometric data in support of its use. A sample of over 1000 male and female student pilots provide thorough norming, additional evidence of reliability, and further construct validity.

The Armstrong Laboratory Aviation Personality Survey (ALAPS): Norming and Cross-validation.

Paul D. Retzlaff

Introduction

The psychological assessment of pilots through testing has a long history with many valuable contributions (Hormann & Maschke, 1996; Dolgin & Gibb, 1988; Picano, 1991; Retzlaff & Gibertini, 1987; Retzlaff and Gibertini, 1988; Flynn, Sipes, Grosenbach, and Ellsworth, 1994; Siem, 1992; King, 1994; King and Flynn, 1995; King, Retzlaff, and McGlohn, in press). Traditional psychological tests, however, are of less than optimal value when applied to the assessment of aviator's personality, psychopathology, and interpersonal interaction.

There are a few specialized tests used for pilot and astronaut selection. They, however, are not published and hence tend to be obscure. Often they have no standardized administration form, manual, or psychometric data. Tests must have established norms, reliabilities, and validities in order to be properly evaluated.

ALAPS Description

The purpose of the Armstrong Laboratory Aviation Personality Survey (ALAPS; Retzlaff, King, McGlohn, and Callister, 1996) is to provide an inventory with appropriate scales, established norms, high reliability, and solid validities for the aviation industry. The ALAPS was developed using the domain theory test construction model (Nunnally, 1978). This model uses most other construction approaches in a systematic and integrative manner.

It includes, in appropriate order, clinical content development, internal statistical homogeneity item selection, and, finally, validity estimate establishment. A sample of 200 student pilots served in the developmental sample. The outcome of these procedures (see Appendix A, available from the author) included 15 scales each with 16 items.

Format The ALAPS is a 240 item test (see Appendix B, available from the author). The subject is requested to respond in a "true" or "false" manner as each item applies to the subject. The test usually takes between 20 and 30 minutes to complete. The test may be used in paper-and-pencil format or by computer administration.

Scales There are 15 scales divided into personality, psychopathology, and crew interaction categories. The Personality scales include Confidence, Socialness, Aggressiveness, Orderliness, and Negativity. The Psychopathology scales include Affective Lability, Anxiety, Depression, and Alcohol Abuse. Finally, the Crew Interaction scales include Dogmatism, Deference, Team Oriented, Organization, Impulsivity, and Risk Taking.

Personality Scales:

CONFIDENCE: High scorers view themselves as highly capable, intelligent, and talented. This can include the negative elements of arrogance, manipulation, and condescension. Clinically these traits may suggest narcissism.

SOCIALNESS: High scorers are extremely social and outgoing.

They enjoy others and are socially comfortable. They see themselves as friendly and charming. Clinically this may include elements of histrionic personality.

<u>AGGRESSIVENESS:</u> High scorers are assertive to the point of being aggressive. They take strong stands and tolerate little criticism. They are verbally and emotionally combative. This quality probably does not rise to the level of antisocial personality.

<u>ORDERLINESS:</u> High scorers are orderly in a behavioral and environmental way. Their lives are structured and neat. They are methodical and disciplined. This may clinically rise to the level of compulsive personality disorder.

<u>NEGATIVITY:</u> High scorers are angry, negative, and cynical. They are socially punitive and not pleasant to be around. Clinically this may rise to the level of negativistic or passive- aggressive personality.

<u>Psychopathology Scales:</u>

<u>AFFECTIVE LABILITY:</u> High scorers are generally emotional and reactive. They can be situationally anxious, depressed, and frightened. Moods are seen as changing quickly with little provocation. Affect is volatile.

<u>ANXIETY:</u> High scorers are chronically anxious. They worry and brood. The anxiety interferes with their lives and occupational functioning.

DEPRESSION: High scorers are depressed. Problems include dysphoric affect as well as the cognitive and vegetative symptoms of depression. They report being pessimistic, unhappy, and guilty. Extreme elevations may include clinical major depression.

ALCOHOL ABUSE: High scorers like to drink, drink a great deal, and get intoxicated. Functioning is impaired and there may be social and occupational problems.

Crew Interaction scales:

DOGMATISM: High scorers believe what they believe is always correct and are not open to change. They are authoritarian interpersonally. They are intolerant of other people, ideas, and actions.

DEFERENCE: High scorers are deferent to a fault. They are submissive and quiet. They concentrate on their job and are uncomfortable questioning the status quo.

TEAM ORIENTED: High scorers enjoy and believe in team work. They value the team effort and team rewards. They do not enjoy working alone and may be inefficient when working alone.

ORGANIZATION: High scorers are systematic and organized. They coordinate and plan all elements of a project. They think things through thoroughly.

IMPULSIVITY: High scorers act first and think second. They often act and talk without sufficient forethought. They see themselves as spontaneous. Others may be less generous in their

assessment.

RISK TAKING: High scorers enjoy danger and risk. New activities and situations are not frightening. They are adventurous, unafraid, and fun-loving. They are not necessarily impulsive about their activities; their actions may be calculated and include a rational appreciation of the inherent danger.

Purpose: The intent of the current work is to provide additional evidence of reliability and validity for the ALAPS. Further, with a large sample better norming is possible.

METHOD

Subjects: A total of 1131 student pilots volunteered to take part in this study. Of this number, 124 were female and 1007 were male. The average age of the subjects was 22.6 (sd=2.9).

Procedure: All subjects were tested during Enhanced Flight Screening (King and Flynn, 1995; Callister and Retzlaff, 1996). Approximately 40% of the subjects were tested at the United States Air Force Academy and the rest at Brooks Air Force Base during their time at the Hondo, TX, facility. The Hondo facility provides screening for those having received commissioning through Officer Training School, Reserve Officer Training Corps, the Air National Guard, and the Air Force Reserve.

NORMING

Table 1 provides the means, standard deviations, and ranges for all 1131 subjects for each of the 15 ALAPS scales. As can be seen, most means are relatively in the middle of the ranges. The

notable exceptions are the clinical scales such as Anxiety and Depression. While these traits are relatively uncommon in the population, there were subjects who endorsed most, if not all, of the items given the range statistics. Additionally, the standard deviations show reasonable distribution of scores and resolution of the sample.

Table 2 includes the descriptive statistics for the male and female subjects individually. T-tests were conducted to determine gender differences. Males were found to have higher Confidence and Dogmatism scores. Females had higher Affective Lability, Anxiety, and Depression scores. Perhaps surprisingly, scales such as Aggressiveness and Risk Taking showed no gender differences.

Percentile transformations by gender are provided in Tables 3 and 4. Percentile within the normative sample may be found by crossing the scale name row with the raw score column. For example, a male subject with a raw score of 2 on the Confidence scale would be at the 1st percentile of the normative sample. This subject would probably have a problem with confidence. A subject with a raw score of 15 on the Alcohol Abuse scale would be in the top 99th percent of the sample. This subject would be exhibiting a very high level of alcohol use and be of great clinical concern.

RELIABILITY

Internal consistencies for both the developmental and current samples are presented in Table 5. Here Cronbach alphas

have been calculated for each scale. In general, it is necessary to have internal consistencies at least in the .70's and preferably in the .80's (Nunnally, 1978). There has been little change in the reliabilities across the two samplings. For the current sample of 1131, none are below .70 and 9 of the 15 scales are .80 or above. The median reliability for the construction sample was .82 and for the cross-validation sample the median is .83.

INTERNAL CONSTRUCT VALIDITY

Table 6 provides the first validity analysis. This univariate intercorrelation matrix of the 15 scales indicates the degree of scale co-variance and overlap. It is desirable to have scales with relatively low intercorrelations to ensure scale specificity. Scales with higher correlations should be theoretically similar in content.

Across the matrix it is apparent that there is not undue scale overlap. Scales are relatively specific. Scales that are correlated are of similar content vein. The highest correlation in the matrix is between Orderliness and Organization. Again, this is appropriate in that those two dimensions are similar. Orderly individuals tend also to be organized. The .77 correlation for these two scales, however, is probably higher than is desirable. Other than that correlation, there are no intercorrelations in the .60's and only 3 in the .50's.

Table 7 is a principal components analysis of the 15 ALAPS scales. This is done to determine the underlying dimensionality of the scales. The eigenvalues relatively cleanly suggest a four

factor solution. The first factor appears to be an affective factor with Negativity, Affective Lability, Anxiety, and Depression loading highly. The second factor encompasses the shared variance in the Confidence, Aggressiveness, and Risk Taking scales. The third factor includes the highly correlated Orderliness and Organization scales. Finally, the fourth factor is a social factor with Socialness and Team Oriented scales. In general, this is a very interpretable underlying factor structure. This and the univariate correlations suggest the ALAPS scales are internally valid.

EXTERNAL CONSTRUCT VALIDITY

This cross-validation sample was also administered the NEO-PI-R (Costa & McCrae, 1992). Correlations between the ALAPS scales and the five main NEO-PI-R scales are found in Table 8 (available from the author). The first NEO-PI-R scale, Neuroticism, is correlated with the affect oriented ALAPS scales, Negativity, Affective Lability, Anxiety, and Depression. The Extraversion scale is correlated with the ALAPS Socialness scale at a very high level and to a lesser degree the ALAPS Team Oriented scale. The Openness NEO-PI-R scale taps a subject's openness to new experiences. It has no high correlations with ALAPS scales. It has a modest negative correlation with the ALAPS Dogmatism scale which makes sense. The Agreeableness scale negatively correlates with the ALAPS Aggressiveness, Confidence, and Dogmatism scales. Finally, the Conscientiousness scale correlates highest with the Organization and Orderliness scales and negatively with the Impulsivity scale. In general, these

correlations are logical and of appropriate magnitude. These data support the external construct validity of the ALAPS scales.

Tables 9 through 13 (available from the author) provide the correlations between the ALAPS scales and the 30 subscales of the NEO-PI-R. Each of the 5 main NEO-PI-R scales have 6 subscales of similar but more focal content. These correlations provide a more narrow analysis of the construct validity of the ALAPS scales. In Table 9, it should be noted that the highest correlation with the NEO-PI-R Anxiety scale is with the ALAPS Anxiety scale. The highest correlation with Angry is with Negativity. The highest correlation with the NEO-PI-R Depression scale is with the ALAPS Depression scale. The NEO-PI-R Self-Conscious scale has no peer on the ALAPS. The Impulsive scale, again, has the highest correlation with the ALAPS Impulsiveness scale. Vulnerable has no complement in the ALAPS.

Similar convergence can be seen in the other tables whenever scales have similar names. For example, in Table 13 the NEO-PI-R Order scale correlates highest with the ALAPS Order scale. Indeed, the correlation here is .68 which is typical of these convergent validities and very strong. Again, construct validity for most of the ALAPS scales is seen.

As a multivariate approach to the external construct validity, a principal components analysis was done using the five main NEO-PI-R scales and the ALAPS scales. Table 14 (available from the author) shows the five factor solution. Factor One nicely encompasses the neurotic and affective elements of the two

tests. Factor Two is an aggressive dimension with negative loadings for the NEO-PI-R Agreeableness scale and positive for the ALAPS Confidence and Aggressive scales. Factor Three includes the NEO-PI-R Conscientiousness scale as well as the ALAPS Orderliness and Organization scales. Impulsivity on the ALAPS has a negative loading on this factor. The fourth factor has the Extraversion NEO-PI-R scale and high loadings on the ALAPS Socialness and Team Oriented scales. Finally, factor Five is anchored by the NEO-PI-R Openness scale and has negative loadings on the ALAPS Dogmatism and Deference scales. In summary, this is a remarkably clean factor solution and supportive of the ALAPS dimensions.

In summary, the psychometrics of the ALAPS continue to be very strong. The scales are highly internally consistent and, as such, highly reliable. The cross-sample validity estimates against the NEO-PI-R are high and appropriate. These psychometric statistics are highly supportive of the utility of the ALAPS.

References

Costa, P. T. & McCrae, R. R. (1992). NEO PI-R: Professional Manual. Odessa, FL: Psychological Assessment Resources.

Dolgin, D. and Gibb, G. D. (1988). Personnel assessment and aviation selection: Past, present, and future. In R. S. Jensen (Ed.), Aviation Psychology (3rd ed., pp. 288-320). London: Gower.

Flynn, C. F., Sipes, W. E., Grosenbach, M. J., and Ellsworth, J. (1994). Top performer survey: Computerized psychological assessment of aircrew. Aviation, Space, and Environmental Medicine, 65, 39-44.

Hormann, H. and Maschke, P. (1996). On the relation between personality and job performance of airline pilots. International Journal of Aviation Psychology, 6, 171-178.

King, R. E. (1994). Assessing aviators for personality pathology with the Millon Clinical Multiaxial Inventory (MCMI). Aviation, Space, and Environmental Medicine, 65, 227-231.

King, R. E. and Flynn, C. F. (1995). Defining and measuring the "Right Stuff": Neuropsychiatrically Enhanced Flight Screening (N-EFS). Aviation, Space, and Environmental Medicine, 66, 951-956.

King, R. E., Retzlaff, P., & McGlohn, S. E. (in press). Female United States Air Force pilot personality: The new right stuff. Military Medicine.

Nunnally, J. C. (1978). _Psychometric Theory._ New York: McGraw-Hill.

Picano, J. J. (1991). Personality types among experienced military pilots. _Aviation, Space, and Environmental Medicine, 62,_ 517-520.

Retzlaff, P. and Gibertini, M. (1988). The objective psychological testing of Air Force officers in pilot training. _Aviation, Space, and Environmental Medicine, 59,_ 661-663.

Retzlaff, P. and Gibertini M. (1987). Air Force pilot personality: Hard data on "The Right Stuff". _Multivariate Behavioral Research, 22,_ 383-399.

Retzlaff, P., King, R. E., McGlohn, S. E., & Callister, J. D. (1996). _The development of the Armstrong Laboratory Aviation Personality Survey (ALAPS). AL/AO-TR-1996-0108._ Brooks AFB: Armstrong Laboratory.

Siem, F. M. (1992). Predictive validity of an automated personality inventory for Air Force pilot selection. _The International Journal of Aviation Psychology, 2,_ 261-270.

Table 1

ALAPS Norms

Scale	MEAN	SD	Range
PERSONALITY (BEHAVIORAL STYLES)			
CONFIDENCE	9.55	3.08	0-16
SOCIALNESS	12.46	3.41	0-16
AGGRESSIVENESS	9.28	3.02	0-16
ORDERLINESS	12.11	3.43	0-16
NEGATIVITY	5.64	3.29	0-16
PSYCHOPATHOLOGY (COPING STYLES)			
AFFECTIVE LABILITY	5.37	4.15	0-16
ANXIETY	2.84	3.71	0-16
DEPRESSION	2.01	2.76	0-15
ALCOHOL ABUSE	7.04	4.15	0-16
CREW INTERACTION (INTERPERSONAL STYLES)			
DOGMATISM	5.90	3.08	0-16
DEFERENCE	6.36	2.79	0-15
TEAM ORIENTED	11.85	3.81	0-16
ORGANIZATION	12.52	3.36	0-16
IMPULSIVITY	7.34	3.65	0-16
RISK TAKING	12.17	2.96	0-16

note: N=1131.

Table 2

Means and Standard Deviations for Males and Females with T-tests.

Scale	Males MEAN	Males SD	Females MEAN	Females SD	t	p
PERSONALITY (BEHAVIORAL STYLES)						
CONFIDENCE	9.71	3.06	8.27	2.97	4.93	.0000*
SOCIALNESS	12.53	3.34	11.87	3.87	2.05	.0407
AGGRESSIVENESS	9.34	3.00	8.81	3.19	1.85	.0639
ORDERLINESS	12.14	3.41	11.83	3.56	0.95	.3396
NEGATIVITY	5.59	3.22	6.02	3.80	-1.39	.1632
PSYCHOPATHOLOGY (COPING STYLES)						
AFFECTIVE LABILITY	5.10	4.01	7.49	4.67	-6.14	.0000*
ANXIETY	2.73	3.63	3.75	4.27	-2.90	.0038*
DEPRESSION	1.91	2.68	2.80	3.23	-3.38	.0007*
ALCOHOL ABUSE	7.07	4.20	6.78	3.74	0.74	.4615
CREW INTERACTION (INTERPERSONAL STYLES)						
DOGMATISM	6.06	3.08	4.64	2.75	4.90	.0000*
DEFERENCE	6.42	2.78	5.90	2.87	1.96	.0501
TEAM ORIENTED	11.95	3.74	11.06	4.27	2.45	.0144
ORGANIZATION	12.50	3.40	12.65	3.06	-0.46	.6421
IMPULSIVITY	7.32	3.69	7.44	3.40	-0.34	.7327
RISK TAKING	12.22	2.93	11.78	3.17	1.56	.1178
N=	1007		124			

Note: * denotes significance at .0100 or less with 1129 degrees of freedom.

Table 3

ALAPS Percentile Conversion Table for Males.

Scale	0	1	2	3	4	5	6	7	8	9	10	11	12	13	14	15	16
	Raw Score																
CONFID	<	<	1	3	5	10	16	25	34	45	57	69	81	89	96	99	>
SOCIAL	<	<	1	2	4	5	7	10	13	18	23	29	37	47	64	85	>
AGGRES	<	<	1	3	6	10	17	27	39	53	65	76	85	91	95	99	>
ORDERC	<	1	2	3	5	7	9	11	13	18	24	31	42	56	72	91	>
NEGATI	5	10	19	28	40	51	63	72	81	88	93	96	98	99	>	>	>
AFFECT	8	21	33	43	54	62	69	73	78	83	87	91	93	96	99	>	>
ANXIET	38	55	65	72	77	81	85	88	91	93	95	96	97	98	99	>	>
DEPRES	38	61	75	83	87	91	93	94	96	97	98	99	>	>	>	>	>
ALCOHO	9	15	20	25	29	35	42	49	60	69	77	84	89	95	98	99	>
DOGMAT	1	5	11	21	33	48	60	71	80	87	91	94	96	98	99	>	>
DEFERE	1	3	7	14	25	40	54	68	79	87	92	95	98	99	>	>	>
TEAMOR	<	1	2	3	5	8	12	16	20	25	30	36	42	53	67	86	>
ORGANI	<	<	1	3	4	6	8	10	13	17	23	30	38	49	65	83	>
IMPULS	2	5	9	17	25	34	43	53	63	72	80	85	90	93	96	99	>
RISKTA	<	<	<	1	2	3	5	8	11	17	24	35	45	60	75	91	>

note: N=1007

Table 4

ALAPS Percentile Conversion Table for Females.

Scale	Raw Score 0	1	2	3	4	5	6	7	8	9	10	11	12	13	14	15	16
CONFID	<	1	3	8	12	18	26	40	52	64	77	85	92	98	99	>	>
SOCIAL	<	<	1	3	7	10	12	19	24	27	28	36	43	52	65	87	>
AGGRES	1	2	3	7	10	16	20	32	41	62	75	80	90	91	94	99	>
ORDERC	1	2	3	4	6	8	11	13	17	19	24	33	48	65	76	90	>
NEGATI	7	11	21	26	40	47	63	68	73	79	84	89	96	97	98	99	>
AFFECT	4	11	18	24	33	38	47	56	57	64	69	76	82	89	90	95	>
ANXIET	26	44	56	61	69	74	78	82	85	87	89	90	93	97	98	99	>
DEPRES	22	44	65	73	81	83	89	91	92	94	95	96	97	98	99	>	>
ALCOHO	4	9	17	23	31	37	46	52	67	75	83	88	94	97	99	>	>
DOGMAT	4	10	23	39	52	67	78	86	89	93	98	99	>	>	>	>	>
DEFERE	2	4	9	19	32	52	67	74	81	87	93	95	97	99	>	>	>
TEAMOR	1	2	3	6	8	14	16	26	32	36	42	45	50	60	66	89	>
ORGANI	<	1	2	3	4	5	6	7	10	11	18	30	40	54	68	83	>
IMPULS	2	3	7	11	18	32	44	52	62	72	81	90	93	95	98	>	>
RISKTA	<	<	<	1	2	3	5	11	21	27	30	38	51	65	78	89	>

note: N=124

Table 5

ALAPS Scale Internal Consistencies.

Scale	Development Sample	Cross-Validation Sample
CONFID	.71	.73
SOCIAL	.85	.83
AGGRES	.73	.73
ORDERC	.83	.84
NEGATI	.74	.75
AFFECT	.85	.86
ANXIET	.86	.90
DEPRES	.76	.83
ALCOHO	.89	.87
DOGMAT	.73	.75
DEFERE	.75	.73
TEAMOR	.84	.87
ORGANI	.83	.84
IMPULS	.82	.81
RISKTA	.80	.76

Note: Alpha is a Cronbach Alpha internal consistency (reliability) statistic.

Table 6

ALAPS Intercorrelation Matrix

	CON	SOC	AGG	ORD	NEG	AFF	ANX	DEP	ALC	DOG	DEF	TEA	ORG	IMP	RIS
CONFID	-														
SOCIAL	29	-													
AGGRES	55	16	-												
ORDERC	02	-00	-00	-											
NEGATI	-01	-31	34	-04	-										
AFFECT	-22	-03	05	-06	42	-									
ANXIET	-32	-13	-03	09	39	54	-								
DEPRES	-30	-27	-06	-08	48	49	53	-							
ALCOHO	12	20	17	-14	09	14	06	05	-						
DOGMAT	22	-13	37	07	43	10	20	13	08	-					
DEFERE	-21	-21	-25	21	05	01	17	18	-12	08	-				
TEAMOR	-02	48	-07	01	-28	-01	-06	-17	02	-31	-10	-			
ORGANI	07	02	00	77	-18	-21	-06	-23	-15	-02	12	05	-		
IMPULS	14	16	27	-35	25	33	12	15	29	11	-18	00	-42	-	
RISKTA	30	19	27	-19	04	01	-10	-04	25	01	-23	01	-17	42	-

Note: Decimals omitted.

Table 7

ALAPS Factor Structure

Rotated Factor Loadings

	FACTOR1	FACTOR2	FACTOR3	FACTOR4	H2
CONFID	-0.362	0.750	0.096	-0.044	0.705
SOCIAL	-0.088	0.373	0.034	0.744	0.702
AGGRES	0.039	0.824	0.081	-0.164	0.714
ORDERC	0.051	-0.011	0.909	0.035	0.830
NEGATI	0.598	0.287	-0.048	-0.499	0.692
AFFECT	0.817	0.044	-0.122	0.075	0.690
ANXIET	0.824	-0.105	0.115	-0.041	0.704
DEPRES	0.737	-0.164	-0.141	-0.238	0.645
ALCOHO	0.223	0.397	-0.202	0.217	0.295
DOGMAT	0.233	0.452	0.171	-0.541	0.580
DEFERE	0.186	-0.380	0.287	-0.226	0.312
TEAMOR	0.004	-0.025	0.062	0.800	0.644
ORGANI	-0.159	-0.010	0.884	0.089	0.815
IMPULS	0.338	0.471	-0.513	0.121	0.613
RISKTA	-0.038	0.539	-0.328	0.139	0.418
Accounted for Variance	2.669	2.523	2.203	1.970	9.365
%	18	17	15	13	62

Note: H2 are the communalities which are the sum of the squared loadings for each variable. This statistic summarizes the quality of the solution's "fit" for each variable. For the purpose of scree analysis, the first 6 Eigenvalues are 3.125, 2.771, 1.976, 1.493, 0.876, and 0.816.

MODELING HEAT FLUX THROUGH FABRICS EXPOSED TO A RADIANT SOURCE AND ANALYSIS OF HOT AIR BURNS

David B. Reynolds
Associate Professor
Department of Biomedical and Human Factors Engineering

Wright State University
207 Russ Engineering Center
Dayton, OH 45435-0001

Final Report for:
Summer Faculty Research Program
Armstrong Laboratory

Sponsored by:
Air Force Office of Scientific Research
Bolling Air Force Base, DC

And

Armstrong Laboratory

August, 1997

MODELING HEAT FLUX THROUGH FABRICS EXPOSED TO A RADIANT SOURCE AND ANALYSIS OF HOT AIR BURNS

David B. Reynolds
Associate Professor
Department of Biomedical and
Human Factors Engineering
Wright State University

Abstract

We studied previously measured heat flux data through a variety of fabrics of interest to the Air Force, including Nomex, PBI-Kevlar, and aluminized versions of the latter. The fabrics were irradiated with a quartz source at incident heat fluxes ranging from 2.2 to 4.0 $cal/cm^2 \cdot s$. Lumped heat capacity analysis of the data satisfactorily explained the shape of the experimental curves studied, but due to lack of data for optical and thermal properties, some of the parameters were found by curve-fitting. However, some of these compare favorably with those obtained from other studies. In another study, we also successfully simulated hot air skin burns using the BURNSIM model and other engineering data for heat transfer coefficients.

MODELING HEAT FLUX THROUGH FABRICS EXPOSED TO A RADIANT SOURCE AND ANALYSIS OF HOT AIR BURNS

David B. Reynolds

Introduction

Although much research has been done on understanding and predicting skin burns as a function of the amount and nature of the incident heat on the skin and exposure time, comparatively little has been done with predicting burns with clothing on. This may be due to the variety of clothing ensembles and the paucity of information about thermal and optical properties.

We have studied and modeled some of the heating experiments previously done in AL/CFBE at WPAFB, OH. In those experiments, several fabrics were exposed to a radiant quartz lamp source for 3 to 6 seconds and incident and transmitted heat fluxes were measured with calorimeters. For the fabrics which were not appreciably damaged by the exposure, we found reasonably smooth transmitted heat flux curves in response to the step change in incident heat flux. This led us to hypothesize that a thermal lumped capacitance approach may explain the transmitted heat flux, which would also be the incident flux on the skin, if the latter does not affect the process. For several of the fabrics we have successfully modeled the transmitted flux with this approach, using a combination of thermal parameters found in the literature and the optical properties found by curve-fitting. Additional temperature, thermal and optical property measurements need to be done to validate the lumped capacitance approach, but these preliminary results are promising.

Theory and Modeling

Radiant heat transfer through fabric

When analyzing a transient heat transfer problem, such as the present one involving heat transfer through a single or multiple fabric layers, the first approach to consider is the "lumped capacitance method" (Incropera and DeWitt, 1996). In this method, we assume that temperature gradient within the lump or lumps (the size is determined by the analyzer) is small, usually with respect to temperature gradients at the interface between the lump and surrounding fluid (gas or liquid). The method can even be extended to numerical solutions involving many lumps, a thermal resistance and capacity formulation of the energy balance equation (Holman, 1997). These solutions would be equivalent to the more commonly used finite difference methods, which discretize the transient heat conduction equation. The latter approach is used in BURNSIM for example.

The following analysis attempts to model some experimental data previously obtained in the Escape and Impact Protection Branch of the Armstrong Laboratory at Wright-Patterson AFB (AL/CFBE). In these experiments, a radiant heat source irradiated individual fabrics and fabric layers, including

Nomex and Nomex III, two weights of Kevlar fabric, aluminized Kevlar and aluminized PBI/Kevlar. Some experiments had an additional 1/8 in air space or cotton t-shirt material between the fabric and backside calorimeter. Previous workers studied incident heat fluxes in the range 2.0 - 4.0 $cal/cm^2 \cdot s$ for exposure times of 3 or 6 s (Knox, et al, 1997).

The incident radiative flux q_i is absorbed by the fabric, transmitted through the fabric or reflected, i.e.

$$q_i = q_a + q_t + q_r \tag{1}$$

where q_a, q_t, and q_r are absorbed, transmitted and reflected fluxes, respectively. Now q_t is assumed to have no interaction with the fabric and directly and instantaneously impinges upon the calorimeter in the experimental setup. The transmissivity $\Im$ may be defined as q_t/q_i. The q_a is mainly determined by the surface absorptivity coefficient α $(\equiv q_a/q_i)$, which is a complex function of the incident radiation direction and spectrum (Incropera and DeWitt). For example, human skin has $\alpha = 0.97$ for infrared radiation, independent of skin color, but $\alpha = 0.65\text{-}0.82$ for visible light, depending on whether it is white or dark, respectively (Cooney, 1976). The heat absorbed is then stored and conducted through the fabric and over the heating time, radiated and convected off the backside of the fabric to the calorimeter.

The heat flux received by the calorimeter is then comprised of two parts: the direct transmission q_t and the flux convected/radiated off the back surface of the fabric. We have considered two lumped thermal capacitance models for experiments analyzed to date: (1) a single-layer fabric model and (2) a double-layer fabric model.

Single Layer Model, Heating Phase

The lumped capacitance method or model (LCM) uses an energy balance on each lump (layer) to formulate the governing differential equation. The general form on a flux basis is

$$\dot{E}_{in} - \dot{E}_{out} + \dot{E}_{gen} = \dot{E}_{sto} \tag{2}$$

where $\dot{E}_{in}$, $\dot{E}_{out}$, $\dot{E}_{gen}$, and $\dot{E}_{sto}$ represents energy flux coming into the layer, energy flux leaving the layer, energy generated in the layer per unit surface area, and rate of energy stored in the layer per unit surface area, respectively. The $\dot{E}_{gen}$ term could arise from chemical reactions in the layer or effective internal heat generation at depth from laser irradiation, for example. For the present situation, we will neglect this term. The term $\dot{E}_{in} = q_a$, but the $\dot{E}_{out}$ term potentially has two components: heat convected/radiated from the back and front sides of the fabric. Due to the proximity and high temperature of the heat source and low view factor of the front side to cooler structures, we will ignore the latter component during the heating phase. However, this may be a significant mode of heat loss on the subsequent cooling phase. The $\dot{E}_{out}$ term is then modeled by the expression $(T - T_c)/R$, where T is the fabric temperature (assumed uniform in a single-layer LCM), T_c is the calorimeter temperature (assumed constant) and R is the effective thermal resistance to heat transfer between the fabric and the calorimeter.

The energy storage term per unit area ($\dot{E}_{sto}$) is given by $\rho c L \frac{dT}{dt}$, where ρ is the fabric density, c is the fabric heat capacity, L is the fabric thickness, and t is time.

Inserting the above relations into (2) yields

$$q_a - \frac{(T - T_c)}{R} = \rho c L \frac{dT}{dt} = C \frac{dT}{dt} \tag{3}$$

where $C = \rho c L$, a thermal capacitance per unit surface area.

The usual procedure for solving (3), subject to knowing the initial fabric temperature, is to let $\theta = T - T_c$ and therefore, $dT/dt = d\theta/dt$ for T_c constant and separate variables and integrate with the initial condition that at t=0, $T = T_c$ or $\theta = 0$. However, there is a complicating factor in that the calorimeter used to measure heat flux from and through the fabric has a time constant $\Im_c$ of just over 200 msec. ($\Im_c$ was estimated to be 204.8 msec $\pm$4.82% for nine studies of its output for a step input in heat flux. The fluxes in these studies ranged from 0.20 to 4.0 (cal/cm^2·s). The response to the step input also indicated that the calorimeter can be treated as a first-order sensor. Schematically, we may diagram the fabric and sensor models as shown in Figure 1.

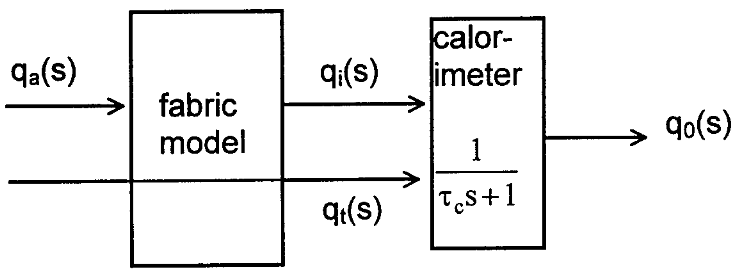

Figure 1: Block diagram of fabric and calorimeter models with inputs and outputs in Laplace (s) domain. q_a and q_t have been defined, q_i is the heat flux from the back side of the fabric and q_o is the calorimeter output.

Taking the Laplace transform of (3) and substituting $\theta = T - T_c$ gives

$$q_a(s) - \frac{\theta(s)}{R} = C\big(s\theta(s) - \theta(0)\big) = Cs\theta(s) \tag{4}$$

assuming $\theta(0)=0$. Solving for $\theta(s)/R = q_i(s)$ gives

$$\frac{\theta(s)}{R} = q_i(s) = \frac{q_a(s)}{RCs + 1} \tag{5}$$

where $q_i(s)$ is the radiation/convection flux into the calorimeter. For q_a constant, which is approximately true for the experimental data we will analyze, then

$$q_i(s) = \frac{q_a}{s(\Im_f s + 1)} \tag{6}$$

where $\Im_f$ = RC. Now the total input to the calorimeter $q_i(s) + q_t(s)$, where q_t is the directly transmitted portion of the incident radiation. The calorimeter output $q_0(s)$ is then given by

$$q_0(s) = \left(q_i(s) + q_t(s)\right)\frac{1}{\Im_c s + 1} \tag{7}$$

If we also assume that q_t is a constant for a given experiment, then inserting (6) into (7) yields

$$q_0(s) = \left(\frac{q_a}{s(\Im_f s + 1)} + \frac{q_t}{s}\right)\frac{1}{\Im_c s + 1} \tag{8}$$

Taking the inverse Laplace transform of (8) gives the calorimeter output in the time domain:

$$q_0(t) = q_a\left(1 - \left(\frac{\Im_f}{\Im_f - \Im_c}\right)e^{-t/\Im_f} + \left(\frac{\Im_c}{\Im_f - \Im_c}\right)e^{-t/\Im_c}\right) + q_t\left(1 - e^{-t/\Im_c}\right) \tag{9}$$

Note that the second term on the rhs of (9) is initially zero, so even though a direct radiant transmission may occur, it is not seen in the output recording of the calorimeter. For good data, $\Im_c$ should be at least 10 times smaller than $\Im_f$. Once the unknown parameters are found, the actual heat flux through the fabric and presumably incident on the skin may be found by setting $\Im_c$=0 in (9), resulting in

$$q_{i,sk} = q_a\left(1 - e^{-t/\Im_f}\right) + q_t \tag{10}$$

To incorporate this input in BURNSIM, an appropriate skin absorption coefficient is required. Because the first term in (10) is a combination of convection and longer wavelength radiation, a coefficient near one is likely. The second term is radiation in the visible spectrum and the coefficient depends upon skin color, but is likely to be lower.

An alternative approach in time domain is to write an additional equation for the calorimeter:

$$\frac{\theta}{R} + q_t = q_0 + \Im_c\frac{dq_0}{dt} \tag{11}$$

Eqs (3) and (11) could be simultaneously solved for the calorimeter output q_0. The inital condition for (11) is that $q_0(0)$=0. We also can readily appreciate that as $\Im_c \to 0$, the calorimeter output q_0 will become the sum of the radiated/convected heat from the fabric (θ/R) and the directly transmitted heat (q_t).

Double Layer Model

In the single layer model, the fabric is treated as a single lump, i.e. uniform in temperature. In a two layer model, we may divide the fabric up into two parts, a front part and a back part. While in each of these parts temperature is uniform, in this model a temperature difference can exist between the front and back parts.

For the front side layer, the energy balance equation is similar to (3):

$$q_a - \frac{(T_1 - T_2)}{R_1} = C_1\frac{dT_1}{dt} \tag{12}$$

where subscripts 1 and 2 refer to the front and back layers, respectively and R_1 is a thermal resistance

connecting layer 1 and 2 and $C_1 = \rho_1 c_1 L_1$ is the thermal capacitance per unit surface area of layer 1.

As for the single layer model, we assume no heat loss from the front side toward the heat source. Again, this formulation is for the heating phase. The thermal resistance $R_1 = L_1/k_1$ where L_1 and k_1 are the thickness and thermal conductivity of the fabric.

Layer 2 has the following energy balance equation:

$$\frac{T_1 - T_2}{R_1} - \frac{(T_2 - T_c)}{R_2} = C_2 \frac{dT_2}{dt} \tag{13}$$

where R_2 is a thermal resistance connecting the fabric back side to the calorimeter and C_2 is the thermal capacitance of layer 2, $\rho_2 c_2 L_2$. However, because an air gap exists between the fabric and calorimeter, some contribution from the latter may need to be included in R_2 and C_2.

Finally, just as in (11), the calorimeter input/output equation can be written:

$$\frac{T_2 - T_c}{R_2} + q_t = q_0 + \Im_c \frac{dq_0}{dt} \tag{14}$$

After transforming the temperature differences: $\theta_1 = T_1 - T_c$ and $\theta_2 = T_2 - T_c$, where T_c is again assumed constant, the set of coupled Eqs (12), (13) and (14) can be written:

$$q_a - \frac{(\theta_1 - \theta_2)}{R_1} = C_1 \frac{d\theta_1}{dt} \tag{15a}$$

$$\frac{(\theta_1 - \theta_2)}{R_1} - \frac{\theta_2}{R_2} = C_2 \frac{d\theta_2}{dt} \tag{15b}$$

$$\frac{\theta_2}{R_2} + q_t = q_0 + \Im_c \frac{dq_0}{dt} \tag{15c}$$

Initial conditions are $\theta_1(0)=0$, $\theta_2(0)=0$ and $q_0(0)=0$, i.e. initial temperatures of fabric and calorimeter are equal and no initial output of the calorimeter.

The general solution of (15a,b,c) is complex and with readily available computational power, solving these equations numerically is easier. However, in light of heat flux measurements of certain fabrics which show a nearly linear portion of the calorimeter heat flux vs. time curve, we solved these equations under certain conditions that result in a linear term in the solution.

The approach is the same as for the one layer model, except that (15a,b) are Laplace transformed and solved for $\theta_2 / R_2 = q_i$, the heat flux radiated/convected to the calorimeter. We noted that when $\Im_1\Im_2 = (R_1C_1)(R_2C_2) >> 0$, then following the same procedure as in (5) through (8) above, the following calorimeter heat flux solution resulted:

$$q_0(t) = q_a\left[\frac{t}{\Im} - \frac{1}{\Im}(\Im' + \Im_c) + \frac{(\Im_1\Im_2)^2}{\Im^3(\Im' - \Im_c)} e^{-t/\Im'} - \frac{\Im_c^2}{\Im(\Im' - \Im_c)} e^{-t/\Im_c}\right] + q_t\left(1 - e^{-t/\Im_c}\right) \tag{16}$$

where $\Im = \Im_2 + \Im_1(1 + R_2/R_1)$ and $\Im' = \Im_1\Im_2/\Im$.

As in Eq (10), the actual heat flux can be found by setting $\Im_c = 0$, yielding

$$q_{i,sk} = q_a\left[\frac{t}{\Im} + \frac{\Im'}{\Im}\left(e^{-t/\Im'} - 1\right)\right] + q_t \tag{17}$$

Analysis Methodology

Up to this point, the double layer model is quite general, requiring inputs of q_a, q_t, R_1, R_2, C_1, C_2 and $\Im_c$ for solution. Ideally, values of these parameters should be obtained from other experimental data, for example, fabric thermal resistance R=L/k from fabric thickness and thermal conductivity. Paucity of such data exists in the literature (Lawson, personal communication). Moreover, parameters such as thermal conductivity, heat capacity and density may be functions of temperature. Absorptivity and transmittivity are also functions of the fabric surface and construction as well as the spectrum of the incident radiation. Consequently, our approach was to estimate parameters for which some data was available and adjust others so that we could reasonably fit previously obtained radiant exposures of several fabrics. Specifically, we used values of density, heat capacity and thermal conductivity given in the Aerotherm report and then used least squares to fit the analytical solution, Eq. (9). Although in principle this procedure could also be done for the double layer solutions given by Eq. (16), we have not done this at this time because additional decisions about the relative size of thermal resistances and capacitances of the layers needs to be resolved. With no other data than the heat flux reaching the sensor, this is pure guesswork. If, however, temperatures of the front and back faces of the material were known, we could determine whether a two layer model was appropriate and attempt to partition the total thermal resistance and capacitance for use in the double layer model.

To date, the approach outlined above has been used to model Nomex III data from 1995 studies done in the THEFT laboratory in AL/CFBE. The NOMEX studies were chosen for analysis because some properties of this material were given in the Aerotherm report. Additionally, the calorimeter heat flux curves for this material indicated a smoothly rising, asymptotic curve resembling a solution of the single layer model. Of course, with the right parameter values, the double layer model could also be used, but we thought that without temperature information referred to above, the simpler model would be appropriate.

Theory for Hot Air Study

We also attempted to predict burn injury from hot air jets impinging on bare forearm skin (Ft. Knox study, 1944). The details of the experimental procedure in these studies are sketchy, particularly regarding the mass flow rates of air. Volumetric flow rate of 6 L/min is given, but temperature and pressure at which this flow was measured are not. Of course, this information is especially important for gas flows.

The main problem in this forced convection study is estimating the local convection heat transfer coefficient, h. The convection coefficient is mainly a function of the Reynolds number at the jet outlet, air thermal conductivity, the distance from the nozzle outlet to the skin, and the distance from the stagnation point (site on skin directly opposite the centerline of the jet) to the point of interest on the skin surface. Reynolds number at a circular jet nozzle of diameter D is given by

$$Re = \frac{\rho V D}{\mu} = \frac{4\dot{m}}{\pi D \mu} \tag{18}$$

where ρ, μ are gas density and viscosity, respectively, V is average gas velocity at the nozzle, and $\dot{m}$ is the gas mass flow rate.

We initially estimated $\dot{m} = \rho\dot{V}$ ($\dot{V}$ is the volumetric flow rate) by estimating gas density assuming 1atm pressure and room temperature, 20°C. Correlations of h for impinging gas jets are given by Martin (1977). We assumed the jet was about 2 nozzle diameters (nozzle diameter was 1 cm) from the skin and since the highest h values are for the stagnation point, this point or nearby it would produce the worst burn for a given exposure time. The convective heat flux q_c is given by

$$q_c = h(T_a - T_s) \tag{19}$$

where T_a is the jet temperature and T_s is the skin temperature. Because of present input limitations of BURNSIM, we assumed T_s was constant, and thus (19) produces a constant heat flux. Of course, T_s would increase over the time of exposure, so using (19) should produce a high estimate of the flux, especially for the longer exposure times for the lower temperature air jets.

However, in all cases (air jets of 100°C, 200°C, 300°C, 400°C and 500°C were studied in the Ft. Knox report), BURNSIM produced no burn at exposures reported to produce second degree burns. We noted that estimated Reynolds numbers were about 1/4 to 1/3 of the lowest values reported in the Martin study. We consequently believe that mass flow rates were underestimated and we used h values from Martin at the lowest Re's studied in his report. These Re were in the range of 2000 to 3300. Interestingly, the highest Re were for the lowest temperature and vice versa. This is due to the fact that higher temperature gas has higher viscosity. The increased thermal conductivity of air with temperature reverses the Re effect, and h increases with increasing air temperature. As shown later, using heat fluxes computed from these h values in BURNSIM showed better agreement between BURNSIM and the data.

Results and Discussion

Fabric heat flux studies

Nomex III

Although the heat transfer resistance of the fabric is supposed to be negligible in the single layer model (Eq(3)), where resistance R is the thermal resistance <u>between</u> the fabric and calorimeter, we decided to try to compute R from fabric properties, i.e., R=L/k, where L is fabric thickness and k is fabric thermal conductivity. Thickness of the Nomex III sample was 0.066 cm and $k=7.5 \times 10^{-5}$ cal/cm·s·°C as recomputed from the Aerotherm report, p.106. Resistance is thus 880 cm^2·s·°C/cal. Thermal heat capacity $C=\rho cL=2.8\times10^{-2}$cal/$cm^2$·°C, where Aerotherm values of density and heat capacity are 1.4 g/cm^3 and 0.30 cal/g·°C, respectively. Note that this results in a fabric time constant $\Im_f$ =RC=24.6s. We used this value of $\Im_f$ and the calorimeter time constant $\Im_c$=0.2048s in (9) and used a least squares curve fitting routine (ProStat, Poly Software International, Salt Lake City, UT) to compute q_a and q_t from a 1995 study

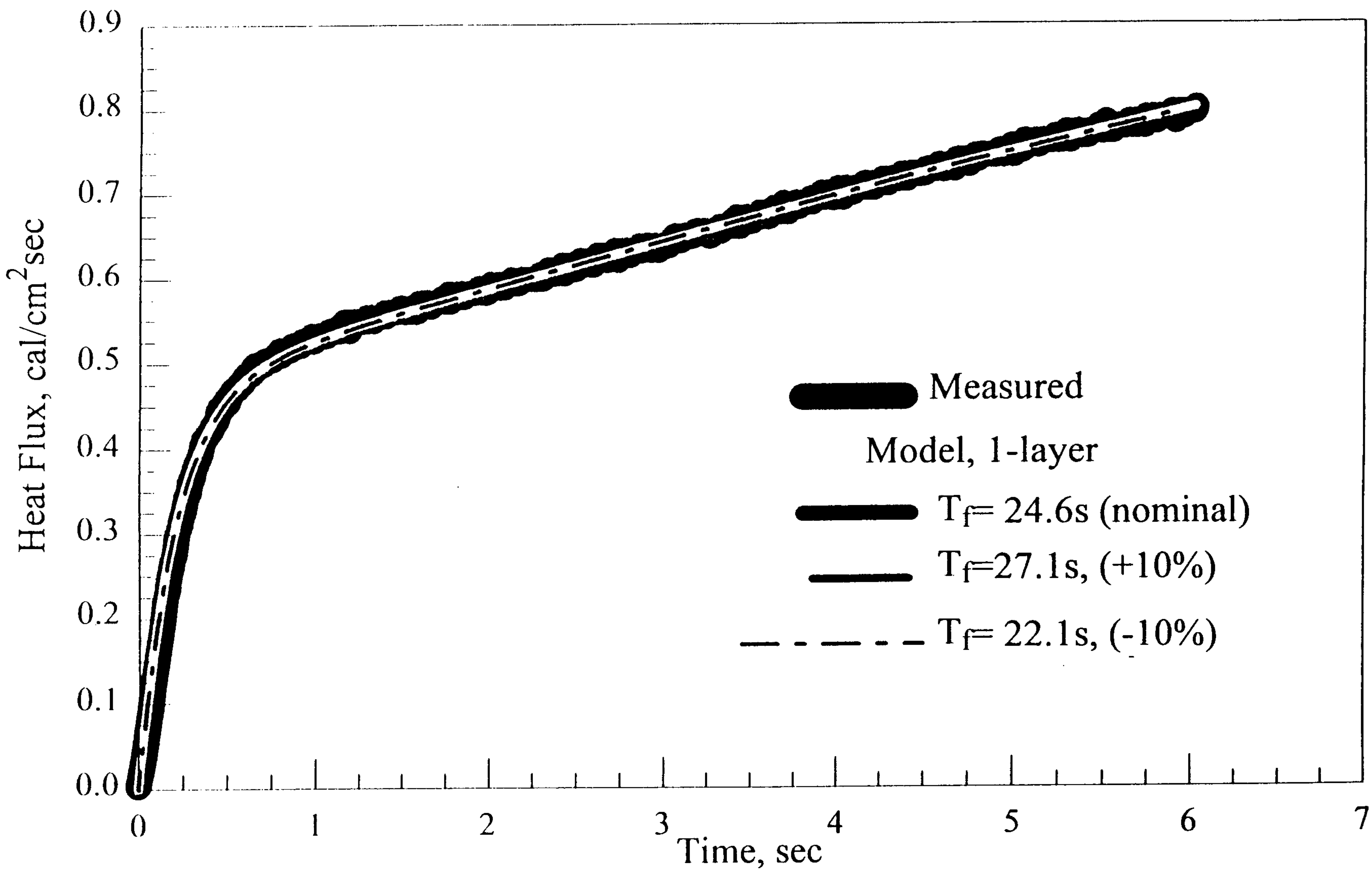

Fig. 2. Heating Curve for Nomex III, 6s Exposure, test AG2B1, 4 Oct 95
Incident Heat Flux = 2.2 cal/cm^{2}sec

in the THEFT lab which had an incident quartz lamp radiation of 2.2 cal/cm^2·s. The graphical results are shown in Fig.2. We also looked at the fit when $\Im_f$ was increased or decreased by 10%. We found very little difference in the overall fit, but there were some differences in the values of q_a and q_t, as shown in Table 1.

Table 1. Calculated and estimated parameters for Nomex III, Test AG2B1, incident flux of 2.2 cal/cm^2·s

$\Im_f$ (sec)	$q_a(\mathrm{cal/cm^2 s})$	$q_t(\mathrm{cal/cm^2 s})$	α	$\Im$
24.6	1.52	0.482	0.691	0.219
27.1(+10%)	1.65(+8.5%)	0.483(+0.21%)	0.750	0.219
22.1 (-10%)	1.38(-9.2%)	0.481(-0.21%)	0.627	0.219
17.5*	1.13	0.479	0.514	0.218

*$\Im_f$, q_a, q_t allowed to vary to find least squares fit.

Note that ±10% changes in the estimated value of $\Im_f$ produced nearly equal percent changes in estimated q_a, but very little change in estimated q_t. The calculated absorptivity α and transmissivity $\Im$ are given in the last two columns. Our absorptivity value is considerably higher than reported in the Aerotherm report (p.83) for virgin state Nomex at quartz lamp temperature (2480°C), where they report α=0.32. However, $\Im$ values are much closer in agreement, 0.250 vs. 0.219. Thus, we may have overestimated $\Im_f$, which would lead to overpredicting q_a and α with very slight effects on q_t and $\Im$. For example, if we let the fitting routine find the least squares fit by also allowing $\Im_f$ to vary, we obtain q_a=1.13 cal/cm^2·s, q_t =0.479 and $\Im_f$=17.5 s. This yields α=0.514 and $\Im$=0.218, considerably closer to the Aerotherm data. Also, we must note that our sample of material was NOMEX III, a more recent version of NOMEX containing 5% Kevlar. This may also account for differences in property values from those given in the Aerotherm report. Finally, we note that the actual flux reaching the calorimeter and presumably incident on the skin would be given by (10), using values from Table 1.

Aluminized PBI-Kevlar

The 1995 studies at the THEFT facility in AL/CFBE also looked at aluminized PBI-Kevlar. Not having found any data on optical and thermal properties of this material, we decided to approach the analysis using the same approach as immediately above, i.e. estimate $\Im_f$ as well as q_a and q_t. This appeared especially promising as the data exhibited an asymptotically rising curve as shown in Figure 3.

The results of least-squares fitting is given in Table 2. Also given are coefficients of variation, i.e. the standard deviation as a percentage of the best fit value. We note that the estimated fabric time constant is about an order of magnitude smaller than for NOMEX III, however it is still about an order of magnitude larger than the calorimeter time constant, so results should be reliable. Computed absorptivity and transmissivity for quartz lamp radiation are both much smaller than for NOMEX III, but this is to be expected for materials with an aluminum coating. We would expect that α would be larger for a radiation spectrum simulating fires and the effect of soot on the

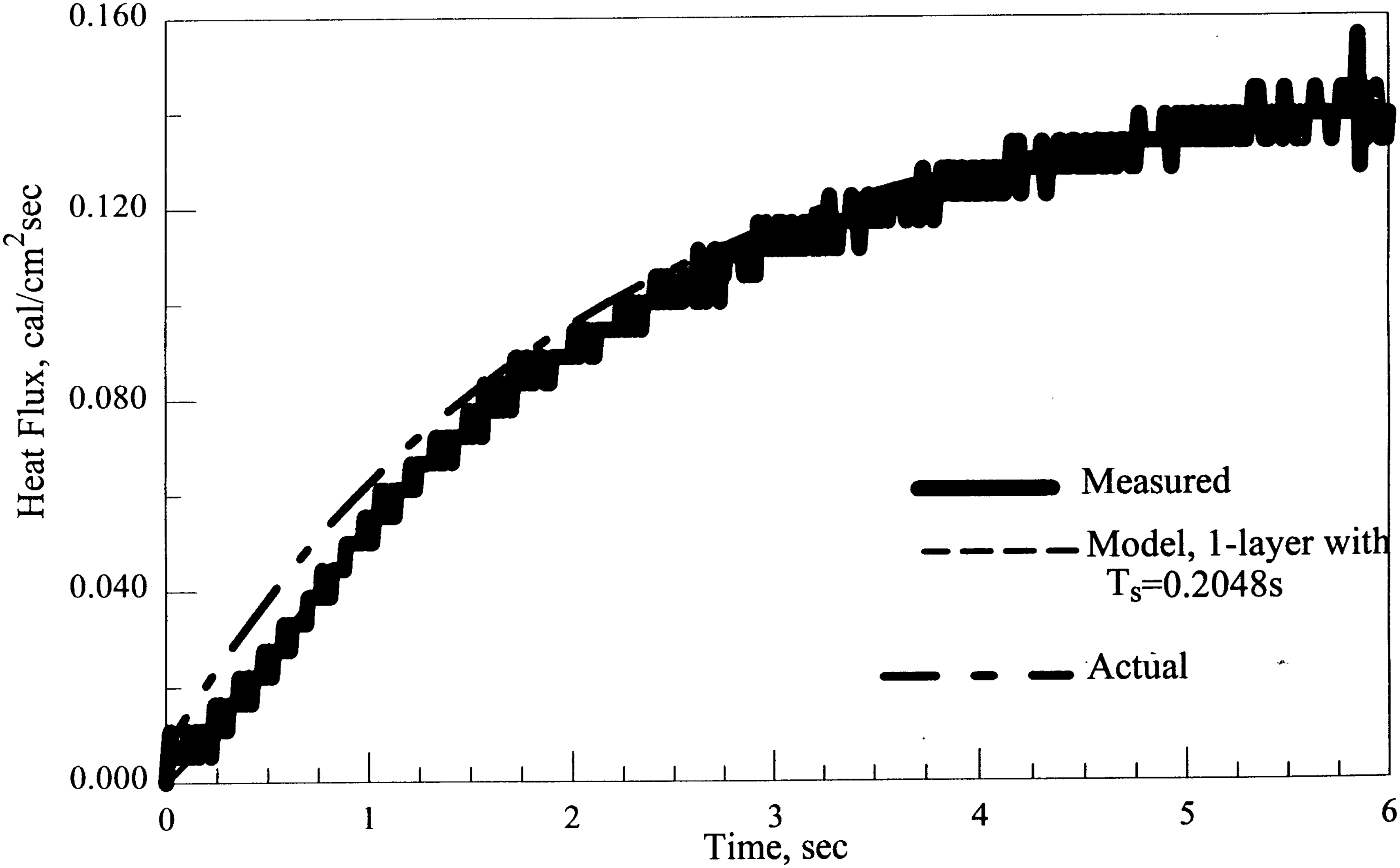

Fig.3. Heating Curve of Aluminized PBI/Kevlar,Test AD10B1, 6s Exposure
Incident Flux = 2.2 cal/cm^{2}sec

surface layer would probably cause an additional increase. This outer layer probably blocks pores in the material and thus the low $\Im$ value. Thermal resistance and capacitance of the material are probably mainly determined by the underlying PBI-Kevlar because the aluminum coating is very thin. Also note that due to the low q_t, calorimeter measurement and predicted actual heat flux are nearly

Table 2. Estimated parameters for aluminized: PBI/Kevlar and Kevlar, and non-aluminized PBI/Kevlar, Test AD1OB1, AC1A1 and AE2B1 respectively. Incident heat flux of 2.2 cal/cm^{2}s in all tests.

	$\Im_f$ (sec)	q_a(cal/cm^{2}s)	q_t(cal/cm^{2}s)	α	$\Im$
Alum. PBI/Kevlar	$1.99 \pm 1.205\%$	$0.140 \pm 0.372\%$	$0.00731 \pm 7.95\%$	0.064	0.0033
Alum. Kevlar	$2.48 \pm 3.127\%$	$0.122 \pm 1.515\%$	$0.00563 \pm 7.64\%$	0.056	0.0026
PBI/Kevlar	$10.7 \pm 6.44\%$	$1.133 \pm 4.792\%$	$0.4122 \pm 0.496\%$	0.515	0.187

the same.

Aluminized Kevlar

The radiant heating plot for this material and least squares parameter values are given in Fig. 4 and Table 2. Parameter values for aluminized Kevlar are similar to those of aluminized PBI/Kevlar, although the thermal time constant for aluminized Kevlar is about 25% larger.

Non-Aluminized PBI/Kevlar

The heating plot and least squares parameter values of 6 oz/yard PBI/Kevlar are given in Fig. 5 and Table 2. This heating curve has an unusual inflection point at 1.8 seconds, which was even more pronounced in the 7.5 oz/yard sample (not shown). These results make the single-layer model suspect. For example, using the two-layer model (Eq (16)) on these results, we have noted a similar inflection point. However, a general least squares fit using Eq (16) leads to unreasonably large standard deviations of some of the estimated parameters, or sometimes, unreasonably large values of the parameters themselves. Thus, Eq (16) is much better suited to a fit where more of the parameters are known, eg., R_1, R_2, C_1 and C_2 and therefore, $\Im_1$ and $\Im_2$. Front and backside temperature measurement would also be helpful in validating a two-layer model of the fabric.

Hot Air Burns Study

The first item to estimate in the Ft. Knox hot air burns study is the mass flow rate of air, presumed constant for each temperature studied. We initially assumed that where the Ft. Knox investigators measured an air volume flow of 6 L/min, the temperature and pressure were 20°C and 1 atm, respectively. Air density at this temperature and pressure is 1.210 kg/m^3, resulting in a mass flow rate of 1.21×10^{-4} kg/s.

The main problem in convection is determining the convective heat transfer coefficient, h, in

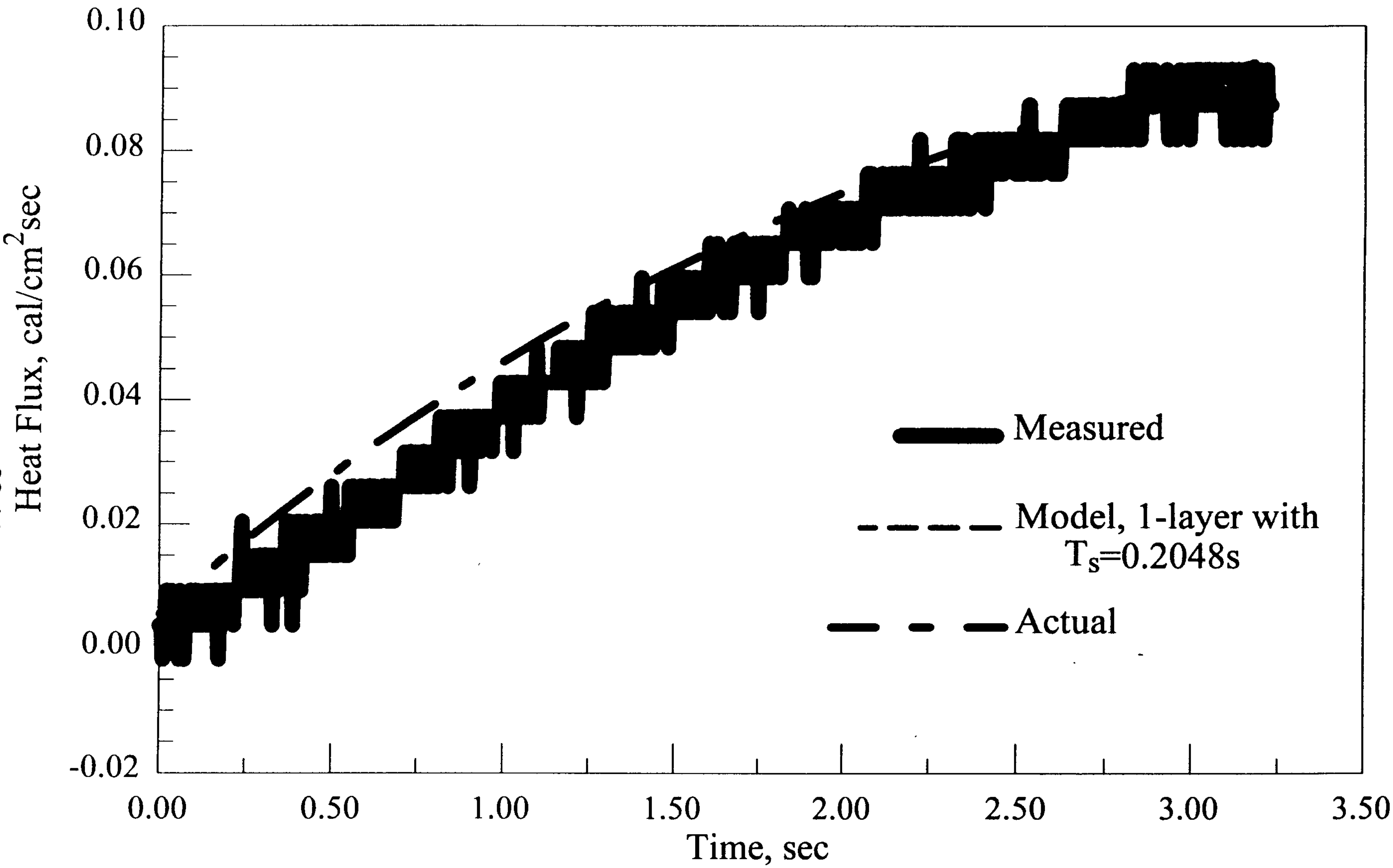

Fig.4. Heating Curve of Aluminized Kevlar, Test AC1A1, 3 s Exposure. Incident Heat Flux = 2.2 cal/cm^2sec.

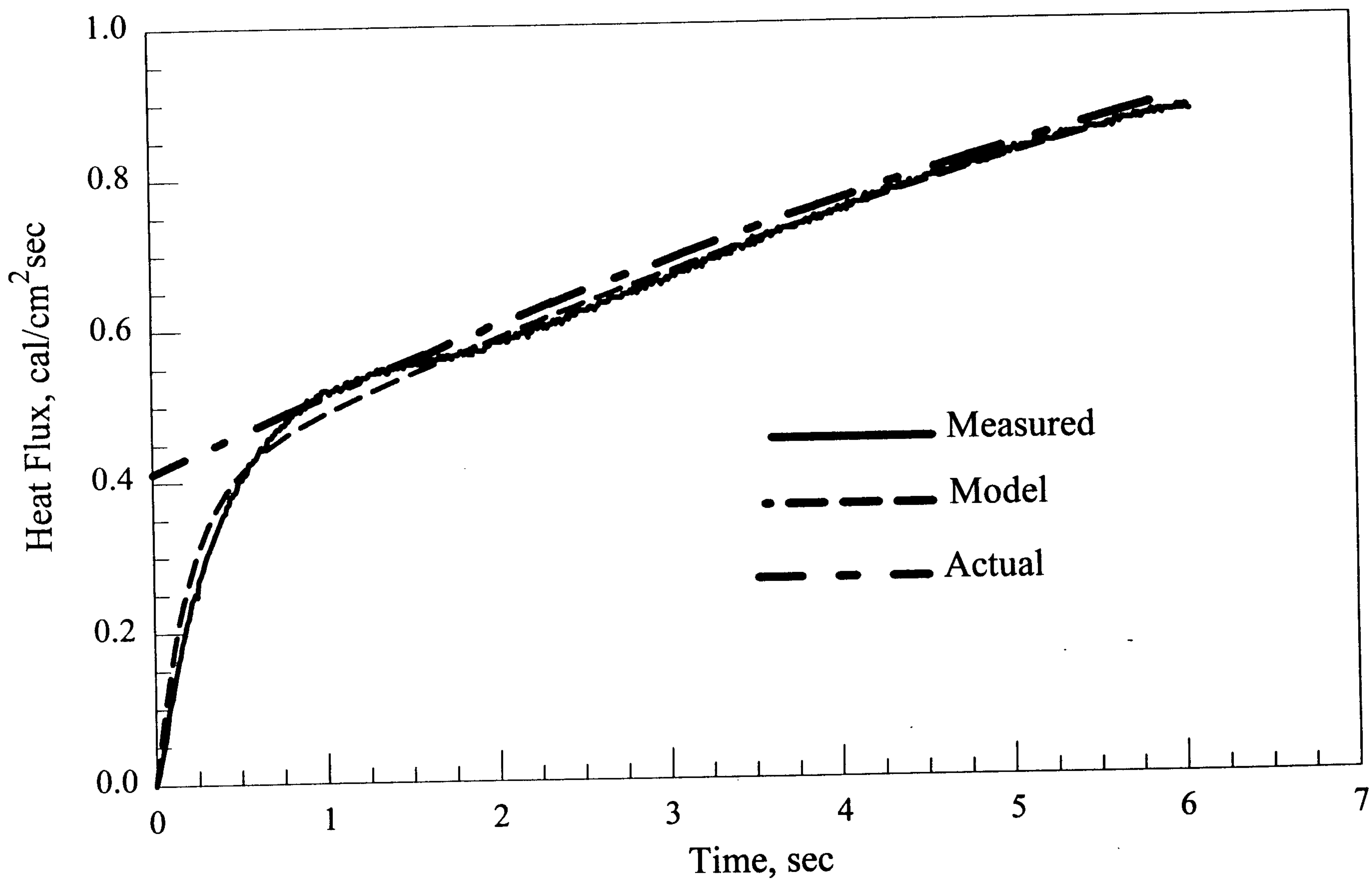

Fig.5. Heating Curve of 6.0 oz/y PBI/Kevlar, Test AE2B1, 6 sec Exposure.
Incident Heat Flux = 2.2 cal/cm^{2}sec.

this case the local value for an air jet impinging upon a nearly flat surface. Martin has extensive data on these coefficients, and for the region near the stagnation point, only graphical results are available. However, except for a very minor correction term, i.e., close to unity, the results for local h for the case in which the nozzle is 2 nozzle diameters (in this case, 2 cm) away from stagnation point is approximately given by

$$Nu = hD/k \approx 1.12\, Re^{0.5}\, Pr^{0.42} \qquad (20)$$

where Nu is the Nusselt number, k is fluid thermal conductivity, and Pr (Prandtl number) is the ratio of fluid kinematic viscosity to thermal diffusivity. For the five temperatures studied, we tabulate the important parameters in Table 3. As mentioned earlier, we chose Re = 2000 as the lowest value, which is for 500°C air. If we used Re based on the $\dot{m}$ value given above, then no burn was predicted by BURNSIM. This finding indicates that pressure and/or temperature was actually higher than what we have assumed. A Re = 2000 was also chosen because it is the lowest value given in the Martin study.

Results of modeling the Ft. Knox study are summarized in Table 3. Convection heat flux q_c was computed by Eq (19) using estimated h and skin surface temperature of 34.5°C, assumed constant. This produces a constant heat flux given also given in the table. Assuming a constant surface temperature will overestimate the heat flux, especially for the lower temperature air at longer exposure times. We found a reasonable prediction of 1st and 2nd degree burns by BURNSIM at each temperature, with a tendency to overpredict exposure times for a given burn at higher flux, shorter duration exposures and underpredict times for lower flux, longer duration exposures.

Conclusions and Recommendations

The following conclusions about the modeling of the THEFT laboratory experiments and the use of BURNSIM to model hot air burns in the Ft. Knox study may be made:

1. For certain experiments, a single-layer LCM is consistent with observed results. For other fabrics, a double or even multilayer approach is probably required. The modeling described here is only appropriate for cases in which fabric properties are reasonably constant over time and temperature and no chemical reactions are occurring.
2. So that modeling is less of an exercise in curve-fitting, thermal and optical properties of the fabrics should be measured independently as functions of temperature and radiation spectrum.
3. Although we obtained reasonable predictions of 1st and 2nd degree hot air burns, insufficient data on the methodology in the Ft. Knox studies required crude estimates of the most important parameter, the convection heat transfer coefficient.

We recommend for future studies of heat flux through protective fabrics that two heat sources be used, one simulating the radiation from fires and another that from higher temperature radiation. Temperatures should be measured at the front and back sides of the fabric to aid in model validation. For multiple fabric layers, additional interfacial temperatures should be measured.

Table 3: Estimated Parameters, BURNSIM simulations and burn data for the Ft. Knox hot air burn study.

Air Temp. (°C)	Re	Pr	k cal/cm·s·°C	H cal/cm²·s·°C	q_c cal/cm²·s	BURNSIM Exposure Time, s	Range of Actual Exposure Time, s	Predicted Burn
500	2000	0.705	1.34×10^{-4}	5.79×10^{-4}	2.70	0.22	0.065-0.15	1st degree
						0.25	0.08-0.3	2nd degree
400	2188	0.692	1.22×10^{-4}	5.47×10^{-4}	2.00	0.33	0.16-0.25	1st degree
						0.38	0.025*	2nd degree
300	2438	0.684	1.08×10^{-4}	5.09×10^{-4}	1.35	0.59	0.50-1.0	1st degree
						0.65	0.75-1.6	2nd degree
200	2786	0.685	0.932×10^{-4}	4.70×10^{-4}	0.780	1.35	1.0-2.0	1st degree
						1.50	2.0-2.5	2nd degree
100	3313	0.695	0.760×10^{-4}	4.20×10^{-4}	0.277	6.1	4.0-8.0	1st degree
						6.9	7.0-10.0	2nd degree

* one case of 2nd degree burn

REFERENCES

Analysis of the Thermal Response of Protective Fabrics, Tech. Rep. AFML-TR-73-14, Aerotherm Division/Acurex Corp, 1973.

Cooney, D.O. Biomedical Engineering Principles, Ch. 5, Dekker, 1976.

Holman, J.P., Heat Transfer, 8th Ed., Ch. 4, McGraw-Hill, 1997.

Incropera, F.P. and D.P. DeWitt, Fundamentals of Heat and Mass Transfer, 4th Ed., Ch. 5, Wiley, 1996.

Knox, F.S., C. Perry, B. Billotte and S. Ringhand, Burn Hazard in Aircraft Fires, NATO AGARD-CP-587, 1997, p.32-1-10.

Lawson, R., Personal Communication, NIST, Gaithersburg, MD.

Martin, H., Heat and Mass Transfer between Impinging Gas Jets and Solid Surfaces, Adv. in Heat Transfer, V. 13, 1977, p. 1-60.

Methods of Protection Against Flash Burns, U.S. Army Med. Res. Lab., Ft. Knox, KY, Proj. 14, AD657228, 1944.

DESORPTION AND BIODEGRADATION OF DINITROTOLUENES IN AGED SOILS

Barth F. Smets
Associate Professor
Environmental Engineering Program

University of Connecticut
241 Glenbrook Road
Storrs, CT 06269

Final Report for:
Summer Research Program
Armstrong Laboratory

Sponsored by:
Air Force Office of Scientific Research
Bolling Air Force Base, Washington, DC

And

Armstrong Laboratory

August 1997

Desorption and Aerobic Biodegradation of Dinitrotoluenes in Aged Soils

Barth F. Smets
Assistant Professor
Environmental Engineering Program
University of Connecticut

Abstract

A study on the desorption kinetics and the biodegradation of dinitrotoluenes in aged soils was performed. Aged clayey soil contaminated with 2,4-DNT, 2,6-DNT, and 2,4,6-TNT was obtained from the Volunteer Army Ammunitions Plant in Chattanooga, Tennessee. The average extractable concentrations of 2,4-DNT, 2,6-DNT, and 2,4,6-TNT were 0.278 (±.004), 0.079 (±.002), and 0.297 (±.004) mg/g, respectively. The organic carbon content (f_{oc}) was 0.70 (± 0.09)%. Using Tenax beads as an infinite sorptive sink, sequential desorption experiments were performed to measure the long-term desorption of DNT and TNT from the soil: 76% and 89% of the extractable nitrotoluenes were desorbed from the soil in one and three days, respectively. Biodegradation of the DNTs was measured in factorial soil slurry experiments. 2,4-DNT was readily available for degradation by the indigenous microorganisms. Complete mineralization, as evidenced by near stoichiometric NO_2^--N release, was achieved within 5 days. Addition of a known 2,4-DNT and 2,6-DNT degrading bacterial strain did not show any benefit. Little mineralization of 2,6-DNT was observed. Additional experiments were performed to evaluate the toxicity or inhibition of 2,6-DNT and TNT towards 2,6-DNT mineralization. The addition of either Tenax beads to reduce the aqueous concentration of 2,6-DNT and TNT or an induced 2,6-DNT degrader (JS922) to the soil slurries did not stimulate 2,6-DNT biodegradation. In separate experiments, it could not be confirmed that TNT at 25 mg/L negatively impacted 2,6-DNT mineralization by JS922. The above work indicates that rapid desorption of nitrotoluenes from the clayey soil tested makes compounds such as 2,4-DNT and 2,6-DNT readily available for biodegradation; that indigenous microorganisms can readily mineralize 2,4-DNT; while stimulation of 2,6-DNT mineralization appears difficult.

DESORPTION AND BIODEGRADATION OF NITROTOLUENES FROM AGED SOILS

by

Barth F. Smets

INTRODUCTION

Significant contamination of nitrotoluenes in soil and groundwater around the world has prompted an interest in their cleanup. Because nitrotoluenes are toxic, mutagenic and/or potentially carcinogenic they pose a human health risk (6). Although 2,4-dinitrotoluene and 2,6-dinitrotoluene contamination is historically of military origin resulting from TNT manufacturing, they also occur in industry as precursors in polyurethane production. As a result, millions of pounds of DNT are released into the environment each year (6).

Both anaerobic and aerobic biotransformation of DNTs has been reported (12). Anaerobic biotransformation typically is the result of an unspecific reduction of the nitro groups to nitroso, hydroxylamino, and eventually amine groups (12). The potential accumulation of the nitroso and hydroxylamino intermediates, which are more toxic than the parent compounds, plagues anaerobic processes for DNT biotransformation. Many pure cultures have been isolated that can completely mineralize both 2,4 and 2,6-DNT as a sole carbon and energy source. Aerobic biodegradation of DNT involves oxygenolytic denitration pathways, releasing nitro groups as NO_2^- (12, 13).

The overall rate of biodegradation of a compound is determined by its bioavailability (10). Contaminants released in soils can become less bioavailable by sorption into soil organic matter and micropore diffusion into soil particles preventing contact between the contaminant and microorganisms. As the soil ages, the pollutants can diffuse deeper into the soil particle or become covalently bound with the soil organic matter. As a result, aging can further decrease bioavailability.

There were three main objectives to this research. The first objective was to measure the desorption kinetics of DNT in aged contaminated soils in sequential desorption experiments. Second, DNT mineralization kinetics in aged contaminated soil were measured in factorial soil slurry experiments. Finally, the toxicity/inhibition effects of 2,6-DNT and TNT on the biodegradation of 2,6-DNT were investigated.

MATERIALS AND METHODS

Bacterial Inoculum

JS922, a bacterial strain known to degrade both 2,4-DNT and 2,6-DNT, was used for all experiments. It was pregrown at 30°C in shake flasks containing a mineral medium supplemented with 2,4-DNT or 2,6-DNT. The medium contained XAD-7 Tenax beads (Sigma, St. Louis, MO) at 10 g/L to maintain a sub-toxic, aqueous concentration of DNTs. The mineral salts medium, termed MM-C, was a 1/100 dilution of Stanier's mineral salts medium (14) but free of inorganic nitrogen, and provided macronutrients and 0.5 mM pH buffering capacity. The total ionic strength of the mineral salts medium was 3.3 mM. The addition of 50 mg/L or 200 mg/L of $HgCl_2$ increased the ionic strength to 3.5 and 4.3 mM, respectively.

HPLC Analysis

In all experiments performed, high performance liquid chromatography (HPLC) separation followed by a UV-detection at 540 nm was used to measure DNT concentrations. The method used a C6-hexyl column (Spherisorb, Alltech, Deerfield, IL) and a solvent system consisting of 70% deionized water and 30% methanol. Confirmation of HPLC peaks during initial analysis of soils was performed using a second HPLC method using a CN column (Zorbax, Hewlett Packard) and a solvent system consisting of 30% acetonitrile and 70% deionized water (7).

Nitrate Analysis

Samples were centrifuged at 14,000 rpm for 5 min. and the supernatant was analyzed with a Dionex DX-300 Series Chromatography System equipped with a Dionex AS11 column and CDM-2 conductivity detector (Dionex, Sunnyvale, CA). The eluent was 19 mM NaOH at a flow rate of 0.65 ml/min.

Nitrite Analysis

Nitrite analysis was performed by a modified standard method (4). A 0.7 ml sample was centrifuged at 14,000 rpm for 5 min. The supernatant was analyzed colorimetrically by mixing 1 ml of deionized water and 0.1 ml of sulfanilamide with 0.1 ml of sample. The solution was allowed to react for 5 min. before 0.1 ml of N-(napthyl)diethylenediamine was added. Samples were vortexed and allowed to react for 15 min. prior to reading their absorbance at 543 nm using a UV-spectrophotometer.

Soil Treatment

Three different soil samples were received from the Volunteer Army Ammunitions Plant in Chattanooga, Tennessee. The soils were expected to contain large quantities of 2,4-DNT, 2,6-DNT, and 2,4,6-TNT. The concentration of total extractable DNTs and TNT were measured according to established protocols(7). Two gram aliquots of soil (air dried and homogenized with mortar and pestle to pass through a 30 mesh sieve) were measured in a Teflon® lined vial containing 10 ml of methanol as the extracting agent. The vials were mixed by vortexing for one min. and were shaken at 200 rpm overnight at 30°C. The vials were removed and allowed to settle for 30 min.. A 5 ml aliquot of the sample combined with 5 ml of $CaCl_2$ (5 g/L) was centrifuged at 740 g for 5 min. to separate the soil fines. The supernatant fraction was analyzed by HPLC for total extractable nitrotoluenes.

Cell enumeration

Cells were dislodged from soil by a modification of a published protocol (2). A 2 g aliquot of wet soil was mixed with 20 ml of a solution consisting of 0.5% sodium pyrophosphate (v/v) and 0.05% polyvinyl pyrrolidone at pH 7 and kept in a 50 ml polyprolylenene centrifuge. This mixture was intermittently mixed by vortexing for 30 min. Then 20 ml of $CaCl_2$ (5 g/L) was added and the suspension was centrifuged at 750 g for 5 min. @ 15°C. The soil free supernatant was transferred to a clean tube and used for MPN or AODC analysis. For enumeration of microbial populations from soil slurry experiments, 1 volume of soil slurry was mixed with 2 volumes of the sodiumpyrophosphate/polyvinyl pyrrolidone solution. This mixture was vigorously shaken by intermittent vortexing before MPN or AODC analysis.

AODC analysis was done according to the protocol of Nishino (9) with cells preserved with acidified Lugol's solution. A microwell MPN protocol was developed to enumerate DNT degrading population and total heterotrophic population. The mineral salts medium used was derived from the Stanier's mineral salts medium (14) with the absence of an inorganic nitrogen source, phosphate buffer added at 0.5 mM and all other compounds at 1% of the full medium strength. Individual DNT isomers were added at 10 mg/L. The final pH was between 7.0 and 7.2. Enumeration of the total heterotrophic fraction used the non-specific R2A medium (11). Ten-fold serial dilutions were made using a 96 microwell plate. Individual wells contained 90 µl of growth medium, and 10 µl of cell suspensions were transferred by means of a multichannel pipetter. Six replicates per dilution were performed. Plates were incubated at 30°C for at least 7 days. After incubation, nitrite formation in each well of the DNT plates was quantified by adding 10 µl sulfanilamide solution and 10 µl N-(1-naphthyl)ethylenediamine solution to each well . Color intensity was measured at 562 nm with a EL340 Biokinetics Reader (BioTek Instruments) plates after approx. 15 to 30 min. vs control wells that contained no cell suspension. Cell activity in the R2A plates was measured by addition of 10 µl of 0.5% INT [0.25 g INT in 50 ml of 10mM phosphate buffer]. Formazan formation after several hours incubation was measured at 562 nm vs control wells. A microcomputer program was used to convert the raw data to MPN values (8).

Synthetic Sorptive Matrix

The effect of sorption on 2,4-DNT and 2,6-DNT biodegradation was evaluated using a synthetic sorptive matrix. A 25 mg/L solution of 2,4-DNT and 2,6-DNT in MM-C was added to a series of flasks that contained 0, 0.1, or 1 g wet weight of XAD-4 Tenax beads (Sigma, St. Louis, MO). rinsed with MeOH and H_2O. Flasks were equilibrated for 24 hours prior to addition of a 1 ml inoculum of JS922. Subsequently, flasks were incubated at 30°C with shaking at 200 rpm and mineralization was monitored by periodic sampling and analysis of NO_2^--N and DNT concentration.

Long-Term Desorption Experiments

Two sets of experiments were performed to monitor the long term desorption of nitrotoluenes from the soils. Both experiments used XAD-4 Tenax beads as a sorptive sink with a large capacity for the DNTs and TNT. In the first set of experiments, soil/bead mixtures were incubated for a fixed time period and the beads were separated and replaced by fresh beads and a fresh aqueous phase (3). In the second type of experiment, no sequential addition of beads occurred (2).

One gram of soil was placed in Teflon® lined vials with 0.25 grams of XAD-4 Tenax beads and 10 ml of a MM-C containing 50 mg/L of $HgCl_2$ (to inhibit biological activity). Vials were incubated on a shaker table (200 rpm) at 30°C. After one day of incubation, the beads from quadruplicate vials were collected. By adding 1 gram of KCl, the density of the aqueous solution was increased causing the beads to float. The beads could then be separated from the aqueous phase using a separatory funnel (Kimax, Fisher, Pittsburgh, PA). Five ml of methanol was used to extract the beads for 24 and 48 hours. Samples from the MeOH extract were analyzed by HPLC. To the remaining soil, 10 ml of fresh MM-C solution and 0.25 g of XAD-4 Tenax beads were added and the vials were reincubated. This procedure was repeated on days 3, 7, 14, 21, and 28. Non-sequential desorption experiments were set up exactly as described for sequential desorption experiments, but duplicate samples were analyzed on days 1, 3, 7, 14, 21 and 28.

Soil Slurry Experiments

Soil slurry experiments were performed in flasks that contained 25 grams of soil B plus 250 ml of MM-C solution. Three different treatment conditions were examined during phase I and phase II of the experiment. All treatments were performed in duplicates. Table 1 lists the treatments used in phase I and in phase II.

Table 1 - Different Treatments in soil Slurry Systems

	Phase I		Phase II	
Flask #	**$HgCl_2$ (50 mg/L)**	**Bioaugmented**	**XAD-4 (0.1 g)**	**Bioaugmented**
1	Yes	No	Yes	No
2	Yes	No	No	No
3	No	No	Yes	No
4	No	No	No	No
5	No	Yes	Yes	Yes
6	No	Yes	No	Yes

If bioaugmented, flasks were inoculated with 1 ml of JS922 pregrown on 3 mM 2,6-DNT resuspended in 1 ml of MM-C (at a dose of approximately 4.8×10^7 cells/g soil). Flasks were placed on a rotary shaker (200 rpm) at 30°C. Nitrite and nitrate production were monitored colorimetrically and by ion chromatography, respectively. Aqueous TNT and DNT concentrations were analyzed by HPLC. Samples of the soil phase were removed weekly and were MeOH extracted and analyzed for total TNT and DNT.

After several weeks, further treatments were performed (phase II) that involved a second addition of JS922 (at a dose of approximately 3.3×10^8 cells/g soil) or the addition of XAD-4 resin beads to decrease the aqueous concentration of 2,6-DNT and 2,4,6-TNT. Table 1 lists to which flasks XAD-4 resin beads had been added and whether the flasks were re-inoculated with JS922 during phase II.

Toxicity/Inhibition of TNT and 2,6-DNT

The growth of JS922 on 2,6-DNT in the absence and presence of TNT was evaluated. Media containing 2,6-DNT at 10 mg/L and TNT at 25 mg/L or 0 mg/L was prepared in flasks and then diluted to 50 ml with MM-C. The media were then inoculated with JS922 pregrown on a 3 mM solution of 2,6-DNT. The flasks were incubated at 30°C on a shaker table (200 rpm) and nitrite production was monitored.

RESULTS

The soil characteristics of the Volunteer Army Ammunitions Plant soil are presented in Table 2. All three soils were examined for their total MeOH extractable nitrotoluenes. Soil pH was measured by equilibrating 2 g of dried soil with 20 ml of deionized water and measuring the aqueous phase pH. pH of each soil was well within the range permissible for microbial activity. As all soils were derived from the vadose zone, f_{oc} values were within the expected range; soil B had the highest organic carbon content at 0.7%. The mean MeOH extractable 2,4-DNT, 2,6-DNT, and 2,4,6-TNT concentrations for soil B were 0.278 (± 0.004),

0.079 (± 0.004), and 0.297 (± .004) mg NT/g soil, respectively. Because of its high nitrotoluene concentration, soil B was chosen for the experiments.

Table 2 - Characteristics of Soil from the Volunteer Army Ammunitions Plant

	pH	f_{OC} (%)		2,4-DNT mg/g		2,6-DNT mg/g		2,4,6-TNT mg/g	
		Mean	SD	Mean	SD	Mean	SD	Mean	SD
A	5.5	0.465	0.058	3.88E-3	1.33E-4	5.03E-3	1.22E-4	ND	
B	6.4	0.701	0.088	2.78E-1	3.84E-3	7.87E-2	1.59E-3	2.97E-1	3.58E-3
C	8.5	0.226	0.005	3.51E-4	2.49E-5	3.51E-4	2.49E-5	ND	

Most probable number enumeration on soil B revealed a resident bacterial population able to denitrate 2,4-DNT (2.7 10^4/g soil) and 2,6-DNT (0.38 10^3/g soil). The total cultivable population was 1.0 10^6/g soil and reflected approx. 10% of the total acridine orange direct count.

Figure 1 shows the results of the sequential and non-sequential desorption experiments for 2,4-DNT (Panel A), 2,6-DNT (Panel B), 2,4,6-TNT (Panel C). Rapid partitioning of the desorbable nitrotoluenes was observed from the aqueous phase into the sorptive sink. The sequential desorption data (1, 3, 7, 14, 21, and 28 days) indicate that after 7 days all the desorbable NTs were removed from soil. The non-sequential desorption (3, 7, 14, 21, and 28 days) data confirms this result by showing all the desorbable NTs captured by the sorptive sink after 7 days.

The cumulative mass of desorbable nitrotoluenes is plotted in Figure 2. A first order desorption rate expression was used to fit the cumulative desorbable NT data.

$$M_{d,t} = M_o(1-e^{-kt})$$

M_o = total mass of desorbable NTs (mg)

$M_{d,t}$ = total amount of NTs desorbed at time t (mg)

First order desorption rate coefficients were estimated at 3.56, 1.19, and 1.80 day^{-1} for 2,4-DNT, 2,6-DNT, and 2,4,6-TNT, respectively. These very high rate coefficients confirm the very rapid desorption. After 1 day of incubation 68% (2,4-DNT), 96% (2,6-DNT), and 78% (2,4,6-TNT), of the total MeOH extractable NTs were desorbed from the soil and 83% (2,4-DNT), 100% (2,6-DNT), and 100% (2,4,6-TNT) were desorbed after 28 days.

The kinetics of the biodegradation of 2,4-DNT and 2,6-DNT sorbed onto a synthetic matrix were measured for JS 922. The addition of Tenax beads progressively reduced the aqueous concentration of DNTs causing the rate of DNT biodegradation, as measured by NO_2^- evolution, to decrease.

Factorial soil slurry experiments were performed to measure the bioavailability of DNT for biodegradation and confirm the rapid desorption found in the long-term desorption experiments. The 2,4-DNT degradation and nitrite profiles of phase I are shown in Figure 1. In the abiotic control flasks, $HgCl_2$ at 50 mg/L suppressed microbial activity for up to 10 days. However, after 10 days 2,4-DNT disappearance occurred in these flasks with a near stoichiometric release of nitrite. As 2,4-DNT disappearance and concomitant NO_2^- accumulation was observed in the control soil slurry vessels, the total microbial population and DNT degradation population was enumerated. Enumeration on R2A and 2,4-DNT revealed cell concentration of 6.9 10^6 and 1.7 10^7 cells/ ml, respectively. No growth was observed on 2,6-DNT. In addition, no growth was observed when enumerations were performed in the presence of $HgCl_2$ (@ 50 mg/L. This suggests that biological activity in the control flasks was due to the unavailability of $HgCl_2$ (because of its binding to the soil or volatilization), rather than the outgrowth of a $HgCl_2$ resistant population. Subsequent to this finding, additional $HgCl_2$ dosing (up to 200 mg/L) was performed. Microbial activity was not halted by increasing the concentration of $HgCl_2$ to 200 mg/L on day 19. A progressive decline in NO_2^- concentration in the control flasks, as well as all other flasks, suggests the occurrence of nitrification.

The DNT profile in Figure 3, Panel A again indicates rapid desorption of the DNTs. Approximately 0.14 mM of desorbable 2,4-DNT was present in all flasks. The near stoichiometric release of nitrite observed in Panel B and Panel C coinciding with the disappearance of 2,4-DNT reveals that aerobic denitration

pathways were expressed. In Flasks 3,4 (indigenous microorganisms) and 5,6 (supplemented with JS922) an average of 0.22 mM of NO_2^--N is released. Approximately 80% of all the nitro groups available in 2,4-DNT were, therefore, released as of NO_2^--N. The remaining 20% of the of NO_2^--N are likely used for cell synthesis.

Figures 4 reveals that transformation of 2,6-DNT is limited. Phase II of the experiment examined the possibility of toxicity or inhibition effects of 2,6-DNT or 2,4,6-TNT. The XAD-4 Tenax beads added to flasks 1, 3, and 5 reduced the aqueous concentration of 2,6-DNT and TNT. Active inoculum of 2,6-DNT degrading JS 922 was added to the flasks 5 and 6. The addition of Tenax beads did not appear to enhance 2,6-DNT degradation. The addition of fresh inoculum (JS922) did not appear to enhance 2,6-degradation.

A slow decrease in TNT concentrations are observed in all three treatments (Figure 5). Slow desorption of TNT is observed in the bioaugmented control flasks relative to the abiotic and biotic controls. The same slow desorption is observed with 2,6-DNT in the bioaugmented control flasks.

Figure 6 shows the results of the TNT toxicity/inhibition experiment. The initial rate of 2,6-DNT removal was very similar in the control (0.015 mg L^{-1} hr^{-1}) and TNT supplemented (0.018 mg L^{-1} hr^{-1}) flasks. Thus, at a concentration of 25 mg/L TNT does not impact initial cell activity. Note, however, that only 10% of the initial 2,6-DNT was degraded in these experiments, and the effects of TNT on sustained 2,6-DNT transformation are not clear.

DISCUSSION

Soil B contained large amounts of 2,4-DNT, 2,6-DNT, and 2,4,6-TNT. The rapid desorption of the contaminants, suggests that the nitrotoluenes are not strongly bound to the soil organic matter or present deep in the soil micropores. Recently, it has been demonstrated that nitroaromatics can adsorb specifically and reversibly to clay surfaces (5). This adsorption occurs via an electron acceptor-donor complex formation between the electron deficient nitroaromatic nucleus and the electron dense oxygen ligands at the clay surface (5, 16). The dominant mineral in the examined soil was kaolinite (15). Therefore, the majority of the desorbable NTs were probably adsorbed to the clay surface rather than partitioned in the soil organic matter. Changes in ionic strength from 0.1 mM to 0.1 M have little effect, while the type of exchangeable cations can have a large effect on NT adsorption to clays (5). Thus, a difference in the ionic solution between the site geochemistry, which is unfortunately unknown, and the mineral salts solution used in these experiments may account for the rapid desorption observed in the lab *vs* their persistence in the field.

The indigenous microorganisms present in soil B were capable of complete mineralization of 2,4-DNT. Near stoichiometric release of nitrite accompanied the degradation of the desorbable 2,4-DNT. Because nitrite was released in near stoichiometric quantities, aerobic denitration pathways are inferred. This contrast with a recent report on aerobic 2,4-DNT transformations in soil microcosms by indigenous microorganisms where only 28% mineralization was observed, and 28% of the original compound was transformed to reduced intermediates (1). Because of the activity of the indigenous microbial community, addition of a known 2,4/2,6-DNT degrader (JS922) was not beneficial.

No mineralization of 2,6-DNT was found during these experiments. MPN enumeration on the soil, however, revealed a population with 2,6-DNT denitrating activity. A small fraction of 2,6-DNT was mineralized (8%) in the reported aerobic microcoms studies, but in that case TNT was absent and the initially applied DNT concentrations were not reported (1). Possibly, toxicity or inhibition exerted by the high aqueous concentrations of 2,6-DNT and/or 2,4,6-TNT impair 2,6-DNT biotransformation. After 25 days of incubation, MPN analysis was performed on a soil slurry supplemented with JS 922 and one that only contained the indigenous microflora. MPNs on R2A and 2,4-DNT for the indigenous and augmented slurry reactors were 3.5 10^7 and 9.18 10^4 and 4.62 10^7 and 1.8 10^5 cells/ml for respectively. Thus, a slightly higher active 2,4-DNT degrading population was present with JS 922 supplementation. However the measured 2,4-DNT degrading population was nearly 3 orders of magnitude below the initial JS 922 cell concentration. Enumeration on 2,6-DNT revealed no cell count for either condition. This suggests that either the added 2,6-DNT degraders have disappeared (because of toxicity of the environment), or are unrecoverable after 25 days on a medium containing 2,6-DNT as sole C source. Neither the addition of a sorptive matrix to decrease the aqueous concentration of 2,6-DNT and TNT in the soil slurry experiments (phase II), nor the addition of an induced culture (JS922) grown on 2,6-DNT enhanced 2,6-DNT degradation. MPN enumeration of the 2,4-DNT and 2,6-DNT degrading fraction was performed 10 days after the onset of phase II. 2,4-DNT and 2,6-DNT MPN were 4.9 10^5 and 4.9 10^6 cell/ml when XAD-4 was present, while those numbers were 3.6 10^3 and 3.6 10^2 in the absence of XAD-4. These results suggest that the reduction of aqueous phase TNT concentration increases the recoverability of DNT

degrading organisms, and potentially the survivability of JS 922. However, 2,6-DNT mineralization was not observed (i.e. no NO_2^- production) even after the combined treatment of XAD-4 addition and a second inoculation, indicating that other factors impede activity of JS 922.

We postulate that the observed decrease in the aqueous phase concentration of 2,4,6-TNT (Figure 5) is not due to biotic transformations. No additional peaks reflective of aminodinitrotoluenes isomers were observed on the HPLC chromatographs suggesting that nitro reductive pathways were not significant. Furthermore, no organisms have so far been isolated that can aerobically mineralize TNT as sole carbon and nitrogen source. TNT loss by volatilization is also unlikely, as the Henry's law coefficient for TNT, 2,4-DNT and 2,6-DNT are 1.1 10^{-8}, 1.86 10^{-7}, and 4.86 10^{-7} atm m^3 mol^{-1} indicating that TNT is the least volatile of the three nitrotoluenes. The reasons for the TNT disappearance remain, therefore, elusive.

REFERENCES

1. **Bradley, P. M., F. H. Chappelle, J. E. Landmeyer and J. G. Schumacher.** 1997. Potential for intrinsic bioremediation of a DNT-contaminated aquifer. Groundwater **35:**12-17.
2. **Carmichael, L. M., R. F. Christman and F. K. Pfaender.** 1997. Desorption and mineralization kinetics of phenathrene and chrysene in soils. Environ. Sci. Technol. **29:**126-132.
3. **Carroll, K. M., M. R. Harkness, A. A. Bracco and R. R. Balcarel.** 1994. Application of a permeant/polymer diffusion model to the desorption of polychlorinated biphenyls from Hudson river sediments. Environ. Sci. Technol. **28:**253-258.
4. **Eaton, A. D., L. S. Clesceri and A. E. Greenberg.** 1995. Standard Methods for the Examination of Water and Wastewater. American Puclic Health Association,Washington, DC
5. **Haderlein, S. B., K. W. Weissmahr and R. P. Schwarzenbach.** 1996. Specific adsorption of nitroaromatic explosives and pesticides to clay minerals. Environ. Sci. Technol. **30:**612-622.
6. **Haigler, B. E. and J. C. Spain.** 1996. Degradation of nitroaromatic compounds by microbes. SIM News **46:**59-68.
7. **Jenkins, T. F., M. E. Walsh, P. W. Schumacher, P. H. Miyares, C. F. Bauer and C. J. Grant.** 1989. Liquid chromatographic method for determination of extractable nitroaromatic and nitramine residues in soil. J. Assoc. Off. Anal. Chem. **72:**890-899.
8. **Klee, A. J.** 1993. A computer program for the determination of most probable numbers and its confidence limits. J. Microb. Meth. **18:**91-98.
9. **Nishino, S. F.** 1986. Direct acridine orange counting of bacteria preserved with acidified lugol iodine. Appl. Environ. Microbiol. **52:**602-604.
10. **Ramaswami, A. and R. G. Luthy.** 1997. Measuring and modeling physicochemical limitations to bioavailability and biodegradation, p. 721-729. *In* C. J. Hurst, G. R. Knudsen, M. J. McInerney, L. D. Stetzenbach and M. V. Walter (ed.), Manual of Environmental Microbiology, ASM Press, Washington, DC.
11. **Reasoner, D. J. and G. E. E.** 1985. A new medium for the enumeration and subculture of bacteria from potable water. Appl. Environ. Microbiol. **49:**1-7.
12. **Spain, J. C.** 1995. Biodegradation of nitroaromatic compounds. Ann. Rev. Microbiol. **49:**523-555.
13. **Spanggord, R. J., J. C. Spain, S. F. Nishino and K. E. Mortelmans.** 1991. Biodegradation of 2,4-dinitrotoluene by a *Pseudomonas* sp. Appl. Environ. Microbiol. **57:**3200-3205.
14. **Stanier, R. Y., N. J. Palleroni and M. Doudoroff.** 1966. The aerobic pseudomonads: A taxonomic study. J. Gen. Microbiol. **43:**159-171.
15. **TRW.** 1996. Site characterization report for the Volunteer Army Ammunition Plant National Environmental Technology Test Site. Site characterization report no. SFIM-AEC-ET-CR-96154. US Army Environmental Center.
16. **Weissmahr, K. W., S. B. Haderlein, R. P. Schwarzenbach, R. Hany and R. Nüesch.** 1997. *In situ* spectroscopic investigations of adsorption mechanisms of nitroaromatic compounds at clay minerals. Environ. Sci. Technol. **31:**240-247.

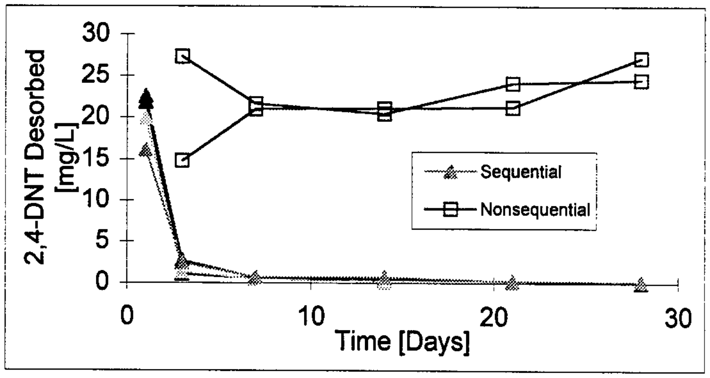

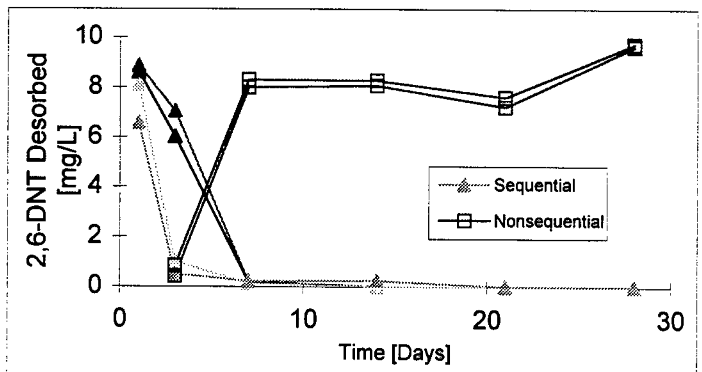

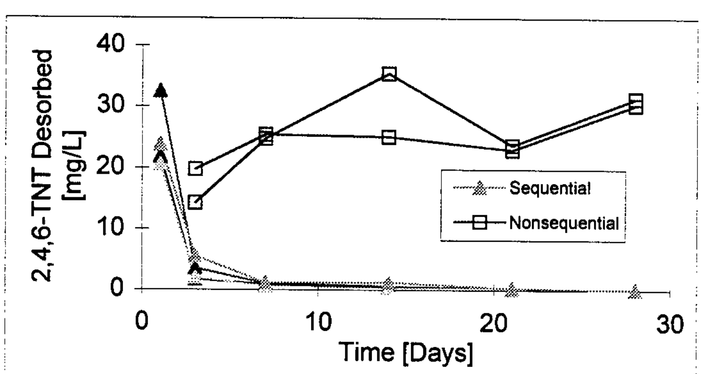

Figure 1 - Desorption of 2,4-DNT (Top), 2,6-DNT (Center), and 2,4,6-TNT (Bottom) from Soil B using XAD-4 Tenax Beads.

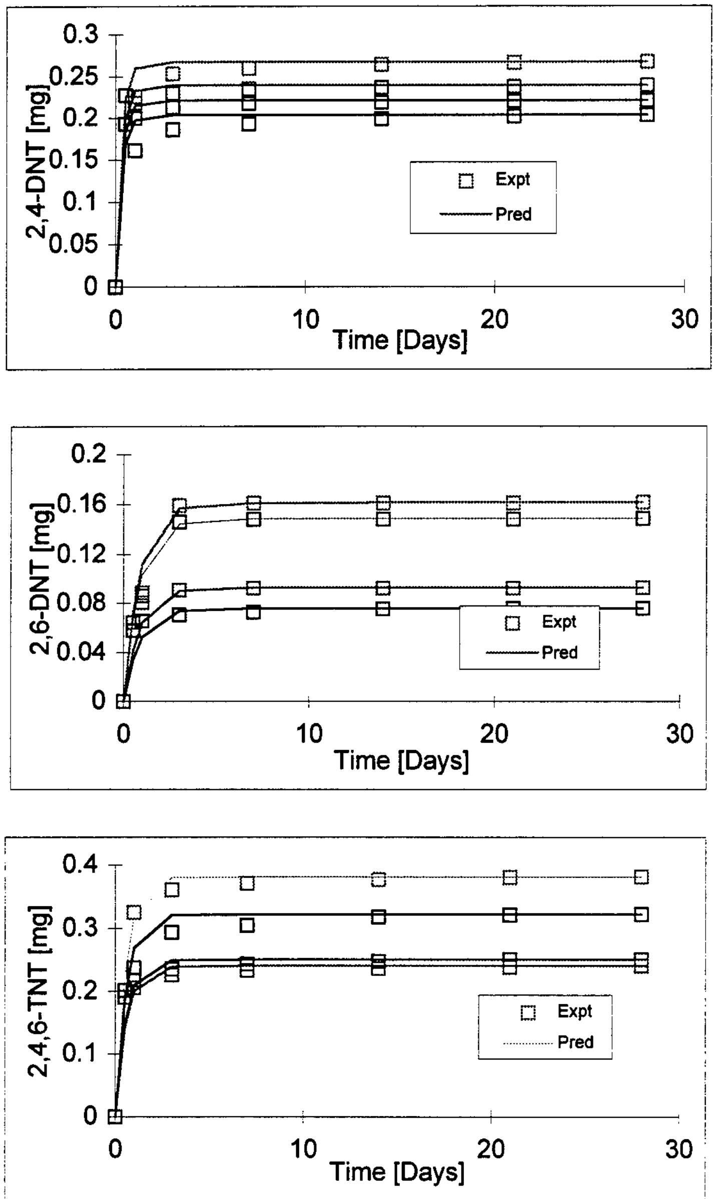

Figure 2 - Cumulative desorption of 2,4-DNT (Top), 2,6-DNT (Center), and 2,4,6-TNT (Bottom) from Soil B using XAD-4 Tenax Beads. Data fit used a first order desorption model.

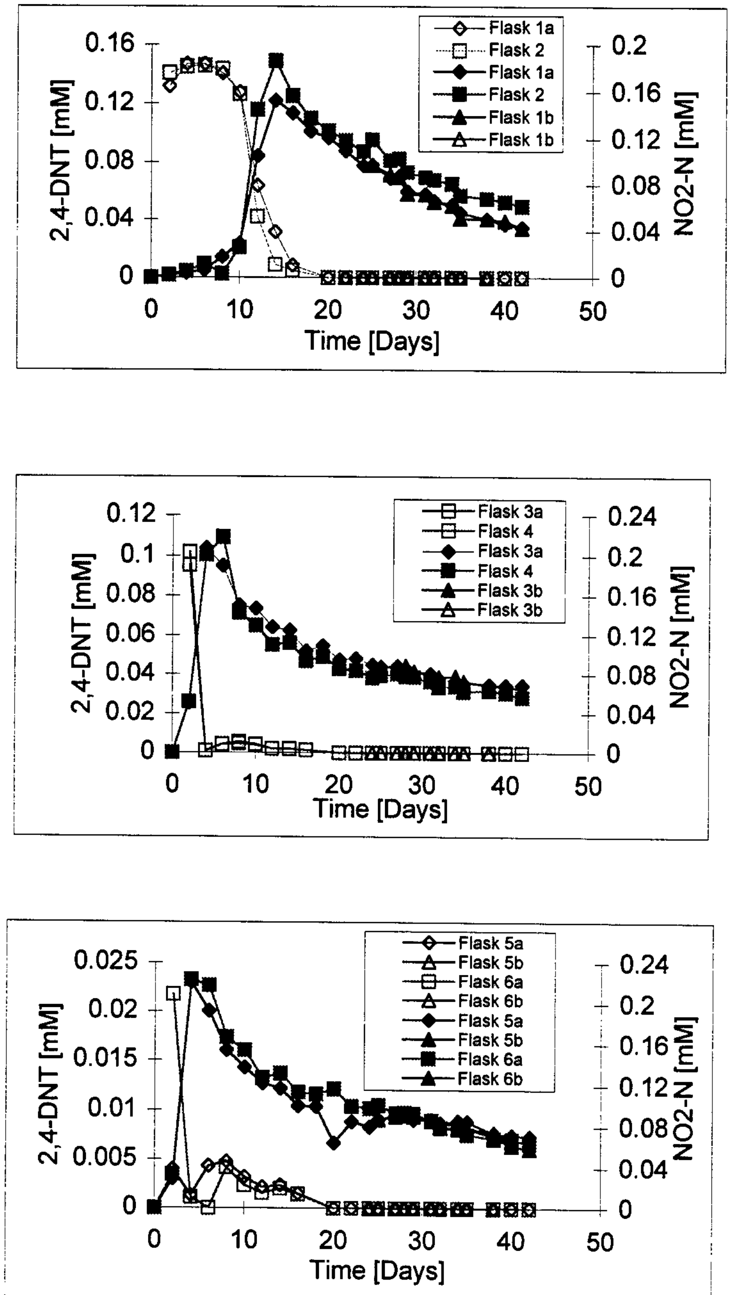

Figure 3 - 2,4-DNT (open symbols) and nitrite (closed symbols) profiles in abiotic control (Top), biotic control (Center), and JS922 supplemented tests (Bottom).

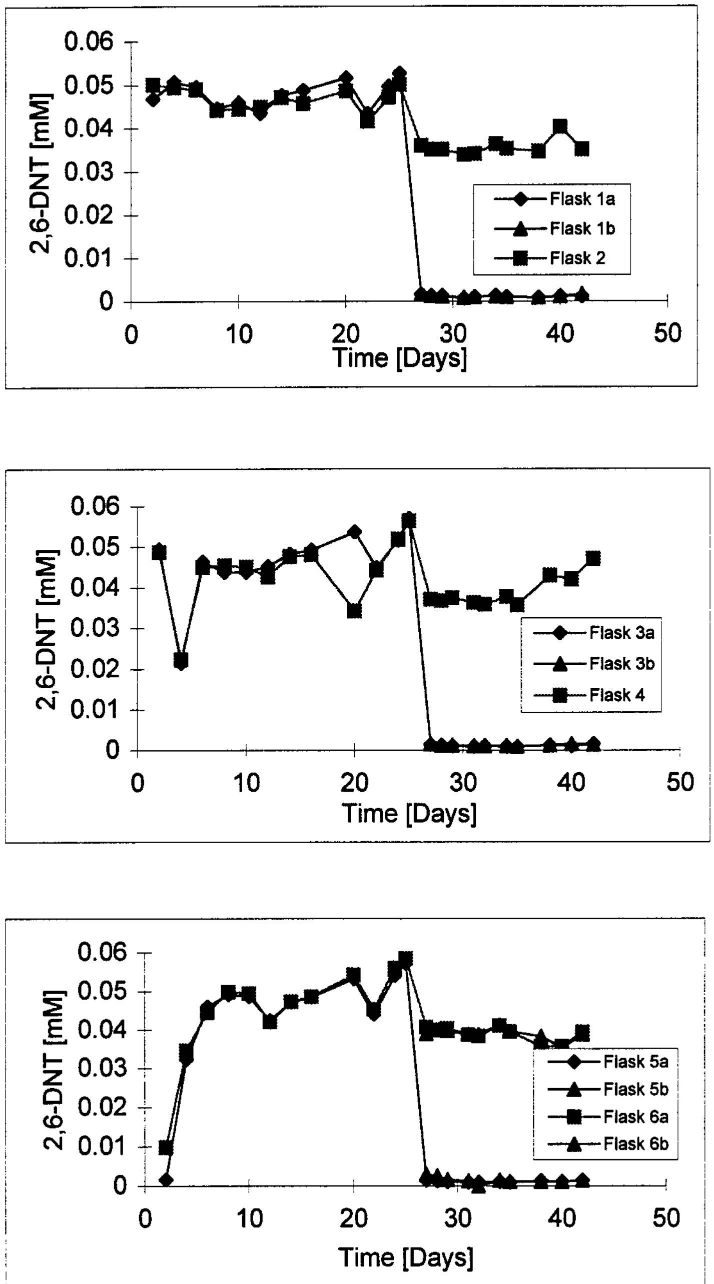

Figure 4 - 2,6-DNT profiles in abiotic control (Top), biotic control (Center), and JS922 supplemented tests (Bottom).

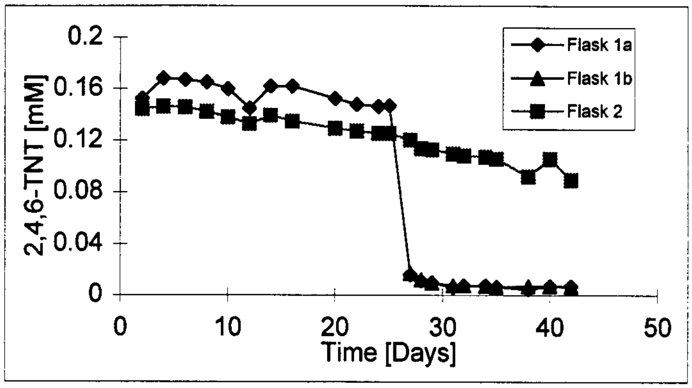

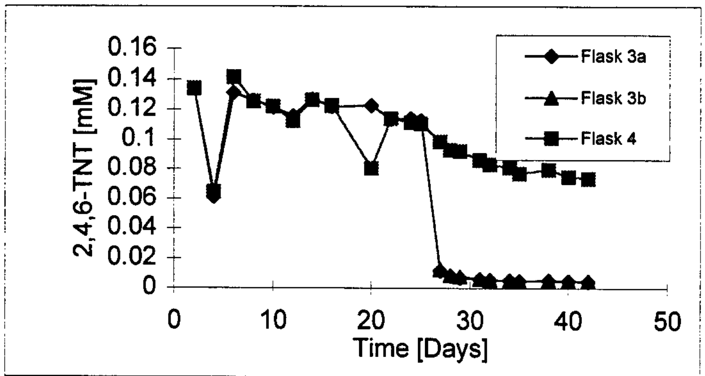

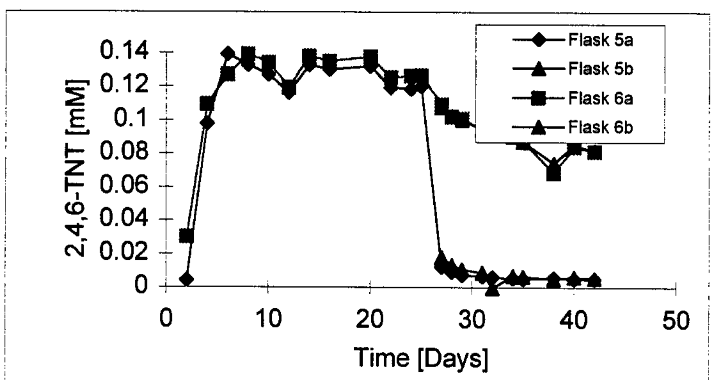

Figure 5 - TNT profiles in abiotic control (Top), biotic control (Center), and JS922 supplemented tests (Bottom).

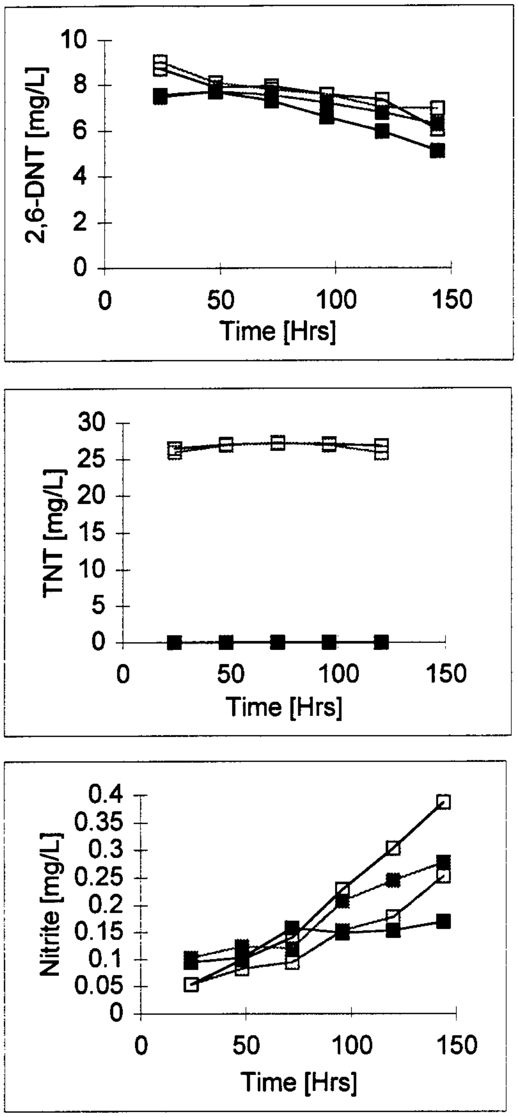

Figure 6 - 2,6-DNT (Top), TNT (Center), and nitrite-N (Bottom) profiles during TNT toxicity/inhibition experiments. Open and filled symbols refer to TNT supplemented and non-supplemented flasks, respectively.

Pharmacological Intervention to Increase the Time before Acceleration (+Gz) Induced Loss of Consciousness in Rats: Electroencephalographic Monitoring

William B. Stavinoha, Ph.D.
Professor of Pharmacology
Department of Pharmacology

7703 Floyd Curl Drive
University of Texas Health Science Center
San Antonio, Tx 78284

Final Report for:
Summer Faculty Research Program
Armstong Laboratory

Sponsored by:
Air Force Office of Scientific Research
Bolling Air Force Base, DC

and

Armstrong Laboratory

September 1997

Pharmacological Intervention to Increase the Time before Acceleration (+Gz) Induced Loss of Consciousness in Rats: Electroencephalographic Monitoring

William B. Stavinoha, Ph.D.
Professor of Pharmacology

Abstract

Pilots flying missions in high performance aircraft are exposed to high acceleration forces which can cause gravity induced loss of consciousness(GLOC). Physical and physiological methods have been extensively studied and utilized to increase the time of consciousness by decreasing pooling of blood in the periphery of the body during high (+Gz). Little research has been done on pharmacological intervention to extend the time to GLOC, primarily due to the lack of a suitable animal model. This study on rats was designed to develop techniques to monitor the conscious state and to apply that information to the study of the consciousness extending effects of caffeine during high (+Gz). In rats accelerated to GLOC, the electroencephalographic (EEG) power spectrum within 1-40Hz was studied using fast Fourier transforms (FFTs). The power spectrum of 39-40Hz (gamma) appeared to be the most sensitive spectrum for predicting GLOC. Caffeine at 30 and 60mg/kg ip was again found to significantly extend the time before the occurrence of GLOC.

PHARMACOLOGICAL INTERVENTION TO INCREASE THE TIME DELAY BEFORE ACCELERATION (+Gz) INDUCED LOSS OF CONSCIOUSNESS IN RATS: ELECTROENCEPHALOGRAPHIC MONITORING.

Introduction

Pilots flying high performance aircraft are exposed to high acceleration forces. When a circular pattern acceleration causes a head to foot inertial load (high +Gz) blood is forced from the head to the body. This loss of blood from the brain, ischemia, can cause a dangerous loss of consciousness (GLOC). GLOC is a significant concern both in terms of pilot safety and the limits its potential occurrence places on aircrew performance (Burton, 1988). There are two major approaches to mitigating the problem (1) Maintaining blood flow to the brain as long as possible and (2) Maintaining the homeostatic process of consciousness as long as possible. A physical and physiological approach to problem (1) is the use of an anti-G suit which inflates to increase pressure on the periphery of the body to limit blood pooling and maintain blood flow to the brain. This procedure provides some extension of time before the occurrence of GLOC (Forster et al, 1994). For problem (2), studies of the central responses to GLOC in baboons GLOC was observed in 16-25sec of 8+Gz but carotid blood flow to the brain ceased during the first few seconds (Werchan et al., 1996). Studies in rats delineated the energy metabolism and neurotransmitter responses of the brain to GLOC and found that the administration of glucose to rodents extended the time to GLOC (Shahed et al., 1995). These findings indicate the importance of the central nervous system homeostatic mechanisms in the extension of time of consciousness during exposure to acceleration that can result in GLOC. An important extension to these findings is the use of the extensive metabolic changes found to occur during the initial phases of ischemia to identify and study drugs that can modify the chemical cascade that occurs with ischemia. In initial studies we found that caffeine administration could significantly increase the time to GLOC as

identified by an isoelectric electroencephalograph (EEG) (Stavinoha, 1996). This indicates a very severe state of ischemia, that is seldom if ever attained in human studies. Therefore studies were undertaken this summer to establish an earlier and more sensitive EEG end point for studying the benefits of caffeine on extending the time to GLOC. This approach involved the extensive analysis of EEG patterns in rats extending the analysis to the gamma (39-40 Hz) frequency domain using Fourier Transform analysis.

Methods

Small Animal Centrifuge: The centrifuge is 1.52m in diameter and is capable of +1-85Gz with an offset rate of +20Gz/s. The operation is computerized and is equipped with a video camera and amplifiers for monitoring the EEG.

Animal preparation: Adult male Sprague-Dawley CD-VAF/Plus rats from Charles River Laboratories, Wilmington, MA were provided free access to food and water. Rats were implanted with biparietal lateral EEG electrodes and the first centrifuge studies were done 2-3 hours later when they were full awake. Each rat was placed in a plexiglass holder and the holder was clamped to the arm of the centrifuge with the head facing the center shaft.

Drug: Caffeine was given in normal saline at doses of 15, 30. or 60 mg/kg IP thirty minutes before centrifugation. The controls received only saline.

EEG: The EEG configuration was essentially as previously described (Lukatch et al., 1997). Four EEG electrodes provided simultaneous recording of two differential EEG signals. One signal was intra-hemispheric; right frontal-right parietal. The second signal was inter-hemispheric; left parietal-right parietal. For EEG data, each 30 second centrifuge acceleration period was preceded by 5 seconds of no acceleration and 30 seconds of recovery time. EEG spectral quantitation was done through use of fast Fourier transforms (FFTs) on

contiguous 1 second epochs of unprocessed EEG data (LabView software). Power within delta(1-4Hz), theta(5-8Hz) alpha (9-12Hz), beta(13-30 Hz) and gamma (39-40 Hz) frequency bands was calculated for each one second epoch.

Results

The data utilizing the 5 EEG frequency bands which included the gamma frequency is still being analyzed so that only the preliminary results can be included in this report. In the original report caffeine, an adenosine A1 receptor blocking agent increased the time to GLOC based on time to isoelectric EEG from a control time of 14.5±2.3 seconds to 35±13.2 seconds. The data this summer confirmed this extension in time. The current analysis is based on the quantitative analysis of G-force induced alterations of rat EEG activity reported from this laboratory by Lukatch et al,(1997). Because the analysis using this system did not present an easily identified end point, the studies were extended to include the gamma frequency which has been investigated by R. Eichon in this laboratory. The preliminary EEG data is presented in figure 1. This shows the decrease in EEG amplitude (isoelectric phase) at 25 Gz. The centrifuge run time is shown at the top as a plateau in a straight line. The plot of the gamma frequency as shown in figure 2 exhibits the rigor which the gamma frequency indicates GLOC indicating its possible use in the evaluation of pharmacologic agents such as caffeine in extending the time to GLOC. Figures 3-5 show the plots of the FFT analysis of the power in five frequencies during 10, 17.5 and 25 +Gz centrifuge runs.

Discussion

Review of the literature on techniques or approaches to increasing the time to GLOC reveals major effort in the physiological and physical approach. Very little research has been carried out involving the central nervous system in a biochemical and pharmacological approach to the problem that occurs

following the loss of blood flow to the brain. This is an important aspect, for consciousness is maintained for many seconds following cessation of blood flow. The early research on pharmacological agents was done before information on brain metabolism and neurotransmitter responses to ischemia were known. Their failure to influence the time of GLOC provoked a very negative feeling toward subsequent pharmacologic research. In fact a recent review on maximizing +Gz tolerance used only 31 lines on drugs out of 87 pages most lines discussing the doubtful usefulness of drugs because of the incidence of side effects (Fong, 1993) The drugs studied in the past that evoked that negative response were analeptics, adrenaline, atropine, amphetamine anti-malarial agents, adrenocorticoids, oestrodiol and testosterone. None of this group could be justified on the basis of recent research into brain responses to ischemia(Shahed et al., 1995). Based on current central nervous system research in this laboratory, it was possible to identify at least two drugs that profoundly affected the time to GLOC. The drugs were 3,4-diaminopyridine and caffeine. Since caffeine is considered a relatively safe drug we chose to do further studies on it.

The excellent study by Lukatch et al.,(1997) from this laboratory indicated that quantitative analysis of EEG activity presented the possibility of predicting GLOC. The studies this summer attempted to extend the studies to the gamma frequency. This was attempted because synchronous high frequency cortical responses in the gamma band have been found in animals to reflect stimuli perceived and responses executed(Singer and Gray, 1995). Gamma responses increased when subjects saw patterns of moving bars(Lutzenberger et al., 1995). Llinas and Ribary,(1993) propose that 40Hz oscillation is a correlate of cognition. This gamma relationship to cognition and consciousness should provided a basis for its usefulness in GLOC studies and the figure 2 indicates that possibility.

Caffeine at 30-60mg/kg significantly extended the time before GLOC in rats.

During the ischemia resulting from high acceleration adenosine is released in the brain (Jiang et al., 1997). This release acting on the adenosine A1 receptors diminishes the release of neurotransmitters and decreases the activity of the brain and lowers the level of consciousness (Rainnie et al.,1994). Caffeine is an adenosine A1 receptor blocking agent(Nehlig et al., 1992) and presumably acts through this mechanism.

Conclusions

1. Caffeine has potential as an agent to extend the time to GLOC.
2. The gamma frequency of the EEG appears to provide the possibility of a quantitative indicator of future GLOC

38 - 40 Hz EEG POWER REDUCTION AT 12- 13 SECONDS :

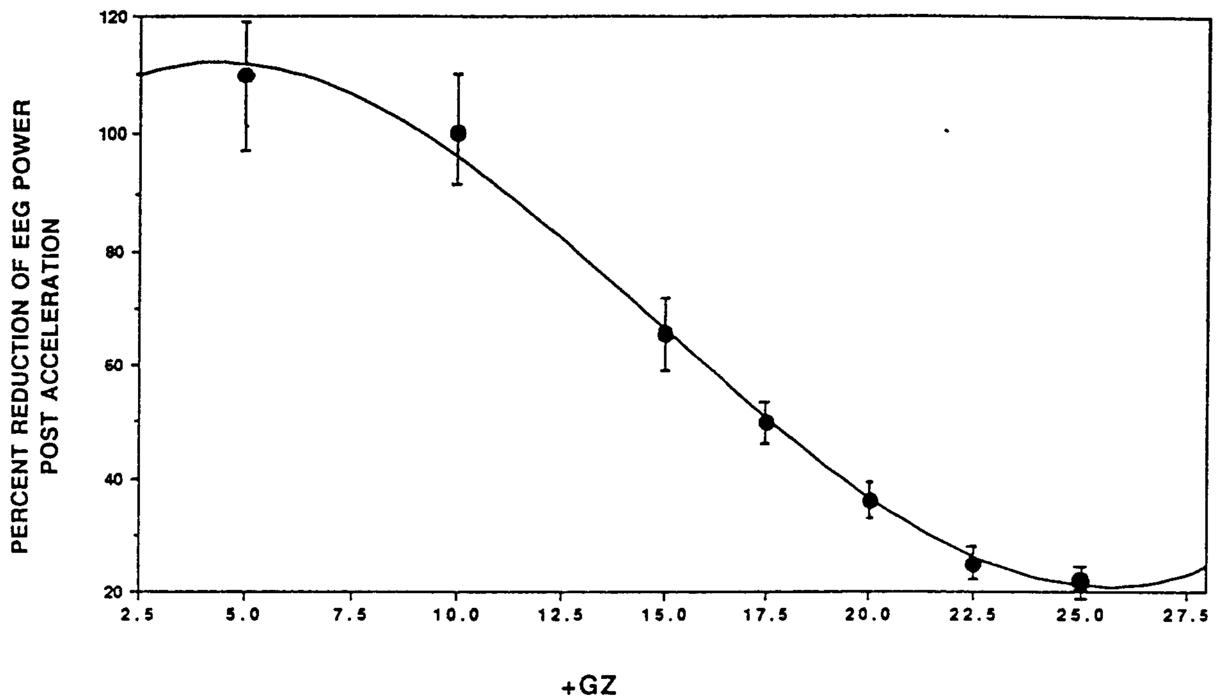

MEAN

FFT ANALYSIS R96-94 : 10 +Gz (UNPROTECTED) BASELINE

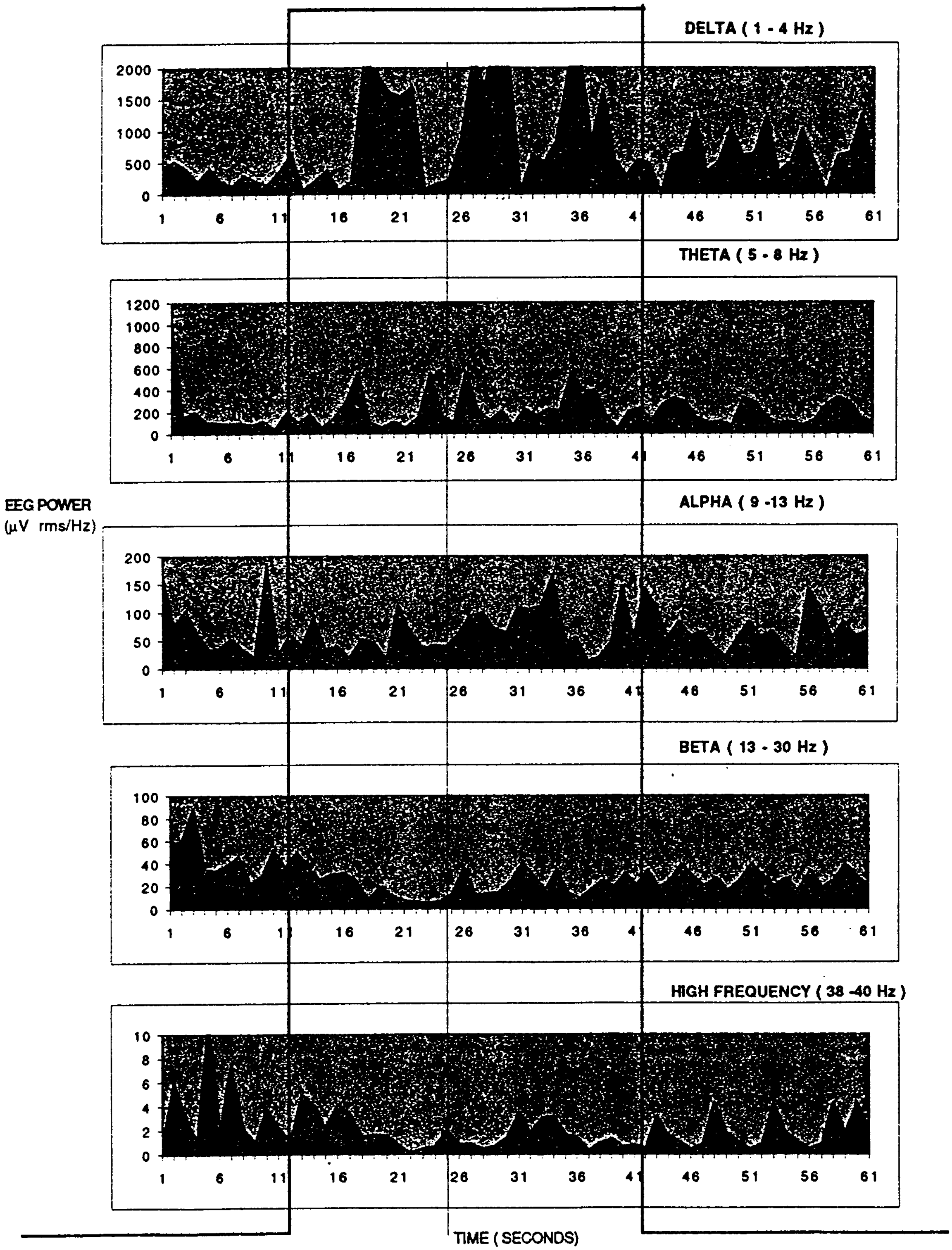

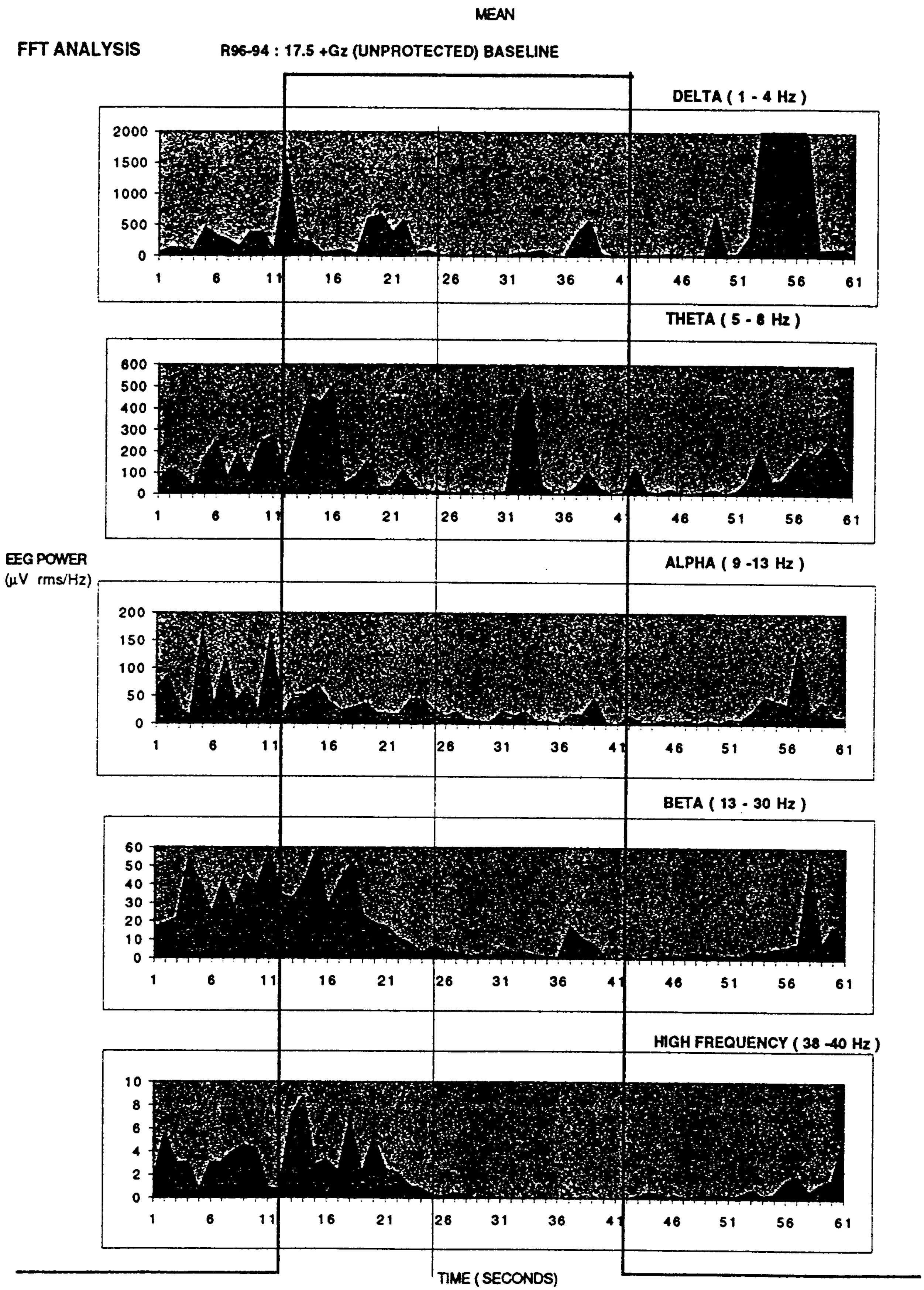
MEAN
FFT ANALYSIS
R96-94 : 17.5 +Gz (UNPROTECTED) BASELINE
DELTA (1 - 4 Hz)
THETA (5 - 8 Hz)
ALPHA (9 -13 Hz)
BETA (13 - 30 Hz)
HIGH FREQUENCY (38 -40 Hz)
EEG POWER
(µV rms/Hz)
TIME (SECONDS)

MEAN

FFT ANALYSIS R96-94 : 25 +Gz (UNPROTECTED) BASELINE

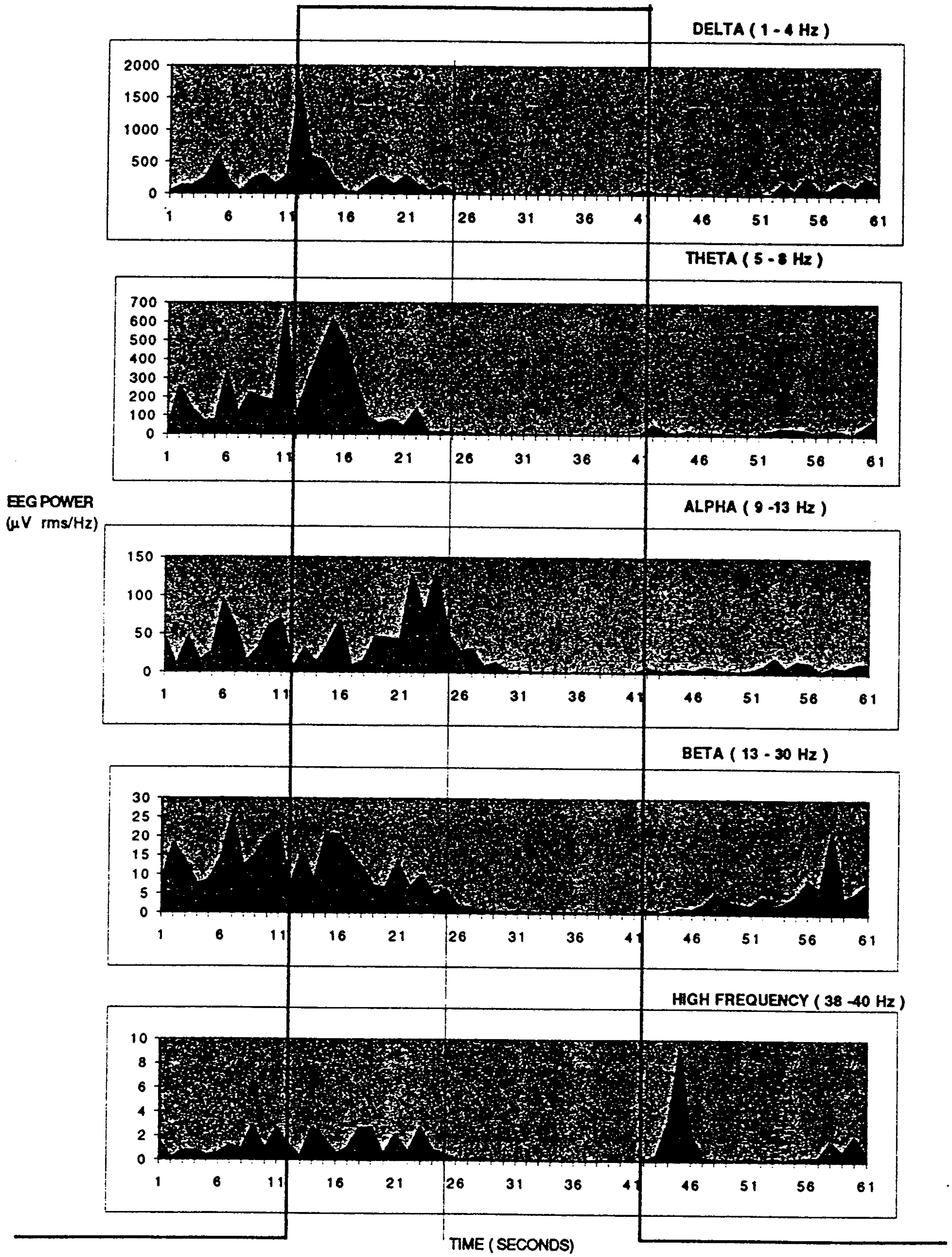

References:

Burton, R. (1988). G-induced loss of consciousness: definition, history, current status. Aviation, space,and enviormental medicine, 59(January), 2-5.

Fong, K. (1993). Maximizing +Gz tolerance in pilots of high performance combat aircraft. Air Force Material Command Wright-Patterson Air Frce Base Ohio, AL-SR-1993-0001, 1-87.

Forster, E., Cammarota, J., & Whinnery, J. (1994). G-LOC recovery with and without G-suit inflation. Aviation,space, and enviormental medicine, 65(March), 249-253.

Jiang, N., Kowaluk, E., Lee, C.-H., Mazdiyasni, H., & Chopp, M. (1997). Adenosine kinase inhibition protects brain against transient focal ischemia in rats. European J of Pharmacology, 320, 131-137.

Llinas, R., & Ribary, U. (1993). Coherent 40-Hz oscillation characterizes dream state in humans. Proc. national academy science USA, 90(March), 2078-2081.

Lukatch, H., Echon, R., Maciver, M., & Werchan, P. (1997). G-Force induced alterations in rat EEG activity: A quantitative analysis. Electroencephalography and Clinical Neurophysiology, in press.

Lutzenberger, W., Preissl, H., Birbaumer, N., & Pulvermuller, W. (1997). High-frequency cortical responses: do they not exist if they are small? Electroencephalography and clinical neurophysiology, 102, 64-66.

Nehlig, A., Daval, J.-L., & Debry, G. (1992). Caffeine and the central nervous system: mechanisms of action, biochemical, metabolic and psychostimulant effects. Brain Research Reviews, 17, 139-170.

Rainnie, D., Heinz, C., Grunze, C., McCarley, R., & Greene, R. (1994). Adenosine inhibition of mesopontine cholinergic neurons: Implications for EEG arousal. Science, 263, 689-692.

Shahed, A., Barber, J., Galindo, J. S., & Werchan, P. (1995). Rat brain glucose and energy metabolites: Effect of +Gz (head to foot inertial load) exposure in a small animal centrifuge. J of Cerebral Blood Flow and Metabolism, 15, 1040-1046.

Singer, W., & Gray, C. (1995). Visual feature integration and the temporal correlation hypothesis. Annu rev neuroscience, 18, 555-583.

Stavinoha, W. (1995). Pharmacological interventioin to increase the time before gravity induced loss of consciousness in rats and mice. USAF summer research program reports, 2, 35 1-35 18.

Werchan, P., Schadt, J., Fanton, J., & Laughlin, M. (1996). Total and regional cerebral blood flow during recovery from G-LOC. Aviation, space and enviormental medicine, 67(8), 751-758.

FORCE-REFLECTING TELEOPERATION CONTROL ARCHITECTURE

Robert L. Williams II
Assistant Professor
Department of Mechanical Engineering

Ohio University
257 Stocker Center
Athens, OH 45701-2979

Final Report for:
Summer Faculty Research Program
Armstrong Laboratory

Sponsored by:
Air Force Office of Scientific Research
Bolling Air Force Base, DC

and

Armstrong Laboratory

August 1997

TELEROBOTIC CONTROL ARCHITECTURE INCLUDING FORCE-REFLECTING TELEOPERATION

Robert L. Williams II
Assistant Professor
Department of Mechanical Engineering
Ohio University

Abstract

This report summarizes the author's work in the *AFOSR* 1997 Summer Faculty Research Program, based in the Human Sensory Feedback (*HSF*) Laboratory of Armstrong Laboratory, located at Wright-Patterson *AFB*. A powerful and general control architecture is presented for real-time, sensor-based, rate-based, shared control of general telerobotic systems including force-reflecting hand controllers (*FRHCs*). Implementation is discussed to specific *Freflex/Merlin* hardware in the *HSF* Lab. A *Matlab* simulation of *Freflex/Merlin* teleoperation under joint and Cartesian pose and rate control was developed and delivered to the *HSF* Lab. This marks the first time the *Freflex* exoskeleton has been used to control the *Merlin* slave manipulator. A major focus is force-reflecting teleoperation to increase telepresence in remote operations. This architecture has been partially implemented in hardware and the work is progressing. Additional accomplishments are the novel Naturally-Transitioning Rate-to-Force Controller (*NTRFC*) and mathematical modeling for the planar version of the novel cable-suspended haptic interface.

TELEROBOTIC CONTROL ARCHITECTURE INCLUDING FORCE-REFLECTING TELEOPERATION

Robert L. Williams II

1 Introduction

Teleoperation of remote manipulators is greatly enhanced by using a force-reflecting input device. This force/moment haptic feedback increases the sense of telepresence (where the user feels part of the remote or virtual environment) by enabling the operator to feel through the force-reflecting master the forces and moments exerted by the slave manipulator on the environment. The Human Sensory Feedback (*HSF*) Laboratory of Armstrong Laboratory located at Wright-Patterson *AFB* has a world-class capability for experimentation in force-reflecting teleoperation for Air Force and *NASA* applications: The unique *Freflex* force reflecting exoskeleton master (Odetics, 1992) and a *Merlin* industrial manipulator slave (American Robot Corporation, 1985). The purpose of this report is to document the author's summer 1997 work at the *HSF* Lab in *Freflex/Merlin* force-reflecting teleoperation, sponsored by the *AFOSR* Summer Faculty Research Program.

The *HSF* Lab has been involved with force-reflecting teleoperation research for more than a decade. Bryfogle (1990) presents algorithms for force-reflecting exoskeletons. Rosenberg (1992) applies virtual fixtures to improve teleoperator performance and later extends the concept to include time-delayed teleoperation (1993). Huang (1993) presents equations for *Freflex* exoskeleton inputs and *Merlin* inverse pose solution, optimized for minimal on-line computation. Dr. Repperger has been very active in force-reflection research, focusing on the operator side of teleoperation (Repperger et.al., 1991; Repperger, 1991; Repperger, 1995; and Repperger et.al., 1995). Haptic feedback can include both force and tactile information; Hasser (1995) combines touch and force feedback in an experimental device.

The author assisted implementation of a unique experimental sensor-based real-time telerobotic system including force-reflecting hand controllers (*FRHCs*) while employed at *NASA* Langley Research Center (Williams et.al., 1997; Williams et.al., 1996; Willshire et.al., 1992). The control architecture in the current report is an extension and adaptation of that system, which includes multiple control modes and shared human/autonomous control. Ohio University graduate student Mark Murphy assisted the author during the summer 1997 work in the *HSF* Lab. His companion report (Murphy, 1997) focuses on practical implementation. For a more complete report of the summer's work, please see Williams and Murphy (1997a). The author accomplished three basic results in summer 1997 work: 1) Development of control architecture for general telerobotic systems including *FRHCs*. Simulation of *Freflex/Merlin* teleoperation and assistance of partial implementation in hardware (currently in progress). 2) Controls design, modeling, simulation, and draft journal article (Williams and Murphy, 1997b) for the novel Naturally-Transitioning Rate-to-Force Controller (*NTRFC*), which is part of 1). 3) Mathematical modeling, algorithm development, and draft journal article (Williams and Roberts, 1997) for the planar version of the author's novel cable-suspended haptic interface. This report summarizes these accomplishments, primarily for the first since draft articles are available from the author for the latter two efforts.

2 System Description

This report assumes the following system characteristics. One or more slave manipulators is to be controlled to accomplish various tasks. The manipulator(s) may be controlled by human operator (teleoperation), autonomously (robotic) or a combination (telerobotic). A six degree-of-freedom (dof) master device (joystick, hand controller, exoskeleton) is used for teleoperation inputs. Since Cartesian commands from the master are sent as Cartesian commands to the manipulator(s), the master and slave need not be kinematically similar. Cartesian/Cartesian master/slave control has more capability than joint/joint control. If two slave manipulators are working independently, two master devices may be used. If two slave manipulators are coupled through a common payload, a single master is sufficient. Figure 1 shows coordinate frame definitions which apply to masters and slaves.

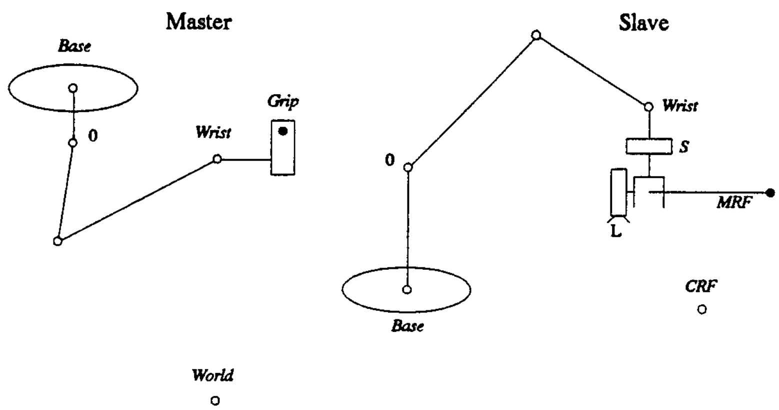

Figure 1. Master and Slave Coordinate Frames

For clarity, dextral *XYZ* Cartesian coordinate frames are represented by dots in Fig. 1. The *World* frame is an inertially-fixed reference frame for all devices. The Master and Slave each have separate *Base*, 0, and *Wrist* frames. The *Base* frame is attached before the first moving joint; 0 is the kinematic base frame; the *Wrist* frame is attached to the last moving link at its joint. The Master and Slave each have coordinate frames attached to each active joint between 0 and *Wrist* (not shown for generality and clarity). The Master *Grip* frame is centered at the human operator's hand grasp point. The Slave has the following frames: *MRF (Moving Reference Frame)* is a user-defined frame which is being controlled. The *MRF* can be placed anywhere as long as it is rigidly attached to the last manipulator link (such as on a grasped payload or even off the physical link). The *CRF (Control Reference Frame)* is a user-defined frame with respect to which the *MRF* is controlled. Cartesian velocities may be commanded in the coordinates of any frame, but all motion relates the *MRF* to the *CRF*. The frames *L* and *S* are the camera lens (for machine vision and/or remote operator views) and force/torque (*F/T*) sensor frames; both are rigidly attached to the Slave *Wrist* and *MRF* frames.

The control frames in Fig. 1 are defined for generality. The *CRF* can be moving and the *Base* can also be moving independently with respect to the *World*. The *MRF* can be changed during tasks and is defined to facilitate task completion. (For example, the *MRF* can be the beam node in a beam assembly task. In this case the *CRF* would be the target connecting node location.) The inclusion of the *MRF* and *CRF* is intended to decouple the

Cartesian task (including a human operator) from the slave manipulator. Figure 2 shows the general control flow in a force-reflecting teleoperated system (*Pose* stands for Cartesian position and orientation and *Wrench* stands for Cartesian force and moment vector). In this report a force-reflecting master will be generically referred to as a force-reflecting hand controller (*FRHC*).

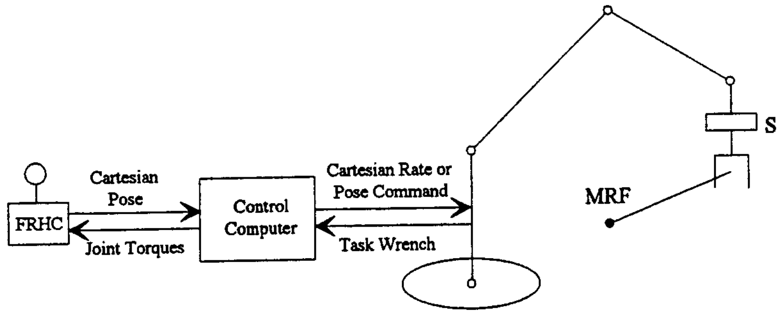

Figure 2. Force-Reflecting Teleoperated System

The author also further developed a concept (Williams and Roberts, 1997) during the summer 1997 period (for which Ohio University has obtained a provisional patent) for a novel cable-suspended haptic interface with force/moment and tactile fusion. This device (when built) could perform as the force-reflecting master.

The *HSF* Lab has the following devices. The methods of this report were implemented on these devices in simulation and hardware implementation is currently progressing. A single *Merlin 6500* robot arm (Fig. 3, from the American Robot Corporation, 1985) is the slave manipulator. This six-dof spatial device consists of six revolute (*R*) joint axes in series. A second *Merlin* may be available in the future to implement dual-arm control. The master is the seven-dof, seven-*R* *Freflex* (Force-reflecting exoskeleton, Fig. 4, a unique device from an Odetics, Inc. *SBIR*, 1991). For a detailed description of the *Merlin/Freflex* control and communications hardware, see Murphy (1997).

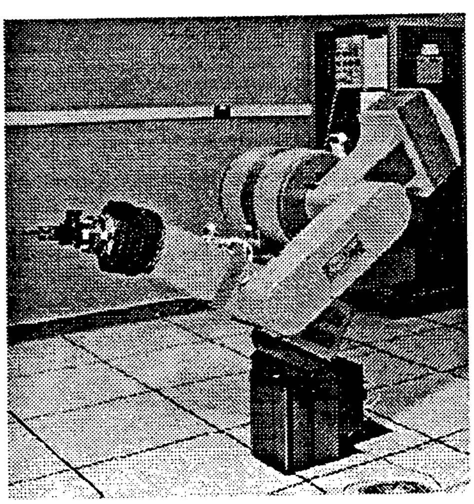

Figure 3. Merlin Slave Manipulator

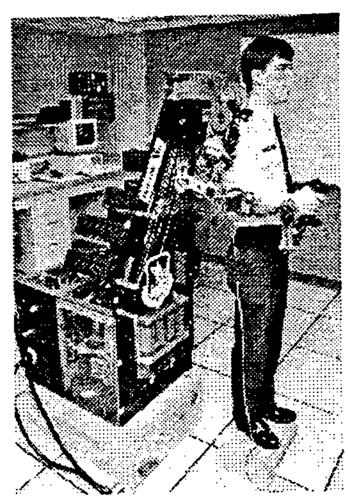

Figure 4. Freflex Force-Reflecting Exoskeleton

3 Kinematics

The telerobotic control architecture presented in this report requires kinematics transformations which relate Cartesian and joint variables within the master and slave devices. Specifically, this section presents the *DH* parameters, forward kinematics transformation, and Jacobian matrices for the *Freflex* master and *Merlin* slave. Huang (1993) presents these equations derived for minimal on-line computation. The equations in this section, used in the simulation and hardware implementation, do not attempt symbolical or numerical computation optimization. Numerical recursion is used. Huang's equations (1993) were implemented on the *Freflex* hardware and our hardware implementation makes use of that existing code insofar as possible. Huang's equations were never implemented on the *Merlin* and so the current report equations are used. Computational efficiency can be improved over the equations presented in this report by using symbolic computer algebra to derive the equations or a numerical approach similar to Huang's.

3.1 DH Parameters

The Denavit-Hartenberg (*DH*) parameters provide a standard manner to describe the joint/link geometric relationships in a serial manipulator. Unfortunately, two possible *DH* standards have arisen, the Paul (1981) convention and the Craig (1989) convention. Craig convention is used in the current report and Odetics (1992), while Huang (1993) uses Paul convention. Figure 5 shows the *Merlin* and Fig. 6 the *Freflex* kinematic diagrams, from which the *DH* parameters of Tables 1 and 2 (Craig, 1989) are derived. All angular units are *degrees*. If the θ_i angular offset of rows 3 and 6 are included for the *Merlin* and *Freflex*, respectively, Figs. 5 and 6 show the zero-joint-angle configurations. Nominal *Merlin* and measured *Freflex* joint angle limits are also given.

Nominal values for the *Merlin* lengths are: $a_2 = 17.375$, $d_2 = 11.9$, $d_4 = 17.25$, and nominal values for the *Freflex* lengths are: $a_3 = 1.969$, $a_4 = -1.969$, $d_3 = 14.64$, $d_4 = 0.625$, $d_5 = 11.77$. All linear units are *inches*.

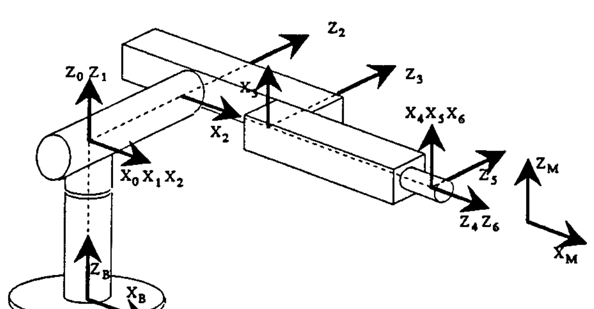

Figure 5. Merlin Kinematic Diagram

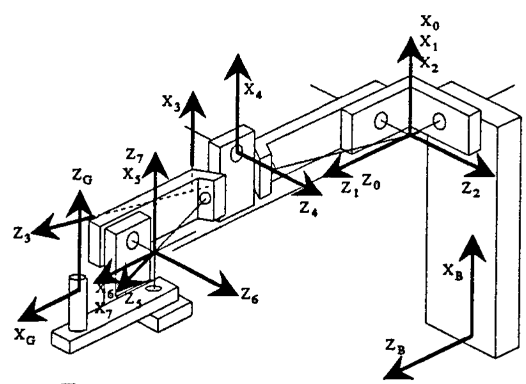

Figure 6. Freflex Kinematic Diagram

3.2 Forward Kinematics

The forward kinematics transformation gives the position and orientation (pose) of the moving frame of interest n with respect to the kinematic base frame 0 (Craig, 1989):

$$ {}^{0}_{n}T = \begin{bmatrix} \begin{bmatrix} {}^{0}_{n}R \end{bmatrix} & \left\{ {}^{0}P_n \right\} \\ 0 \quad 0 \quad 0 & 1 \end{bmatrix} \qquad {}^{0}X_n = \left\{ x \quad y \quad z \quad \gamma \quad \beta \quad \alpha \right\}^T \tag{1} $$

The pose can be represented by ${}^{0}_{n}T$ (the 4x4 homogeneous transformation matrix with the 3x3 orientation matrix ${}^{0}_{n}R$ and the 3x1 position vector ${}^{0}P_n$) or ${}^{0}X_n$ (whose first 3 components are ${}^{0}P_n$ and second 3 are orientation numbers extracted from ${}^{0}_{n}R$, e.g. *Z-Y-X* Euler convention, see Eq. 10). Given one row in a *DH* parameter table, the homogeneous transformation matrix relating the pose of neighboring frames in a serial chain is:

$$ {}^{i-1}_{\;\;\;i}T = \begin{bmatrix} c\theta_i & -s\theta_i & 0 & a_{i-1} \\ s\theta_i c\alpha_{i-1} & c\theta_i c\alpha_{i-1} & -s\alpha_{i-1} & -d_i s\alpha_{i-1} \\ s\theta_i s\alpha_{i-1} & c\theta_i s\alpha_{i-1} & c\alpha_{i-1} & d_i c\alpha_{i-1} \\ 0 & 0 & 0 & 1 \end{bmatrix} \tag{2} $$

where $c\theta_i = \cos(\theta_i)$, $s\theta_i = \sin(\theta_i)$, etc. The forward kinematics transformation for active joints is:

$$ {}^{0}_{n}T = \prod_{i=1}^{n} {}^{i-1}_{\;\;\;i}T = {}^{0}_{1}T\,{}^{1}_{2}T \cdots {}^{n-1}_{\;\;\;\;n}T \tag{3} $$

The overall forward kinematics for the *Merlin* and *Freflex* are given below on the left and right, respectively (Note the *Merlin* and *Freflex* each have *Base*, 0, and *Wrist* frames which must be distinguished, see Fig. 1):

$$ {}^{Wo}_{M}T = {}^{Wo}_{B}T\,{}^{B}_{0}T\,{}^{0}_{W}T\,{}^{W}_{M}T \qquad {}^{Wo}_{G}T = {}^{Wo}_{B}T\,{}^{B}_{0}T\,{}^{0}_{W}T\,{}^{W}_{G}T \tag{4} $$

where *M*, *B*, 0, *W*, and *G* stand for the *MRF*, *Base*, 0, *Wrist*, and *Grip* frames. The world frame *Wo* is common.

Table 1. *Merlin DH* Parameters

i	α_{i-1}	a_{i-1}	d_i	θ_i	*Limits*
1	0	0	0	θ_1	±147
2	-90	0	d_2	θ_2	+56,-230
3	0	a_2	0	$\theta_3 - 90$	+56,-230
4	-90	0	d_4	θ_4	±360
5	90	0	0	θ_5	±90
6	-90	0	0	θ_6	±360

Table 2. *Freflex DH* Parameters

i	α_{i-1}	a_{i-1}	d_i	θ_i	*Limits*
1	0	0	0	θ_1	18,-28
2	90	0	0	θ_2	+130,-52
3	-120	0	d_3	θ_3	±90
4	120	a_3	d_4	θ_4	-3,-166
5	-70	a_4	d_5	θ_5	±90
6	70	0	0	$\theta_6 + 90$	+128,+51
7	90	0	0	θ_7	+57,-52

3.3 Jacobian Matrices

The Jacobian matrix ${}^{k}J$ for a serial chain maps joint rates $\dot{\Theta} = \left\{ \dot{\theta}_1 \quad \dot{\theta}_2 \quad \cdots \quad \dot{\theta}_n \right\}^T$ into Cartesian rates ${}^{k}\dot{X} = \left\{ \dot{x} \quad \dot{y} \quad \dot{z} \quad \omega_x \quad \omega_y \quad \omega_z \right\}^T$ of the frame of interest with respect to the base, expressed in any frame k:

${}^{k}\dot{X}={}^{k}J\dot{\Theta}$. The i^{th} column of ${}^{k}J$ is the Cartesian velocity of the point of interest due to joint rate i alone (with $\dot{\theta}_i$ factored out). This fact leads to the following formula for the i^{th} column of ${}^{k}J$, where ${}^{i}z_i = \{0 \quad 0 \quad 1\}^T$:

$$
{}^{k}J_i = \begin{Bmatrix} {}^{k}_{i}R\left({}^{i}z_i \times {}^{i}P_n\right) \\ {}^{k}_{i}R\,{}^{i}z_i \end{Bmatrix} \tag{5}
$$

Equation 5 is applied for each moving joint to yield the 6x6 *Merlin* and 6x7 *Freflex* Jacobian matrices, each relating the motion of the respective *Wrist* with respect to *Base*, expressed in k (k can be different for *Merlin* and *Freflex* and is chosen as the respective 0 frames in this report).

4 Control Architecture

This section presents the general real-time telerobotic control architecture for implementation in the *HSF* Lab. It is adapted from a unique hardware system at *NASA* Langley (Williams et.al., 1997). The sensor-rich system is rate-based but allows input from various control modes simultaneously: pose, rate, vision, force; others may be added. The architecture provides shared telerobotic control, defined as concomitant human, automated, and sensor-based inputs. All modes can operate on all Cartesian axes simultaneously (which can lead to conflicts of which the operator must be aware). During tasks one or more control modes may be activated during task steps by entering non-zero gain matrices. In the current report, only joint control, pose control, and rate control are implemented for a single slave manipulator and force-reflecting master. This may be expanded in the future as needed (e.g. additional sensory feedback modes such as machine vision and laser proximity, dual-slave-arm operations, kinematically-redundant slave manipulators; see Williams et.al., 1997). Huang's (1993) control mode for the slave manipulator allows only inverse pose control and is based on the complex, multiple solution inverse pose kinematics results. The current rate-based method does not use these equations, but instead requires the slave manipulator Jacobian matrix. Even though not as widely applied as inverse pose control, rate control has several benefits: linear equations, unique solution, and inputs from multiple control modes are linearly summed. Both inverse rate and inverse pose suffer from the same manipulator kinematic singularities.

4.1 Control Diagram

The real-time, sensor-rich, rate-based, shared telerobotic control architecture is shown in Fig. 7 for a single slave manipulator. The following subsections present the control modes and algorithms.

4.1.1 Resolved-Rate Control. The resolved-rate control algorithm is used for motion control from all input sources: master, pose, and force controllers. The algorithm implemented is based on Whitney's method (1969). This section assumes a static *Base* and *CRF*; the method can be extended to handle moving *Base* and *CRF* frames for dynamic tasks. The time-varying manipulator Jacobian matrix maps joint rates to Cartesian rates of the *Wrist*: ${}^{k}\dot{X}_W={}^{k}J\dot{\Theta}$. The Cartesian rates ${}^{k}\dot{X}_W={}^{k}\{\underline{v}_W \quad \underline{\omega}_W\}^T$ express the translational and rotational velocities of

the *Wrist* with respect to the *Base*, expressed in the coordinates of any frame k. Common choices are k = *Wrist*, 0, or *Base*; simplest symbolic terms for the Jacobian matrix result when k is the frame midway between the *Base* and *Wrist*, often the *Elbow* frame. The equation ${}^k\dot{X}_W = {}^kJ\dot{\Theta}$ must be inverted (or, more efficiently, solved by Gaussian elimination) at each control step. First, however, the input *MRF* Cartesian rates ${}^j\dot{X}_M$ (the sum of all control inputs for the *MRF* frame, expressed in any frame j) must be converted to the resolved rate input ${}^k\dot{X}_W$ (the equivalent Cartesian velocities of the *Wrist* frame to produce $\dot{X}_M$). This rigid-body velocity transformation and coordinate transformation is given in Eq. 6 (Craig, 1989).

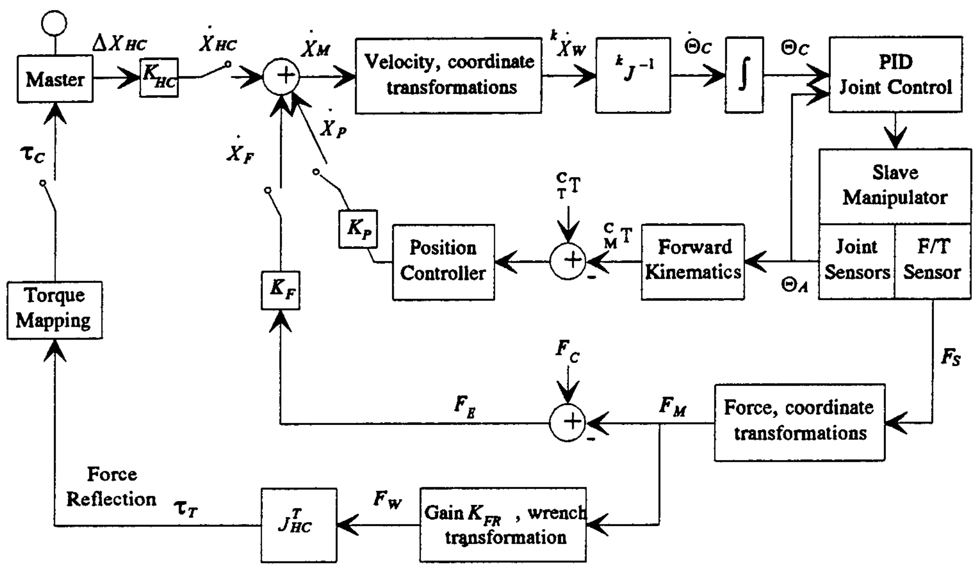

Figure 7. Telerobotic Control Architecture

$$ {}^k\dot{X}_W = {}^k\begin{Bmatrix} \underline{v}_W \\ \underline{\omega}_W \end{Bmatrix} = \begin{bmatrix} {}^k_jR & {}^k_WR\,{}^WP_{MRF} \times {}^k_jR \\ 0 & {}^k_jR \end{bmatrix} {}^j\begin{Bmatrix} \underline{v}_{MRF} \\ \underline{\omega}_{MRF} \end{Bmatrix} \tag{6} $$

$\dot{X}_M$ always gives the six-dof velocity of *MRF* with respect to *Base*, but can be expressed in any coordinates j (e.g. *CRF*, *Base*, 0, or *World*). Now the rate equation is inverted to calculate the instantaneous joint rates necessary to obtain the commanded ${}^k\dot{X}_W$:

$$ \dot{\Theta}_C = {}^kJ^{-1}\,{}^k\dot{X}_W \tag{7} $$

The commanded joint rates are numerically integrated to commanded joint angles Θ_C. These angles are commanded to the manipulator and achieved using linear independent *PID* control laws. Joint encoder feedback Θ_A is used to form the errors for servo control.

This algorithm is sensitive to kinematic singularities, where the manipulator loses freedom to move in one or more Cartesian direction. In the neighborhood of singularities, extremely high joint rates are theoretically required to satisfy a finite Cartesian command. To deal with this problem, the determinant of the Jacobian matrix ${}^{k}J$ must be monitored. When the determinant approaches zero, the matrix inverse (or Gaussian elimination) in Eq. 7 is replaced by a matrix pseudoinverse based on Singular Value Decomposition (*SVD*). Near singularities, the exact Cartesian command ${}^{k}\dot{X}_{W}$ cannot be satisfied, but the *SVD* will yield bounded joint rates which will move the manipulator through the singular neighborhood until Eq. 7 can take over again.

For teleoperation, the displacement ΔX_{HC} of the operator's hand with the master device is interpreted to be the rate $\dot{X}_{HC}$ after applying matrix gain K_{HC}, as discussed in Section 4.2.1.2.

4.1.2 Pose Control. Resolved-rate control may be used to command manipulator poses by closing a position loop around the rate system. The difference between the commanded (${}^{C}_{T}T$, frame T stands for *Target*) and current (${}^{C}_{M}T$) manipulator poses must be calculated. The target pose may be commanded by the operator through teleoperation master (Section 4.2.1.1) or keyboard input, an automated path planner, or some sensor-based algorithm (e.g. machine vision). The current pose is found from the forward kinematics transformation of joint encoder feedback Θ_{A} and other known homogeneous transformation matrices.

$$ {}^{C}_{M}T = {}^{C}_{WO}T\,{}^{WO}_{B}T\,{}^{B}_{W}T(\Theta_{A})\,{}^{W}_{M}T \tag{8} $$

The translational error vector is found by algebraic subtraction of the position vectors: ${}^{C}P_{T-M} = {}^{C}P_{T} - {}^{C}P_{M}$. However, because the orientation cannot be represented by vectors the angular velocity error must be calculated using a rotation matrix "difference".

$$ {}^{M}_{T}R = {}^{C}_{M}R^{-1}\,{}^{C}_{T}R = {}^{C}_{M}R^{T}\,{}^{C}_{T}R \tag{9} $$

Three orientation numbers (e.g. Euler *Z-Y-X* α,β,γ, Craig 1989) are extracted from the difference rotation matrix ${}^{M}_{T}R$, as given in Eq. 10.

$$ R = [r_{ij}] = \begin{bmatrix} c\alpha c\beta & -s\alpha c\gamma + c\alpha s\beta s\gamma & s\alpha s\gamma + c\alpha s\beta c\gamma \\ s\alpha c\beta & c\alpha c\gamma + s\alpha s\beta s\gamma & -c\alpha s\gamma + s\alpha s\beta c\gamma \\ -s\beta & c\beta s\gamma & c\beta c\gamma \end{bmatrix} \qquad \begin{aligned} \beta &= a\tan 2\left(-r_{31}, \pm\sqrt{r_{11}^{2} + r_{21}^{2}}\right) \\ \alpha &= a\tan 2(r_{21}/c\beta, r_{11}/c\beta) \\ \gamma &= a\tan 2(r_{32}/c\beta, r_{33}/c\beta) \end{aligned} \tag{10} $$

where $c\beta = \cos(\beta)$, $s\beta = \sin(\beta)$, etc. The α,β,γ solution in Eq. 10 has two results represented by the $\pm$ in the β solution. The solution is subject to a $\beta = \pm 90^{\circ}$ singularity (Craig, 1989, presents an alternative solution for the singular case). Taking these three numbers α,β,γ as both the Euler angles and respective rates ($\dot{\gamma} = \gamma$, $\dot{\beta} = \beta$,

and $\dot{\alpha} = \alpha$), the commanded angular velocity error vector is calculated using the appropriate rotational kinematic differential equations in Eq. 11 (Kane et.al., 1983).

$$\begin{Bmatrix} \omega_x \\ \omega_y \\ \omega_z \end{Bmatrix} = \begin{bmatrix} 1 & 0 & -s\beta \\ 0 & c\gamma & c\beta s\gamma \\ 0 & -s\gamma & c\beta c\gamma \end{bmatrix} \begin{Bmatrix} \dot{\gamma} \\ \dot{\beta} \\ \dot{\alpha} \end{Bmatrix} \tag{11}$$

The position and orientation error vector is converted to a rate $\dot{X}_P$, added into the summing junction in Fig. 7, after applying the vector gain K_P (with translational units $1/s$ and unitless rotational components).

<u>4.1.3 Force Control.</u> An active force controller has been implemented in the resolved-rate scheme to command forces to the environment with the manipulator. This active force controller is basically a general impedance controller (Hogan, 1985) with only the damping term. A six-dof *F/T* sensor (with frame *S*) mounted after the last joint reads the contact wrench $F_S = \{f_S \quad m_S\}^T$. The weight and gravity-moment of the end-effector mounted outboard of the *F/T* sensor (transformed to *S*) must be subtracted from the sensor reading. This modified sensor reading in *S* must be transformed by rigid body transformations and coordinate rotations (Craig, 1989) to the equivalent *MRF* wrench:

$$F_M = \begin{Bmatrix} f_M \\ m_M \end{Bmatrix} = \begin{bmatrix} {}^M_S R & 0 \\ {}^M P_S \times {}^M_S R & {}^M_S R \end{bmatrix} \begin{Bmatrix} f_S \\ m_S \end{Bmatrix} \tag{12}$$

A wrench error vector $F_E = F_C - F_M$ is formed from the difference of the sensed and commanded wrenches in the *MRF*. Since both force and moment are vector quantities, algebraic subtraction applies. The wrench error is converted to a rate $\dot{X}_F = K_F F_E$ which is sent to the summing junction in Fig. 7. This rate drives the manipulator motion so the desired force is achieved continuously. The diagonal gain matrix K_F has units *m/Ns* and *rad/Nms* for translational and rotational terms, respectively. If zero wrench is commanded and the manipulator contacts the environment, the motion will automatically align the manipulator end-effector for minimal Cartesian contact wrench and misalignments. This is called *force/moment accommodation* (*FMA*) (Williams et.al., 1996; Williams and Murphy, 1997b).

If a *FRHC* is used, the sensed *MRF* wrench can also be sent so the operator's hand feels the task wrench exerted by the manipulator. The required transformation is (Craig, 1989):

$$\tau_T = J_{HC}^T F_W \tag{13}$$

where τ_T is the vector of *FRHC* joint torques/forces required to feel the task wrench and J_{HC} is the *FRHC* Jacobian matrix. The task wrench F_M is scaled by matrix gain K_{FR} and sent as the *FRHC* grip wrench. If the *FRHC* Jacobian is derived for the *Wrist* relative to the *Base*, a rigid body wrench transformation (similar to Eq. 12)

is required to transform this scaled task wrench from *Grip* to *Wrist*, obtaining F_W for use in Eq. 13. The joint torques are achieved by torque mapping, sending τ_C to the *FRHC* (e.g. see Section 4.2.5.2).

4.1.4 Simultaneous Control. In the control architecture of Fig. 7, all input sources (i.e. master, position, and force) can be enabled simultaneously for all Cartesian axes. In most other experimental telerobotics systems the author is acquainted with, only one input source is enabled at any one time and changing between sources requires artificial software or hardware switches. Often different input sources will result in competing goals (e.g. different poses commanded by the operator and automated path planner). Therefore, software switches are included (set by script file keyboard input) to enable or disable each input source during the execution of tasks. Also, zero values in the vector gains K_{HC}, K_P, and K_F can be used to disable some or all Cartesian axes from the input sources. See Section 5 for an example of simultaneous inputs from two control modes which is complimentary, not competing. A limitation of the proposed control architecture is that the gains are tuned heuristically. Gain scheduling is allowed but there is no theoretical basis for computing the gains. As the manual gain selection is necessarily conservative to achieve stability, it is likely that suboptimal performance is obtained.

4.1.5 Shared Control. The proposed control architecture allows shared control, which is control by a human operator (teleoperation), autonomous sensor-based control (robotic), or a combination of both (telerobotic). In this system the human controls the system via the master or through keyboard inputs. The master input is integrated seamlessly. For instance, if it appears the automated system will drive the end-effector into an obstacle the operator can modify the trajectory in real-time by using the master. After the danger is past and the master input is zero the original target pose is still reached by the manipulator.

4.2 Force-Reflecting Master Control Diagram

Figure 8 shows the control flow for the implementation of a Cartesian *FRHC* commanding inputs and reflecting wrenches with a telerobotic system in Cartesian space. There is some overlap between Figs. 7 and 8; Fig. 8 shows more detail. Figure 8 assumes Cartesian rate inputs; the difference for Cartesian pose inputs is minor (discussed below). This method has not yet been fully implemented in hardware. The following subsections present the algorithms for Fig. 8. For more detail, see Williams (1997).

4.2.1 *FRHC* Cartesian Input Commands. Let us start with the block "*FRHC* Including Operator" in Fig. 8. The user must first define the desired *FRHC* reference pose via a switch. This pose (calculated from forward kinematics ${}^{0}_{G_0}T = {}^{0}_{1}T\,{}^{1}_{2}T \cdots {}^{6}_{7}T\,{}^{7}_{G_0}T$ when the switch is hit) can be any convenient pose in the *FRHC* workspace which represents zero Cartesian input to the manipulator. The operator may redefine this pose at any time. This feature is intended to decouple the Cartesian input from the *FRHC* base frame and allow generality for commands.

During any control cycle when the operator has moved the *FRHC* grip from the reference pose, the input command to the manipulator is determined as follows. First the *FRHC* joint sensors are read and *FRHC* forward kinematics calculates the current grip frame pose relative to the *FRHC* base frame: ${}^{0}_{G}T = {}^{0}_{1}T\,{}^{1}_{2}T \cdots {}^{6}_{7}T\,{}^{7}_{G}T$. Now a difference homogeneous transformation matrix is calculated to represent the input (inverse given in Craig, 1989):

$$ {}^{G_0}_{G}T = {}^{0}_{G_0}T^{-1}\, {}^{0}_{G}T \tag{14} $$

At this point, the Cartesian pose and rate input cases differ.

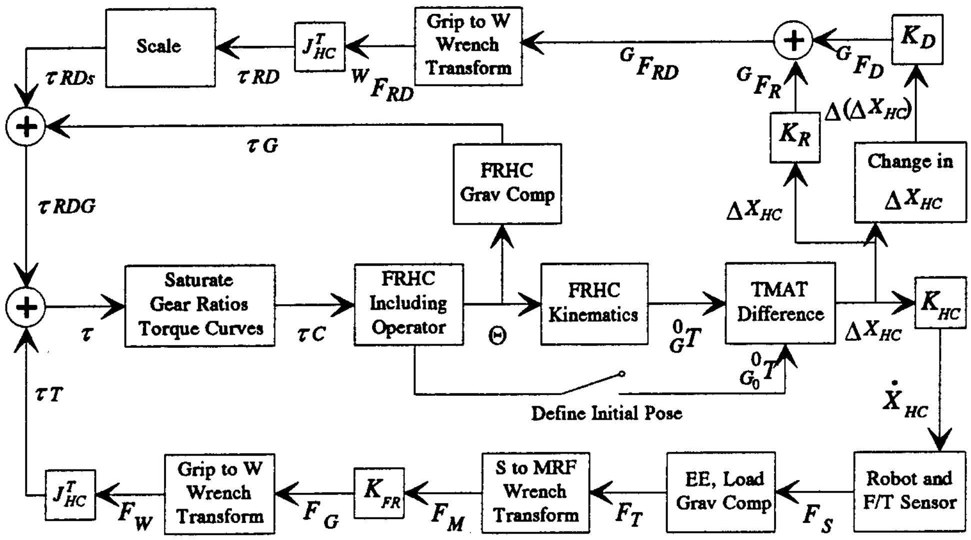

Figure 8. Cartesian FRHC Control Diagram

4.2.1.1 Cartesian Pose Input. The difference matrix ${}^{G_0}_{G}T$ is interpreted as the commanded slave pose ${}^{M_0}_{T}T$ (where M_0 is the reference *MRF* frame, which can also be redefined using *FRHC* pose indexing). M_0 is fixed once defined, as opposed to the constantly changing *MRF* in pose control (Eq. 8 in Section 4.1.2). The pose input is then (see Section 4.1.2) ${}^{C}_{T}T = {}^{C}_{M_0}T\, {}^{M_0}_{T}T = {}^{C}_{M_0}T\, {}^{G_0}_{G}T$. This is not pictured in Fig. 8.

4.2.1.2 Cartesian Rate Input. This procedure is similar to formation of rate signal $\dot{X}_P$ for resolved-rate-based pose control (Section 4.1.2). A set of difference numbers $\Delta X_{HC} = \{x \quad y \quad z \quad \gamma \quad \beta \quad \alpha\}^T$ is extracted from the difference matrix ${}^{G_0}_{G}T$. The translational part $\{x \quad y \quad z\}^T$ is the fourth column of ${}^{G_0}_{G}T$ excluding row 4, while α, β, γ are the *Z-Y-X* Euler angles (Craig 1989) extracted from the difference rotation matrix ${}^{G_0}_{G}R$. This is labeled as "*TMAT* Difference" in Fig. 8. For Cartesian rate input, the translational terms are the first three terms of ΔX_{HC} scaled by the first three K_{HC} diagonal elements (units sec^{-1}). In Fig. 8 all gain matrices K_m are order 6x6 and (generally) diagonal matrices of gains. Because a static *FRHC* orientation must be converted into a Cartesian rotational rate, we again use $\dot{\gamma} = \gamma$, $\dot{\beta} = \beta$, and $\dot{\alpha} = \alpha$ in the rotational rate kinematics transformation Eq. 11. Then the angular velocity command is $\{\omega_x \quad \omega_y \quad \omega_z\}^T$, scaled by the second three K_{HC}

diagonal elements (unitless). The total teleoperated Cartesian rate command to the *MRF* ($\dot{X}_{HC}$) is formed from these translational and rotational rate terms. Note this process is not shown in Fig. 8, but is inside the K_{HC} block.

The lower path in Fig. 8 presents reflection of the Cartesian task wrench to the operator, discussed in Section 4.1.3. Previously-presented algorithms are sufficient to command a manipulator and feed back task wrenches simultaneously with a *FRHC* in Cartesian space. However, the next section presents the additional features of Fig. 8 to improve operator loading and *FRHC* stability.

4.2.2 Improved Operator Loading and Stability. One benefit of wrench-reflection to the operator is increased feeling of telepresence which enables teleoperation tasks to be completed more easily and with lower contact wrenches. However, one drawback is the potential for increased operator loading, including fatigue from resisting wrenches through the *FRHC* and supporting a portion of the *FRHC* weight. In the last section, the end-effector and payload weights and moments were subtracted to remove that static loading from the operator (this information is not required for tasks). To improve telepresence quality, the payload weight may be included.

In the current section, *FRHC* gravity compensation is presented to further unload the operator's arm. Also, for Cartesian rate inputs, a unique return-to-center method is developed which assists the operator in finding the zero input *FRHC* pose when zero inputs are desired in between commanded motions. For both rate and pose inputs, a damping term is also added to improve relative *FRHC* stability. It is crucial that these operator aids do not mask the task Cartesian contact wrench.

4.2.2.1 FRHC Gravity Compensation. Many *FRHCs* are mini-articulated robots which must be supported by the operator. *FRHC* gravity compensation applies configuration-varying joint torques so the *FRHC* supports most (theoretically, all) of its static weight. At the *CG* of *FRHC* link *i*, the weight $m_i g$ acts. If a fictitious force $f_{icomp} = m_i g$ is provided equal and opposite of the weight vector, that link will be balanced. The joint torques required to support this f_{icomp} may be calculated using $\tau_i = J_i^T f_{icomp}$, where J_i is the Jacobian matrix relating the center of mass of link *i* to the base. Only motors 1 through *i* support the weight of link *i*. By summing all links' τ_i (vectors of increasing dimension 1 through *n* for links 1 through *n*) we calculate the joint torques τ_G in Fig. 8 required to unload the operator's arm by commanding the *FRHC* to support its own weight. Huang (1993) presents an alternative gravity compensation algorithm; simulation demonstrated identical results for the two methods. Section 4.2.5.3 presents the nominal mass and mass center parameters.

4.2.2.2 Constant-Force Return-to-Center and Virtual Walls. For Cartesian rate input commands, the manipulator will move with a commanded velocity when the *FRHC* Cartesian pose is different from its reference pose G_0. Therefore, a return-to-center (*RTC*) force should be provided to assist the operator's hand in finding the zero input *FRHC* pose. As a first try (at *NASA* Langley Research Center), this *RTC* force was calculated using Hooke's law with a virtual spring: ${}^{G}F_R = -K_R \Delta X_{HC}$. The *FRHC* grip wrench is calculated for each Cartesian axis (3 translations, 3 rotations) independently; the negative sign is to draw the operator's hand

back toward the zero pose. However, it was found that the *FRHC* workspace far from the defined reference pose generated large *RTC* forces unnecessarily due to the linearly increasing relationship.

Therefore, a novel constant-force return-to-center (*CFRTC*) approach was developed. Figure 9 shows the *CFRTC* force as a function of scalar displacement ΔX_{HCi} from the zero reference, for one of the 6 Cartesian axes. ΔX_{HCi} represents any one of the six terms in the relative Cartesian pose ΔX_{HC}. $\Delta X_{HCi}, i = 1,2,\cdots,6$ are found from *FRHC* joint sensors as discussed previously. The magnitudes in Fig. 9 are arbitrary and must be determined for specific *FRHCs* based on performance requirements and *FRHC* workspace. The *CFRTC* is symmetric about $\Delta X_{HCi} = 0$; each side displays three distinct (but continuous) regions. The first is the deadband, serving two purposes: a) providing a small region of zero input surrounding the zero pose; and b) providing a parabolic virtual wall which the operator must overcome if an input is to be commanded in that particular Cartesian axis. The second, largest, zone is the working range which provides the *CFRTC* (as opposed to Hooke's law) virtual spring. The third zone provides a stiff virtual spring to alert the operator when the edge of the *FRHC* workspace is encountered. In practice it was found that this stiff spring was unnecessary so the flat *CFRTC* zone was extended to the workspace boundary. In this case, the operator must be aware of the workspace boundaries, but the effective *FRHC* range is extended.

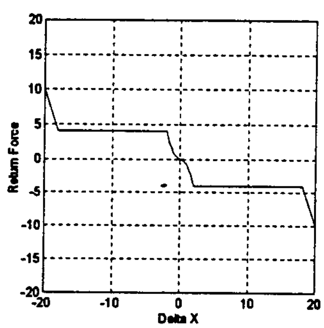

Figure 9. CFRTC for One Cartesian Axis

The i^{th} term for the Cartesian *CFRTC* wrench ${}^{G}F_R$ is expressed in Eq. 15. Note translational pose terms correspond to return forces while rotational pose terms correspond to return moments.

$$\begin{aligned} \left({}^{G}F_R\right)_i &= -a_i \Delta X_i^2; \Delta X_i \le \Delta X_{iDB} \\ &= -a_i \Delta X_{iDB}^2; \Delta X_i > \Delta X_{iDB} \end{aligned} \qquad (15)$$

where the constant ΔX_{iDB} is the i^{th} axis deadband value, a_i is the i^{th} axis parabolic constant, and the subscript *HC* was dropped for clarity. If $\Delta X_i \le \Delta X_{iDB}$, no Cartesian command is sent out for the i^{th} axis. If $\Delta X_i > \Delta X_{iDB}$, ΔX_{iDB} must first be subtracted from ΔX_i before it is used in a Cartesian pose or rate command. Figure 9 and Eq.

15 are represented on Fig. 8 by the virtual spring characteristics K_R (more complicated than the other Fig. 8 matrix gains due to the different zones). The rotational deadband should be applied at the angular velocity level due to the Euler angle coupling in R matrices.

4.2.2.3 Damping Term. To increase relative *FRHC* stability, a damping term is added. If the *FRHC* pose is static, there is zero damping term. However, if the operator is making *FRHC* pose changes with respect to time, the damping term applies a resistive wrench ${}^G F_D$ (opposite to the velocity direction of each Cartesian pose term) at the *FRHC* grip. This dampens rapid changes in the manipulator Cartesian commands.

The $\Delta(\Delta X_{HC})$ vector is calculated via a simple difference in the current and previous ΔX_{HC} values. In this case we have small angle motion (for $\Delta(\Delta X_{HC})$, not for ΔX_{HC}) so the entire pose representation ΔX_{HC} may be subtracted algebraically to yield $\Delta(\Delta X_{HC})$, rather than using the form of Eq. 11. ${}^G F_D$ is calculated by applying a diagonal matrix of damping gains K_D (with negative signs) to $\Delta(\Delta X_{HC})$.

$$\left({}^G F_D\right)_i = -K_{Di}\Delta(\Delta X_{HC})_i \tag{16}$$

The stability issue is important in a wrench-reflecting system. If the operator makes contact between the manipulator and its environment at a high rate, a large wrench will be reflected, which pulls the operator's hand back. In turn, the manipulator will reverse, only to be returned with the command from the operator's hand recovering forward. This situation can lead to an oscillating instability. This is extremely difficult to model due to environment stiffness uncertainties and lack of a good model and variability for human operators. In the experimental system, stability was aided by the *FRHC* damping term, but operator training and heuristic gain tuning also helped stabilize the system. A future goal is to better ensure stability.

4.2.2.4 Total Assist Terms. The return-to-center and damping operator assist terms are summed to determine the required assist wrench ${}^G F_{RD}$ at the *FRHC* grip: ${}^G F_{RD} = {}^G F_R + {}^G F_D$. As with the task wrench case, ${}^G F_{RD}$ must be converted to the equivalent wrench for the W frame (Eq. 12 with proper indices) before using an equation of the Eq. 13 form to calculate the joint torques/forces τ_{RD} to achieve the assist features. In order to ensure that the task wrench dominates, the assist wrench τ_{RD} is first scaled uniformly to a given fraction of the *FRHC* joint torque limits to yield τ_{RDs}. The gravity compensation joint commands τ_G cannot be likewise scaled if they are to support the entire *FRHC* mass. The total assist joint torques are thus: $\tau_{RDG} = \tau_{RDs} + \tau_G$.

<u>4.2.3 Total *FRHC* Joint Commands.</u> The total joint torques/forces commanded to the *FRHC* joints are the sum of those required for the task wrench (with end-effector and payload removed, if desired) and those required for the assist wrench: $\tau = \tau_T + \tau_{RDG}$. In order to calculate the final joint commands τ_C, a final uniform scaling (saturation) must be performed if one or more of the commanded joint torques τ exceed the motor capabilities. Also, gear ratios and torque calibration curves must be implemented. Now the discussion of Fig. 8 is

complete. The operator feels any task wrenches and continuously updates the Cartesian manipulator commands, while being assisted by gravity compensation, return-to-center (for rate inputs), and *FRHC* damping.

4.2.4 Pose vs. Rate Cartesian Commands. The experimental systems implemented allowed both pose and rate inputs. Figure 8 is developed for the rate case, but the pose case is very similar. For the pose case, the input is discussed in Section 4.2.1.1. In pose mode, the *CFRTC* assist wrench is not required because a static *FRHC* pose yields a static manipulator pose (rather than moving with constant velocity). The deadband and virtual walls were first implemented at *NASA* but not found to be as useful as in the rate case. However, the same *FRHC* gravity compensation and damping terms apply well to the pose case.

4.2.5 Implementation Issues.

4.2.5.1 Switches. A *FRHC* should have at least three switches. The most prominent should be used as a deadman switch (must be continuously held by the operator to send commands to the robot and receive wrench reflection back). A second switch can be used to define the *FRHC* reference pose as shown in Fig. 8. This same switch may be used as an index button to command the entire slave robot workspace with a limited *FRHC* workspace, when using pose input mode. The third switch can be used to enable/disable wrench reflection from the task to the *FRHC*. The second and third switches do not need to be depressed continuously.

4.2.5.2 Torque Coupling. The seven *Freflex* joints are actuated via seven base-mounted motors through complex cable-drive systems. Therefore, the joint angles and joint torques are coupled functions of the motor angles and torques. Huang (1993) uses a constant global coupling matrix A to describe the kinematic coupling: $\Delta\Theta_{joint} = A\Delta\Theta_{motor}$. By the principle of virtual work, the same matrix is used in the torque coupling: $\tau_{motor} = A^T \tau_{joint}$. Huang (1993) presents a method to experimentally determine the matrix A using redundant measurements and a least squares fit. Ideally, A is a lower triangular matrix because motor i torque should only depend on outboard links. Huang (1993) reports an experimentally-determined A.

4.2.5.3 Mass Parameters. The *Freflex* links' mass m_i and center of mass CG_i (vector from origin of frame i to CG_i, expressed in i coordinates) are critical for the *Freflex* gravity compensation algorithm. Odetics (1992) gives conservative values for these parameters, used for worst-case motor sizing. Huang (1993) does not report these parameters, but they appear in the original *Freflex* code and are given in Table 3. Unfortunately, there is no explanation as to how these values were obtained. The current gravity compensation works on the *Freflex* hardware, but it needs improvement. The Table 3 values should be re-calibrated: Starting with the seventh link, m_7 and CG_7 should be tuned until each link supports itself against gravity. This process should be repeated for links six through one. For simulation purposes and also future hardware implementation, the *Freflex* code CG_i values (derived for Paul *DH* parameters) were transformed to equivalent values with Craig *DH* convention; these are reported in Table 4. Of course, m_i does not change with *DH* convention.

Table 3. ***Freflex* Mass Parameters, Paul**

Link	m_i	CG_{ix}	CG_{iy}	CG_{iz}
1	0.02163	1.15	-7.28	-4.40
2	0.01684	0.00	1.58	7.55
3	0.00958	-1.57	-1.36	-0.09
4	0.01036	0.17	0.10	2.62
5	0.00389	0.00	-3.69	-3.90
6	0.00285	0.00	-4.00	-3.50
7	0.00437	-0.58	0.00	-2.60

Table 4. ***Freflex* Mass Parameters, Craig**

Link	m_i	CG_{ix}	CG_{iy}	CG_{iz}
1	0.02163	1.15	4.40	-7.28
2	0.01684	0.00	5.75	2.41
3	0.00958	0.40	0.76	-1.13
4	0.01036	-1.80	2.50	0.80
5	0.00389	0.00	2.40	-4.80
6	0.00285	0.00	3.50	-4.00
7	0.00437	1.10	0.00	-2.60

5 Naturally-Transitioning Rate-to-Force Controller (*NTRFC*)

Raibert and Craig (1981) present a method for hybrid position/force control where certain Cartesian axes are chosen for position control and the remaining ones for force control. The current system can achieve this by proper placement of zeros in K_P and K_F in Fig. 7. However, excellent free motion to contact characteristics are achieved in by combining rate control and force-moment accommodation (*FMA*) on all axes simultaneously. This is termed Naturally-Transitioning Rate-to-Force Control.

The Naturally-Transitioning Rate-to-Force Controller (*NTRFC*) is applicable to control of any manipulator(s) with wrist-mounted force/torque sensor, rate inputs, and contact with the environment. The concept was developed heuristically at *NASA* Langley Research Center (Williams et.al., 1996) and demonstrated to be very effective in experiments (Willshire et.al., 1992). The system behaves as a rate controller in free motion and as a force controller in contact. The transition requires no mode changes, logical switches, or gain changes in the controller software or hardware and thus is termed a natural transition. The transition is a consequence of the physics of manipulator contact with the environment when using rate control with force/moment accommodation (*FMA*). The *NTRFC* concept was extended during summer 1997 at the *HSF* lab by the author. Rigorous modeling was performed and design procedures were developed (Williams and Murphy, 1997b). The *NTRFC* is currently being implemented in the *Freflex/Merlin* system and evaluation experiments are planned.

6 Simulation

A *Matlab* simulation was developed for the *Freflex/Merlin* system with the control architecture of this report. This simulation is useful to validate algorithms, test new ideas safely, compare data from hardware implementation, and view simulated motions. This code (developed under *Matlab* 5.0 but compatible with previous versions) was delivered to *HSF* personnel at the end of the summer 1997 period. This section presents the required m-files and their hierarchy. Joint, pose, and rate control modes are available. The menu-driven simulation is invoked by typing ***fremer*** at the *Matlab* prompt.

fremer.m	Main *Freflex/Merlin* routine; calls:
merlinDH.m	*Merlin DH* parameters and other constants
freDH.m	*Freflex DH* parameters and other constants

merfk.m	*Merlin* forward kinematics including animation vectors
frefk.m	*Freflex* forward kinematics including animation vectors
Fmplot.m	Display *Freflex* and *Merlin* in current poses (animation)
fretrq.m	Calculate *Freflex* force/torque algorithms; calls **Fj0** and **fregc**
frein.m	Simulate user input on *Freflex*, apply deadbands
Fpose.m	Move *Freflex* to user-specified pose; calls **Frr**
Mpose.m	Move *Merlin* to user-specified pose using resolved-rate; calls **Mrr**
Mpose2.m	Move *Merlin* to user-specified pose using inverse pose; calls **smoothie**
plotres.m	Plot simulation results, if user desires
Fj0.m	Calculate *Freflex* Jacobian and additional kinematics
fregc.m	Calculate *Freflex* gravity compensation
Frr.m	*Freflex* resolved-rate, for simulation **Fpose** only!
Mrr.m	*Merlin* Jacobian and resolved-rate
smoothie.m	*Merlin* joint angle interpolation, inverse pose only
required functions:	
dhfun.m	Evaluate Eq. 2 given one row of *DH* parameters
inv_homo.m	Invert homogeneous transformation matrix (Craig, 1989)
inv_euler.m	Extract *Z-Y-X* Euler angles from a rotation matrix, Eq. 10

7 Conclusion

A powerful and general control architecture is presented for real-time, sensor-based, rate-based, shared control of general telerobotic systems including force-reflecting hand controllers (*FRHCs*). A *Matlab* simulation of *Freflex/Merlin* teleoperation under joint and Cartesian pose and rate control was developed and delivered to the *HSF* Lab. This architecture has been partially implemented in hardware and the work will continue. This work is the first time the *Freflex* exoskeleton has been used for force-reflecting teleoperation of the *Merlin* slave manipulator to increase telepresence in remote operations. Additional accomplishments are the novel Naturally-Transitioning Rate-to-Force Controller (*NTRFC*) and mathematical modeling for the planar version of the novel cable-suspended haptic interface.

Acknowledgments

The author gratefully acknowledges support for this research from the Air Force Office of Scientific Research and Armstrong Laboratory in the Summer Faculty Research Program. Many thanks also to Captain Debra North for support and facilities in the Human Sensory Feedback Lab at Wright-Patterson *AFB*. The following researchers helped make the summer work more productive and enjoyable: Lieutenant Kurtis Johnson, Dr. Dan Repperger, Jim Berlin, and Lieutenant Mike Krier. The author thanks graduate student Mark Murphy for unwavering support in the face of theory and hardware.

References

American Robot Corporation, 1985, "*Service manual for the System II Merlin Intelligent Robot*".

M.D. Bryfogle, 1990, "*Force Reflection Algorithms for Exoskeleton Controllers*", AAMRL-TR-90-090.

J.J. Craig, 1989, **Introduction to Robotics: Mechanics and Control**, Addison Wesley Pub. Co., Reading, MA.

C.J. Hasser, 1995, "*Tactile Feedback for a Force-Reflecting Haptic Display*", AL/CF-SR-1996-0134.

N. Hogan, 1985, "*Impedance Control: An Approach to Manipulation*", ASME Journal of Dynamic Systems, Measurement, and Control.

M.Z. Huang, 1993, "*Efficient Coordination of an Anthropomorphic Telemanipulation System*", AL/CF-TR-1995-0120.

T.R. Kane, P.W. Likins, and D.A. Levinson, 1983, Spacecraft Dynamics, McGraw-Hill.

M.A. Murphy, 1997, "*Implementation of Freflex/Merlin Teleoperation*", Final Report, *AFOSR* Summer Graduate Student Research Program, Armstrong Laboratory.

Odetics Inc., 1992, "*Exoskeleton Master Arm, Wrist, and End-Effector Controller with Force-Reflecting Telepresence*", Phase II Final Report, Contract No. F33615-89-C-0587.

R.P. Paul, 1981, **Robot Manipulators**, MIT Press, Cambridge, MA.

M. Raibert and J.J. Craig, 1981, "*Hybrid Position/Force Control of Manipulators*", ASME Journal of Dynamic Systems, Measurement, and Control.

D.W. Repperger, E.L. Scarborough, and T.L. Chelette, 1991, "*Construction of a Dual Axis Force Reflection Stick and Test Station*", AL-TR-1992-0041.

D.W. Repperger, 1991, "*Active Force Reflection Devices in Teleoperation*", IEEE Control Systems Magazine, 52-56, January.

D.W. Repperger, C.A. Phillips, and T.L. Chelette, 1995, "*A Study on Spatially Induced "Virtual Force" with an Information Theoretic Investigation of Human Performance*", IEEE Transactions on Systems, Man, and Cybernetics, 25(10):1392-1404.

D.W. Repperger, 1995, "*Biodynamic and Spasticity Reduction in Joystick Control via Force Reflection*", AL/CF-TR-1995-0152.

L.B. Rosenberg, 1992, "*The Use of Virtual Fixtures as Perceptual Overlays to Enhance Operator Performance in Remote Environments*", AL/CF-TR-1994-0089.

L.B. Rosenberg, 1993, "*The Use of Virtual Fixtures to Enhance Operator Performance in Time Delayed Teleoperation*", AL/CF-TR-1994-0139.

D.E. Whitney, 1969, "*Resolved Motion Rate Control of Manipulators and Human Prostheses*", IEEE Transactions on Man-Machine Systems.

R.L. Williams II and M.A. Murphy, 1997a, "*Telerobotic Control Architecture Including Force-Reflecting Teleoperation*", Armstrong Lab Technical Report.

R.L. Williams II and M.A. Murphy, 1997b, "*Naturally-Transitioning Rate-to-Force Control*", submitted to the ASME Journal of Dynamic Systems, Measurement, and Control.

R.L. Williams II, 1997, "*Cartesian Control of Force-Reflecting Hand Controllers*", Conference on Applied Mechanisms and Robotics, Cincinnati, OH.

R.L. Williams II and R.G. Roberts, 1997, "*Modeling and Analysis of Cable-Suspended Robots*", submitted to the 1998 ASME Design Technical Conferences, Atlanta, GA.

R.L. Williams II, F.W. Harrison, and D.I. Soloway, 1997, "*Shared Control of Multiple-Manipulator, Sensor-Based Telerobotic Systems*", 1997 IEEE International Conference on Automation and Robotics, Albuquerque, NM.

R.L. Williams II, F.W. Harrison, and D.I. Soloway, 1996, "*Naturally-Transitioning Rate-to-Force Controller for Manipulators*", 1996 IEEE International Conference on Automation and Robotics, Minneapolis, MN.

K. Willshire, F.W. Harrison, E.F. Hogge, R.L. Williams II, and D.I. Soloway, 1992, "*Results of Telerobotic Hand Controller Study Using Force Information and Rate Control*", *AIAA* Paper 92-1451, *AIAA* Space Programs Conference, Huntsville.

AN PSYCHOMETRIC EXAMINATION OF THE MULTIDIMENSIONAL WORK ETHIC PROFILE AMONG AIRFORCE ENLOISTED PERSONNEL

David J. Woehr
Associate Professor
Department of Psychology

Texas A&M University
College Station, Texas 77843-4235

Final Report for:
Summer Faculty Research Program
Armstrong Laboratory

Sponsored by:
Air Force Office of Scientific Research
Bolling Air Force Base, DC

And

Armstrong Laboratory

August, 1997

AN PSYCHOMETRIC EXAMINATION OF THE MULTIDIMENSIONAL WORK ETHIC PROFILE AMONG AIR FORCE ENLISTED PERSONNEL

David J. Woehr
Associate Professor
and
Michael J. Miller
Graduate Student

Department of Psychology
Texas A&M University
College Station, Texas 77843-4235

Abstract

The present study examines the psychometric properties of the Multidimensional Work Ethic Profile (MWEP) developed by Michael Miller and David Woehr (Woehr & Miller, 1997, Miller and Woehr, 1997) with Air Force enlisted personnel. The MWEP is a multidimensional measure of work ethic based on previous literature and research focusing on work ethic and job performance. Originally developed based on a sample of university students, the MWEP has demonstrated good psychometric characteristics including reliability and validity. The MWEP has been suggested as a potentially valuable screening tool with Air Force enlisted personnel. The purpose of the present study was to provide a preliminary evaluation of the measure among Air Force enlisted personnel. Results indicate that the measure does demonstrate similar psychometric characteristics among Air Force enlisted personnel as with the original developmental sample. The MWEP provides reliable and valid measures of multiple dimensions underlying the work ethic construct. These results indicate that the MWEP may be a useful screening tool for Air Force Personnel.

AN PSYCHOMETRIC EXAMINATION OF THE MULTIDIMENSIONAL WORK ETHIC PROFILE AMONG AIR FORCE ENLISTED PERSONNEL

David J. Woehr
and
Michael J. Miller
Texas A&M University

Introduction

History and Definition of Work Ethic

The term "work ethic" was coined centuries ago by post-Reformation intellectuals who opposed the practice of social welfare and professed the importance of individualism (Byrne, 1990). They espoused the belief that human beings must assume full responsibility for their lot in life and the poor were no exception. As such, hard work was viewed as a panacea and through it, one could improve his or her condition in life. Implicit in this assumption was the belief that the poor simply needed to help themselves through diligent labor and all life's ills would vanish. Such were the harsh origins of the construct.

Modern formulations of the work ethic construct stem from the work of the German scholar Max Weber. It was in 1904 and 1905 that Weber wrote a two-part essay entitled "The Protestant Ethic and the Spirit of Capitalism". In this essay Weber advanced the thesis that the introduction and rapid expansion of capitalism and the resulting industrialization in Western Europe and North America was in part the result of the Puritan value of asceticism (i.e., scrupulous use of time, strict self-denial of luxury, worldly pleasure, ease, and so on to achieve personal discipline) and the belief in a calling from God (Byrne, 1990; Charlton, Mallinson, & Oakeshott, 1986; Fine, 1983; Furnham, 1990a; Green, 1968; Lehmann, 1993; Maccoby, 1983; Nord, Brief, Atieh, & Doherty, 1988; Poggi, 1983). It was the practice of asceticism that Weber believed produced the celebrated 'work ethic'--the complete and relentless devotion to one's economic role on earth (Lessnoff, 1994). An individual's economic role was prescribed by the belief in a calling (Gilbert, 1977). The manifestation of occupational rewards through success in one's calling came to be revered as a sign of being one of the elect (i.e., chosen by God to receive salvation). Thus, economic activity was a vehicle toward economic success and economic success was a sign of salvation.

Weber maintained that other Protestant faiths (e.g., Calvinism, Methodism, Pietism, and Baptists) shared common theological underpinnings in terms of being proponents of asceticism and the spirit of capitalism (Bouma, 1973; Nelson, 1973); thus the term "Protestant Work Ethic" (PWE). However, the premise that work ethic is a religiously oriented concept was contested then and since. In fact, researchers have found little relationship between religious orientation and endorsement of the work ethic (Giorgi & Marsh, 1990; Ray, 1982). Ray (1982) concluded that all religious orientations currently share the attributes associated with the work ethic to the same degree. He states that the Protestant ethic, "...is certainly not yet dead; it is just no longer Protestant" (p. 135). This is consistent with Pascarella's (1984) contention that all major religions have espoused the importance of work. Thus, it appears that what was originally conceived as a religious construct is now likely secular and is best viewed as general work ethic and not the PWE.

Since work ethic is not a surrogate for religious orientation the question becomes, What is it? Current conceptualizations tend to view work ethic as an attitudinal construct pertaining to work oriented values. An individual espousing a high work ethic would place great value on: hard work, autonomy, fairness, wise and efficient use of time, delay of gratification, and the intrinsic value of work (Cherrington, 1980; Dubin, 1963; Furnham, 1984; Ho & Lloyd, 1984; Weber, 1958; Wollack, Goodale, Wijting, & Smith, 1971). Therefore, work ethic seems to be made up of multiple components. These components appear to include: industriousness, asceticism, self-reliance, morality, delay of gratification, and the centrality of work. In the absence of a firmly accepted conceptual and operational definition it is posited that work ethic is a construct that reflects a constellation of attitudes and beliefs pertaining to work oriented behavior. Characteristics of "work ethic" are that it: (a) is multidimensional; (b) pertains to work and work related activity in general, not specific to any particular job (yet may generalize to domains other than work - school, hobbies, etc.); (c) is learned (not dispositional); (d) refers to attitudes and beliefs (not necessarily behavior); (e) is intendend as a motivational construct (should be reflected in behavior); and (e) is secular, not necessarily tied to any one set of religious beliefs.

Relevance of Work Ethic to the Air Force

As previously defined, individual differences in work ethic should reflect differences among individuals in terms of their attitudes and beliefs with respect to the value of work and work-related behavior. An important

consideration for industrial psychology is the relationship between these attitudes and beliefs and actual work behavior. While industrial psychologists interested in the work ethic have typically explored its relationship with other attitudinal variables such as job satisfaction (e.g., Aldag & Brief, 1975; Blood, 1969; Stone, 1975, 1976; Wanous, 1974), job involvement (e.g., Blau, 1987; Randall & Cote, 1991; Saal, 1978), and organizational commitment (e.g., Kidron, 1978; Morrow & McElroy, 1987), there have been relatively few studies (e.g., Khaleque, 1992; Orpen, 1986), focusing on the relationship of work ethic with actual job performance. A possible reason for this is the lack of distinction between task and contextual aspects of job performance.

Recently several models of job performance have been proposed which attempt to describe a set of underlying dimensions that are representative of performance in all jobs (Borman & Motowidlo, 1993; Campbell, 1990; Campbell, McCloy, Oppler, & Sager, 1993). For example, Campbell (1990) argues that all jobs are made up of eight factors, including: job-specific task proficiency, non-job-specific task proficiency, written and oral communication, demonstrating effort, maintaining personal discipline, facilitating team and peer performance, supervision and leadership, and management and administration. Campbell's formulation distinguishes between behaviors that contribute to organizational effectiveness through their focus on task proficiency and those behaviors that help the organization in other ways (Motowidlo & Van Scotter, 1994). Task proficiency behaviors are formally prescribed by the organization whereas other behaviors, though not formally a part of the job, are still very valuable for organizational effectiveness (Borman & Motowidlo, 1993).

Borman and Motowidlo (1993) place performance behaviors not prescribed by the organization under the rubric of contextual activities. Examples include:

(1) Volunteering to carry out task activities that are not formally a part of the job.
(2) Persisting with extra enthusiasm or effort when necessary to complete own task activities successfully.
(3) Helping and cooperating with others.
(4) Following organizational rules and procedures even when personally inconvenient.
(5) Endorsing, supporting, and defending organizational objectives. (p. 73)

Using a sample comprising Air Force mechanics, Motowidlo and Van Scotter (1994) demonstrated that supervisors consider task performance and contextual performance separately when providing performance ratings. It is the contextual component of job performance in which work ethic may offer substantial predictive utility.

Specifically, it may be possible to predict with a measure of work ethic the extent to which an individual would engage in contextual performance of value to the unit. Further, the work ethic may demonstrate a relationship with technical school training success, job performance, and tenure in the Air Force.

Measurement of Work Ethic

Of paramount concern for research focusing on the understanding of the work ethic construct as well as the relationship between work ethic and work behavior is the ability to accurately measure the construct. There are at least seven work ethic measures in existence which purport to provide reliable and valid measures of this construct. However, there are a number of problems with these measures. First and foremost, they focus on the measurement of a single construct by providing a global "work ethic" score. This is a considerable shortcoming as, since its inception, Weber believed the work ethic to be a multidimensional construct; a position that has subsequently been supported by numerous researchers (Bouma, 1973; Cherrington, 1980; Furnham, 1984; Oates, 1971).

From a psychometric as well as a conceptual perspective, the lack of focus on the multidimensional nature of the work ethic is troubling. The use of a single overall score could potentially cause the loss of information with regards to the different components of work ethic as well as their relationships with other constructs (Carver, 1989; McHoskey, 1994). Further, the use of a single score in studies using different instruments to measure the work ethic may at least partially explain the equivocal results often found in the literature (Furnham, 1984). That is, one cannot be sure if the conflicting results are due to a lack of robustness in the studies, the scales measuring different components of the work ethic, or deficiencies in terms of construct relevance and psychometric properties (Furnham, 1990b).

A second concern is that the various measures appear to tap different components of the work ethic and not the construct in its entirety. This has often led to poor intercorrelations among measures. For example, Furnham (1990b) administered seven measures of the work ethic to 1,021 participants and found that the correlations between the various measures ranged from 0.19 - 0.66 with a mean r of 0.36. One would expect the values to be much higher if the scales were indeed measuring the same thing.

Finally, another potential problem with existing work ethic measures is that these measures are relatively dated. The mean time since publication for the previous measures is 23 years. The age of the measures poses the

problem of many dated items. For example, some of the items contain sex-biased language such as: "Hard work makes a man a better person", "The man who can approach an unpleasant task with enthusiasm is the man who gets ahead", and "To be superior a man must stand alone".

Factor analytic investigations of the various measures have found the existence of several identifiable factors (Furnham, 1990b; Heaven, 1989; Tang, 1993; Mirels & Garrett, 1971; McHoskey, 1994). For example, McHoskey (1994) factor analyzed Mirels and Garrett's Protestant Ethic scale. His analysis yielded a 4-factor solution which he labeled, "success", "asceticism", "hard-work", and "anti-leisure". However, McHoskey was quick to point out that though this scale was multidimensional, other important aspects of the PWE were absent. Specifically, it in no way measured an individual's attitudes toward morality, self-reliance, or delay of gratification. This lack of comprehensiveness in measuring the work ethic has been levied against other scales as well and limits their utility (Furnham, 1984, 1990a, b; McHoskey, 1994).

In an effort to ameliorate the shortcomings in previous attempts to measure the work ethic, Woehr and Miller (1997) and Miller and Woehr (1997) developed the Multidimensional Work Ethic Profile (MWEP). The goal in the development of such a measure was to build on and extend previous measures in an attempt to capture the multidimensionality of the construct. The MWEP is a 65-item measure assessing 7 dimensions related to the work ethic construct. These dimensions are: *"Delay of Gratification"*, *"Hard Work"*, *"Morality/Ethics"*, *"Self-Reliance"*, *"Leisure"*, *"Wasted Time"*, and *"Centrality of Work"*. Complete definitions of these dimensions are provided in table 1.

Originally developed based on a sample of university students, the MWEP has demonstrated good psychometric characteristics including reliability and validity. Specifically, Miller and Woehr (1997) report 3 - 4 week test-retest reliabilities of 0.83 - 0.95 and internal consistency coefficient alphas of 0.78 - 0.89 for the dimensions of work ethic. With regards to construct-related validity the MWEP demonstrated discriminant relationships with personality, cognitive ability, and manifest needs. Lastly, the criterion-related validity of the MWEP was evaluated by relating it to academic effort indices pertinent to the university student sample. The MWEP was shown to be significantly related to hours studying per week (0.21), hours watching TV per week (0.36), hours in extracurricular activities per week (0.26), and classes missed (0.30).

Table 1.

Dimension definitions for the 7 work ethic dimensions assessed by the MWEP.

Dimension:	**Definition:**
Centrality of Work	Belief in the virtues of hard work.
Delay of Gratification	Striving for independence in one's daily work.
Hard Work	Pro-leisure attitudes and beliefs in activities that serve a rejuvenating function.
Leisure	Belief in work for work's sake and the importance of work.
Morality/Ethics	Believing in a just and moral existence.
Self-Reliance	Orientation toward the future; the postponement of rewards.
Wasted Time	Attitudes and beliefs reflecting active and productive use of time.

Present Study

Given the previous evaluations of the MWEP and the potential for use as a screening measure among Air Force enlisted personnel, the objective of this study was to empirically determine the extent to which the psychometric properties of the MWEP that have been found with a university student sample would generalize to Air Force enlisted personnel. Measurement stability across the samples would allow for greater confidence with regards to measurement equivalence and provide an initial indication of the viability of the MWEP for use in the Air Force.

As noted, the primary objective of the present study was to compare the psychometric characteristics of the MWEP with Air Force personnel relative to the original student development sample. This comparison focused on: (1) the mean score levels on each dimension, (2) score variability for each dimension, (3) the reliability for each dimension, and (4) the overall pattern of correlations among dimensions. If the MWEP functions similarly across the two samples no differences in dimension variability, dimension reliability, or the overall pattern of correlations among dimensions should be found. However, differences in mean levels on each dimension are likely given the actual differences across the two samples. That is, the student sample represents 18 to 22-year-old college students. Alternately, the Air Force sample represents an 18 to 22-year-old non-college bound sample. It is likely that actual

differences in work ethic attitudes and beliefs exist across the two groups. Such differences would be reflected in mean dimension score differences.

Method

University Participants.

The university student sample comprised 598 participants (52% female and 48% male). Subject participation was voluntary and subjects received partial course credit for taking part in the study. Mean age of the participants was 19.2 and ranged from 17 to 27.

Air Force Participants.

Participants in the present study were 268 Air Force enlisted personnel that participated in the study during Basic Military Training (BMT). The participants were 95% male and 5% female. Further, 71% were White, 15% Black, 8% Hispanic, 4% Asian, and 2% Other. Mean age of the participants was 19.95 and ranged from 18 to 35.

Multidimensional Work Ethic Profile (MWEP) Measure.

The MWEP was originally developed as a 65 item paper-and-pencil measure. The measure requires responses to items on a 5 point Likert-type scale ranging from 1(strongly disagree) to 5 (strongly agree). In order to facilitate data collection in the present study the MWEP was included as part of a computer-administered battery of questionnaires. Thus a computer administered version of the MWEP was developed. Although computer-administered this version was highly similar to the paper-and-pencil version. Both items and response options were displayed in the same manner in both forms. Participants were asked to respond to each of the items via the numbers on the computer keyboard.

Procedure.

The MWEP was administered as part of an extensive battery of computer-administered questionnaires completed in a single 4 hour session during the first week of BMT. Subjects were seated at individual computer terminals and given the measures. Administration of the measures was counterbalanced across experimental sessions.

Results

Comparison of the MWEP in the two samples focused on: (1) the mean score levels on each dimension, (2) score variability for each dimension, (3) the reliability for each dimension, and (4) the overall pattern of correlations among dimensions. Mean scores for each of the 7 work ethic dimensions for both the Air Force and student samples are presented in Table 2.

Table 2.

Means and standard deviations for the 7 work ethic dimensions for both the Student and Air Force Samples.

	Student Sample N = 598		Air Force Sample N = 268		
Dimension:	**Mean**	**SD**	**Mean**	**SD**	**t**
Centrality of Work	24.34	6.04	20.79	6.03	8.01*
Delay of Gratification	16.95	4.52	14.08	4.18	8.85*
Hard Work	22.09	5.86	16.81	5.45	12.52*
Leisure	28.63	5.86	31.50	5.81	-6.68*
Morality/Ethics	16.08	4.45	13.90	3.21	8.15*
Self-Reliance	26.11	6.88	24.84	6.79	2.51
Wasted Time	19.96	4.71	16.10	4.34	11.41*

*$p < .01$.

Tests for differences between the mean scores for each dimension are also presented in Table 2. These results indicate significant mean differences for all dimensions except the self-reliance dimension. Further, means are higher for the student sample than for the Air Force sample for all dimensions except the leisure dimension. Thus, the student sample had significantly higher mean scores for the *"Centrality of Work"*, *"Delay of Gratification"*, *"Hard Work"*, *"Morality/Ethics"*, and *"Wasted Time"* dimensions. The Air Force sample had a significantly higher mean score on the leisure dimension and no significant difference was for the self-reliance dimension.

Table 3 provides the results of a comparison of the variance of each dimension across samples. These

results indicate no significant differences for any of the dimensions across samples except *"Morality/Ethics"*. For the morality/ethics dimension there is significantly less variability in scores for the Air Force sample than for the student sample.

Table 3.

Test for equality of variances across student and Air Force Samples.

			Levine's Equality of	Test for Variances
Dimension	**Student Sample Variance**	**Air Force Sample Variance**	**F**	**Significance**
Centrality of Work	36.48	36.36	.088	.767
Delay of Gratification	20.43	17.47	2.60	.107
Hard Work	34.33	29.70	1.173	.279
Leisure	34.33	33.76	.187	.665
Morality/ethics	19.80	10.30	26.301	.000
Self-Reliance	47.33	46.10	.136	.713
Wasted Time	22.18	18.84	1.586	.208

Dimension reliabilities (coefficient α) for both samples are presented in table 4. Examination of these results indicate no differences in dimension reliabilities across samples except for the *"Morality/Ethics"* dimension. Specifically, all dimension reliabilities are within .03 of each other across samples except for the *"Morality/Ethics"* dimension for which the reliability is substantially lower in the Air Force sample.

Finally, the dimension intercorrelations for both the Air Force and student samples are presented in table 5. In order to assess the extent to which the dimension intercorrelations differed across samples, we used LISREL 8.14 (Joreskog & Sorbom, 1993) to provide an overall test of the equivalence of the 2 correlation matrices. Specifically, we tested a model in which correlations among the 7 work ethic dimensions were set equal to the student sample

based correlations and the correlations for the Air Force sample were constrained to be equal to those from the student sample. Using this approach, the overall model fit indices derived from the LISREL analyses provide an indication of the overall equality of the correlations across samples. Results of this analysis are provided in Table 6 and indicate that the two sets of correlations are generally equivalent.

Table 4.

Test for equality of reliabilities across student and Air Force Samples.

Dimension	Student Sample Reliability	Air Force Sample Reliability
Centrality of Work	.84	.85
Delay of Gratification	.79	.78
Hard Work	.85	.87
Leisure	.87	.87
Morality/ethics	.78	.55
Self-Reliance	.89	.86
Wasted Time	.79	.77

Discussion

The present study presents an examination of the psychometric properties of the Multidimensional Work Ethic Profile (MWEP) developed by Michael Miller and David Woehr (Woehr & Miller, 1997, Miller and Woehr, 1997). The MWEP is a 65 item measure of work ethic based on previous research and literature focusing on work ethic and job performance. An important characteristic of the MWEP is that it assess 7 conceptually and empirically distinct facets of the work ethic construct. Originally developed based on a sample of university students, the MWEP has demonstrated good psychometric characteristics including reliability and convergent and discriminate validity. Further, the MWEP has been suggested as a potentially valuable screening tool with Air

Table 5.

Work ethic dimension intercorrelations for the student and Air Force samples.

	Student Sample						
Dimensions:	1	2	3	4	5	6	7
1. Centrality of Work	1.0						
2. Delay of Gratification	.38	1.0					
3. Hard Work	.33	.33	1.0				
4. Leisure	-.47	-.12	-.08	1.0			
5. Morality/Ethics	.17	.25	.22	.08	1.0		
6. Self-Reliance	.20	.21	.38	.10	.13	1.0	
7. Wasted Time	.56	.40	.38	-.28	.21	.32	1.0
	Air Force Sample						
1. Centrality of Work	1.0						
2. Delay of Gratification	.52	1.0					
3. Hard Work	.48	.56	1.0				
4. Leisure	-.44	-.26	-.23	1.0			
5. Morality/Ethics	.34	.44	.48	-.16	1.0		
6. Self-Reliance	.20	.11	.23	-.02	.18	1.0	
7. Wasted Time	.62	.55	.59	-.34	.46	.26	1.0

Student Sample $N = 598$. All correlations are significant ($p < .01$).

Air Force Sample $N = 268$. All correlations greater than .17 are significant ($p < .01$).

Table 6.

Goodness of fit indices for the test of intercorrelation equivalence.

χ^2	**df**	χ^2/df	**RMSEA**	**GFI**	**NFI**	**CFI**	**RFI**
72.30	42	1.72	.04	.92	.95	.98	.95

Force enlisted personnel. The purpose of the present study was to provide a preliminary evaluation of the measure among Air Force enlisted personnel. Results indicate that the measure does in fact demonstrate highly similar psychometric characteristics among Air Force enlisted personnel as with the original developmental sample. The MWEP provides reliable and valid measures of multiple dimensions underlying the work ethic construct. These results indicate that the MWEP may be a useful screening tool for Air Force Personnel.

Specifically, results of the present study found no differences across samples for the dimension variances, reliabilities, and intercorrelations across dimensions. One exception to these findings was for the *"Morality/Ethics"* dimension. For this dimension the results indicated significantly less variance as well as substantially lower reliability with the Air Force sample relative to the student sample. One possible explanation for this finding may lie in differences in the work settings of the two samples. That is, the student sample was assessed in a non-job setting while the Air Force sample was assessed in an actual job setting. It is likely that the items comprising the *"Morality/Ethics"* dimension are fairly transparent and actual job incumbents may not respond as truthfully as non incumbents. This would explain the restricted variance found in the Air Force sample. This reduced variance would in turn result in a lower reliability estimate. Counter to this explanation, however, was our finding that the mean response for the *"Morality/Ethics"* dimension was actually significantly lower in the Air Force sample relative to the student sample. If the items were relatively transparent and the incumbent sample was simply responding in a more socially desirable manner then one would expect a higher mean score. It is difficult at this point to determine the exact reasons for the differences found across samples for this dimensions. The lack of differences across the other, more work-related, dimensions however is encouraging.

The results of the present study do indicate significant mean score differences for 6 of the 7 dimensions across samples. These differences are not unexpected and do not call into question the measurement equivalence of the MWEP in either sample. Rather these differences are to a certain extent consistent with expected differences between the two samples. The student sample represents young adults attending college. Alternately, the Air Force sample represents young adults not attending college but directly entering the work force. Thus differences in work ethic scores most likely reflect actual differences between samples.

Conclusion

The prediction of job performance is one of the benchmarks of industrial psychology. Though the field has relied primarily on cognitive ability measures to predict performance, it has also pursued the use of alternative predictors (Arvey & Sackett, 1993). One of the most prevalent alternative predictors has been personality variables (Adler, 1996; Barrick & Mount, 1991; Goffin, Rothstein, & Johnston, 1996; Hogan, Hogan, & Roberts, 1996; Horman & Maschke, 1996; Tett, Jackson, & Rothstein, 1991). Though measures of personality have not resulted in adverse impact, many researchers have found a low relationship with actual criterion measures of job performance (Ones, Mount, Barrick, & Hunter, 1994). Another potential problem is that personality variables may not function in a linear fashion. Attitudinal variables such as work ethic may bridge the gap between cognitive ability and personality variables.

The present study demonstrates that one such attitudinal measure, the MWEP, a multidimensional measure of work demonstrates good psychometric characteristics in two diverse samples. This suggests that the MWEP is a potentially valuable pragmatic measure for either sample. Certainly, the next step is to examine the predictive utility of the MWEP in an Air Force context. A proposed avenue of research for the future would be an examination of the relationship of the work ethic to technical school training success, job performance, and tenure in the Air Force. This could be achieved through the administration of the MWEP to enlisted personnel while in BMT and following up on their respective progress in the Air Force. The criteria in this example might be technical school final grades, performance evaluations while at the duty station, and fulfilment of enlistment tour requirements.

References

Aldag, R. J. & Brief, A. P. (1975). Some correlates of work values. Journal of Applied Psychology, 60, 757-760.

Blau, G. J. (1987). Using a person-environment fit model to predict job involvement and organizational commitment. Journal of Vocational Behavior, 30, 240-257.

Blood, M. R. (1969). Work values and job satisfaction. Journal of Applied Psychology, 53, 456-459.

Borman, W. C., & Motowidlo, S. J. (1993). Expanding the criterion domain to include elements of contextual performance. In N. Schmitt & W. C. Borman (Eds.), Personnel selection in organizations (pp. 71-98). San Francisco: Jossey-Bass.

Bouma, G. D. (1973). Beyond Lenski: A critical review of recent "Protestant Ethic" research. Journal for the Scientific Study of Religion, 12, 141-155.

Byrne, E. F. (1990). Work, inc.: A philosophical inquiry. Philadelphia: Temple University Press.

Campbell, J. P. (1990). Modeling the performance prediction problem in industrial and organizational psychology. In M. D. Dunnette & L. M. Hough (Eds.), Handbook of industrial and organizational psychology (Vol 1, 2nd ed., pp. 687-732). Palo Alto, CA: Consulting Psychologists Press.

Campbell, J. P., McCloy, R. A., Oppler, S. H., & Sager, C. E. (1993). A theory of performance. In N. Schmitt & W. C. Borman (Eds.), Personnel selection in organizations (pp. 35-70). San Francisco: Jossey-Bass.

Carver, C. S. (1989). How should multifaceted personality constructs be tested? Journal of Personality and Social Psychology, 56, 577-585.

Charlton, W., Mallinson, T., & Oakeshott, R. (1986). The Christian response to industrial capitalism. London: Sheed & Ward.

Cherrington, D. J. (1980). The work ethic: Working values and values that work. New York: AMACOM.

Dubin, R. (1963). Industrial worker's worlds: A study of the 'central life interests' of industrial workers. In E. O. Smigel (Ed.), Work and Leisure (pp. 53-72). New Haven: College and University Press.

Fine, R. (1983). The Protestant ethic and the analytic ideal. Political Psychology, 4, 245-264.

Furnham, A. (1984). The Protestant work ethic: A review of the psychological literature. European Journal of

Social Psychology, 14, 87-104.

Furnham, A. (1990a). The Protestant work ethic: The psychology of work-related beliefs and behaviours. London: Routledge.

Furnham, A. (1990b). A content, correlational, and factor analytic study of seven questionnaire measures of the Protestant work ethic. Human Relations, 43, 383-399.

Gilbert, J. B. (1977). Work without salvation: America's intellectuals and industrial alienation, 1880-1910. Baltimore: Johns Hopkins University Press.

Giorgi, L., & Marsh, C. (1990). The Protestant work ethic as a cultural phenomenon. European Journal of Social Psychology, 20, 499-517.

Green, A. W. (1968). Sociology: An analysis of life in modern society. New York: McGraw-Hill.

Ho, R., & Lloyd, J. I. (1984). Development of an Australian work ethic scale. Australian Psychologist, 19, 321-332.

Heaven, P. C. L. (1989). Structure and personality correlates of the Protestant work ethic among women. Personality and Individual Differences, 10, 101-104.

Joreskog, K. G., Sorbom, D. (1993). LISREL-8: Structural equation modeling with the SIMPLIS command language. Chicago, IL: Scientific Software International Inc.

Khaleque, A. (1992). Work values, attitudes and performance of industrial workers in Bangladesh. Social Indicators Research, 27, 187-195.

Kidron, A. (1978). Work values and organizational commitment. Academy of Management Journal, 21, 239-247.

Lehmann, H. (1993). The rise of capitalism: Weber versus Sombart. In H. Lehmann & G. Roth (Eds.), Weber's Protestant ethic: Origins, Evidence, Contexts (pp. 195-208). Washington, D. C.: Cambridge University Press.

Lessnoff, M. H. (1994). The spirit of capitalism and the Protestant ethic: An Enquiry into the Weber thesis. Brookfield, VT: E. Elgar.

Maccoby, M. (1983). The managerial work ethic in America. In J. Barbash, R. J. Lapman, S. A. Levitan,

& G. Tyler (Eds.), The work ethic--A critical analysis (pp. 183-196). Madison, WI: Industrial Relations Research Association.

McHoskey, J. W. (1994). Factor structure of the Protestant work ethic scale. Personality and Individual Differences, 17, 49-52.

Mirels, H. L., & Garrett, J. B. (1971). The Protestant ethic as a personality variable. Journal of Consulting and Clinical Psychology, 36, 40-44.

Morrow, P. C., & McElroy, J. C. (1987). Work commitment and job satisfaction over three career stages. Journal of Vocational Behavior, 30, 330-346.

Motowidlo, S. J., & Van Scotter, J. R. (1994). Evidence that task performance should be distinguished from contextual performance. Journal of Applied Psychology, 79, 475-480.

Nelson, B. (1973). WeberÕs Protestant ethic: Its origins, wanderings, and foreseeable future. In C. Glock & P. Hammond (Eds.), Beyond the classics (pp. 71-130). New York: Harper & Row.

Nord, W. R., Brief, A. P., Atieh, J. M., & Doherty, E. M. (1988). Work values and the conduct of organizational behavior. Research in Organizational Behavior, 10, 1-42.

Poggi, G. (1983). Calvinism and the capitalist spirit: Max Weber's Protestant ethic. Amherst: University of Massachusetts Press.

Miller, M. J., & Woehr, D. J. (1997). Work ethic: The development and evaluation of a multidimensional measure. Manuscript submitted for publication.

Oates, W. (1971). Confessions of a workaholic: The facts about work addiction. New York: World Publishing Company.

Pascarella, P. (1984). The new achievers: Creating a modern work ethic. New York: Free Press.

Randall, D. M. & Cote, J. A. (1991). Interrelationships of work commitment constructs. Work and Occupations, 18, 194-211.

Ray, J. J. (1982). The Protestant ethic in Australia. Journal of Social Psychology, 116, 127-138.

Saal, F. E. (1978). Job involvement: A multivariate approach. Journal of Applied Psychology, 63, 53-61.

Stone, E. F. (1975). Job scope, job satisfaction, and the Protestant ethic: A study of enlisted men in the

U.S. Navy. Journal of Vocational Behavior, 7, 215-234.

Stone, E. F. (1976). The moderating effect of work-related values on the job scope-job satisfaction relationship. Organizational Behavior and Human Performance, 15, 147-167.

Tang, T. L. -P. (1993). A factor analytic study of the Protestant work ethic. The Journal of Social Psychology, 133, 109-111.

Wanous, J. P. (1974). Individual differences and reactions to job characteristics. Journal of Applied Psychology, 59, 616-622.

Weber, M. (1958). The Protestant Ethic and the spirit of capitalism (T. Parsons, Trans.). New York: Charles Scribner's Sons.

Woehr, D. J. & Miller, M. J. (1997, April). The meaning and measurement of work ethic. Paper presented at the annual Southeastern Industrial/Organizational Psychology Meeting, Atlanta, GA.

Wollack, S., Goodale, J. G., Wijting, J. P., & Smith, P.C. (1971). Development of the Survey of Work Values. Journal of Applied Psychology, 55, 331-338.

MODES OF HUMAN HEAD/NECK RESPONSE TO VERTICAL IMPACT

Mariusz Ziejewski Ph.D.
Associate Professor
Department of Mechanical Engineering

North Dakota State University
Dolve 111
Fargo, ND 58105

Final Report for:
Summer Research Program
Armstrong Laboratory

Sponsored by:
Air Force Office of Scientific Research
Bolling Air Force Base, Washington, DC

And

Armstrong Laboratory

August 1997

MODES OF HUMAN HEAD/NECK RESPONSE
TO VERTICAL IMPACT

Mariusz Ziejewski, Ph.D.
Associate Professor
Mechanical Engineering Department
North Dakota State University

Abstract

Helmet-mounted systems, such as night vision goggles and helmet-mounted displays, have come into increased demand in recent years. Though these devices enhance the pilot's performance, they may also increase the chance of neck injury during ejection. The helmet-mounted systems change the helmet's mass properties such as weight, moment of inertia, and center of gravity location, which may alter the head/neck response and possibly change the pattern of neck loading. To define the specifications or criteria for allowable head mounted mass and center of gravity location that is safe for the crew members, identification of the head/neck responses and the factors influencing those responses is necessary. The objectives of this study were to identify the modes of head/neck response to vertical impacts, to determine and assess the parameters influencing head/neck response and to determine a method of predicting mode of head/neck response for a given subject under given conditions. The data used in this study came from five test cells of the Female Impact Program (FIP) study performed by the USAF Armstrong Laboratory on their Vertical Deceleration Tower (VDT) facility. The subjects were exposed to acceleration levels comparable to those experienced in the catapult phase of ACES II ejections. The peak acceleration level for the tests used in this study was 10 G. Each of the subjects wore the same type of helmet. However, the weight and inertial properties of the helmet were varied to simulate those of current helmet-mounted systems.

Five modes of head/neck response for vertical impact were identified and characterized. Modes A and B represent forward neck and head rotation. Modes C and D represent forward neck rotation and rearward head rotation. Mode E of head/neck response represent no significant neck or head rotation. Two experimental parameters, namely, initial linear x-acceleration of the head at the mouthpiece and head pitch as measured by the motion of the mouthpiece LED with respect to the shoulder LED, were found to be sufficient to uniquely define the mode of head/neck response. Three categories of parameters have been identified and suggested to be the determining factors in a given subject's mode of response for a given condition. The categories include initial position, anthropometry, and other factors such as helmet, weight, helmet center of gravity location and impact acceleration level.

MODES OF HUMAN HEAD/NECK RESPONSE TO VERTICAL IMPACT

Mariusz Ziejewski, Ph.D.

INTRODUCTION

Helmet-mounted systems, such as night vision goggles and helmet-mounted displays, have come into increased demand in recent years. Though these devices enhance the pilot's performance, they may also increase the chance of neck injury during ejection. The helmet-mounted systems change the helmet's mass properties such as weight, moment of inertia, and center of gravity location, which may alter the head/neck response and possibly changing the pattern of neck loading.

There are two mechanisms of neck injury, direct impact to the neck and inertial loading of the head. During the ejection phase of escape, a direct impact to the pilot's neck is unlikely. However, the pilots are subjected to inertial loading of the head. During inertial loading of the head, forces are transmitted by the neck structure to the torso. The magnitude of the transmitted load is dependent on the inertia of the head/helmet system, the initial orientation of the cervical spine, and the direction of head motion.

The dynamic strength of the human neck is different for different directions of bending. Mertz and Patrick found that resultant bending moment is an excellent indicator of neck strength [1]. For extension, a resultant bending moment of 42 ft-lbs (57 N-m) was proposed as the lower boundary for an injury tolerance level. For flexion, a resultant bending moment of 140 ft-lbs (190 N-m) was suggested as the injury tolerance level. Based on these bending moment tolerance levels, the neck appears to be at least three times stronger in resisting flexion than extension.

The United States Air Force initiated testing to evaluate the effect of acceleration levels to human neck response during ejection procedures. The main objective of their study was to define neck response during the catapult or impact acceleration phase of the ejection. High-speed film footage clearly showed that for identical test conditions, some subjects responded with neck flexion, while others responded with neck extension. To accomplish the ultimate objective of defining the specifications or criteria for allowable head mounted mass and center of gravity location that is safe for the crewmembers, identification of the head/neck responses and the factors influencing those responses is necessary.

OBJECTIVES

1. To identify the modes of head/neck response to vertical impacts.
2. To determine and assess the parameters influencing head/neck response.
3. To determine a method of predicting mode of head/neck response for a given subject under given conditions.

EXPERIMENTAL DATA

The data used in this study came from five test cells of the Female Impact Program (FIP) study performed by the USAF Armstrong Laboratory on their Vertical Deceleration Tower (VDT) facility [2].

The VDT is composed of an impact carriage mounted on two vertical guide rails. The test assembly, including a generic ejection seat, a restraint harness, and the instrumentation, is mounted to the impact carriage. The carriage is then raised and allowed to free-fall along the vertical rails onto a water reservoir (hydraulic decelerator) at the base of the tower. A contoured piston mounted on the bottom of the carriage is guided into the reservoir where the displacement of water around the piston decelerates the carriage and produces an upward (+Gz) acceleration. The subjects are positioned in the VDT seat and restrained with a standard double shoulder strap-lap belt combination. Principal measured parameters include tri-axial linear accelerations at the head (mouthpiece or bitebar) and chest, angular accelerations about the lateral axis at the head and chest, seat and carriage vertical (z-axis) accelerations, and seat pan loads. Body displacements are measured by motion analysis using the SELSPOT infrared detection system.

The subjects were exposed to acceleration levels comparable to those experienced in the catapult phase of ACES II ejections. The peak acceleration level for the tests used in this study was 10 G. Each of the subjects wore the same type of helmet. However, the weight and inertial properties were varied slightly to simulate those of current helmet-mounted systems. The helmet test configurations used are given in Table 1.

Table 1.
Helmet Test Configurations

TEST CELL	ADDED WEIGHT (LB)	WEIGHT PLACEMENT (IN)	Cg SHIFT (IN)	CENTER OF GRAVITY (X.Y.Z) (IN)	MOMENT OF INERTIA (X, Y, Z) (LB-IN^2)	SIW
D	(HELMET ONLY)	N/A	N/A	(-0.89, 0.01, 1.18)	(63.53, 38.63, 57.39)	0.139
E	1.5	0.0	0.1	(-0.79, 0.01, 0.73)	(115.84, 39.78, 110.38)	0.200
F	1.5	5.0	1.59	(0.70, 0.14, -0.10)	(124.46, 71.59, 125.81)	0.324
G	4.5	2.0	1.21	(0.32, 0.06, -0.14)	(211.97, 53.23, 204.85)	0.365
J	1.5	0.0	0.1	(-0.79, 0.01, 0.73)	(115.84, 39.78, 110.38)	0.200

Note that for Cell J, the headrest was moved to 1 inch behind the seatback tangent line.

SIW = Standard Inertial Weight [2]

The study used both male and female subjects of various anthropometric dimensions. The gender, age, selected anthropometry of the test subjects, and test numbers are given in Table 2.

Table 2.
Test Setup

SUBJECT ID	SUBJECT GENDER	AGE (YR)	WEIGHT (LB)	STAND HT. (IN)	SITTING HT. (IN)	TEST CELL				
						D	E	F	G	J
B-9	M	30	155	68.1	34.9	3562	3593	3611	—	—
B-11	M	35	225	72.7	37.5	3686	3723	3810	3827	3825
B-16	F	31	130	65.3	35.2	3718	3742	3756	3829	3820
B-17	F	26	133	67.0	34.8	3584	3602	3673	3716	3746
B-18	F	24	100	64.5	34.3	3652	3670	3741	3752	—
C-12	M	35	185	68.1	36.6	3603	3644	3660	3701	3727
C-15	F	24	126	63.5	34.3	3633	3663	—	—	—
C-17	M	29	160	69.8	38.0	3592	3612	3639	3666	—
E-4	M	35	208	71.5	38.4	3590	3641	3654	3683	3728
G-11	M	29	166	69.5	36.8	3558	3608	3622	3680	3712
H-15	M	24	177	69.2	35.7	3632	3662	3665	3582	—
J-7	M	28	160	67.7	35.6	3667	3691	3743	3753	3824
J-9	F	25	123	61.2	32.0	3563	3587	3613	3640	—
J-10	M	23	200	69.1	36.4	3583	3606	3624	3690	3758
J-11	F	21	159	65.7	34.5	3659	3675	3757	3805	3725
K-9	F	27	137	65.9	34.1	3631	3696	3709	3719	3734
M-21	M	36	150	66.1	34.2	3569	3627	3685	3722	3809
M-30	M	35	183	70.0	37.2	3623	3643	3672	3700	3759
O-3	M	27	135	62.6	33.2	3621	3638	3688	3704	3732
O-5	F	23	145	65.6	35.1	3566	3589	3616	3630	—
P-11	M	24	192	74.0	37.9	3567	3601	3647	3653	3713
R-20	F	26	107	63.6	34.6	3568	3580	3596	3614	3731
R-21	M	36	228	71.3	38.1	3581	3610	3637	3655	3726
S-11	M	32	219	71.2	37.0	3561	3619	3646	3668	3733
S-20	F	27	125	67.4	33.9	3582	3609	3634	3706	3748
V-3	F	26	115	63.9	33.8	3576	3599	3648	3658	3747
W-8	F	30	128	66.8	35.0	3591	3617	3669	3695	3735

---- means the subject did not participate in that testing configuration

MODES OF HEAD/NECK RESPONSE

A schematic diagram of the head/neck anatomical structure, indicating the approximate locations of a reference coordinate system at the first thoracic vertebra (T1), the head anatomical coordinate system, the occipital condylar point and the approximate head center of gravity, is given in Figure 1.

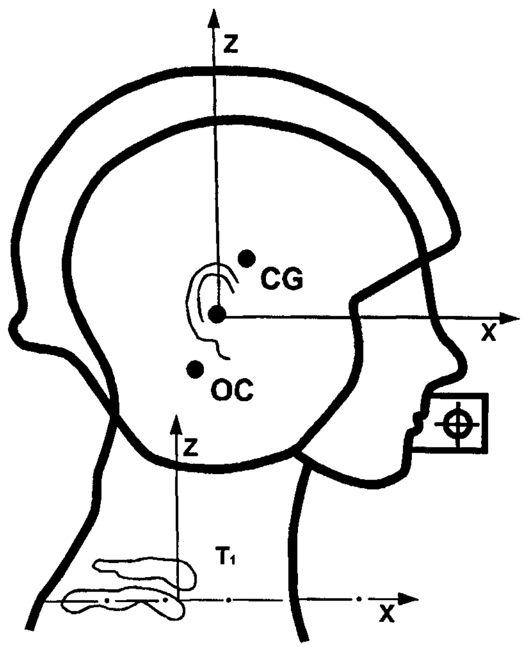

Figure 1. Schematic diagram of head/neck anatomical structure.

In the analysis the head/neck structure can be represented by a two-pivot linkage mechanism as shown in Figure 2. Considering the physical constraints of the experimental setup, there are five possible modes of head/neck response.

The first two modes, Modes A and B, represent forward neck and forward head rotation. Mode A differs from Mode B by the relative angular velocity of the neck in comparison to the head. Mode A has greater initial neck angular velocity than head angular velocity, while Mode B has greater initial head angular velocity than neck angular velocity. A schematic diagram showing the direction of head/neck rotation for Modes A and B is given in Figure 3.

The second two modes, Modes C and D, represent forward neck rotation and rearward head rotation. Mode C differs from Mode D by the relative angular velocity of the neck in comparison to the head. Mode C has greater initial neck angular velocity than head angular velocity. Mode D has greater initial head angular velocity than neck angular velocity. A schematic diagram showing the direction of head/neck rotation for Modes C and D is given in Figure 4.

Mode E of head/neck response has no significant head or neck rotation. The schematic diagram for Mode E is shown in Figure 5.

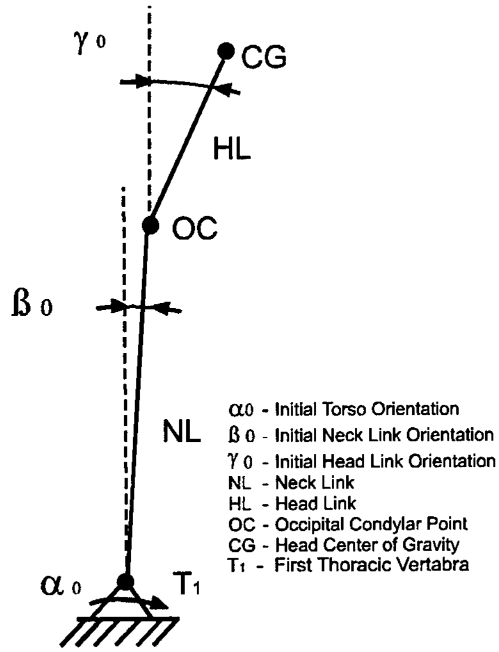

Figure 2. Two-pivot linkage mechanism representing head/neck structure.

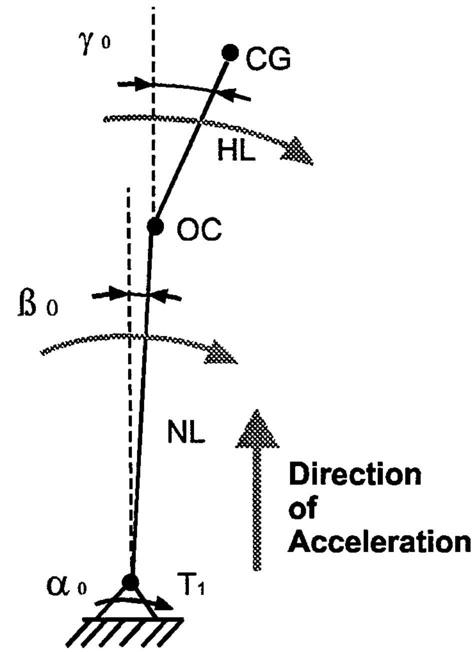

Figure 3. Schematic diagram showing direction of head/neck rotation for Modes A and B.

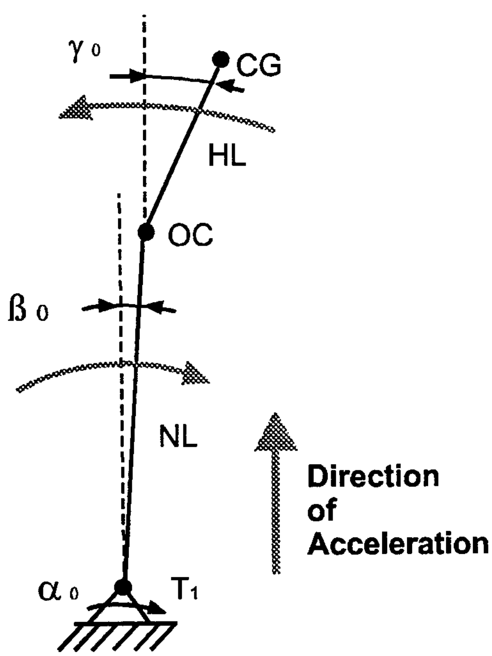

Figure 4. Schematic diagram showing direction of head/neck rotation for Modes C and D.

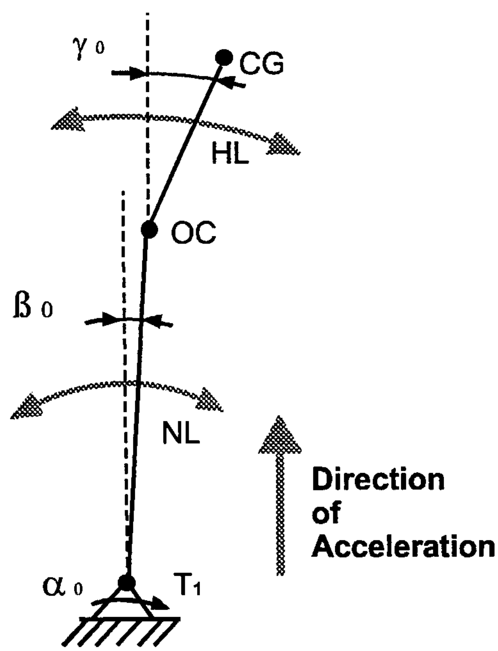

Figure 5. Schematic diagram showing direction of head/neck rotation for Mode E.

The characterized modes of head/neck response are summarized in the upper portion of Table 3.

Table 3.
Modes of Head/Neck Response for Vertical Impact.

		MODES				
		A	**B**	**C**	**D**	**E**
RESPONSE	Neck Rotation (β)	forward	forward	forward	forward	none
	Head Rotation (γ)	forward	forward	back	back	none
	Condition	$\omega_\beta > \omega_\gamma$	$\omega_\beta < \omega_\gamma$	$\omega_\beta > \omega_\gamma$	$\omega_\beta < \omega_\gamma$	none
DIAGNOSTIC PARAMETERS	X - Acceleration *(Initial at mouthpiece)*	+	-	+	-	**0**
	Head Pitch *(Mouthpiece wrt shoulder)*	- (>10°)	- (3°-10°)	+ (>5°)	+ (3°-5°)	**0** (<3°)
CATEGORY 1 *(Initial Position)*	Neck Pitch	*	*	*	*	*
	Head Pitch	*	*	*	*	*
CATEGORY 2 *(Anthropometry)*	Sitting Height (mm)	*	*	*	*	*
	Head Length (mm)	*	*	*	*	*
	Chest Circ. (mm)	*	*	*	*	*
	Weight (kg)	*	*	*	*	*
CATEGORY 3 *(Other Factors)*	Helmet Weight (kg)	*	*	*	*	*
	Helmet C. G.	*	*	*	*	*
	Acceleration Level (G)	*	*	*	*	*

ω_β = angular velocity of the neck
ω_γ = angular velocity of the head

* Indicates the values not available at this time. Values to be determined in the follow up research.

DATA ANALYSIS

For all tests considered in this study, the available measured parameters were considered. In addition, the high-speed film footage was viewed to observe the general trends. Based on the evaluation of the experimental parameters, it was determined that two parameters, namely, initial linear x-acceleration of the head at the mouthpiece and head pitch as determined by the motion of the mouthpiece LED with respect to the shoulder LED, were sufficient to uniquely identify the head/neck mode of response. The directions of the diagnostic parameters are given in Table 3, where positive (+) x-acceleration designates forward acceleration and positive (+) head pitch designates a rearward head rotation.

Based on the evaluation of the experimental head pitch data, it was observed that for Mode A, the head pitch was greater than 10°. For Mode B, the head pitch was between 3° and 10°. For Mode C, the head pitch was greater than 5°. For Mode D, the head pitch was between 3° and 5°. For Mode E, the head pitch was less than 3°. This information is given in Table 3.

Using the described definition of head/neck response modes, all the studied tests were classified in terms of mode of response. The frequency of each response mode for different test cells is given in Table 4. Figures 6 through 10 show the diagnostic parameter trend for each of the modes. Each figure contains data from three experimental tests which have that mode of response. The test numbers are listed in the legend.

Table 4.
Frequency of response mode for different test cells.

		MODE									
CELL	**SIW**	**A**		**B**		**C**		**D**		**E**	
		Ratio	**%**	**Ratio**	**%**	**Ratio**	**%**	**Ratio**	**%**	**Ratio**	**%**
D	.139	4/27	14.8	8/27	29.6	5/27	18.5	8/27	29.6	2/27	7.4
E	.200	3/27	11.1	6/27	22.2	4/27	14.8	5/27	18.5	9/27	33.3
F	.324	7/24	29.2	9/24	37.5	2/24	8.3	4/24	16.7	2/24	8.3
G	.365	6/25	24.0	10/25	40.0	2/25	8.0	2/25	8.0	5/25	20.0
J	.200	1/11	9.0	1/11	9.0	7/11	63.6	1/11	9.0	1/11	9.0

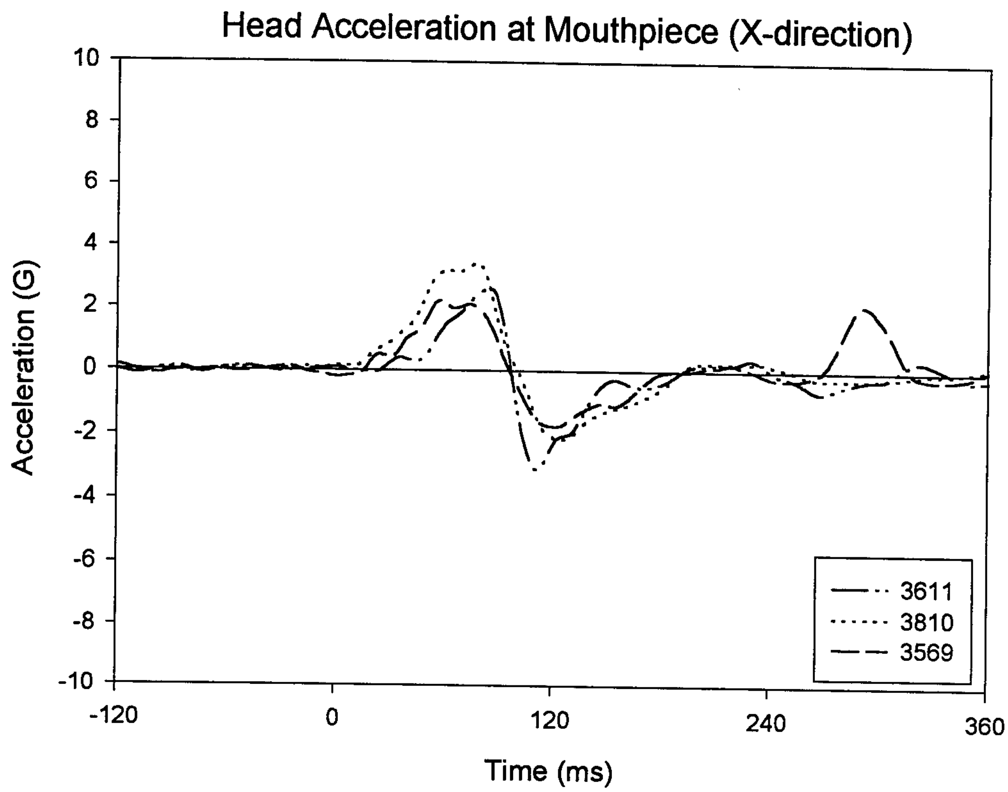

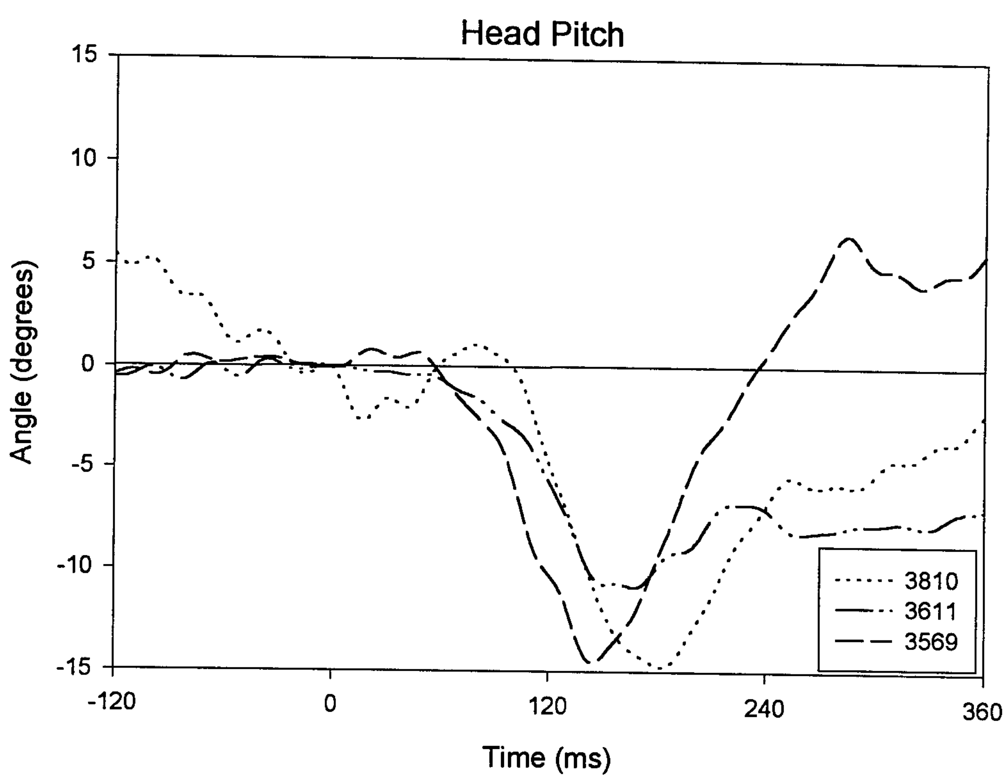

Figure 6. Sample experimental data for linear x-acceleration of the head and head pitch for Mode A.

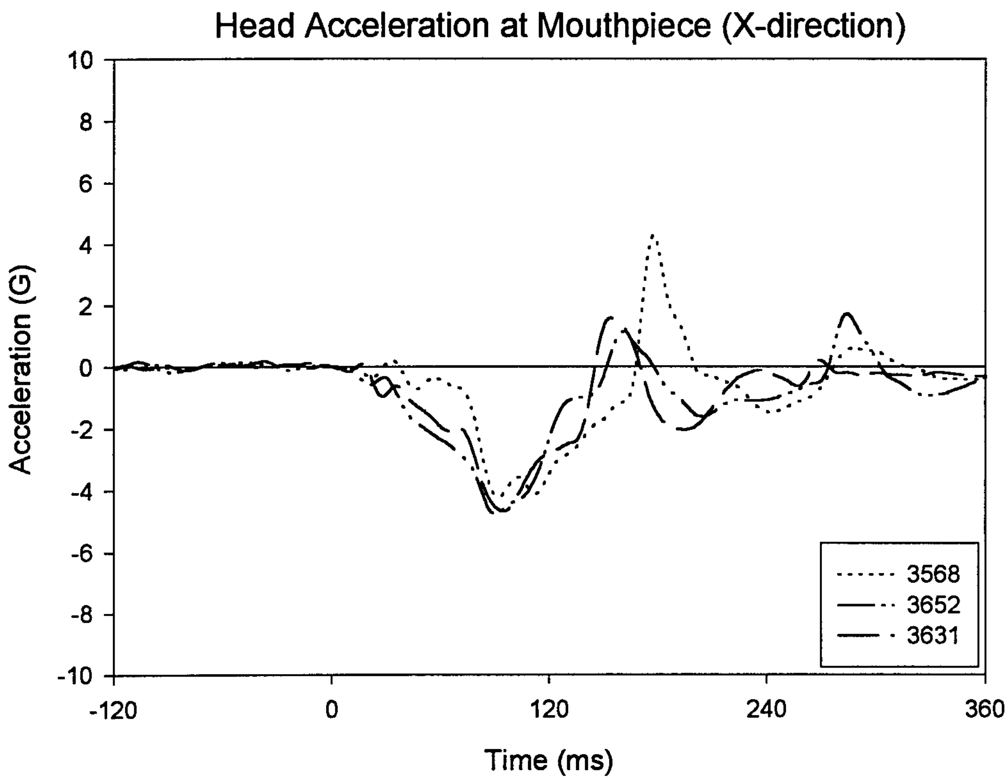

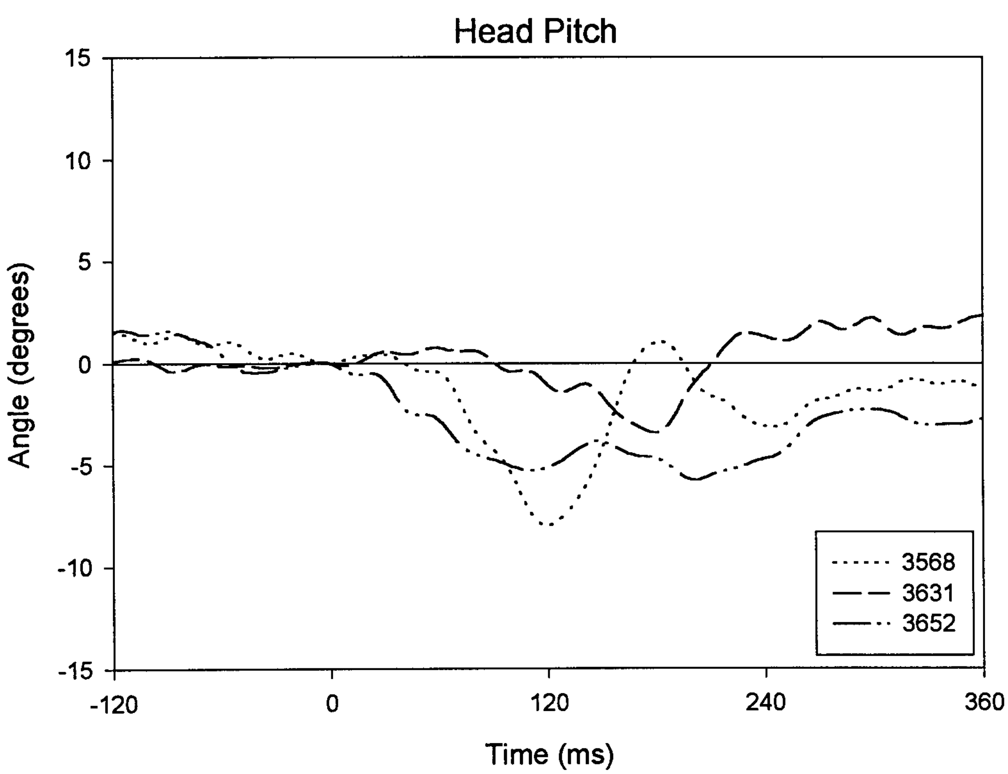

Figure 7. Sample experimental data for linear x-acceleration of the head and head pitch for Mode B.

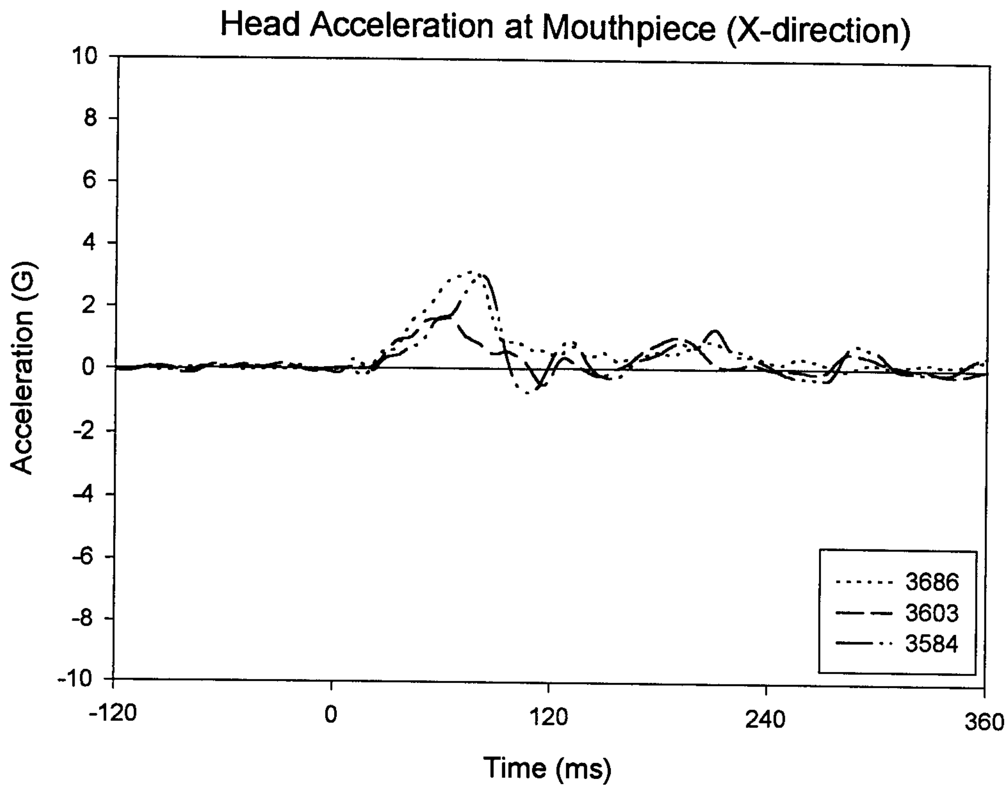

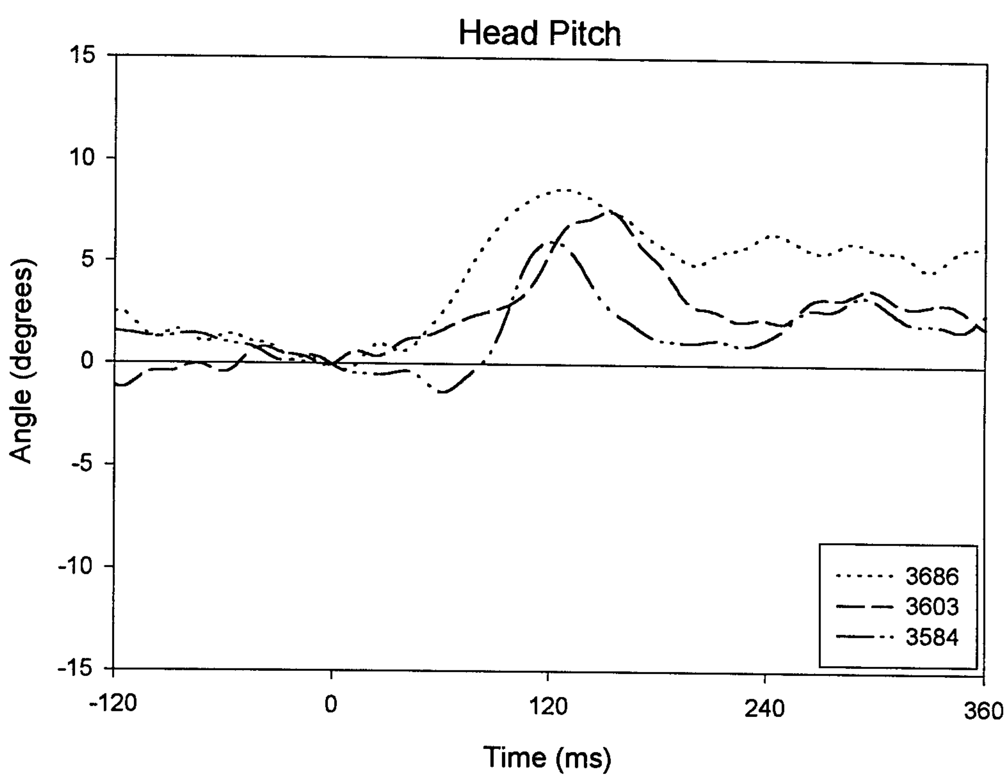

Figure 8. Sample experimental data for linear x-acceleration of the head and head pitch for Mode C.

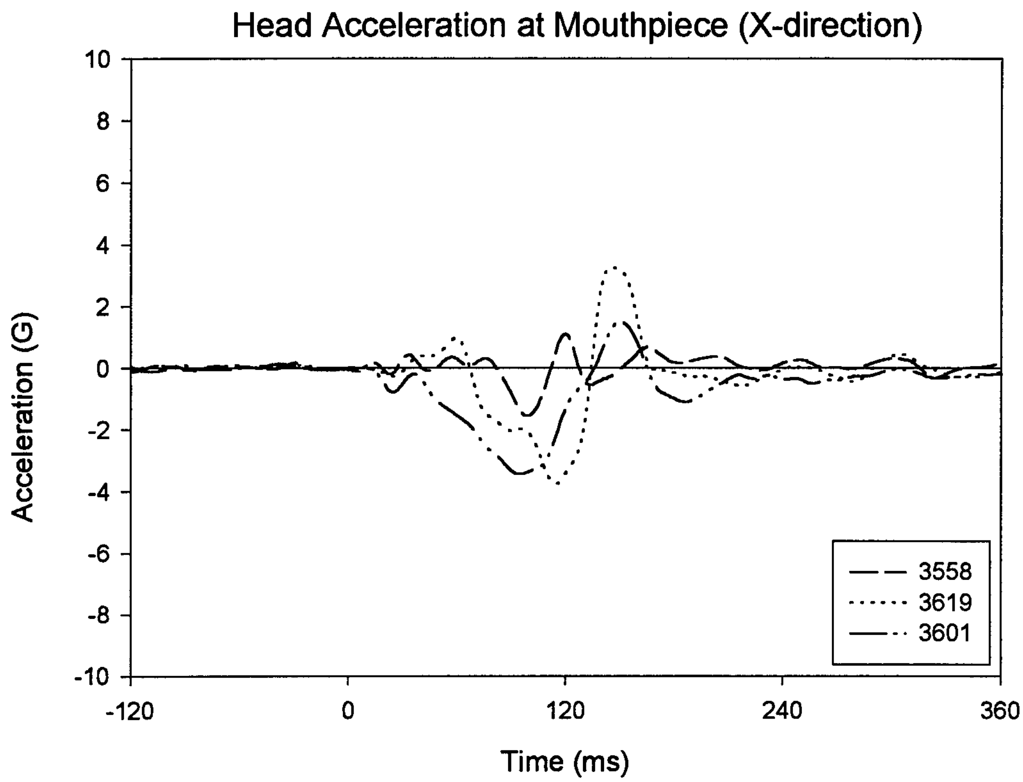

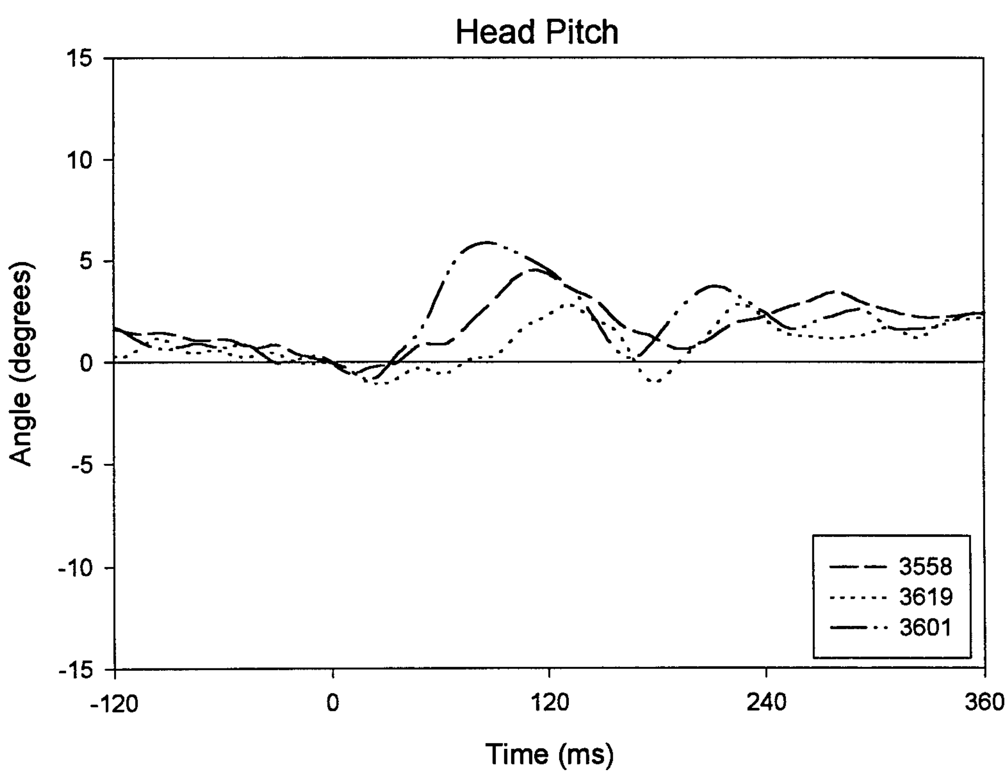

Figure 9. Sample experimental data for linear x-acceleration of the head and head pitch for Mode D.

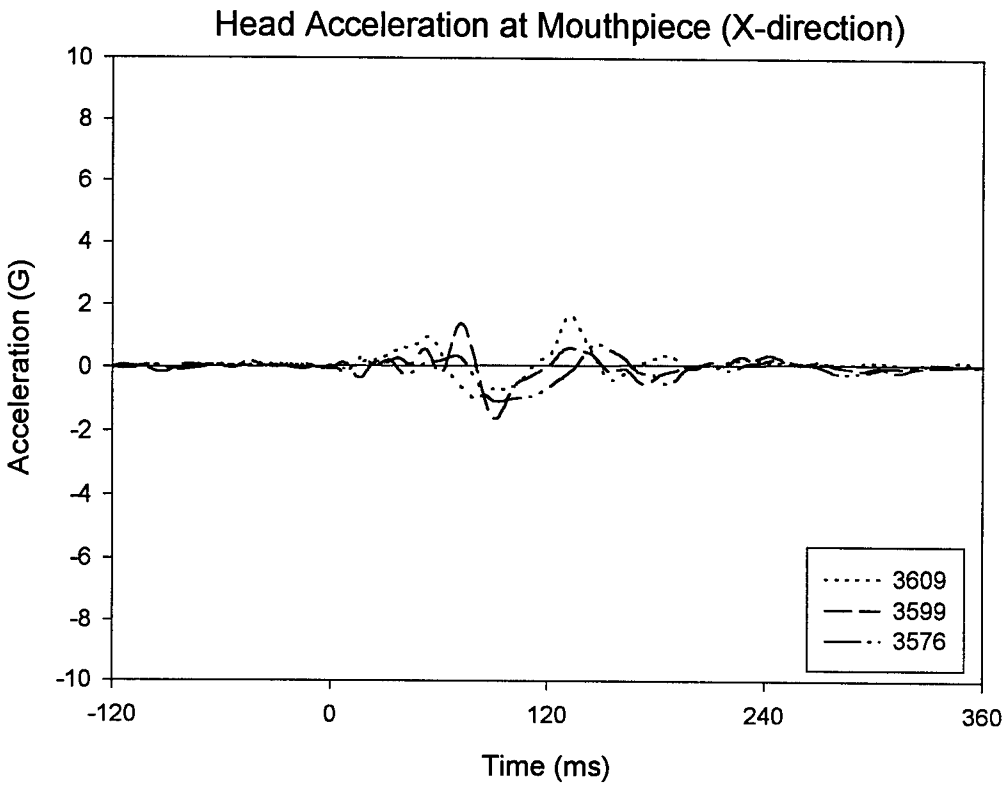

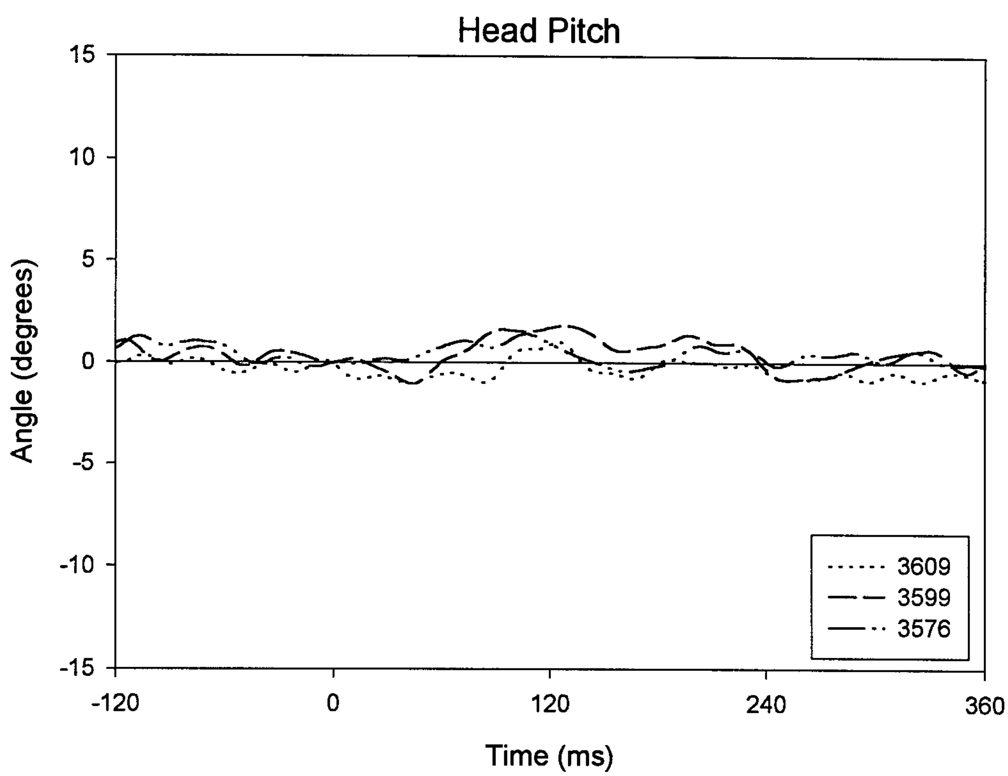

Figure 10. Sample experimental data for linear x-acceleration of the head and head pitch for Mode E.

HIGH SPEED FILM ANALYSIS

Representative examples for different modes based on the cell D, E, F, and J, high speed films visual analysis are given in Figures 11 through 15.

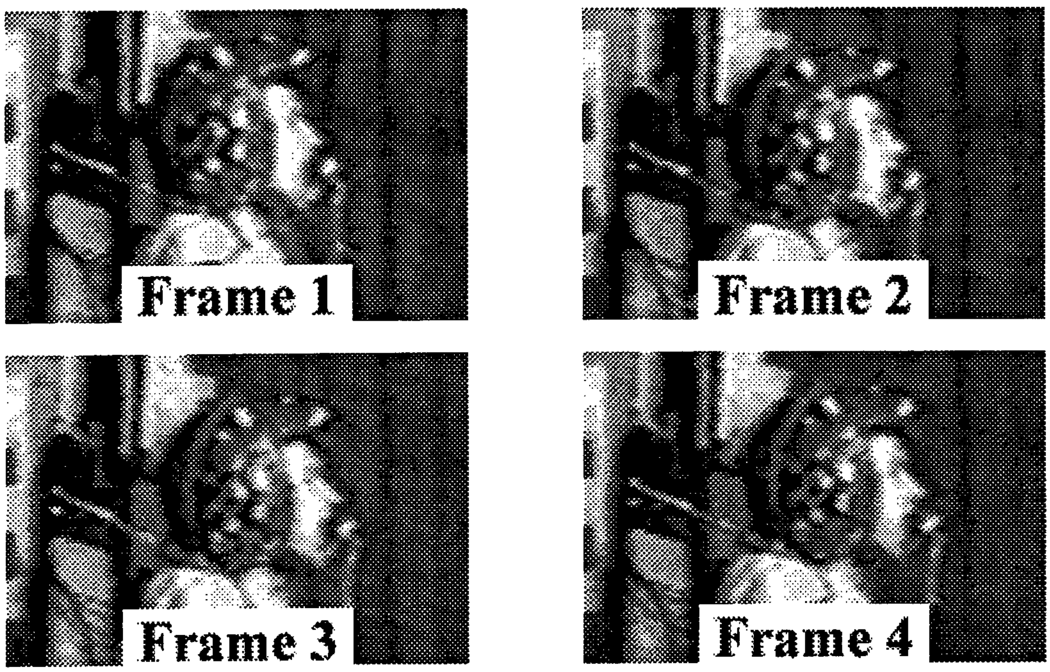

Figure 11. Mode A (Forward neck and head rotation, greater initial neck angular velocity than head angular velocity, test number 3569)

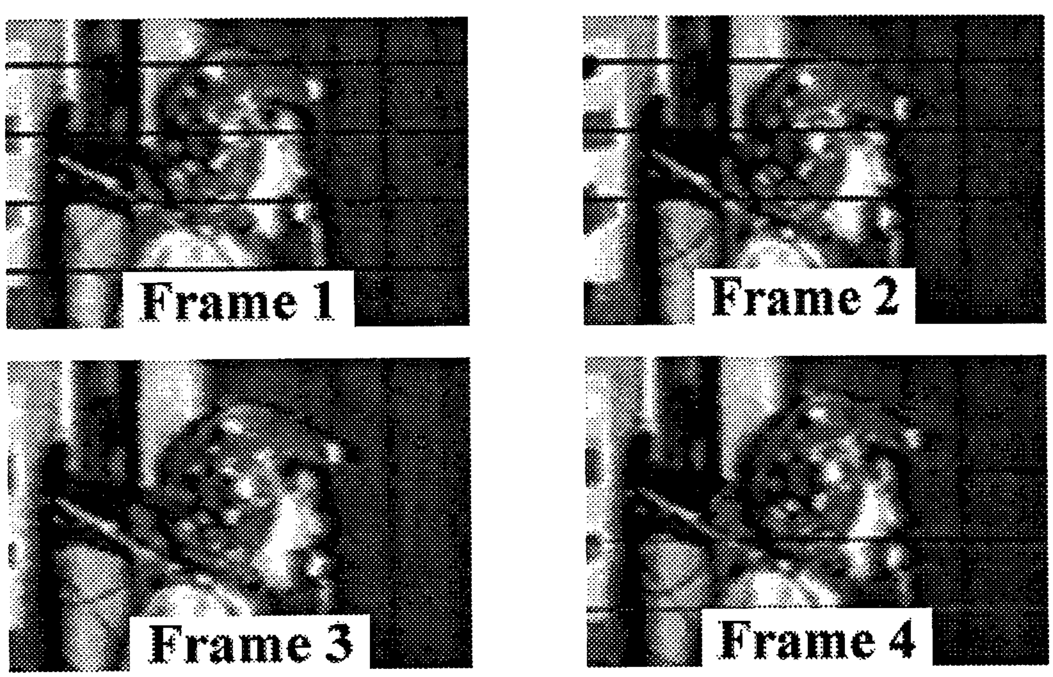

Figure 12. Mode B (Forward neck and head rotation, greater initial head angular velocity than neck angular velocity, test number 3631.)

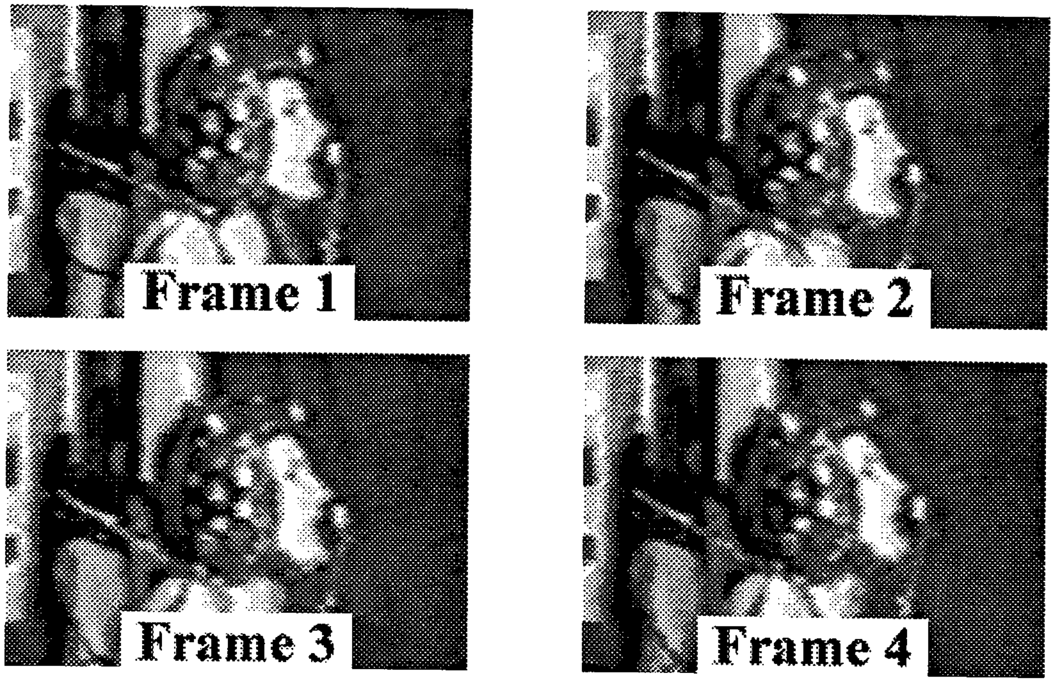

Figure 13. Mode C (Forward neck rotation and rearward head rotation, greater initial neck angular velocity than head angular velocity, test number 3584.)

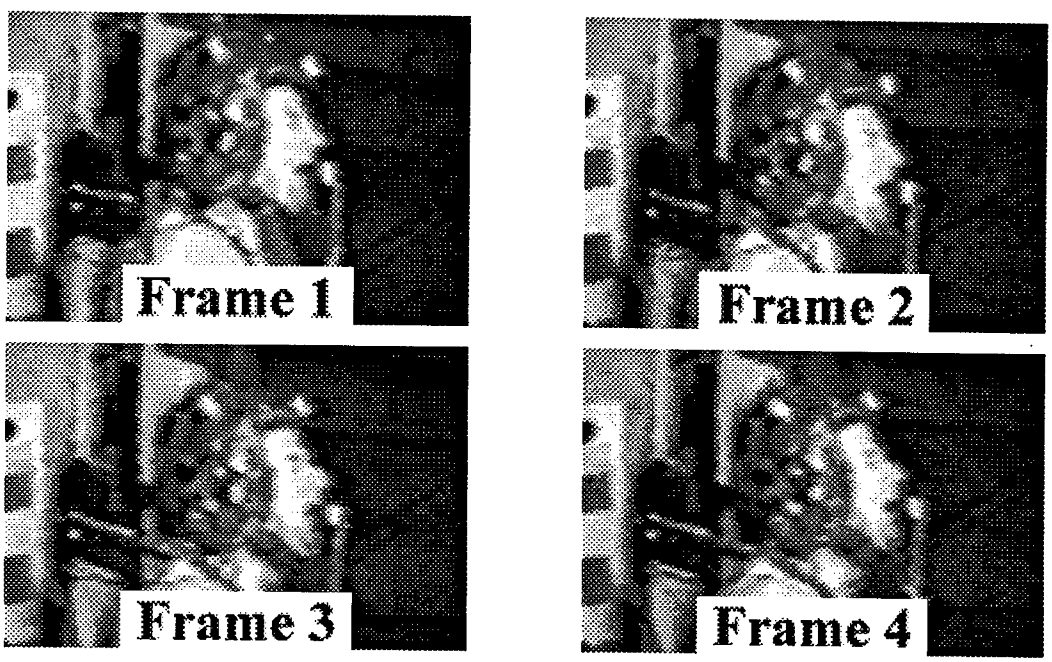

Figure 14. Mode D (Forward neck rotation and rearward head rotation, greater initial head angular velocity than neck velocity, test number 3558.)

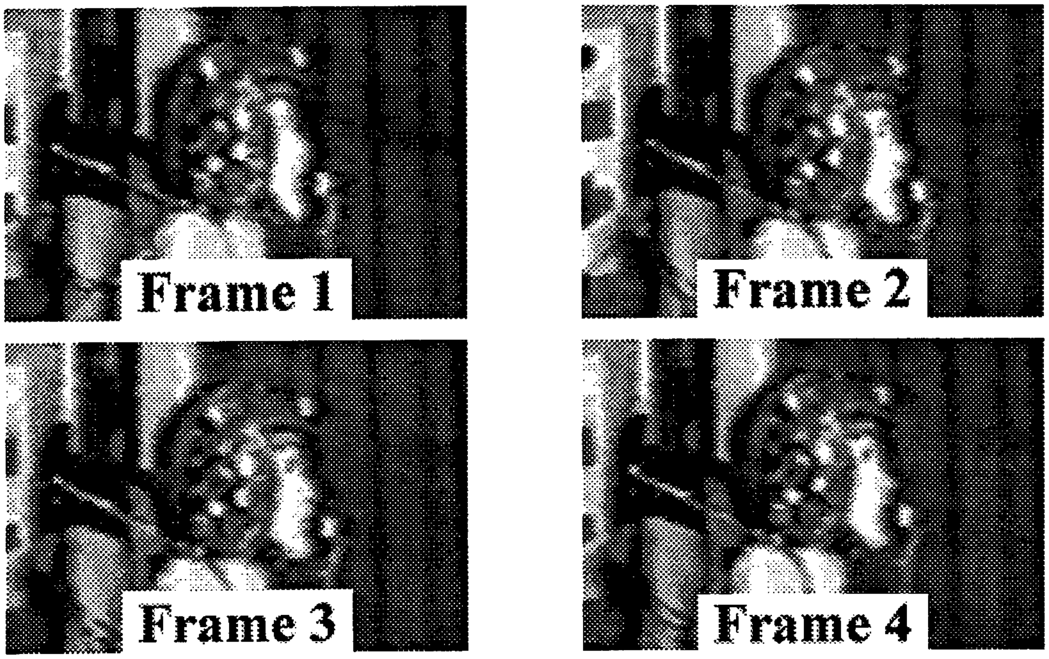

Figure 15. Mode E (No significant head or neck rotation, test number 3576.)

STATISTICAL ANALYSIS

Theoretically, a subject can respond in any of the five modes of response. However, a combination of several parameters will determine the subject's mode of response for the given conditions. These parameters can be classified into three different categories and the role they play in the head/neck response can be determined with the help of statistical analysis. Category #1 is initial position, specifically initial neck pitch and initial head pitch. Category #2 is anthropometry. The third category is labeled as others and includes helmet weight, helmet center of gravity location and impact acceleration level. The values for the parameters in these three categories are not yet available. A follow-up research project could determine those values that would complete Table 3. Thus, providing a tool for predicting head/neck response of a given subject under given conditions.

A preliminary statistical investigation of the influence of anthropometry was performed. Due to lack of sufficient number of observations (tests) to explain the variability present in the experimental data no conclusion can be reached in regard to the tested effects. It appears, however, that four anthropometric variables as sitting height, head length, chest circumference and weight are significant. These anthropometric variables were chosen as a preliminary set of variables to consider in defining the head/neck response modes as given in Table 3. Table 5 gives the influential anthropometry and mode of response for each subject under each test configuration.

Table 5.
Response Mode for Tests

SUBJECT ID	SEATED HT. (IN)	HEAD LENGTH (IN)	CHEST CIRCUMFERENCE (IN)	WEIGHT (LB)	TEST CELL				
					D	E	F	G	J
B-9	34.9	7.8	35.9	155	A	D	A	—	—
B-11	37.5	7.9	43.7	225	C	C	A	A	E
B-16	35.2	7.4	34.3	130	D	B	B	B	B
B-17	34.8	7.7	35.6	133	C	E	B	E	C
B-18	34.3	7.2	29.5	100	B	B	B	E	—
C-12	36.6	7.5	39.4	185	C	C	C	C	C
C-15	34.3	7.8	31.9	126	B	E	—	—	—
C-17	38.0	7.9	39.1	160	C	C	C	C	—
E-4	38.4	9.0	46.3	208	D	E	A	E	C
G-11	36.8	7.7	38.7	166	D	D	E	B	C
H-15	35.7	7.8	40.0	177	D	E	B	D	—
J-7	35.6	7.9	35.1	160	E	C	E	E	C
J-9	32.0	7.0	35.1	123	A	B	B	B	—
J-10	36.4	8.0	40.7	200	B	E	A	B	C
J-11	34.5	7.1	39.5	159	B	A	A	A	E
K-9	34.1	7.0	37.1	137	B	B	B	B	D
M-21	34.2	7.2	32.6	150	A	A	E	A	A
M-30	37.2	7.1	43.3	183	D	D	D	D	*
O-3	33.2	7.6	36.0	135	A	A	A	A	*
O-5		7.6	35.6	145	D	E	D	B	—
P-11	37.9	7.5	39.3	192	D	D	D	D	*
R-20	34.6	7.0	32.1	107	B	B	E	B	*
R-21	38.1	7.9	47.2	228	B	E	B	E	*
S-11	37.0	7.9	45.7	219	D	D	B	B	*
S-20	33.9	7.5	34.0	125	C	E	D	A	*
V-3	33.8	7.0	32.8	115	E	E	A	A	*
W-8	35.0	7.7	34.2	128	B	B	B	B	*

---- subject did not participate in that testing configuration

* test data not available

SUMMARY AND CONCLUSIONS

1) Five modes of head/neck response for vertical impact were identified and characterized. The first two modes, Modes A and B, represent forward neck and forward head rotation. Mode A differs from Mode B by the relative angular velocity of the neck in comparison to the head. Mode A has greater initial neck angular velocity than head angular velocity, while Mode B has greater initial head angular velocity than neck angular velocity. The second two modes, Modes C and D, represent forward neck rotation and rearward head rotation. Mode C differs from Mode D by the relative angular velocity of the neck in comparison to the head. Mode C has greater initial neck angular velocity than head angular velocity. Mode D has greater initial head angular velocity than neck angular velocity. Mode E of head/neck response has no significant head or neck rotation.
2) Two experimental parameters, namely, initial linear x-acceleration of the head at the mouthpiece and head pitch as measured by the motion of the mouthpiece LED with respect to the shoulder LED, were found to be sufficient to uniquely define the mode of head/neck response.
3) Three categories of parameters have been identified and suggested to be the determining factors in a given subject's mode of response for a given condition. The categories include initial position, anthropometry, and other factors such as helmet, weight, helmet center of gravity location and impact acceleration level.
4) With the developed method, one can classify the modes of response for the existing VDT tests. This information can be used to study several different areas of interest such as:
   a) Frequency of response mode
   b) Gender differences
   c) Effect of helmet configurations on head/neck response
5) When completed, the developed method will allow one to predict how a given subject will respond to a given vertical impact condition.

SUGGESTIONS FOR FURTHER WORK

In order to use the developed method as a predictive tool, one must determine the magnitude of the values of each parameter in the three categories identified as influential factors in determining head/neck response including initial position, anthropometry, and other factors such as helmet, weight, helmet center of gravity location and impact acceleration level.

REFERENCES

1. H. J. Mertz and L. M. Patrick, "Strength and Response of the Human Neck." SAE Paper No. 710855, Fifteenth Stapp Car Crash Conference, Nov. 17-19, 1971, Coronado, CA.
2. Perry, C.E., J.R. Buhrman, and F.S. Knox III, "The Effect of Head Mounted Mass on Males and Females Under +Gz Impact Acceleration," Aviation, Space, and Environmental Medicine (ASEMCG 68 {5}:216), Presentation at Annual AsMA Meeting, May 1997.